Osaka University Knowledge Archive

Title	Development of plasma-assisted polishing for highly efficient and damage-free finishing of single-crystal SiC, GaN and VD-SiC
Author(s)	鄧, 輝
Citation	大阪大学, 2016, 博士論文
Version Type	VoR
URL	https://doi.org/10.18910/55988
rights	
Note	

Osaka University Knowledge Archive : OUKA

https://ir.library.osaka-u.ac.jp/

Osaka University

Doctoral Dissertation

Development of plasma-assisted polishing for highly efficient and damage-free finishing of single-crystal SiC, GaN and CVD-SiC

Hui Deng

January 2016

Graduate School of Engineering,
Osaka University

Table of Contents

Page

Chapter 1 Background 1

1.1 Introduction 1

1.2 Difficult-to-machine materials 2

1.2.1 4H-SiC 3

1.2.2 GaN 4

1.2.3 CVD-SiC 5

1.3 Motivation of this study 6

1.4 Thesis organization 6

References 7

Chapter 2 Proposal of plasma-assisted polishing 9

2.1 Introduction 9

2.2 Current polishing techniques 10

2.2.1 Chemical mechanical polishing 10

2.2.2 Mechanochemical polishing 12

2.2.3 Catalyst-referred etching 12

2.2.4 UV-assisted polishing 13

2.2.5 Electro-chemical mechanical polishing 14

2.3 Proposal of plasma-assisted polishing 14

2.3.1 Introduction 14

2.3.2 Plasma chemical vaporization machining 14

2.3.3 Generation of atmospheric-pressure plasma 16

2.3.4 Strategies of PAP for difficult-to-machine materials 20

2.4 Summary 25

References 25

Chapter 3 Development of the PAP machine 29

3.1 Introduction 29

3.2 PAP machines for preliminary experimental study 29

3.2.1 Symmetric PAP machine 29

3.2.2 Two-step PAP process 31

3.2.3 Generation of large-area AP-plasma 33

3.3 Prototype PAP machine 36
3.3.1 Introduction 36
3.3.2 Polishing tool 36
3.3.3 Pressurizing mechanism 38
3.3.4 Cooling system 40
3.3.5 Dresser 41
3.4 Summary 43
References 44

Chapter 4 Application of PAP to 4H-SiC 45
4.1 Introduction 45
4.2 How is a SiC wafer fabricated 45
4.2.1 Introduction 45
4.2.2 Diamond lapping and polishing of 4H-SiC 46
4.2.3 CMP of SiC 48
4.3 Modification of 4H-SiC by AP-plasma irradiation 51
4.4 Application of the symmetric PAP machine 58
4.5 Application of two-step PAP process 63
4.5.1 Oxidation of 4H-SiC (0001) by water-vapor-containing plasma 63
4.5.2 Probable flattening mechanism of PAP 67
4.5.3 Comparison of plasma oxidation and thermal oxidation 68
4.6 Flattening of the C-face of 4H-SiC 75
4.6.1 Conventional CMP 76
4.6.2 Combination of thermal oxidation and CeO_2 slurry polishing 79
4.7 ECMP of 4H-SiC 80
4.8 Summary 86
References 88

Chapter 5 Control of the surface atomic structure of SiC (0001) 91
5.1 Introduction 91
5.2 Crystal structure of 4H-SiC 92
5.3 Probable mechanism for controlling the surface atomic structure of 4H-SiC (0001) 93
5.4 Proof of the proposed mechanism 95
5.5 Summary 101
References 102

Chapter 6 Application of PAP to GaN (0001) **105**
6.1 Introduction 105
6.2 CMP of GaN 105
6.3 Surface modification of GaN by AP-plasma irradiation 108
6.4 Applications of two-step PAP 111
6.4.1 Plasma pretreatment and slurry polishing 111
6.4.2 Plasma pretreatment and dry polishing using grinding stone 115
6.5 Application of prototype PAP machine 122
6.5.1 Optimization of plasma generation conditions 122
6.5.2 Deterioration of grinding stone during polishing 128
6.5.3 Effect of dressing in PAP 133
6.6 Summary 135
References 136

Chapter 7 Plasma-based-figuring and finishing of CVD-SiC **139**
7.1 Introduction 139
7.2 CVD-SiC used in the study 139
7.3 Lapping and CMP of CVD-SiC 141
7.4 AP-plasma-based figuring and finishing of CVD-SiC 143
7.4.1 Concept 143
7.4.2 PCVM of CVD-SiC 144
7.4.3 PAP of CVD-SiC 148
7.5 Summary 150
References 151

Chapter 8 Summary **153**

Acknowledgements **161**

Chapter 1

Background

1.1 Introduction

Advances in human society are always accelerated by the development and applications of new materials and new manufacturing techniques. This principle can be clearly understood by considering the history of humans from the Stone Age to the Bronze Age and Iron Age. This trend also exists in current society with the rapid upgrading of products, especially those based on semiconductors and optics. To improve the performance of semiconductor devices and optical components, research to develop better semiconductor and optical materials and better manufacturing techniques has been widely conducted.

For semiconductor devices, high voltage and current duration, high working frequency, low energy loss and so forth have been strongly required in various fields. Taking these requirements into consideration, the conventional semiconductor material, silicon (Si), has reached its limits. Therefore, semiconductor materials with wide bandgaps, high hardness, strong chemical inertness and high thermal conductivity are required, making wide-gap semiconductor materials, such as silicon carbide (SiC), gallium nitride (GaN) and diamond, the best choices. Therefore, research on the properties and device applications of these next-generation wide-gap semiconductor materials has been widely conducted by industry and academia [1-5].

For optical components, the mold material is even more important than the component material. This is because the quality of optical components, such as the shape accuracy, surface roughness and so forth, is greatly affected by the mold integrity. To obtain optical components with high quality, mold materials with high hardness, strong chemical inertness, high thermal conductivity and a high coefficient of thermal expansion are strongly required, making chemical vapor deposition SiC (CVD-SiC) a very good choice [6-8].

Although the excellent properties of wide-gap semiconductor materials and CVD-SiC have been theoretically proved, there still are several challenges before we can realize their excellent performance in actual products. The first challenge is how to machine these materials from their natural state such as an ingot or block into applicable substrates or components; these materials are well known to be difficult to machine owing to their high hardness and chemical inertness even if hard machine tools are used. The second challenge is that even if these materials can be machined, it is difficult to obtain perfect surfaces with low surface roughness without scratches

or subsurface damage. In particular, in the case of single crystals, the surface atomic structure (step-terrace structure) is important since step-flow epi-growth is usually necessary for electronic device use [9, 10]. The third challenge is to minimize the cost of obtaining these materials with perfect surfaces. The polishing efficiency, the consumable items used in polishing and the posttreatment after polishing should all be taken into consideration.

Many polishing techniques to realize the highly efficient and high-quality polishing of these difficult-to-machine materials have already been proposed, among which chemical mechanical polishing (CMP) is applied in industry [11].

1.2 Difficult-to-machine materials

Two types of difficult-to-machine material are investigated in this study: wide-gap semiconductor materials for power devices and CVD-SiC for optical applications. Usually, semiconductor materials with a bandgap exceeding twice that of Si can be called wide-gap semiconductor materials, which include SiC, GaN and diamond. Table 1.1 shows the electrical and mechanical properties of Si, SiC, GaN and diamond [1, 12, 13]. As we can see from this table, these materials have many excellent properties compared with Si.

Table 1.1 Properties of some semiconductor materials [1, 12, 13]

	Si	4H-SiC	GaN	Diamond
Bandgap (eV)	1.1	3.26	3.39	5.45
Transition type	Indirect	Indirect	Direct	Indirect
Electron mobility (cm^2/Vs)	1350	1000	900	1900
Breakdown field (MV/cm)	0.3	2.0	3.3	5.6
Saturation velocity (cm/s)	1×10^7	2.0×10^7	2.5×10^7	2.7×10^7
Thermal conductivity (W/cmK)	1.5	4.5	1.3	20
Hv (GPa)	14-16	24-28	18-20	70-110
Young's modulus (GPa)	190	441-500	250-330	1050, 1164
Density (10^3 kg/m^3)	2.3	3.2	6.1	3.5
Melting point (℃)	1420	2830±40	>2500	4373 (125 kbar)

1.2.1 4H-SiC

Single crystal SiC has more than 100 polytypes, among which 4H-SiC is the most widely used in electronic devices. Compared with Si, single-crystal 4H-SiC has about three times the bandgap energy, eight times the breakdown electric field, three times the thermal conductivity and only a slightly lower bulk electron mobility. Therefore, SiC is considered a promising next-generation semiconductor power device material for high-power, high-temperature and high-frequency applications [14)].

Since SiC has a wide bandgap, the maximum operation temperature of SiC devices in theory is very high (about 800 ˚C) and much higher than that of Si devices. While most Si-based power devices have a maximum operation temperature of about 200 ˚C, SiC-based metal-oxide-semiconductor field-effect transistors (SiC-MOSFETs) operated at 650 ˚C have been reported recently [15)]. Also, the thermal conductivity of SiC is very high, meaning that the water cooling system for SiC devices can be downsized or even replaced by an air cooling system. This is beneficial for decreasing the cost and miniaturizing devices. Owing to its high breakdown electric field, SiC can be used in high-voltage integrated circuits. SiC-MOSFETs with a breakdown voltage higher than 1.7 kV and SiC diodes with a breakdown voltage higher than 20 kV have been successfully developed [16, 17)]. Also, SiC-based devices have a relatively low on-resistance and tail current in high-frequency devices, therefore their energy loss is much smaller than that of conventional Si-based devices [18)].

The Acheson process, which was proposed in 1891, was the first bulk growth technique developed for single-crystal SiC [19)]. In this process, a mixture of silica, carbon, sawdust and salt is heated to a maximum temperature of 2700 ˚C in a furnace. Chemical reactions occur in this process and SiC is generated. Even nowadays, this process is still used in the fabrication of SiC abrasives. High-quality single-crystal SiC was first obtained by the Lely method proposed in 1955 [19)]. In this method, SiC lumps formed by the Acheson process are sublimated after heating and recrystallized in a low-temperature area. SiC substrates with 15 mm diameter can be obtained with this method. Nowadays, most SiC substrates are fabricated by the modified Lely method proposed in 1978 [20)]. In the modified Lely method, SiC powder is sublimated in an Ar atmosphere and then recrystallized on the surface of a seed SiC crystal owing to the temperature gradient. This technique was later made commercially available by Cree Research Inc.

Currently, SiC chips are fabricated on 76-mm (3 inch)- and 100-mm (4 inch)-diameter substrates. Compared with Si devices fabricated on 300- to 450-mm-diameter substrates, the cost of manufacturing devices on SiC substrates is high. Recently, the fabrication of 150-mm (6 inch)-diameter SiC substrates has been reported [21)], which is expected to lead to a major decrease in the manufacturing cost of SiC power devices.

Before application in power devices, epitaxial growth on bulk SiC substrates is necessary. The

quality of the epitaxially grown layer is greatly affected by the surface morphology of the bulk substrate [9, 10]. Therefore, a perfect SiC surface is necessary. The polishing of SiC is a challenge owing to its high hardness and chemical inertness.

1.2.2 GaN

Single-crystal GaN is also one of the most promising materials for next-generation power device applications. GaN has a wider bandgap and stronger breakdown electric field than SiC and Si. Therefore, GaN is very suitable for high-voltage applications. In 2014, GaN high-electron-mobility transistors (HEMTs) and GaN diodes with a breakdown voltage higher than 600 V were successfully developed for power converter applications [22]. Also, the saturation electron velocity of GaN is much higher than that of Si; thus, it is expected to be used in high-frequency power devices. A GaN-based HEMT operating working with a high frequency of 5.8 GHz has been reported [23]. As shown in Table 1.1, GaN has a direct and wide transition bandgap, therefore it has been widely used in blue light-emitting diodes (LEDs) with a high-efficiency energy transfer [4].

The development history of GaN is not as long as that of SiC. In 1969, a GaN epitaxial layer grown on a sapphire substrate using the technique of hydride vapor phase epitaxy (HVPE) was first reported [24]. After that, GaN LEDs were successfully fabricated and many other epitaxial growth techniques for GaN were developed such as metal-organic chemical vapor deposition (MOCVD) [25], molecular beam epitaxy (MBE) [26], liquid phase epitaxy (LPE) [27] and so forth. However, the direct epitaxial growth of GaN on foreign substrates always resulted in rough and fractured surfaces that were not suitable for device applications [28]. GaN films with smooth surfaces were first obtained in 1986 by the deposition of an AlN intermediate buffer layer [29]. Then, doping techniques to obtain n-type and p-type GaN films were developed and bright blue LEDs with superior performance went into mass production. Recently, the epitaxial growth of GaN on large Si substrates to reduce the defect density and residual stress and decrease the chipping cost has also been reported [30].

Owing to the very limited availability and relatively high cost of sufficiently large GaN single crystals for use as substrates for homoepitaxial growth, the development of GaN-based devices mainly relies on heteroepitaxy, namely crystal growth on a different substrate material. Recently, free-standing 2 inch GaN substrates grown by HVPE have been successfully obtained and considerable efforts has been made to decrease their cost [31].

Similarly to SiC, the polishing of GaN is also difficult. In addition to its high hardness and chemical inertness, the large number of dislocation sites in GaN, where stress exists, also make it difficult to obtain a pit-free surface [32].

1.2.3 CVD-SiC

Materials with high hardness, a light weight and high thermal conductivity are very suitable as bulk materials for space telescope mirrors and mold materials for optical components. For mirror and mold applications, the surface quality is important. Scratches, surface roughness and figure accuracy affect the performance of mirrors and molds, and subsurface damage (SSD) affects the durability of these components.

Table 1.2 shows the mechanical properties of tungsten carbide (WC), reaction-sintered SiC (RS-SiC) and CVD-SiC [33-38]. Compared with WC and RS-SiC, CVD-SiC has a higher hardness, meaning that CVD-SiC has a strong resistance to wear due to abrasion and making it difficult to form scratches and SSD in the abrasive polishing of CVD-SiC. Also, CVD-SiC has high durability against high-temperature oxidation, thus long-life applications can be expected. CVD-SiC has high thermal conductivity and a low thermal expansion coefficient, therefore the likelihood of shape failures caused by nonuniformity of the temperature distribution in the molding process is very small.

Although amorphous CVD-SiC was once reported [39], currently most commercially available CVD-SiC substrates are polycrystalline and grown on foreign substrates such as RS-SiC and graphite. The drawback of CVD-SiC is its poor machinability. Unlike single crystals, the polishing of CVD-SiC is greatly affected by grain boundaries and crystal orientation dependences, make it difficult to obtain an ultrasmooth surface with sub-nanometer roughness by polishing using conventional techniques.

Table 1.2 Properties of typical materials for molding [33-38]

	WC	RS-SiC	CVD-SiC
Hv (GPa)	17-21	24-28	25-35
Durability against high-temperature oxidation	Slightly inferior	Slightly inferior	Good
CTE (10^{-6}/k)	5	3.9	4.0
Thermal conductivity (W/m・K)	70	130	300
Young's modulus (GPa)	190	350	466
Density (10^3 kg/m^3)	14.5	3.05	3.21
Melting point (℃)	2785	1410 (Si)	2830 (35 atm)
Machinability	Comparatively good	Slightly inferior	Inferior

1.3 Motivation of this study

As described in the background, there are several challenges in the polishing of difficult-to-machine materials to realize their excellent properties in actual products. The motivation of this study is to develop a novel polishing technique to resolve the problems of current polishing techniques for these difficult-to-machine materials.

In this study, a novel polishing technique named plasma-assisted polishing (PAP) is proposed and developed. The surface modification of difficult-to-machine materials by atmospheric-pressure plasma (AP-plasma) irradiation and the removal of the modified layer by soft abrasive polishing are effectively combined in PAP.

There are three aims of this study.

1. To propose PAP and demonstrate its applicability by performing fundamental experiments.
2. To develop a prototype PAP machine for polishing large substrates.
3. To investigate the applicability of PAP to other difficult-to-machine materials.

1.4 Thesis organization

This thesis consists of eight chapters.

In this chapter (Chapter 1), the background to this study, the properties and applications of the difficult-to-machine materials that will be polished in this study and the aims of this study are described.

In Chapter 2, PAP is proposed. The current polishing techniques for difficult-to-machine materials are introduced as well as the properties of AP-plasma and its application in plasma chemical vaporization machining (PCVM). PAP is proposed as a means of resolving the problems of conventional polishing techniques.

Chapter 3 presents the development of a PAP machine from preliminary experiments on localized polishing to the fabrication of a prototype for polishing large substrates.

In Chapter 4, PAP is applied to 4H-SiC substrates. The surface modification of SiC (0001) by AP-plasma is experimentally confirmed. The application results for a symmetric PAP machine, two-step PAP and the prototype PAP machine are introduced. Polishing of the C-face of SiC is also investigated. To realize the highly efficient polishing of SiC, electro-chemical mechanical polishing (ECMP) using CeO_2 slurry is also conducted.

The probable mechanism for controlling the surface atomic structure of 4H-SiC (0001) is proposed in Chapter 5. This mechanism is based on the balance between chemical factors and mechanical factors in the polishing process. Experiments that support the proposed mechanism are also conducted.

In Chapter 6, PAP is applied to single-crystal GaN to obtain an atomic-scale flat and pit-free surface. The surface modification of GaN by AP-plasma is confirmed. Two-step PAP and the prototype PAP machine are applied. The mechanism for the pit-free polishing of GaN is also discussed in this chapter.

In Chapter 7, AP-plasma is used for the figuring and finishing of CVD-SiC. PCVM for highly efficient and damage-free figuring and PAP for damage-free and slurryless finishing are combined.

In Chapter 8, the thesis is summarized.

References

1) H. Okumura, Jpn. J. Appl. Phys. 45 (2006) 7565-7586.
2) S. J. Pearton, C. R. Abernathy, D. P. Norton, A. F. Hebard, Y. D. Park, L. A. Boatner and J. D. Budai, Mater. Sci. Eng. R 40 (2003) 137-168.
3) T. Funaki, J. C. Balda, J. Junghans, A. S. Kashyap, H. A. Mantooth, F. Barlow, T. Kimoto and T. Hikihara, IEEE Trans. Power Elect. 22 (2007) 1321-1329.
4) P. Schlotter, J. Baur, Ch. Hielscher, M. Kuner, H. Obloh, R. Schmidt and J. Schneider, Mater. Sci. Eng. B 59 (1999) 390-394.
5) H. Umezawa, M. Nagase, Y. Kato and S. Shikata, Diamond Relat. Mater. 24 (2012) 201-205.
6) C. Hall, M. Tricard, H. Murakoski, Y. Yamamoto, K. Kuriyama and H. Yoko, Proc. SPIE 5868 (2005) 58680V-1-10.
7) N. Ebizuka, Y. Dai, H. Eto, W. Lin, T. Ebisuzaki, H. Omori, T. Handa, H. Takami and Y. Takahashi, Proc. SPIE 4842 (2003) 329-334.
8) J. Casstevens, A. Rashed, R. Plummer, D. Bray, R. Gates, E. Curzio, M. Ferber and T. Kirkland, Proc. SPIE 4451 (2001) 458-467.
9) J. Powell, P. Neudeck, A. Trunek, G. Beheim, L. Matus, R. Hoffman and L. Keys, Appl. Phys. Lett. 77 (2000) 1449-1451.
10) H. Matsunami and T. Kimoto, Mater. Sci. Eng. R20 (1997) 125-166.
11) H. Aida, T. Doi, H. Takeda, H. Katakura, S. Kim, K. Koyama, T. Yamazaki and M. Uneda, Curr. Appl. Phys. 12 (2012) 541-546.
12) V. Domnich, Y. Aratyn, W. M. Kriven and Y. Gogotsi, Rev. Adv. Mater. Sci. 17 (2008) 33-41.
13) J. Qian, G. Voronin, T. W. Zerda, D. He and Y. Zhao, J. Mater. Res. 17 (2002) 2153-2160.
14) J. B. Casady and R. W. Johnson, Solid-state Elect. 39 (1996) 1409-1422.
15) T. Shinohe, Toshiba Review 59 (2004) 49-53. (In Japanese)
16) S. Liebig, J. Engstler, A. Engler and J. Lutz, International Conference on Power Electronics PCIM, 2012.
17) H. Niwa, J. Suda and T. Kimoto, Appl. Phys. Epress 5 (2012) 064001-1-3.

18) P. Friedrichs, T. Kimoto, L. Ley and G. Pensl, (Wiley, New York, 2009) 311-314.
19) Y. M. Tairov and V. F. Tsvetkov, J. Cryst. Grow. 52 (1981) 146-150.
20) G. Ziegler, P. Lanig, D. Theis and C. Weyrich, IEEE Trans. Elect. Devices 30 (1983) 277-281.
21) M. Ogawa, K. Mine, S. Fuchiyama, Y. Tawa and T. Kato, Mater. Sci. Forum 778-780 (2014) 776-779.
22) R. Mitova, R. Ghosh, U. Mhaskar, D. Klikic, M. Wang and A. Dentella, IEEE Trans. Power Electron. 29 (2014) 2441-2452.
23) H. Hasegawa, S. Yoshida, S. Furuta, Y. Moriguchi and S. Kawasaki, Proc. 2014 IEEE wireless power transfer conference (2014) 21-23.
24) H. P. Maruska and J. J. Tiethen, Appl. Phys. Lett. 15 (1969) 327-329.
25) H. M. Manasevit, F. M. Erdmann and W. I. Simpson, J. Electrochem. Soc. 118 (1971) 1864−1868.
26) E. J. Tarsa, B. Heying, X. H. Wu, P. Fini, S. P. DenBaars and J. S. Speck, J. Appl. Phys. 82 (1997) 5472-5479.
27) F. Kawamura, T. Iwahashi, K. Omae, M. Morishita, M. Yoshimura, Y. Mori and T. Sasaki, Jpn. J. Appl. Phys. 42 (2003) L4-L6.
28) F. A. Ponce and D. P. Bour, Nature 386 (1997) 351-359.
29) H. Amano, N. Sawaki, I. Akasaki and Y. Toyoda, Appl. Phys. Lett. 48 (1986) 353-355.
30) D. Zhu, D. J. Wallis and C. J. Humphreys, Rep. Prog. Phys. 76 (2013) 106501.
31) H. J. Lee, K. Fujii, T. Goto, C. Kim, J. Chang, S. K. Hong, M. Cho and T. Yao, Proc. SPIE 7602 (2010) 760202.
32) H. Gong, G. Pan, Y. Zhou, X. Shi, C. Zou and S. Zhang, Appl. Surf. Sci. 338 (2015) 85-91.
33) K. Tsuno, H. Irikado, K. Oono, S. Suyama and Y. Itoh, Proc. 6th Internat. Conf. on Space Optics (2006) 47.
34) S. P. Simner, P. Xiao and B. Derby, J. Mater. Sci. 33 (1998) 5557-5568.
35) V. Rehn and W. J. Choyke, Nucl. Instr. Meth. 177 (1980) 173-178.
36) A. Khounsary, P. Fernandez, L. Assoufid, D. Mills, D. Walters, J. Schwartz and J. Robichaud, Rev. Sci. Instrum. 73 (2002) 1537-1540.
37) J. Li, S. Sugimoto, S. Tanaka, M. Esashi and R. Watanabe, J. Am. Ceram. Soc. 85 (2002) 261-263.
38) H. Kim, I. Shon, I. Ko, J. Yoon, J. Doh and G. Lee, J. Ceram. Proce. Res. 7 (2006) 224-229.
39) L. Tong, M. Mehregany and W. C. Tang, Proc. Micro electro mechanical systems (1993) 242-247.

Chapter 2

Proposal of Plasma-assisted Polishing

2.1 Introduction

As described in Chapter 1, there are three challenges in polishing difficult-to-machine materials: their poor machinability owing to their high hardness and chemical inertness, the difficulty of generating a perfect surface and the high polishing cost. Concerning the machinability, there are two solutions: the use of hard abrasives such as diamond for polishing or modifying the surface to realize soft abrasive polishing. In the case of hard abrasive polishing using diamond, the problem is the formation of scratches and subsurface damage (SSD) and the increase in surface roughness [1, 2]. With the decrease in the size of the diamond abrasives, the surface roughness can be improved and the thickness of the SSD can be decreased, but a damage-free surface with a uniform atomic structure on the surface is difficult to generate owing to the high hardness of diamond. In particular, etching has been considered as a damage-free process, which has been widely used in semiconductor processes. However, the flattening ability of etching is poor since etching is an isotropic process. Thus, the second solution, the combination of surface modification and soft abrasive polishing, appears to be more promising.

In most current polishing techniques for difficult-to-machine materials such as chemical mechanical polishing (CMP) [3, 4], mechanical chemical polishing (MCP) [5], catalyst-referred etching (CARE) [6, 7], UV-assisted polishing [8, 9], electrochemical mechanical polishing (ECMP) [10] and so forth, chemical reactions to induce surface modification and polishing using a soft abrasive are combined. The poor machinability of difficult-to-machine materials can be resolved by surface modification. Optimization of the polishing conditions to obtain perfect surfaces with a relatively low polishing cost and high efficiency has been widely conducted in recent years.

Table 2.1 shows the Vickers hardnesses of some hard-to-machine materials and some abrasive materials. To realize damage-free polishing, the abrasive material should be selected with consideration of the hardnesses of the specimen, the modified layer and the abrasive material. A soft abrasive should be used to polish the modified (softened) layer; however, if the abrasive material is much softer than the modified layer, the material removal rate (MRR) will be very low. Not only the polishing efficiency but also the polishing cost should be taken into consideration. That is to say, the abrasive material used in polishing must be optimized with consideration of the surface quality, efficiency and polishing cost.

Table 2.1 Vickers hardnesses of difficult-to-machine materials and abrasive materials [11-18]

Materials	Vickers Hardness (GPa)	Reference
Diamond	70~110	11
Cubic boron nitride (cBN)	45~50	12
Silicon carbide (SiC)	24~28	11
Gallium nitride (GaN)	18~20	13
Sapphire (Al_2O_3)	12-23	14
Tungsten carbide (WC)	17~21	14
Silicon (Si)	13-16	15
Quartz crystal (SiO_2)	10~12	16
Silica (SiO_2)	7.6	17
Ceria (CeO_2)	5~7.5	18

2.2 Current polishing techniques

2.2.1 Chemical mechanical polishing

CMP has a long history and has been widely used in the fields of optics and semiconductor devices for finishing optical components and Si substrates and chips [19, 20]. Figure 2.1 shows a schematic image of a typical CMP machine for wafer polishing. It can be roughly divided into four parts: a rotary table with a covered polishing pad (a nonwoven type or a suede type), a rotary polishing head (wafer holder), a slurry supplier and a conditioner. For the polishing of a curved surface, localized CMP is usually conducted using a small polishing pad.

In the CMP of SiC, an alkaline colloidal silica slurry has been widely used [3, 4, 21-23]. The probable mechanism is that the SiC surface is first modified (oxidation, hydroxylation and so forth) by the chemicals in the slurry. Then the modified layer is removed by abrasion with a silica abrasive. According to Table 2.1, silica is very soft compared with SiC; thus, no scratches are formed and an atomically flat surface with a root mean square (rms) roughness of less than 0.2 nm has been obtained [22]. However, owing to the chemical inertness of SiC, the surface modification rate of SiC by slurry is very low, resulting in extremely low MRRs for SiC [21].

To increase the MRR of CMP, the efforts of different chemicals and abrasives in the slurry have been investigated. To increase the surface modification rate of SiC in CMP, the addition of potassium manganite ($KMnO_4$), potassium nitrate (KNO_3) and hydrogen peroxide (H_2O_2) to the

slurry has been investigated [24, 25]. It has been demonstrated that the CMP of SiC with added $KMnO_4$ or H_2O_2 is very effective for obtaining high MRRs. On the other hand, a mixed abrasive slurry (MAS) consisting of colloidal silica and nano-diamond has also been developed [26]. The diamond abrasive forms mechanical stress at the surface of SiC and increases the surface modification rate, resulting in an increase in the MRR from 0.06 μm/h to 0.55 μm/h. With the development of the slurry, ultrahigh efficiency CMP with a MRR of 5.8 μm/h has also been realized [27].

Although CMP is the most widely used polishing technique for SiC, it still has several problems. The MRR of CMP for SiC is very low, making the process time-consuming and increasing the polishing cost. Although the MRR of CMP varies with the polishing conditions; usually it is lower than 1.0 μm/h. CMP is used as the final finishing process for SiC. However, even when a scratch-free and ultrasmooth SiC surface was obtained by CMP, residual SSD was still found, which means that the SSD formed by the preprocess was not completely removed [28]. The rms roughness of a SiC surface has been improved to less than 0.2 nm, but the step-terrace structure on the polished surface was not uniform, which would affect the following epitaxial growth process [22]. Also, the use, management and post-treatment of the slurry increase the polishing cost of CMP.

In the case of CMP for GaN, the above problems also occur. The MRR of CMP for GaN is usually lower than 80 nm/h, which is even lower than that for SiC [22]. Moreover, another major challenge of CMP for GaN is the formation of etch pits after polishing [29]. Currently, self-standing GaN substrates are much more expensive than those of SiC and not easily obtainable. Thus, GaN films prepared on a sapphire substrate using MOCVD are widely used. Table 2.2 shows the properties of GaN and sapphire. Many dislocations are formed in the GaN epilayers owing to the large mismatch of the lattice constant and thermal expansion coefficient between GaN and sapphire [30]. It was reported that preferential etching and the removal of these dislocations sites occur in CMP. Therefore,

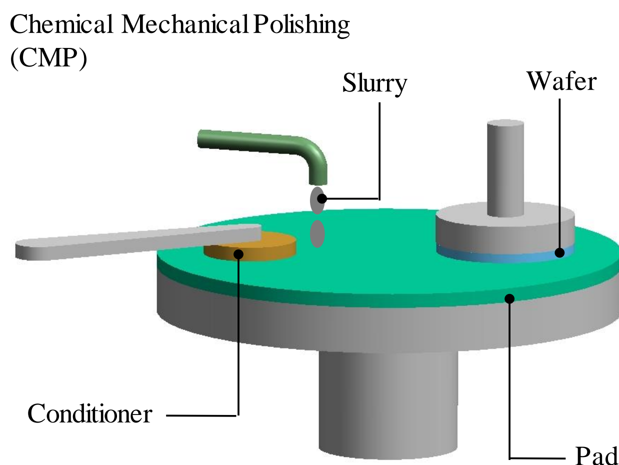

Figure 2.1 Schematic image of conventional CMP for wafer polishing.

Table 2.2 Lattice constant and thermal expansion coefficient of GaN and sapphire [30)]

	Lattice constant (Å)	Thermal expansion coefficient ($\times 10^{-6}$/K)
GaN	a=3.189, c=5.182	5.59 (a), 3.17 (c)
Sapphire	a=4.763, c=13.003	7.5 (a), 8.5 (c)

when a GaN epilayer is processed by CMP using silica slurry, many etch pits originating from the dislocation sites are formed [29)].

2.2.2 Mechanochemical polishing

MCP was proposed by Yasunaga *et al.* for polishing sapphire using steel in a dry ambient [31)]. In MCP, soft abrasives with high affinity to the specimen are used. As shown in Figure 2.2, the abrasives react with the specimen around the contact points, which have a high temperature and a high pressure. The reaction products are adapted to the abrasives and are removed, resulting in the polishing of the specimen.

Kikuchi *et al.* proposed a method of catalytic MCP to polish single-crystal SiC [5)]. A chromium oxide (Cr_2O_3) abrasive was used in their experiments. Cr_2O_3 played two roles in this polishing process. First, it acted as a catalyst to promote the reaction between SiC and oxygen from the ambient. Thus, SiC was oxidized. Second, it acted as an abrasive to remove the oxide layer by abrasion. As a result, a damage-free and scratch-free surface was obtained.

On the basis of the same mechanism, tribo-catalytic-abrasive grinding was proposed by Kido *et al.* for the highly efficient machining of single-crystal SiC [32)]. A specially made grinder using a CeO_2 abrasive was used in their study. Even though a grinding process was performed, a flat surface with a Ra roughness of 0.4 nm was obtained.

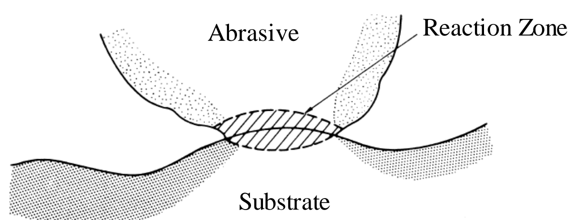

Figure 2.2 Schematic image of MCP [31)].

2.2.3 Catalyst-referred etching

CARE is an abrasive-free etching process, which was proposed by Hara *et al.* [6, 7)]. This technique uses a Pt polishing plate as a catalyst to activate hydrofluoric (HF) acid to react with a substrate, enabling the removal of SiC. In CARE, chemical etching occurs only near the surface of the catalyst plate. The plate has a planar surface that is used as a reference during substrate flattening. The plate plays a similar role to the polishing pad used in CMP. The protrusions of the

substrate are preferentially etched since they first come in contact with the plate. With the removal of the protrusions, an atomically flat surface is finally obtained. Since CARE is an etching process, less damaged surfaces can be obtained compared with conventional abrasive processes such as grinding, lapping and polishing.

CARE has been successfully applied to single-crystal SiC and GaN [6, 7, 33)]. Atomically flat SiC and GaN surfaces with uniform step-terrace structures were obtained. The flattening mechanism of CARE has been widely studied by first-principles calculation. In recent years, HF acid in CARE has been replaced by deionized (DI) water, making this flattening process more practically applicable [34)].

Water-CARE has been conducted on some oxide materials such as sapphire and glass. The surface roughnesses were decreased to 0.2 nm and 0.1 nm, respectively, which indicated the great flattening ability of CARE [35)]. It is noteworthy that the MRR of water-CARE for lanthanum oxide glass is very high (about 84 μm/h), even higher than that of conventional slurry polishing processes [35)]. Recently, studies on the replacement of the catalyst plate with inexpensive metals have also been conducted to reduce the cost of CARE [36)].

2.2.4 UV-assisted polishing

Hong *et al*. proposed photochemical polishing assisted by UV irradiation [8, 9)]. In their study, SiC was polished with a Cr_2O_3 abrasive under the irradiation of UV light. The irradiation of UV light enhanced the oxidation of the SiC surface. The hardness of Cr_2O_3 is similar to that of SiO_2; thus, subsurface damage is minimal in this process. In a later study, Watanabe *et al*. utilized TiO_2 and CeO_2 as abrasive materials. The use of a CeO_2 abrasive greatly improved the removal rate and roughness.

In addition to SiC, this process is highly advantageous for polishing single-crystal diamond [31)]. This polishing process can be considered as an MCP process combined with UV-induced photochemical reactions. A quartz plate has been used as the polishing medium. After UV irradiation, the diamond substrate is activated by a change in the surface termination. The temperature increases in the contact area between the diamond and the quartz plate. Surface carbon atoms are oxidized by active species such as hydroxyl radicals (OH radicals) and oxygen radicals and then removed as CO and CO_2 [31)].

This polishing technique has been successfully applied to single-crystal diamond substrates, chemical vapor deposition (CVD) diamond-coated films and polycrystalline diamond (PCD). A quartz plate is much softer than diamond; thus, it is considered that almost no SSD is formed in this process. With the application of UV-assisted polishing, flat diamond surfaces with Ra roughness of less than 0.2 nm were obtained [37, 38)].

2.2.5 Electro-chemical mechanical polishing

Electro-chemical Mechanical Polishing (ECMP), which combines surface anodic oxidation and slurry polishing, has been proposed for the highly efficient polishing of copper, glassy carbon and so forth. The application of ECMP to single-crystal SiC was first performed by Li *et al.* [10]. A two-step ECMP process has been proposed. In this study, SiC was first oxidized by a mixture of H_2O_2 and KNO_3 electrolytes, then the oxide layer was removed by polishing using colloidal silica slurry. After several cycles of anodic oxidation and slurry polishing, a smooth surface was obtained. Simultaneous ECMP using a colloidal silica slurry was also investigated in their work. However, after polishing for 3 h, many scratches could still be observed on the polished surface.

In Ballarin's work, electrochemical etching using HF acid was proposed for the surface polishing of polycrystalline SiC [39]. This etching process is very effective. However, it is difficult to obtain an ultrasmooth surface since etching is an isotropic process.

2.3 Proposal of plasma-assisted polishing

2.3.1 Introduction

Although the polishing of difficult-to-machine materials can be realized by the above-introduced polishing techniques, there are still some problems, such as the high polishing cost, low polishing efficiency, low surface quality and so forth. In the case of CMP, which is the most widely used polishing technique in industry, it has been reported that the use, management and post-treatment of slurry account for about 50% of the total cost of CMP [40]. Therefore, a slurryless dry polishing technique can potentially greatly reduce the cost of CMP. On the other hand, in polishing techniques combining surface modification and abrasive polishing, the polishing efficiency is limited by the surface modification rate because the reactions (modification) should first occur on the surface of the substrate to form a soft modified layer, otherwise the substrate will hardly be polished (removal). Therefore, a highly efficient surface modification method is required.

This means that it is necessary to efficiently modify the surfaces of difficult-to-machine materials in a dry ambient, without a slurry, making AP-plasma, which has many reactive species and can be generated in a dry ambient, a very promising method.

2.3.2 Plasma chemical vaporization machining

Machining using AP-plasma has been studied by research groups in Osaka University for more than 25 years [41]. A non-contact machining technique named plasma chemical vaporization machining (PCVM) was developed for the ultraprecision and damage-free polishing, thickness correction and figuring of silicon, fused silica, quartz crystal, silicon carbide and diamond [41]. The

mechanism of PCVM is based on chemical reactions (etching) of the substrate induced by AP-plasma irradiation. Since it is a non-contact machining technique, it is possible to maintain the original physical and mechanical properties of the specimen. A similar machining process has already been utilized in plasma etching in LSI manufacturing [42]. However, the removal rate was very low since it was carried out under a low-pressure atmosphere. There was no spatial resolution of the machining because the plasma area expanded under the low-pressure atmosphere. In PCVM, localized AP-plasma is generated only around the electrode and the radical density is very high because of the high-pressure atmosphere. Therefore, numerically controlled (NC) machining with a high spatial resolution is possible, giving PCVM great potential to replace conventional mechanical machining methods.

Figure 2.3 shows a schematic diagram of an NC-PCVM system using an electrode with a small diameter for local etching [43]. A plasma-generating unit is constructed from a coaxially arranged electrode and a dielectric cover to supply the process gas to the vicinity of the electrode. The diameter of the electrode, which is made of aluminum alloy, is changeable depending on the requirements; usually a diameter of 3 mm is used. The composition and flow rate of the process gas are controlled using mass flow controllers (MFCs). A stable plasma is generated in the narrow gap between the electrode and the substrate by applying a high-frequency electric field (f=13.56 MHz, radio frequency). The gap distance can also be varied from sub-mm to mm order. The area reaching with the plasma is localized in the vicinity of the electrode because the mean free path of electrons in the AP-plasma is very small under atmospheric pressure. The relative position and speed between the electrode and the workpiece are controlled using an XY table and an electrode driven by AC servo motors. For the thickness correction of a quartz crystal wafer using PCVM, the initial thickness distribution over the entire wafer is measured. The "removal volume

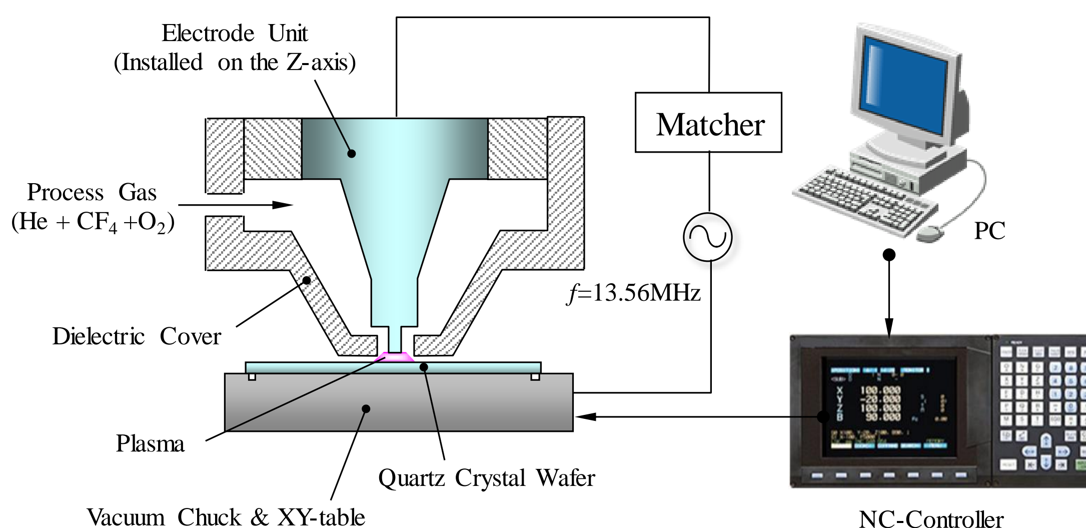

Figure 2.3 Schematic diagram of the NC-PCVM system [43].

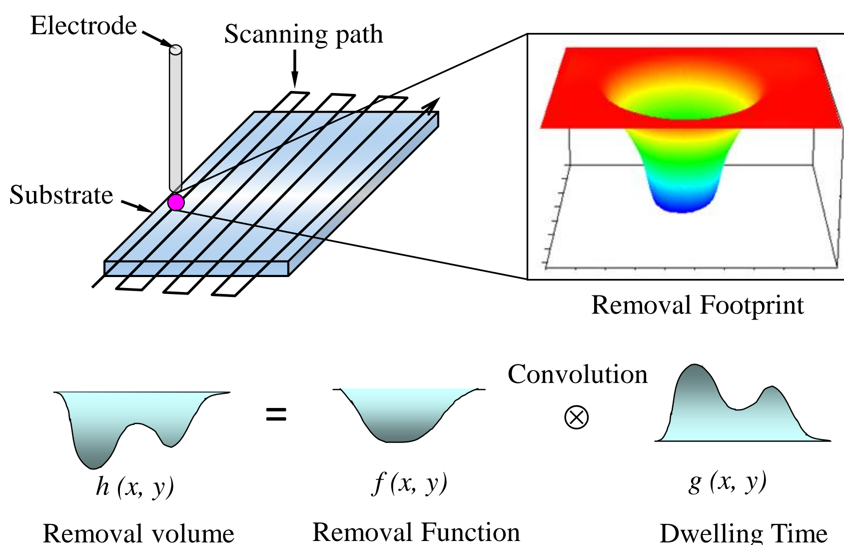

Figure 2.4 Correcting procedures of thickness variation by controlling the scanning speed of the localized plasma [43].

distribution" on the wafer, which represents the volume distribution to be removed, is calculated by subtracting the objective thickness from the measured thickness distribution. On the other hand, the volumetric distribution of the footprint formed in the removal area under the electrode in a unit removal time is expressed by the "removal function", as shown in Figure 2.4 [43]. It has been confirmed that the depth of the footprint increases with the removal time. Therefore, the local removal volume at a certain position can be controlled by controlling the dwelling time of the electrode during scanning. The removal volume distribution on the wafer is determined by the convolution of the removal function and the dwelling time distribution of the electrode. NC scanning is performed by raster scanning then a wafer of uniform thickness is obtained deterministically.

In addition to the thickness correction of quartz crystal wafers [43], PCVM has been successfully applied for the fabrication of focusing elliptical mirrors, the thinning of 6 inch silicon-on-insulator (SOI) substrate [44, 45] and the fabrication of substrates for doubly curved crystal (DCC) spectrometers [46, 47].

2.3.3 Generation of atmospheric-pressure plasma

Although it has been demonstrated that PCVM has major advantages for the high-precision figuring of Si-based materials, the flattening ability of PCVM at the atomic level is lower than that of mechanical processes such as grinding and polishing because PCVM is an isotropic etching process. To combine the advantages of the chemical process in AP-plasma and mechanical abrasive polishing, plasma-assisted polishing (PAP), which combines surface modification by AP-plasma irradiation and the removal of the modified layer by soft abrasive polishing, is

proposed. In this polishing technique, AP-plasma is used to soften the surfaces of difficult-to-machine materials, making it possible to polish them using a soft abrasive. Since surface modification by AP-plasma plays a critical role in PAP, it is necessary to understand the basic generation mechanism and properties of AP-plasma.

As the fourth fundamental state of matter in addition to the solid, liquid and gas states, the word "plasma" was introduced into physic by Langmuir to describe a region of gas discharge in which the numbers of electrons and ions are equal [48)]. Plasma can be generated by applying energy to a gas to induce its dissociation, excitation and ionization. This energy can be thermal or carried by either an electric current or electromagnetic radiation [49)]. Generally, plasmas can be divided into two main categories, thermal plasmas (high-temperature fusion type) and non-thermal plasmas (low temperature). In PAP, non-thermal AP-plasmas that are not in absolute thermodynamic equilibrium and are activated by electric fields are applied.

To describe the gas discharge process in an electric field between negative (cathode) and positive (anode) electrodes, Townsend's theory has been widely used [50)]. In a weakly ionized plasma, collisions from electric-field-accelerated electrons are dominant. The production of electrons in the discharge system can be described by two coefficients, Townsend's first ionization coefficient α and the secondary electron emission coefficient γ. The electron-impact ionization (α-process) results in the generation of ions, which are attracted to the cathode, where secondary electrons are generated with a probability of γ. The initial electrons are finally attracted to the anode and completing their impact ionization process. For a sustainable discharge process, the number of electrons attracted to the anode should be equal to that of newly generated electrons. Thus, the Townsend criterion of breakdown is described as:

$$\gamma\ [exp\ (\alpha d)\ -\ 1]\ =\ 1. \tag{2.1}$$

Conditions for breakdown at different gas pressures were first studied by Paschen *et al.* [51)]. The result is the well-known Paschen curve describing the dependence of the breakdown voltage V_B on the distance d between electrodes and the gas pressure p. On the basis of the Townsend criterion, the Paschen equation can be written as follow:

$$V_B = \frac{Bpd}{\ln(pd)+\ln\left\{ A / \ln(1+1/\gamma) \right\}}\ , \tag{2.2}$$

where A and B are constants dependent on the type of gas.

Figure 2.5 shows the Paschen curves of different gases [52)]. There is always an optimal value of the product (pd) at which the breakdown voltage has its minimum value. On both sides of the minimum value, the breakdown voltage increases. The Paschen curve can be explained as follows: in a discharge system in which the electrode distance (d) is constant, an increase in pressure (p)

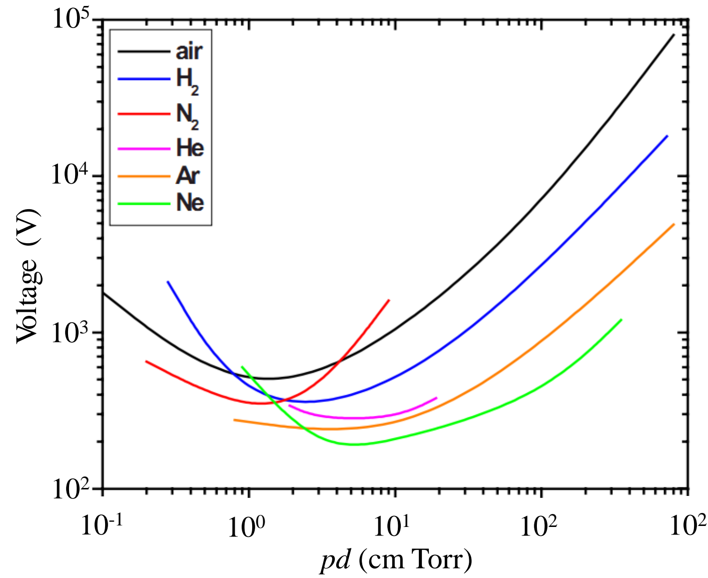

Figure 2.5 Paschen curves of different gases [52].

leads to a small mean free path (λ) and electrons cannot acquire sufficient energy ($eE\lambda$) to ionize. Thus, the applied voltage must be increased to increase the electric field (V/d) and realize a discharge. Also, with a decrease in p, the density of gas particles available for ionization becomes lower, which decreases the collision frequency. Thus, the applied voltage must be increased to increase the ionization probability and realize a discharge [50].

In PAP, the reactive species in AP-plasma are used for the surface modification of difficult-to-machine materials. These species are generated by the collisions in the plasma. Even though the collisions in AP-plasma are complicated, only the collisions from the electric-field-accelerated electrons, which are dominant in a weakly ionized plasma, are considered in this study. During the movement of the accelerated electrons, they collide with the gas atoms/molecules. These collisions result in energy transfer and chemical reactions, which can be generally divided into four groups: elastic collision, excitation, ionization and dissociation.

When an elastic collision occurs between an electron and a gas molecule (atom), very little kinetic energy is transferred to the gas molecule owing to the large mass difference between the electron and the molecule and no chemical reactions occur in this process. When the energy of the electron is higher than the lowest excitation energy of the gas molecule, excitation collisions occur. Neutral atoms/molecules in the ground (lowest) energy state are excited. Once a neutral is excited, it will relax back to its ground state. In this relaxation process, photons with energy (wavelength) equal to the energy gap are emitted. By detecting the energy and intensity of the emitted photons using a multichannel spectrometer, the radicals in plasmas can be identified. This method is called optical emission spectroscopy (OES) and is widely used in PAP study.

Figure 2.6 shows photographs and OES spectra of He and Ar plasmas used in PAP. The color

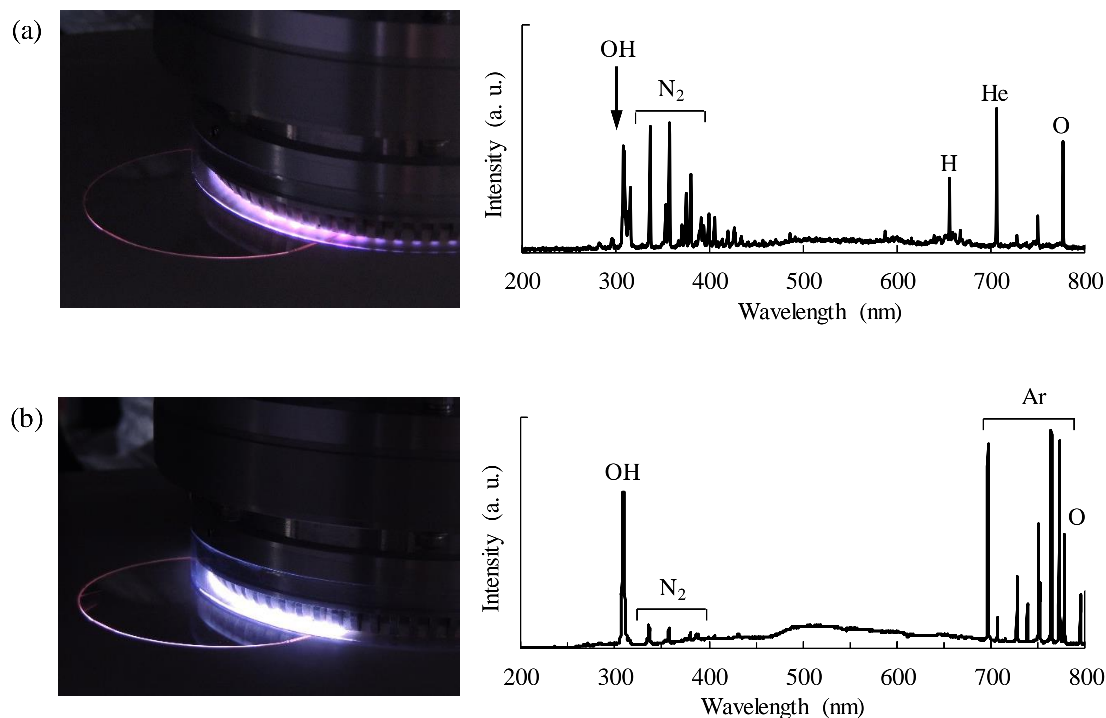

Figure 2.6 Photos and OES spectra of He (a) and Ar (b) plasmas used in PAP.

of the discharge in He is purple while the color of the discharge in Ar is almost white. He has a much lower density than N_2, thus, in a He discharge the inclusion of N_2 from the ambient, which has a very low excitation energy of about 5.23 eV, occurs. Thus, the excitation of N_2 becomes dominant. As shown in the OES spectrum of the He plasma, strong peaks corresponding to the second positive system of N_2 can be observed [53)]. Therefore, the plasma appears purple. In the Ar discharge, the substitution from ambient air to Ar is efficiently conducted because the mass of Ar atoms is very large. Therefore, only very limited emission from N_2 is detected as shown in the OES spectra. Because it is a mixture of photons emitted with different wavelengths, the Ar plasma appears white.

With sufficient kinetic energy, a free electron may cause an electron to detach from an atom or molecule, resulting in the generation of a second free electron and a positive ion. The energy required for this reaction is typically around 10−20 eV and is called the ionization energy. This process is called electron-impact ionization and it is the dominant way that electrons are produced in a non-thermal gas discharge [50)].

If an inelastic collision occurs between an electron and a polyatomic molecule, the molecule will be dissociated if the energy of the electron is higher than the dissociation energy of the molecule. The dissociation process will result in the generation of many radicals (chemical species with an unpaired electron) with strong reaction potentials [54)]. Therefore, usually the

admixing of reactive gases such as O_2, water vapor, SF_6 and CF_4 into the process gas is conducted to increase the reactivity of the plasma and realize chemical reactions. In PAP, admixing is also conducted and OH, O and F radicals are generated owing to the electron impact dissociation of the reactive gases.

To realize a homogeneous glow discharge with a relatively low breakdown voltage, noble gases such as Ar or He are widely used as the carrier gas for AP-plasma generation. There are several reasons why He is widely used: the first reason is its high ionization rate even in a weak electric field [55)]; the second is its high diffusion coefficient [56)]; the third is the expectation of the penning effect (an ionization process resulting from collisions between excited metastable particles and neutral particles with a lower ionization potential than the excitation potential of the metastable particles) [57)]. Although He has the above advantages, its price has gradually increased in recent years owing to an increase in demand, increasing the polishing cost of PAP. Also, since He has a very small mass, the inclusion of N_2 from the ambient inevitably occurs suppressing the generation of reactive radicals. Therefore, Ar is also used as the carrier gas for plasma generation in this study owing to its relatively low price and good substitution effect (large mass). Another advantage of Ar is its low ionization energy. The ionization energy of Ar (15.75 eV) is much lower than that of He (24.58 eV); thus, the electron density in Ar plasma is higher than that in He plasma under the same discharge conditions, resulting in a high radical density. In this study, Ar and He are both used.

2.3.4 Strategies of PAP for difficult-to-machine materials

Owing to the high reactivity of the radicals in AP-plasma, the surface modification of difficult-to-machine materials, which makes them easier to polish, becomes possible. PAP was proposed as a combination of surface modification and soft abrasive polishing [58-62)]. Figure 2.7 shows the

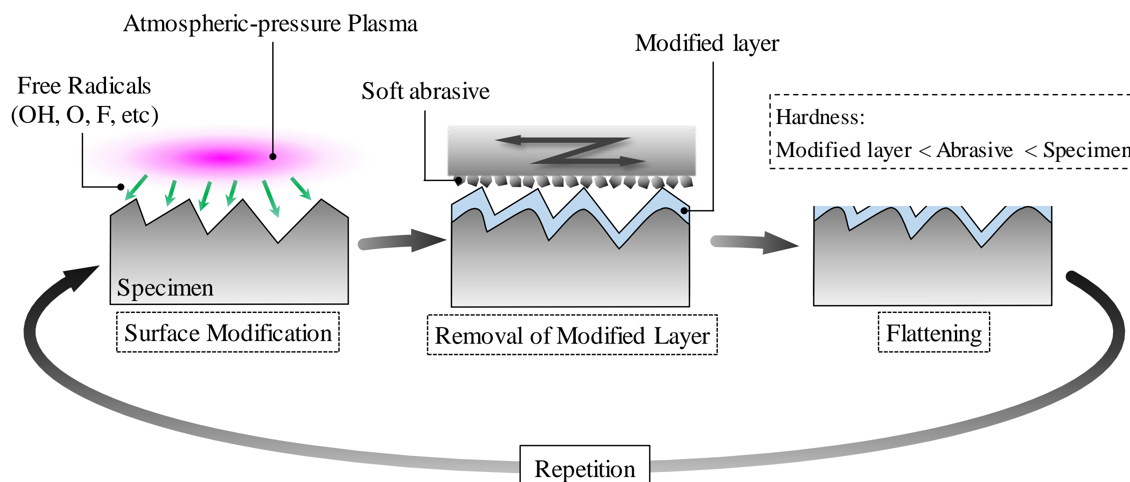

Figure 2.7 Concepts of PAP.

concepts of PAP. The specimen is first irradiated by AP-plasma. The specimen reacts with the radicals and a modified layer is formed. Then, the modified layer, which is usually softer than the specimen, is polished by a soft abrasive and removed. With the repetition of plasma modification and abrasive polishing, the rough specimen surface is gradually flattened. Finally, a damage-free and atomically flat surface is obtained. Compared with conventional polishing techniques such as mechanical polishing and CMP, the following advantages of PAP are expected.

(1) Cost-effectiveness

PAP is a dry polishing process without the use of a slurry, which makes it very cost-effective. In CMP, the use, management and post-treatment of the slurry account for a large percentage of the total cost of the polishing process. As a dry polishing process, the cost of the slurry is avoided. Although a noble gas and grindstones are used in PAP, their cost is expected to be much lower than that of a slurry. Also, in contrast to the low-pressure plasmas used in the semiconductor industry, open-air-type AP-plasmas are used in PAP. Therefore, vacuum systems such as chambers and pumps are not necessary in PAP, also making it a cost-effective polishing process.

(2) Damage-free polishing

For semiconductor materials, surface damage, such as scratches and SSD, greatly affects their electronic properties and the reliability of devices. For die materials, their durability is also greatly affected by SSD. Figure 2.8 shows a comparison of mechanical polishing (MP) and PAP. In MP, scratches and SSD are inevitably formed because a hard abrasive such as diamond is used [63]. In the case of PAP, only the modified layer is removed. The specimen is hardly polished owing to the large difference in hardness between the abrasive and the specimen as shown in Table 2.1. Thus, almost no mechanical damage is formed in PAP. On the other hand, since surface modification is conducted under atmospheric pressure, damaged layers formed by the bombardment of ions in the plasma are not introduced because the

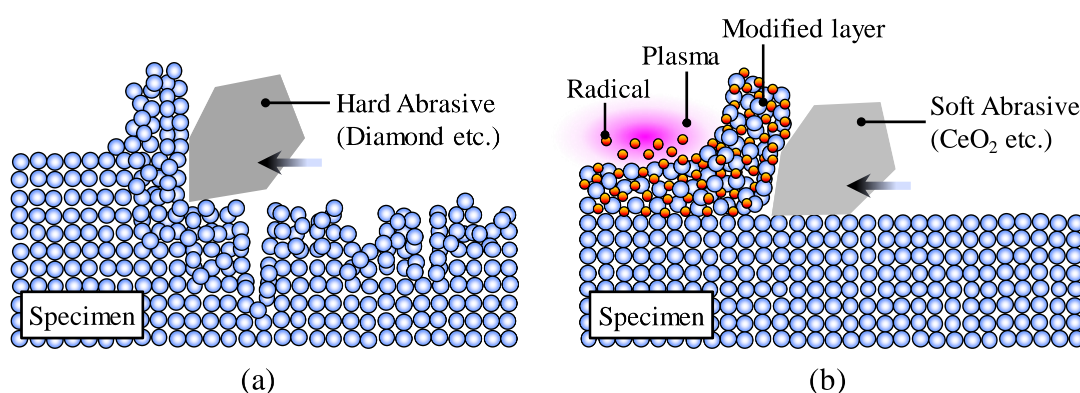

Figure 2.8 Comparison of MP (a) and PAP (b).

kinetic energy of the ions is very low owing to their very small mean free path under atmospheric pressure. Thus, PAP is considered to be a damage-free polishing technique.

(3) High MRR

Most of the current polishing techniques for difficult-to-machine materials are based on a combination of surface modification and abrasive polishing. Since polishing is conducted only after the surface is modified, the MRR of PAP is determined by the surface modification rate. Plasma has a very high surface modification efficiency for difficult-to-machine materials owing to the existence of a large number of reactive radicals. The modification efficiency of AP-plasma can also be increased by optimization of the conditions for AP-plasma generation such as the applied power, the concentration of the reactive gas, the gas and substrate temperature and so forth. Therefore, very high MRRs are expected for PAP.

Figure 2.9 shows the strategies for polishing various difficult-to-machine materials, such as single-crystal SiC, CVD-SiC, GaN, sapphire and diamond, by PAP. For different materials, AP-plasmas with different reactive gases are used for surface modification. Table 2.3 shows the oxidation-reduction potential of different oxidizing species. Fluorine atoms, hydroxyl groups and oxygen atoms have the strongest oxidation-reduction potential. Therefore, it is considered that if the surfaces of the difficult-to-machine materials are exposed to plasma containing CF_4, water vapor or O_2, surface modification will occur. In this study, the modification properties of plasma containing water vapor, O_2 and CF_4 were investigated.

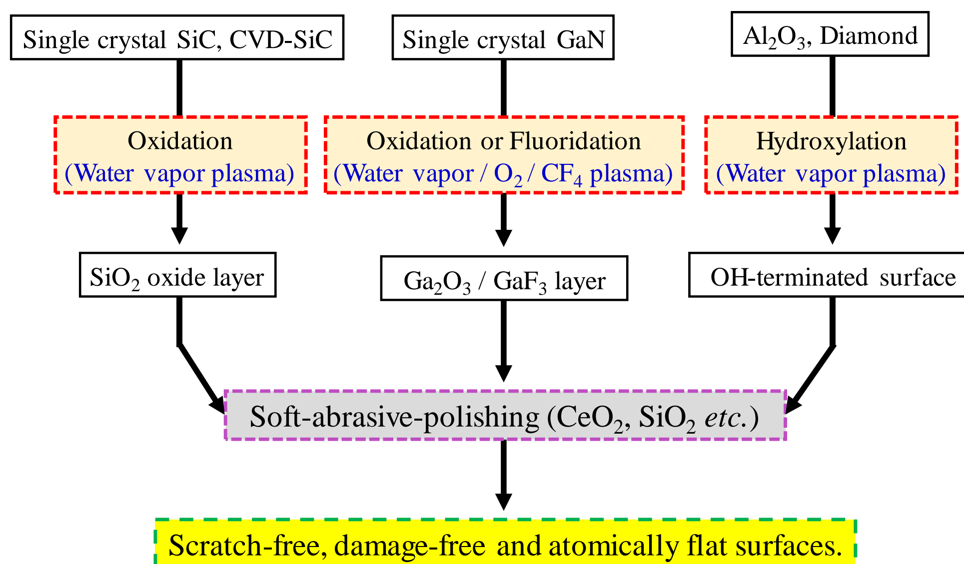

Figure 2.9 Strategies of PAP applied to difficult-to-machine materials.

Table 2.3 Oxidation-reduction potential

Radicals	F	OH	O	O_3	H_2O_2	ClO_2	Cl_2
Oxidation-reduction potential (V)	3.03	2.80	2.42	2.07	1.78	1.49	1.36

(1) Water-vapor-containing plasma

In water-vapor-containing plasma, the generation of OH radicals (in the ground state and excited state) is based on the reactions shown in Table 2.4. For the surface modification of single-crystal SiC, CVD-SiC and GaN, water vapor plasma is used for surface oxidation. It is considered that SiC will be oxidized to SiO_2 while GaN will be oxidized to Ga_2O_3. The oxidized surfaces are considered to be softer than the bulk materials, making it possible to polish the modified surfaces and remove the modified layers by polishing using soft abrasives such as CeO_2, SiO_2 and so forth. The surface oxidation reactions and the changes in the surface hardness resulting from irradiation by water-vapor-containing plasma were experimentally confirmed, which will be described in the following chapters.

Table 2.4 Typical reactions in water vapor contained plasma [63)]

Mechanism	Reaction
Electron impact dissociation of water	$H_2O + e \rightarrow OH\ (X) + H + e$
Direct dissociative electron excitation of water	$H_2O + e \rightarrow OH\ (A) + H + e$
Dissociative recombination of water ion	$H_2O^+\ (H_3O^+) + e \rightarrow OH\ (A) + H$
Dissociative excitation of water with noble gas metastable	$H_2O + M_m^* \rightarrow OH\ (A) + M + H$

In the case of sapphire and diamond, it is not practicable to form a soft surface oxide layer by water vapor plasma irradiation since sapphire is already an oxide and the oxidation products of diamond are volatile (CO and CO_2). However, water-vapor-containing plasma can be used for surface hydroxylation. In the PAP of sapphire and diamond, the substrates and grinding stones are both exposed to OH radicals during polishing and hydroxylation of the substrates and grinding stones occurs. In the contact area, dehydration condensation reactions occur between the OH-terminated substrates and the grinding stones, resulting in the removal (polishing) of the substrates.

(2) Oxygen-containing plasma

Table 2.5 shows the mechanism and reactions of the generation of oxygen radicals in oxygen containing plasma. Similar to water-vapor-containing plasma, oxygen-containing plasma is used in PAP for the surface oxidation of SiC and GaN. Oxygen-containing plasma can also be used to machine diamond by etching with a very high efficiency [64].

Table 2.5 Typical reactions in oxygen contained plasma [52]

Mechanism	Reaction
Electron impact dissociation of oxygen molecule	$O_2 + e \rightarrow O + O + e$
Oxygen molecule dissociation with noble gas metastable	$O_2 + M_m^* \rightarrow O + O + M$
Oxygen molecule dissociation with excited N_2	$O_2 + N_2^* \rightarrow O + O + N_2$

(3) CF_4-containing plasma

Table 2.6 shows the mechanism and reactions of the generation of F radicals in CF_4 plasma. As has been mentioned in 2.3.2, CF_4-containing plasma is used in the PCVM of Si-based materials because the reaction products of CF_4-containing plasma and the substrates are volatile. Therefore, for the PAP of SiC (single-crystal and CVD), in which surface modification is required, CF_4 plasma is not suitable. However, CF_4 plasma can be used for the surface modification of GaN since the reaction product, GaF_3, is non-volatile. In Chapter 4, it will be demonstrated that GaF_3 is softer than GaN. Thus, CF_4 plasma is suitable for the PAP of GaN. It has also been reported that CF_4 plasma can be used for the machining of diamond by etching [65].

Table 2.6 Typical reactions in CF_4 contained plasma [66]

Mechanism	Reaction
Electron impact dissociation of CF_4	$CF_4 + e \rightarrow CF_3 + F + e$
Combination of CF_3 with oxygen molecule	$O_2 + CF_3 \rightarrow COF_2 + OF$
Conversion of OF radical to F atom	$CF_3 + OF \rightarrow COF_2 + F + F$

2.4 Summary

To realize the highly efficient, cost-effective and damage-free polishing of difficult-to-machine materials, which cannot be realized by conventional polishing techniques, PAP is proposed. In this chapter, the conventional polishing techniques, the basics of the generation of AP-plasma, and the concepts and strategies of PAP are described.

(1) The damage-free and ultraprecision polishing of difficult-to-machine materials is difficult owing to their high hardness and chemical inertness. Currently, several polishing techniques are being developed for these materials. However, there are still several challenges associated with these polishing techniques such as the low polishing efficiency and high cost.

(2) AP-plasma has been successfully used in PCVM for the ultraprecision machining of Si-based materials. The major advantages of AP-plasma in machining, such as the high efficiency, good form accuracy, low cost and the ability of damage-free machining, have been proved.

(3) PAP, which combines AP-plasma surface modification and soft abrasive polishing, was proposed, in which the surfaces of difficult-to-machine materials are modified by the irradiation of AP-plasma and a soft modified layer is formed. Then the modified layer is removed by polishing using a soft abrasive. Thus, a damage-free and atomic-scale flat surface can be expected. Plasmas containing water vapor, oxygen and CF_4 are used in PAP for the polishing of different materials.

References

1) J. R. Grim, M. Benamara, M. Skowronski, W. J. Everson and V. D. Heydemann, Semicond. Sci. Technol. 21 (2006) 1709-1713.
2) S. Johansson, J. Schweitz and K. P. Lagerlof, J. Am. Ceram. Soc. 72 (1989) 1136-1139.
3) L. Zhou, V. Audurier, P. Pirouz and J. A. Powell, J. Electrochem. Soc. 144 (1997) L161-L163.
4) C. L. Neslen, W. C. Mitchel and R. L. Hengehold, J. Electron. Mater. 30 (2001) 1271-1275.
5) M. Kikuchi, Y. Takahashi, T. Suga, S. Suzuki and Y. Bando, J. Am. Ceram. Soc. 75 (1992) 189-194.
6) H. Hara, Y. Sano, H. Mimura, K. Arima, A. Kubota, K. Yagi, J. Murata and K. Yamauchi, J. Electron. Mater. 35 (2006) L11-L14.
7) K. Arima, H. Hara, J. Murata, T. Ishida, R. Okamoto, K. Yagi, Y. Sano, H. Mimura and K. Yamauchi, Appl. Phys. Lett. 90 (2007) 202106.
8) S. H. Hong, J. Watanabe, and M. Touge, Int. J. Manuf. Sci. Technol. 9 (2007) 23-28.

9) J. Watanabe, S. H. Hong, K. Yamaguchi, M. Touge, and N. Kuroda, Proc. Advances in Abrasive Technology (ASAAT 2007) (2007) 91-96.
10) C. Li, I. B. Bhat, R. Wang and J. Seiler, J. Electron. Mater. 33 (2004) 481-486.
11) J. Qian, G. Voronin, T. W. Zerda, D. He and Y. Zhao, J. Mater. Res. 17 (2002) 2153-2160.
12) D. He, Y. Zhao, L. Daemen, J. Qian, T. D. Shen and T. W. Zerda, Appl. Phys. Lett. 81 (2002) 643-645.
13) R. Nowak, M. Pessa, M. Suganuma, M. Leszczynski, I. Grzegory, S. Porowski, and F. Yoshida, Appl. Phys. Lett. 75 (1999) 2070-2072.
14) A. Zerr, H. Eschnauer and E. Kny, Wiley-VCH (2012)
15) A. Belger, M. Reibold and P. Paufler, Mater. Sci. Applications. 3 (2012) 185-194.
16) V. Blank, M. Popov, N. Lvova, K. Gogolinsky and V. Reshetov, J. Mater. Res. 12 (1997) 3109-3114.
17) A. Arora, D. B. Marshall, B. R. Lawn and M. V. Swain, J. Non-Crystalline Solids 31 (1979) 415-428.
18) A. B. Shorey, K. M. Kwong, K. M. Johnson and S. D. Jacobs, Appl. Optics 39 (2000) 5194-5204.
19) L. M. Cook, J. Non-Crystalline Solids 120 (1990) 152-171.
20) W. J. Patrick, W. L. Guthrie, C. L. Standley and P. M. Schiable, J. Electrochem. Soc. 138 (1991) 1778-1784.
21) H. Aida, T. Doi, H. Takeda, H. Katakura, S. W. Kim, K. Koyama, T. Yamazaki and M. Ueda, 12 (2012) S41-S46.
22) T. Kato, K. Wada, E. Hozomi, H. Taniguchi, T. Miura, S. Nishizawa and K. Arai, Mater. Sci. Forum 556-557 (2007) 753-756.
23) X. Shi, G. Pan, Y. Zhou, Z. Gu, H. Gong and C. Zou, Appl. Surf. Sci. 307 (2014) 414-427.
24) S. Kurokawa, T. K. Doi, C. Wang, Y. Sano, H. Aida, K. Oyama and K. Takahashi, ECS Trans. 60 (2014) 641-646.
25) Y. Zhou, G. Pan, X. Shi, H. Gong, G. Luo and Z. Gu, Surf. Coat. Technol. 251 (2014) 48-55.
26) H. S. Lee, D. I. Kim, J. H. An, H. J. Lee, K. H. Kim and H. Jeong, Ann. CIRP 56 (2010) 333-336.
27) M. Hirano, J. Inoue, K. Kawada, S. Nagaya, T. Kido, T. Nakayama, G. Sasaki and T. Kato, Advanced Power Semiconductor 1 (2014) 88-89. (In Japanese)
28) S. E. Saddow, T. E. Schattner, J. Brown, L. Grazulis, K. Mahalingam, G. Landis, R. Bertke and W. C. Mitchel, J. Electron. Mater. 30 (2001) 228-234.
29) H. Gong, G. Pan, Y. Zhou, X. Shi, C. Zou and S. Zhang, Appl. Surf. Sci. 338 (2015) 85-91.
30) S. A. Kukushkin, A. V. Osipov, V. N. Bessolov, B. K. Medvedev, V. K. Nevolin and K. A. Tcarik, Rev. Adv. Mater. Sci. 17 (2008) 1-32.
31) N. Yasunaga, A. Obara and O. Imanaka, J. JSPE 44 (1978) 65-71.
32) T. Kido, M. Nagaya, K. Kawata and T. Kato, Mater. Sci. Forum 778-780 (2014) 754-758.
33) J. Murata, S. Sadakuni, K. Yagi, Y. Sano, T. Okamoto, K. Arima, A. N. Hattori, H. Mimura and K. Yamauchi, Jpn. J. Appl. Phys. 48 (2009) 121001.
34) J. Murata, S. Sadakuni, T. Okamoto, A. N. Hattori, K. Yagi, Y. Sano, K. Arima and K. Yamauchi, J.

Cryst. Growth 349 (2012) 83-88.

35) A. Isohashi, S. Sadakuni, T. Sugiura, N. Kidani, T. Inada, W. Yamaguchi, K. Inagaki, Y. Sano and K. Yamauchi, Proc. Euspen (2015) 345-346.
36) A. Isohashi, T. Inada, W. Yamaguchi, T. Sugiura, S. Matsuyama, Y. Sano and K. Yamauchi, Proc. JSPE (2014) 25-26.
37) A. Kubota, S. Fukuyama, Y. Ichimori and M. Touge, Diamond Relat. Mater. 24 (2012) 59-62.
38) J. Watanabe, M. Touge and T. Sakamoto, Diamond Relat. Mater. 39 (2013) 14-19.
39) N. Ballarin, C. Carraro, R. Maboudian and L. Magagnin, Electrochem. Commun. 40 (2014) 17-19.
40) A. Philipossian and E. Mitchell, Jpn. J. Appl. Phys. 42 (2003) 7259-7264.
41) Y. Mori, K. Yamamura, K. Yamauchi, K. Yoshii, T. Kataoka, K. Endo, K. Ingaki and H. Kakiuchi, Nanotechnology 4 (1993) 225-229.
42) R. G. Poulsen, J. Vac. Sci. Technol. 14 (1977) 266-274.
43) K. Yamamura, S. Shimada and Y. Mori, Ann. CIRP 57 (2008) 567-570.
44) Y. Mori, K. Yamamura and Y. Sano, Rev. Sci. Instrum. 75 (2004) 942-946.
45) Y. Sano, K. Yamamura, H. Mimura, K. Yamauchi and Y. Mori, Rev. Sci. Instrum. 78 (2007) 086102.
46) K. Yamamura, K. Ueda, M. Nagano, N. Zettsu, S. Maeo, S. Shimada, T. Utaka and K. Taniguchi, Nucl. Instr. and Meth. A 616 (2010) 281-284.
47) M. Hosoda, K. Ueda, M. Nagano, N. Zettsu, S. Shimada, K. Taniguchi and K. Yamamura, Key Engineering Materials 447-448 (2010) 213-217.
48) E. E. Kunhardt, IEEE Trans. Plasma Sci. 28 (2000) 189-200.
49) C. Tendero, C. Tixier, P. Tristant, J. Desmaison and P. Leprince, Spectrochimica Acta Part B 61 (2006) 2-30.
50) L. Bardos and H. Barankova, Thin Solid Films 518 (2010) 6705-6713.
51) H. Eichhorn, K. H. Schoenbach and T. Tessnow, Appl. Phys. Lett. 63 (1993) 2481-2483.
52) D. Pappas, J. Vac. Sci. Technol. A 29 (2011) 020801.
53) O. Flores, F. Castillo, H. Martinez, M. Villa, S. Villalobos and P. G. Reyes, Phys. Plasmas 21 (2014) 053502.
54) R. A. Wolf, Wiley (2012)
55) T. Tochikubo, T. Chiba and T. Watanabe, Jpn. J. Appl. Phys. 38 (1999) 5244-5250.
56) S. Kanazawa, M. Kogoma, T. Moriwaki and S. Okazaki, J. Phys. D: Appl. Phys. 21 (1988) 838-840.
57) R. Bartnikas, J. Phys. D: Appl. Phys. 1 (1968) 659-661.
58) H. Deng, T. Takiguchi, M. Ueda, A. N. Hattori, N. Zettsu and K. Yamamura, Jpn. J. Appl. Phys. 50 (2011) 08JG05.
59) K. Yamamura, T. Takiguchi, M. Ueda, H. Deng, A. N. Hattori and N. Zettsu, Ann. CIRP 60 (2011) 571-574.
60) H. Deng and K. Yamamura, Ann. CIRP 62 (2013) 575-578.

61) H. Deng, K. Monna, T. Tabata, K. Endo and K. Yamamura, Ann CIRP 63 (2014) 529-532.
62) H. Deng, K. Endo and K. Yamamura, Ann CIRP 64 (2015) 531-534.
63) L. Li, A. Nikiforov, Q. Xiong, N. Britun, R. Snyders, X. Lu and C. Leys, Phys. Plasma 20 (2013) 093502.
64) S. Kiyohara, Y. Yagi and K. Mori, Nanotechnology 10 (1999) 385-388.
65) Y. Ando, Y. Nishibayashi, K. Kobashi, T. Hirao and K. Oura, Diamond Relat. Mater. 11(2002) 824-827.
66) C. J. Mogab, A. C. Adams and D. L. Flamm, J. Appl. Phys. 49 (1978) 3796-3803.

Chapter 3

Development of the PAP machine

3.1 Introduction

As described in Chapter 2, the surface modification (softening) of difficult-to-machine materials by the irradiation of AP-plasma and the removal of the modified layer by soft abrasive polishing are effectively combined in PAP. The combination of AP-plasma modification and soft abrasive polishing can be performed in different manners, separately or simultaneously. The plasma generation system can also be varied from localized plasmas for fundamental experiments to large-area plasmas for polishing large substrates. The abrasive polishing can be conducted using a polishing film, a grinding stone and even slurry.

The development of the PAP machine can be divided into two stages. In the first stage, preliminary experimental studies to demonstrate the usefulness of PAP were conducted using a symmetric PAP machine, and a two-step PAP process was developed to clarify the modification and removal mechanism in PAP. In the second stage, a prototype PAP machine for the highly efficient and dry polishing of 3 inch substrates was developed.

3.2 PAP machines for preliminary experimental study

3.2.1 Symmetric PAP machine

Figure 3.1(a) shows a schematic view of the symmetric PAP machine used for preliminary research. This apparatus consists of a separately installed AP-plasma generation unit and mechanical removal unit. AP-plasma was generated by applying an RF (radio frequency, f =13.56 MHz) electric power, and noble-gas-based water vapor, O_2 or CF_4 is supplied as a process gas. In the case of water-vapor-containing plasma, water vapor was introduced into the process gas by bubbling it through ultrapure water (UPW), and its concentration was measured using a dew-point meter (DPM). In the case of O_2- and CF_4-containing plasmas, two flow paths exist, one for the reactive gas (O_2 or CF_4) and one for the noble gas (He or Ar). The copper electrode used was covered with quartz glass to prevent arc discharge through the generation of dielectric barrier discharge (DBD). As shown in Figure 3.1(b), a localized plasma with a diameter of about 8 mm was generated under the electrode. In the mechanical removal unit, a polishing experiment using a polishing film (ϕ8 mm) was conducted.

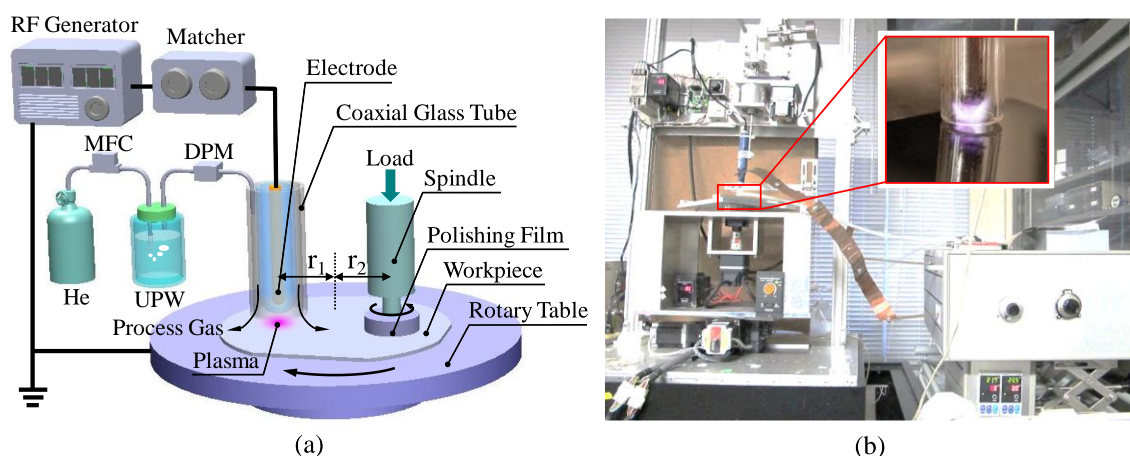

Figure 3.1 Symmetric PAP machine. (a) The schematic view. (b) Photograph of the apparatus.

The specimen was installed on a rotary table, and surface modification by plasma irradiation and mechanical removal using a polishing film supplied by MIPOX Co. Ltd. [1)] were sequentially conducted. The electrode and polishing film were located at the same distance from the center of the rotary table (r_1=r_2 in Figure 1). This is why this machine is called a symmetric machine. The polished area was not the whole surface but an annular shape with a width of about 8 mm.

Figure 3.2 shows the structure and SEM topography of the polishing film used in the symmetric PAP machine. A CeO_2 abrasive with an average grain size of 0.5 μm was used for polishing. During polishing, the wear of the polishing film was very rapid; thus, the polishing film needed to be replaced for the next polishing cycle after a short polishing time such as 1 min. CeO_2 is very soft compared with SiC or GaN, as can be seen from Table 2.1, therefore it is considered that damage-free polishing can be realized.

Frequent replacement of the polishing film greatly lowers the polishing efficiency and this process is not suitable for industry. Therefore, continuous polishing is required and polishing using slurry and grinding stones should be investigated.

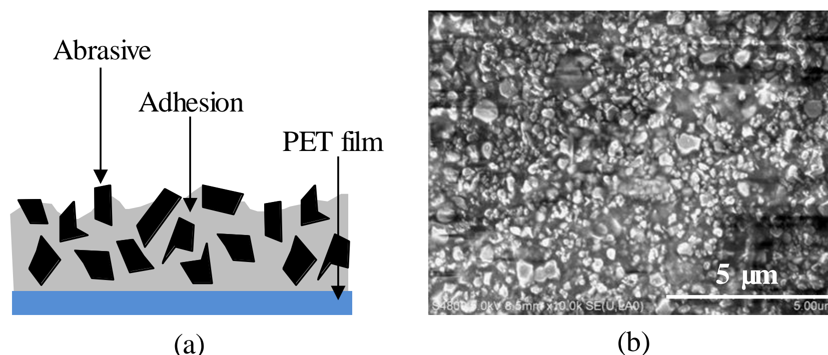

Figure 3.2 (a) Cross-sectional structure of the polishing film. (b) SEM image of the polishing film (CeO_2).

3.2.2 Two-step PAP process

Plasma modification and abrasive polishing can also be performed separately, which is called the two-step PAP process. Figure 3.3 shows the concept of the two-step PAP process. In step one, surface modification by AP-plasma irradiation is conducted and a modified layer is formed on the surface. The modified layer is softer than the substrate, therefore in step two, soft abrasive polishing is conducted to remove only the modified layer and obtain a flat surface.

Figure 3.4(a) shows the experimental setup used for plasma irradiation. A mixture of a noble gas and water vapor, O_2 or CF_4, which were respectively used as the carrier gas and the reactive gas for plasma generation, were supplied from the center of the electrode and flowed through the space between the electrode and the ceramic cover. The flow rates of the carrier gas and reactive gas were controlled using MFCs. The substrate was set on a worktable by a vacuum chuck. In most of the experiments, the gap between the electrode and the substrate was adjusted to less than 2 mm to realize the generation of AP-plasma with a low applied electric power. The diameter of the powered electrode, which was made of aluminum alloy, was 3 mm. An impedance matcher was used to maximize the transfer of power from the power source to the load (plasma area). AP-plasma was generated by applying a 13.56 MHz RF power between the electrode and the

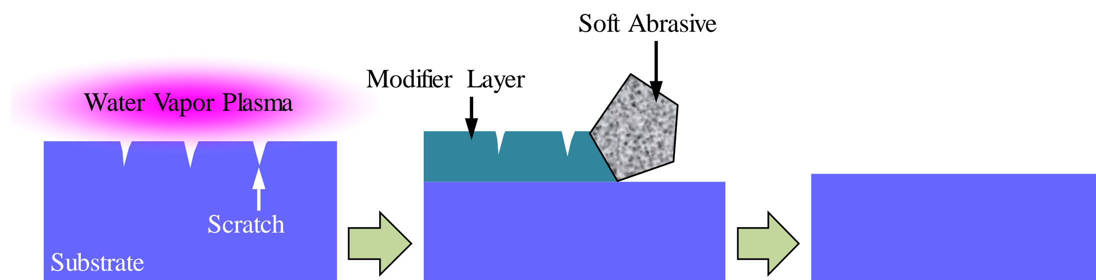

Figure 3.3 Concept of two-step PAP.

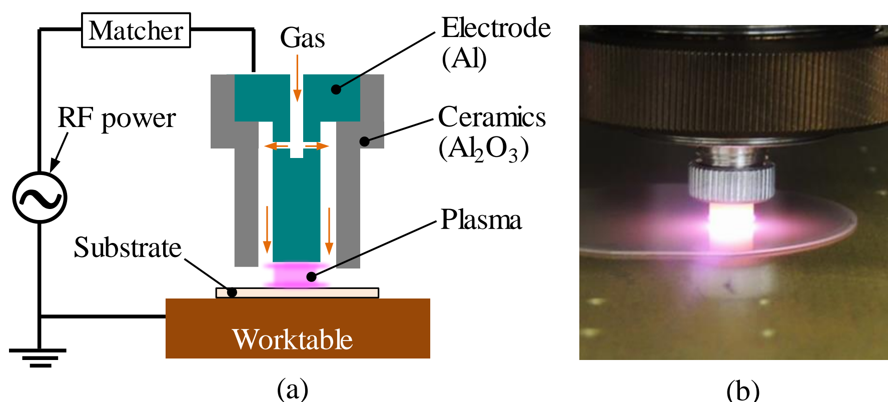

Figure 3.4 (a) Schematic view of the experimental setup used for plasma modification. (b) Image of AP-plasma (CF_4).

worktable. Figure 3.4(b) shows a photograph of plasma irradiation on the surface of a GaN substrate. With the scanning of the X-Y table, the target area on the substrate was modified.

After the substrate was irradiated by AP-plasma, the modified substrate surface was polished using slurry or grinding stones to remove the modified layer and realize a flat surface. In the case of slurry polishing (wet polishing), a polishing pad (NP178) with a diameter of 10 mm supplied by FILWEL Co. Ltd. [2] was used. A commercially available CeO_2 slurry (average diameter: 190 nm) and SiO_2 slurry (average diameter: 72 nm) were both investigated. In the case of grinding stone polishing (dry polishing), resin-bonded CeO_2 and SiO_2 grinding stones supplied by NORITAKE Co. Ltd. [3] were used since the grinding stones were still under development. The average particle size of the CeO_2 abrasive and SiO_2 abrasive, the thickness of the grinding stones and the concentration of the abrasive were varied in different experiments. Also, two types of grinding stone, the fixed type and the loose-hold type (LHA) were used for comparison.

Figure 3.5(a) shows the experimental setup used for abrasive polishing by a grinding stone. The grinding stone was fixed below the rotary spindle. With the scanning of the X-Y table, the substrate was polished by the grinding stone through the application of a constant load. In the case of slurry polishing, the same setup was used with the grinding stone replaced by a polishing pad. A slurry container was installed on the worktable and the substrate was immersed in the slurry.

In the two-step PAP process, plasma modification and abrasive polishing are separately conducted. This process was used to clarify the plasma modification mechanism and mechanical removal mechanism in PAP. The application results of two-step PAP are described in Chapter 4

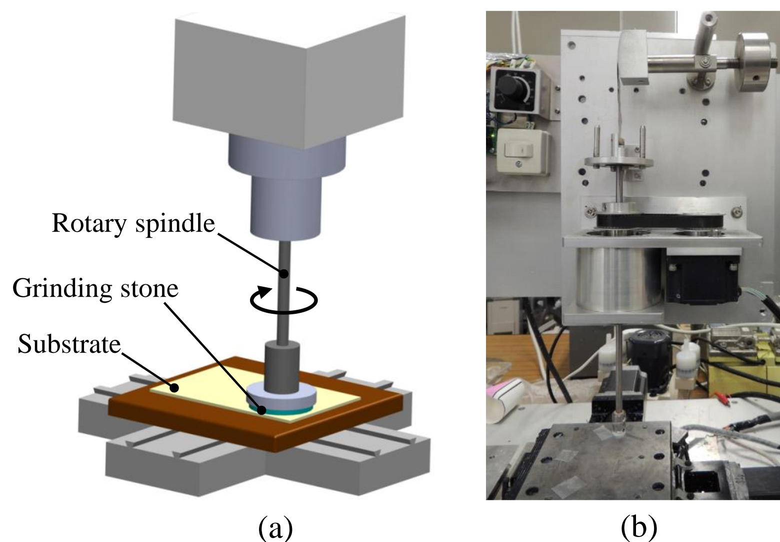

Figure 3.5 (a) Schematic view of the experimental setup used for abrasive polishing. (b) Photograph of the polishing machine.

for SiC and Chapter 6 for GaN. Also, for comparison with PAP, conventional CMP without plasma pretreatment was also conducted using the experimental setup shown in Figure 3.5.

3.2.3 Generation of large-area AP-plasma

As previously mentioned, localized AP-plasmas with a diameter of less than 10 mm were used in the symmetric PAP machine and the two-step PAP process. The whole-surface polishing of large substrates (3 inch and larger) cannot be realized using the symmetric PAP machine and the frequent replacement of the polishing film greatly decreases the polishing efficiency and makes handling difficult. In the two-step PAP process, plasma modification and abrasive polishing are separately conducted, which also lowers the polishing efficiency. To realize the industrial application of PAP, the highly efficient polishing of large substrates is essential. Therefore, it is essential to generate a large-area homogeneous AP-plasma.

Figure 3.6 shows a schematic view of the fundamental AP-plasma generation setup. The gap distance between the two electrodes, which are made of aluminum alloy, is 2 mm. There are many holes in the upper electrode to realize a uniform flow of process gas. The diameter of the electrodes is 85 mm. The generation of AP-plasma can be observed from the side and from the above through the holes. Figure 3.7 shows photographs of the setup before and after AP-plasma generation (carrier gas: He, gas flow rate: 1.5 slm, applied RF power: 200 W). It was confirmed that a homogeneous glow discharge was realized in the area between the two electrodes.

Although a large-area AP-plasma with a diameter of 85 mm was generated, its conditions were considerably different from these of PAP in which abrasive polishing was combined. When plasma generation is combined with polishing, there are extraneous items in the plasma ambient such as grinding stones and dust from the grinding stones and substrate. Also, the rotation and scanning of the polishing tool and substrate affect the stability of the plasma. Thus, the realization of a homogeneous glow discharge in PAP is difficult.

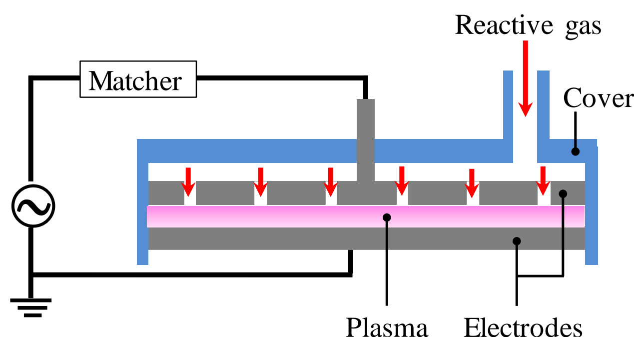

Figure 3.6 Schematic view of a fundamental AP-plasma generation setup (ϕ 85 mm)

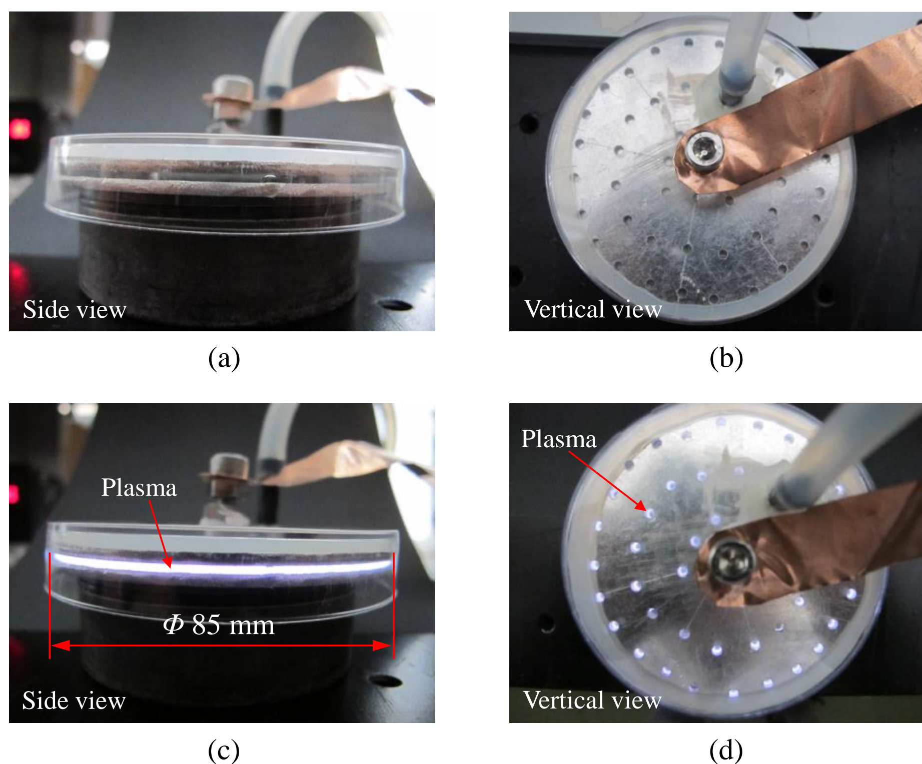

Figure 3.7 Generation of large area AP-plasma (ϕ 85 mm). (a, b) Before plasma generation. (c, d) After plasma generation.

Figure 3.8 shows a schematic view of the PAP machine used for preliminary study. This machine can be divided into two parts: the polishing tool and the stage. The substrate is held on the center of the stage by a vacuum chuck. RF power is applied between the upper electrode and ground electrode. A He- or Ar-based process gas is introduced into the gap area between the two electrodes. The upper electrode and ground electrode are covered with thin ceramic plates to prevent arc discharge through the generation of DBD. The diameter of the upper electrode is 150 mm, making the polishing of large substrates possible. By controlling the pressure of the back air, stretching of the welding bellows occurs. The pressure applied in polishing is controlled by the stretching of the welding bellows. The grinding stones move up and down through the upper electrode. Therefore, the electrode gap is constant in PAP, which keeps the surface modification conditions constant.

Figure 3.9 shows photographs of plasma generation in this machine. Since the discharge area is quite large (ϕ 150 mm), the parallelism of the powered electrode and ground electrode greatly affects the uniformity of the plasma discharge. Figure 3.9(a) shows a photograph of plasma generation with poor parallelism of the two electrodes (applied RF power: 100 W). Discharge only occurs on the left side. With increasing applied RF power, the discharge area expanded; however, arc discharge occurred owing to the concentration of the electric field. By adjusting the

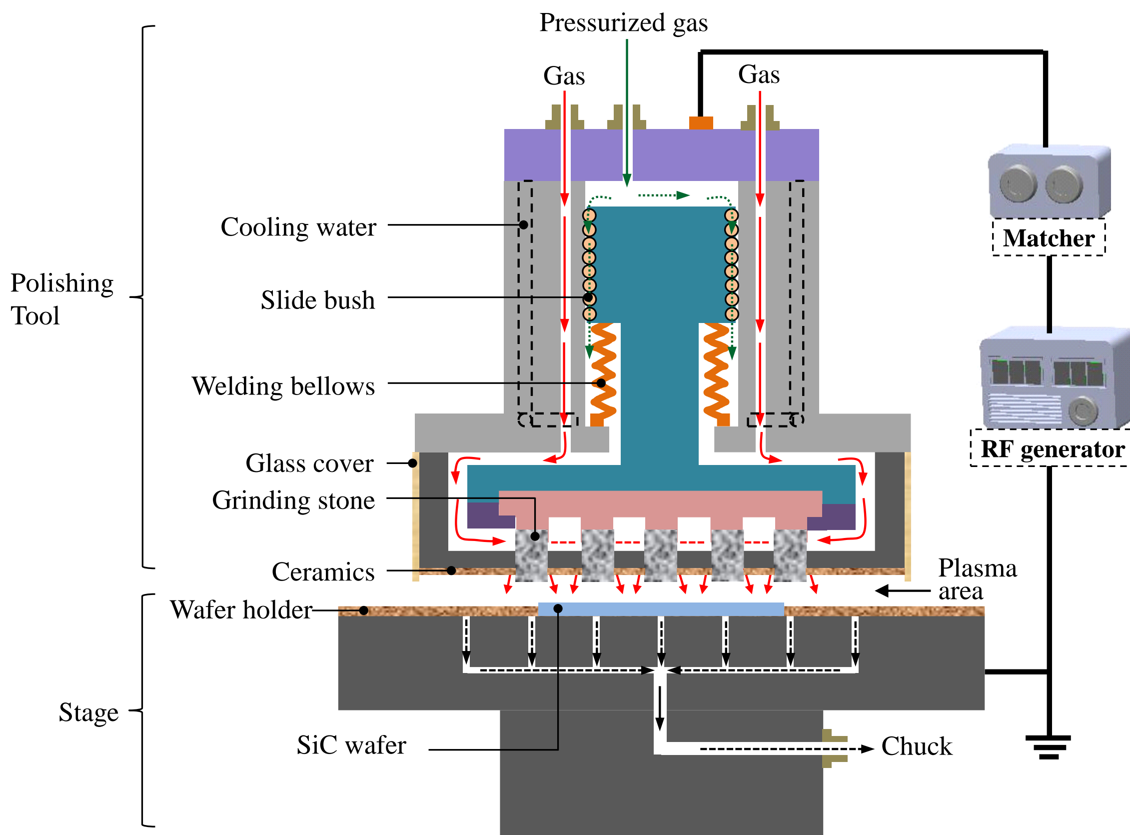

Figure 3.8 Schematic view of a PAP machine for preliminary study.

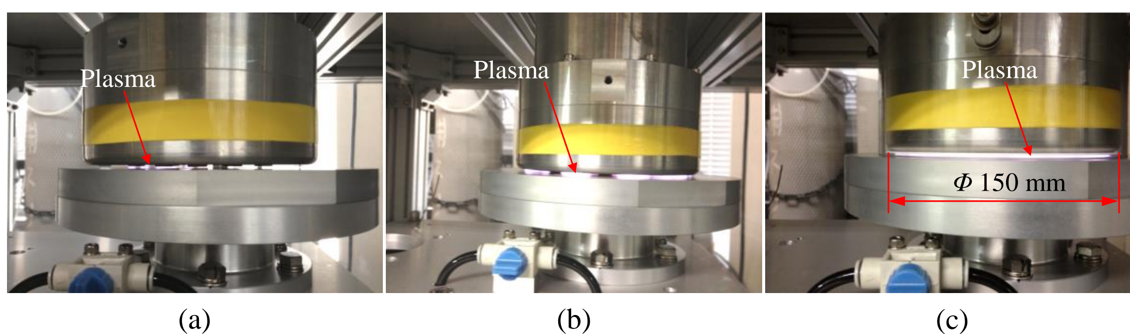

Figure 3.9 Photographs of AP-plasma generation. (a) Before the parallelism adjusted (100 W). (b) After the parallelism adjusted (100 W). (c) After the parallelism adjusted (200 W).

parallelism of the electrodes, the generation of plasma became much more uniform as shown in Figure 3.9(b). After the applied RF power was increased to 200 W, a homogeneous glow discharge with a diameter of 150 mm was generated as shown in Figure 3.9(c).

3.3 Prototype PAP machine

3.3.1 Introduction

As previously mentioned, the symmetric PAP machine was used to demonstrate the usefulness of this novel polishing technique. Then, the two-step PAP process was conducted to clarify the modification and removal mechanism in PAP. Also, the generation of large-area homogeneous AP-plasmas (ϕ85 mm and ϕ150 mm) was experimentally confirmed. On the basis of the previous preliminary study, a prototype PAP machine was developed to realize the highly efficient, damage-free, slurryless and whole-surface polishing of large substrates of SiC, GaN and sapphire.

Figure 3.10(a) shows a photograph of the prototype PAP machine. Three inch SiC, GaN and sapphire substrates can be polished using this machine as well as square single-crystal diamond substrates (20 mm $\times$20 mm). The pressurization is controlled using a servo motor and a load cell. The polishing pressure can be controlled from 0.01 MPa to 0.5 MPa. In this range, the pressure of PAP can be optimized to obtain lower surface roughness and higher polishing efficiency. The maximum rotation speed of the stage is 500 rpm while that for the polishing tool is 2000 rpm. He and Ar can be used as the carrier gas, and the reactive gas is chosen from water vapor, oxygen and CF_4. In addition to the rotation of the polishing head and stage, scanning of the stage is also conducted to realize the uniform polishing of the whole substrate. Figure 3.10(b) shows a photograph of the polishing area in the machine with plasma generated. AP-plasma was generated between the upper powered electrode and the substrate by applying RF power. The substrate was set on the center of the stage using a vacuum chuck. Process gas was supplied from the center of the polishing head. Owing to the structure of the polishing head, this PAP machine can only be used to polish wafer substrates.

3.3.2 Polishing tool

Figure 3.11 shows the structure of the hybrid polishing tool of the prototype PAP machine. This polishing tool consists of many small grinding stones and electrodes as shown in Figures 3.12(a) and (b). The electrodes and grinding stones are alternately arranged in the polishing tool. Between each pair of grinding stones, there is an electrode for plasma generation. The electrodes are made of aluminum alloy and resin-bonded grinding stones are used in this research to realize damage-free polishing.

When PAP is conducted, the grinding stones come in contact with the substrate after pressurization as shown in Figure 3.12(c). The gap distance between the powered electrodes and the substrate is kept constant during polishing. In the gap area, AP-plasma is generated after supplying gas and the application of RF power between the powered electrode and the grounded stage. Therefore, the substrate surface, which is exposed to AP-plasma, is modified (by oxidation,

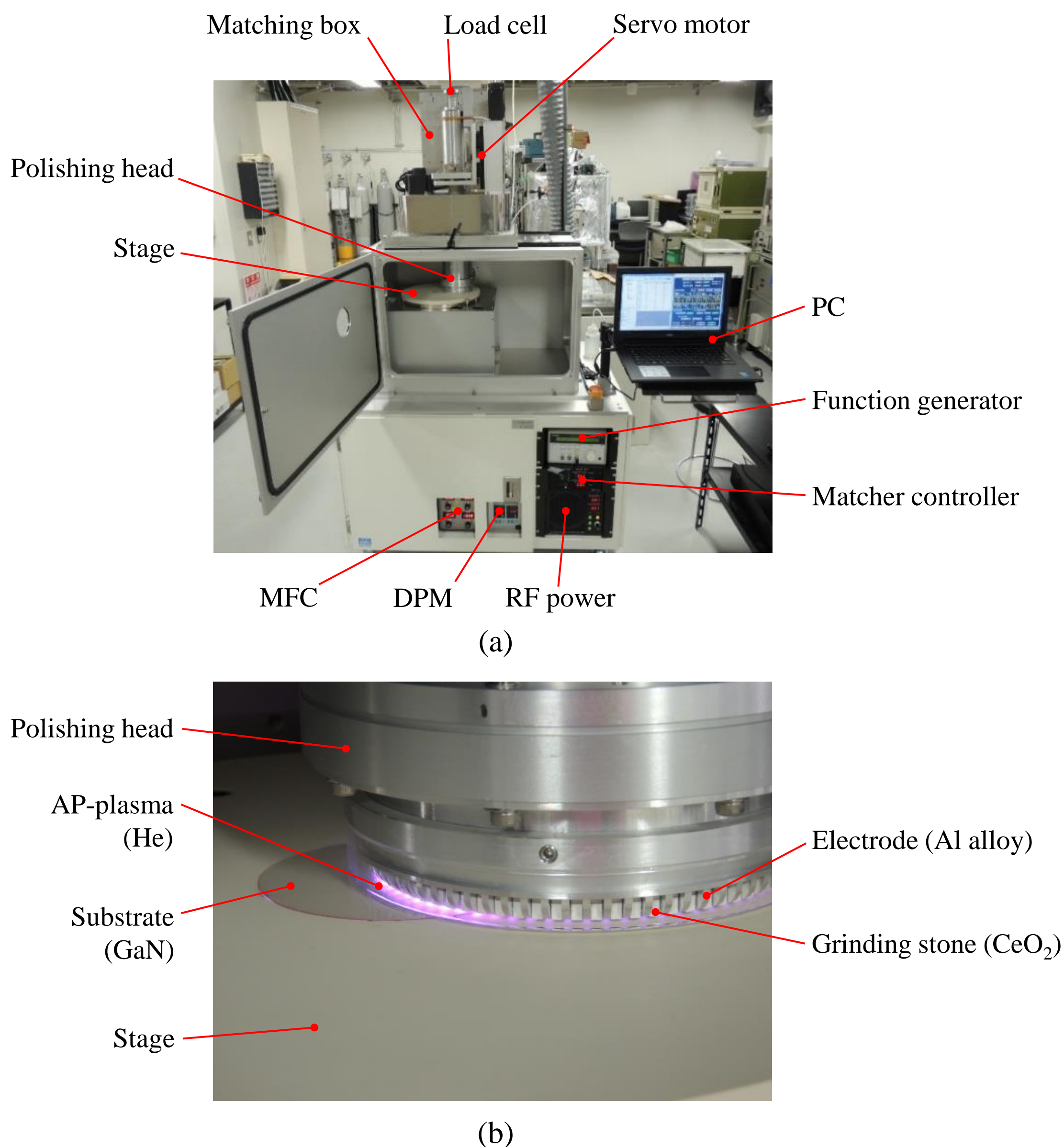

Figure 3.10 (a) Photographs of the prototype PAP machine. (b) Photograph of the AP-plasma (He) generated with the prototype PAP machine.

fluoridation and hydroxylation). Owing to the rotation of the polishing head and the stage, the modified area is immediately polished by the grinding stones. That is to say, using this hybrid polishing tool, surface modification by AP-plasma and soft abrasive polishing by resin-bonded grinding stones are simultaneously conducted. Compared with the symmetric PAP machine and the two-step PAP process, high polishing efficiency is expected.

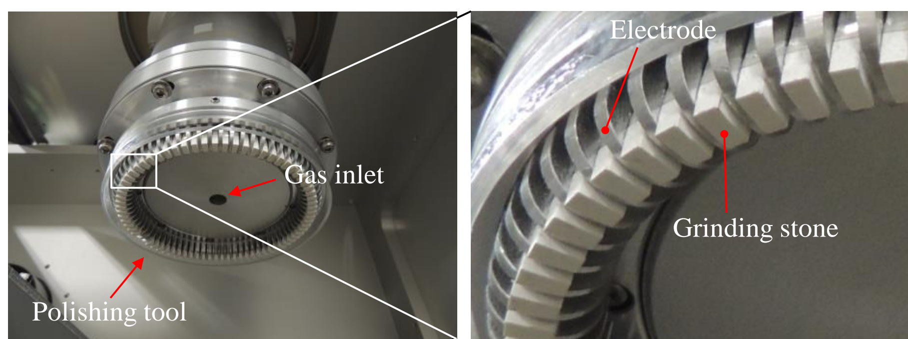

Figure 3.11 Photographs of the polishing tool of the prototype PAP machine.

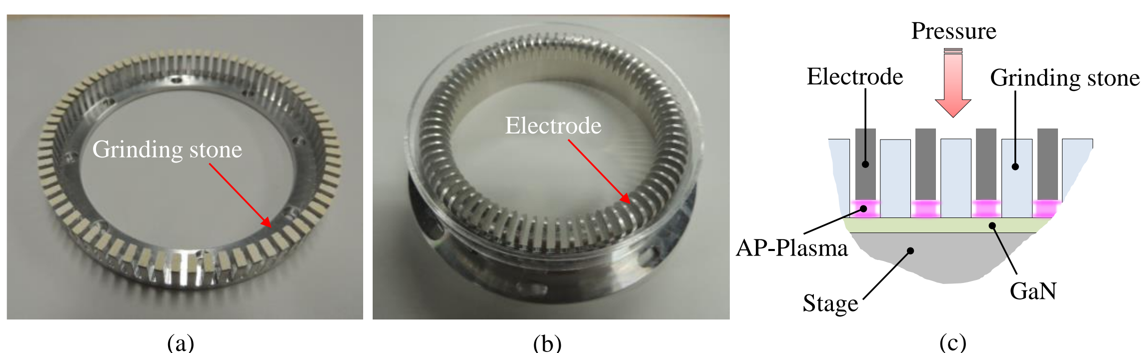

Figure 3.12 (a) Photographs of the grinding stones. (b) Photographs of the electrodes. (c) Schematic view of the hybrid polishing tool.

3.3.3 Pressurizing mechanism

Various pressurizing mechanisms such as weight pressurization, pneumatic pressurization and hydraulic pressurization have been used in different lapping and polishing machines. In PAP, to optimize the surface quality and polishing efficiency, control of the polishing pressure over a large range is necessary. Figure 3.13 shows a schematic view (a) and photograph (b) of the pressurizing mechanism used in the prototype PAP machine. Pressurization is realized using a load cell, a servo motor and three damped springs. The lower two springs are used to cancel the weight of the rotary spindle. Before polishing, the desired pressure is input to the pressure control software. After the substrate has settled, the polishing tool moves downward to the substrate in a manual mode. Once the grinding stones are almost in contact with the substrate, the manual approach stops. Then the generation of AP-plasma and the rotation and scanning of the stage and the polishing tool are conducted in order. After that, pressure control starts and the value of the measured pressure on the load cell is reset to zero. The grinding stones move downward to come in contact with the substrate and the pressure gradually increases to the set value.

In PAP, there is vertical vibration owing to the friction between the grinding stones and the substrate. The force on the load cell is measured in real time. If the measured pressure is lower than the desired value, feedback is transferred to the servo motor and the grinding stones move downward to increase the polishing pressure. On the other hand, if the measured pressure is higher than the desired value, the grinding stones move upward. In this way, PAP is performed on the substrate with a constant polishing pressure. Since the three springs have the same spring constant, the load on the substrate F_r is three times the load on the load cell F_m.

The relationship between F_r and F_m was experimentally investigated. The worktable was replaced by a balance so that the load F_r on the substrate (balance) could be measured. For a desired load F_m, F_r was measured three times to evaluate the repeatability. Figure 3.14 shows the measurement results. It was found that with increasing the F_m, the deviation of Fr obtained from the measured data to the predicted value also increased. Two reasons are considered to explain the deviation. One is the friction between the spindle and the rotary joint. The other is the deformation error from the damped springs. Even though there was deviation of the pressure, the repeatability was found to be very good especially at large pressures. Therefore, good repeatability of the polishing conditions in PAP, especially the polishing pressure, can be expected.

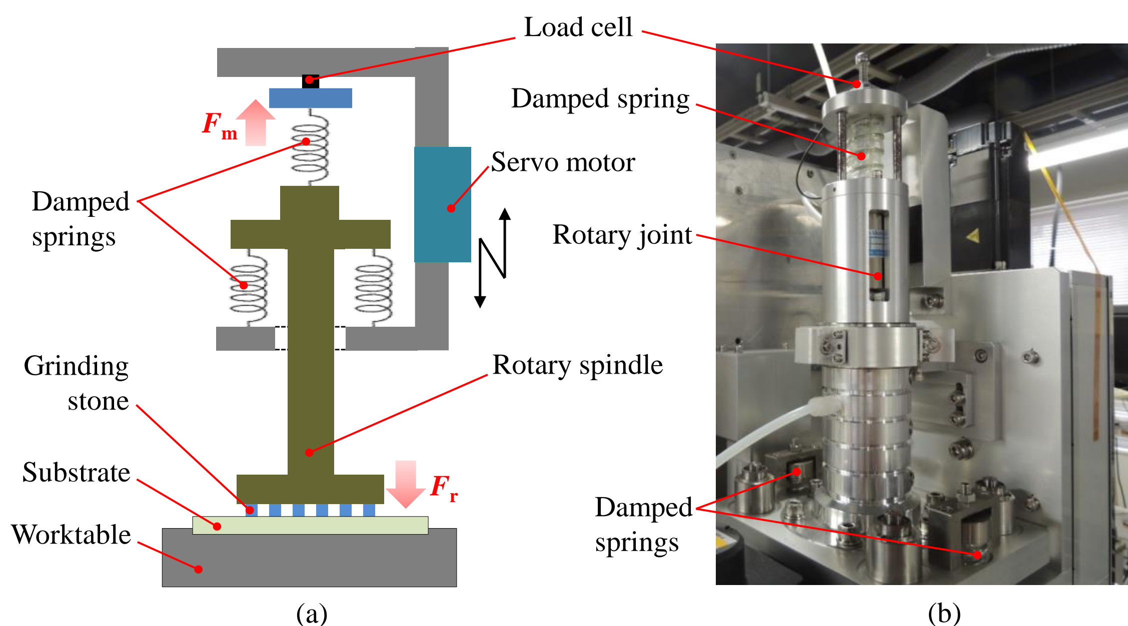

Figure 3.13 Pressurization mechanism of the prototype PAP machine. (a) Schematic view of the pressurization mechanism. (b) Photograph of the pressurization unit.

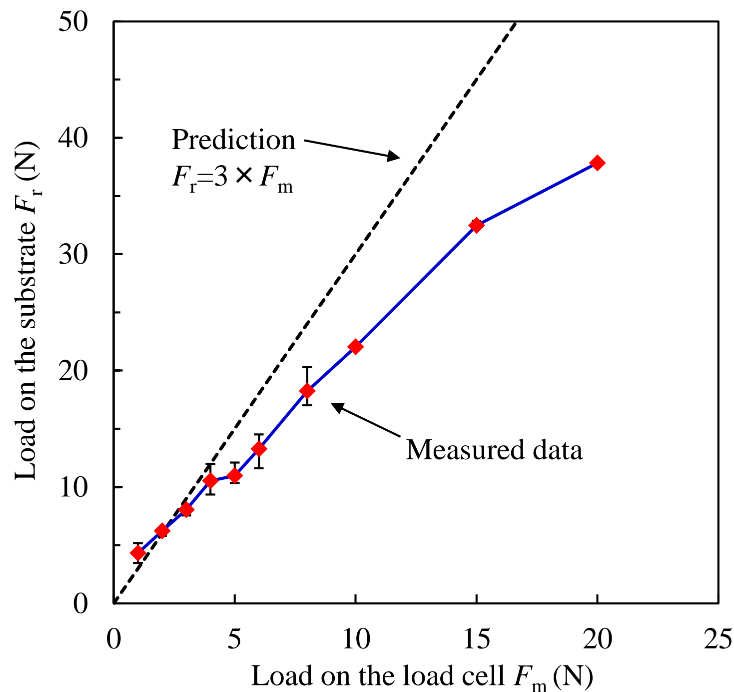

Figure 3.14 Relationship between the load on the substrate (F_r) and the load on the load cell (F_m).

3.3.4 Cooling system

In this prototype PAP machine, a cooling system is necessary for the following two reasons. First, the rotary spindle of the polishing head rotates through a ball spline with a maximum speed of 2000 rpm. The friction heat will affect the durability of the ball spline. Thus, cooling is essential to eliminate the effect of the friction heat. Second, plasma is also a heat source, especially in the case of a large applied RF power. Resin-bonded grinding stones are used in this prototype PAP machine. The heatproof temperature of such grinding stones is less than 150 ℃. These grinding stones are immersed in the plasma ambient and the heat from the plasma will affect the polishing performance of the grinding stones. Therefore, cooling is essential to decrease the temperature of the hybrid polishing tool, including the electrodes and grinding stones.

Figure 3.15 shows the cooling system used in the prototype PAP machine. A coolant water circulation unit in which the temperature can be set from -20 ℃ to 30 ℃ is used. The coolant water flows through the spindle and the polishing tool. With the application of this cooling system, the effect from the increase in temperature in PAP can be suppressed.

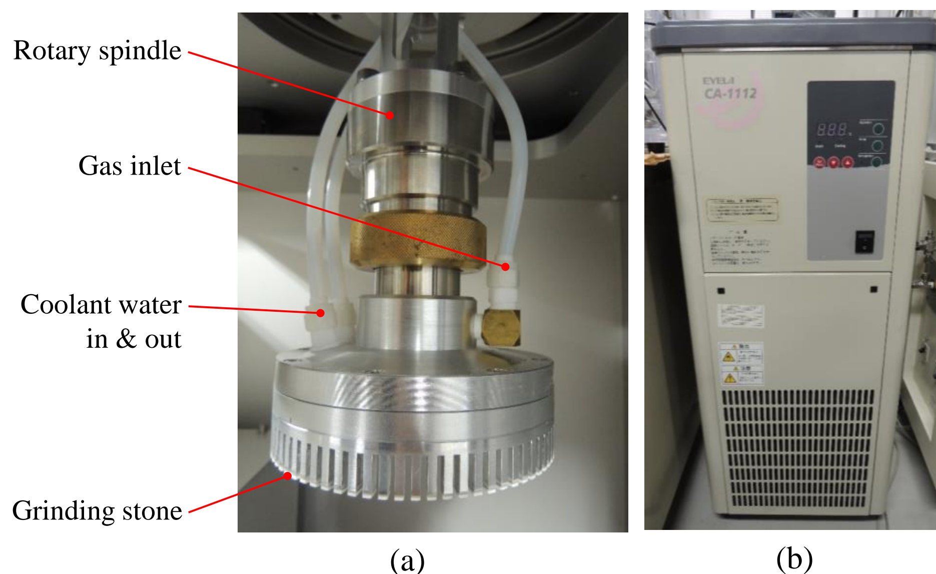

Figure 3.15 Cooling system of the prototype PAP machine. (a) Photograph of the polishing head. (b) Photograph of the coolant water circulation unit.

3.3.5 Dresser

In this prototype PAP machine, plasma modification and grinding stone polishing are simultaneously conducted. After a soft modified layer is generated, it is removed by polishing using the grinding stones. However, surface deterioration such as wear of the grinding stones occurs after polishing, which will degrade the surface quality as well as the polishing efficiency. Thus, a dresser is necessary to refresh the deteriorated grinding stone surfaces. In this prototype PAP machine, diamond plates are used for dressing.

Figure 3.16 shows photographs of the diamond plates and optical microscope images of the diamond grains on the surface of the plates. Three types of diamond plate with diamond grains having different sizes and arrangements are evaluated, #100 grains with an annular distribution, #100 grains with a planar distribution and #200 grains with a planar distribution. The effectiveness of dressing using these diamond plates will be evaluated in following chapters.

Figure 3.17 shows an image of dressing using these diamond plates. The diamond plate is set in the sample holder. Since the plate is much thicker than the SiC or GaN substrate, dressing is conducted after the electrodes are removed from the polishing tool. The dressing conditions are very similar to the PAP conditions, which including rotation, scanning and pressurization. The resin-bonded grinding stones are very soft compared with diamond and only the top surfaces of the grinding stones need to be refreshed. Therefore, dressing is usually conducted at a very low pressure such as 10 kPa and for a very short time such as several seconds.

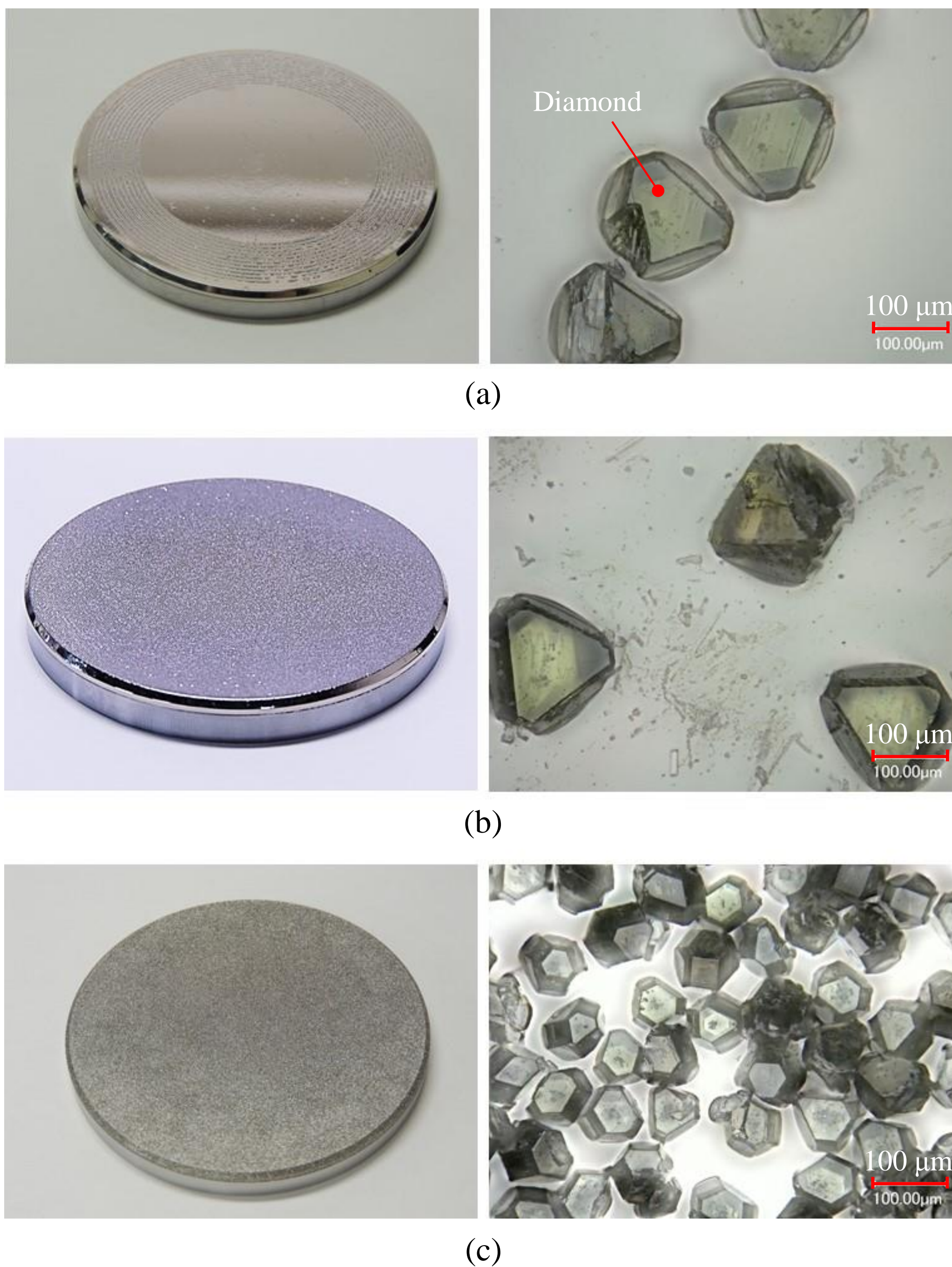

Figure 3.16 Diamond dressers used in the prototype PAP machine. (1) #100, annular distributed type. (b) #100, plane distributed type. (c) #200, plane distributed type unit. Left side: Photographs of the dresser. Right side: Optical microscope images of the diamond grains on the dresser.

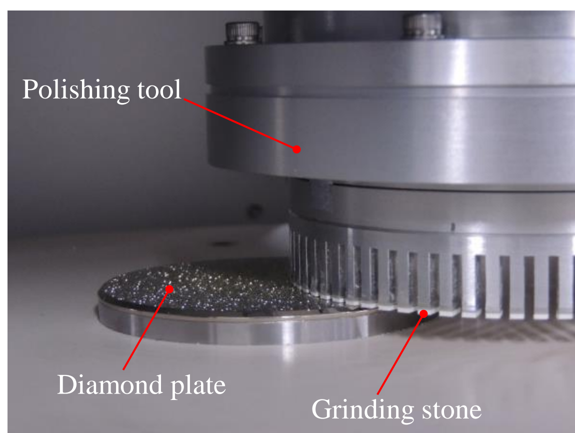

Figure 3.17 Photograph of dressing in the prototype PAP machine.

3.4 Summary

A PAP machine was developed from a symmetric-type machine for fundamental study to a prototype for practical application. In this chapter, the background to the development of the PAP machine and the details of the prototype PAP machine are described.

(1) To demonstrate the usefulness of PAP, a symmetric PAP machine that combines localized AP-plasma modification and polishing using polishing films was developed. An annular polishing area can be obtained after polishing.

(2) To clarify the oxidation and removal mechanism in PAP, a two-step PAP process was developed. The surface modification process by AP-plasma and the removal process by abrasive polishing will be investigated using this machine.

(3) To realize the polishing of large substrates, the generation of large-area AP-plasma was experimentally confirmed. Homogeneous glow discharges in large areas with diameters of 85 mm and 150 mm were realized.

(4) A prototype PAP machine was developed for the practical application of PAP to 3 inch substrates of SiC, GaN and sapphire. Slurry is not used in this machine, which is an open-air-type polishing machine without the use of a vacuum chamber, therefore it is expected to be a very cost-effective polishing technique for difficult-to-polish materials compared with conventional processes.

References

1) http://www.mipox.co.jp/products/lappingfilm_lineup.
2) http://www.filwel.co.jp/pad.html.
3) http://www.noritake.co.jp/company/dev/toryu.html.

Chapter 4 Application of PAP to 4H-SiC

4.1 Introduction

To realize the high-efficiency, low-cost and high-quality polishing of 4H-SiC, the symmetric PAP machine, the two-step PAP process and the prototype PAP machine were developed. The symmetric PAP machine, in which plasma-based modification and abrasive polishing were alternately conducted, was used to demonstrate the usefulness of PAP. The two-step PAP process, in which plasma-based modification and abrasive polishing were separately conducted, was applied to 4H-SiC to investigate the oxidation mechanism and the removal mechanism of the modified layer. Finally, the prototype PAP machine, in which plasma-based modification and abrasive polishing were simultaneously conducted, was applied to realize the whole-surface polishing of large 4H-SiC substrates in a dry ambient.

4.2 How is a SiC wafer fabricated?

4.2.1 Introduction

A brief history of the application of 4H-SiC has been given in Chapter 1. Before SiC can be used in power devices, several procedures are necessary. Figure 4.1 shows the process flow from crystal growth to epi-ready substrates of SiC. Nowadays, the crystal growth of 4H-SiC is usually conducted using the modified Lely method [1]. The obtained SiC ingot is sliced with the desired off-angle, which is usually 0°, 4° or 8°, using diamond wire saws and rough substrates are obtained. After that, grinding using a diamond abrasive is conducted to improve the flatness of the substrate and decrease the thickness of the SSD formed by slicing with high efficiency. Also, the flatness and thickness of the substrate are well adjusted in the grinding process. Next, polishing using diamond slurry is conducted to further remove the SSD and improve the surface roughness. Usually, this polishing process is divided into several steps using diamond slurry with different grain sizes. Finally, as a damage-free finishing process, CMP using a soft abrasive slurry such as SiO_2 is conducted to decrease the surface roughness to the atomic level without the formation of scratches or SSD. After CMP, epi-ready SiC substrates are obtained.

Even though the damage-free polishing of SiC can be realized by CMP [2], its high polishing cost including the use, management and post-treatment of a large amount of slurry is a major drawback. Also, since SiC is a typical difficult-to-machine material with high hardness and strong chemical inertness, conventional CMP of SiC is a time-consuming process owing to its low polishing efficiency, which also increases the polishing cost [3].

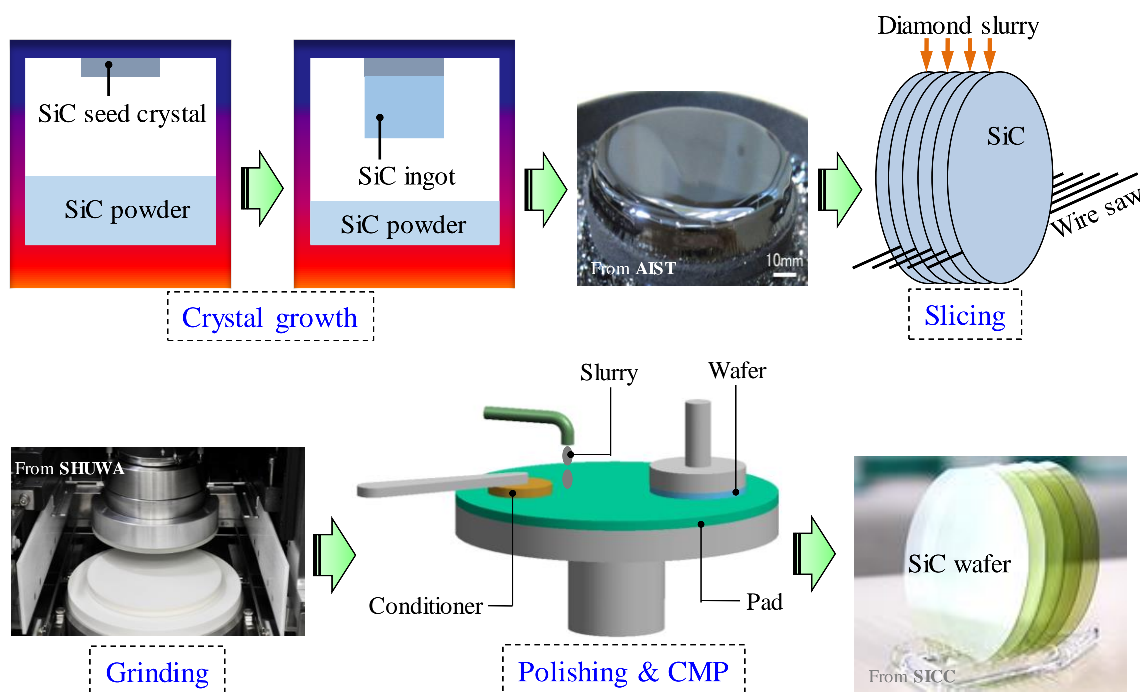

Figure 4.1 Process flow from crystal growth to epi-ready substrates of single crystal SiC [4-6].

The motivation for developing PAP is to resolve these problems and challenges existing in the conventional CMP process to realize the high-efficiency, low-cost, high-quality and slurryless polishing of 4H-SiC substrates.

4.2.2 Diamond lapping and polishing of 4H-SiC

To obtain a better understanding of the manufacturing process of SiC substrates, the lapping and mechanical polishing of 4H-SiC using diamond abrasives were investigated in this study. Table 4.1 shows the conditions of diamond lapping. The Si face of the SiC substrate was lapped with a large load and a long duration.

Figure 4.2 shows a scanning white light interferometer (SWLI) image of a large area (64 μm × 48 μm) and atomic force microscopy (AFM) images of small areas (5 μm × 5 μm and 500 nm × 500 nm) of the lapped SiC surface. Since diamond is much harder than SiC, many scratches were formed. Also, the surface was rough and not suitable for electronic device applications. Even

Table 4.1 Parameters of diamond lapping

Substrate	4H-SiC (on-axis, 0001)
Load	1650 g
Pad rotation speed	1500 rpm
Substrate rotation speed	200 rpm
Abrasive	Diamond (ϕ=5~15 μm)
Time	24 h

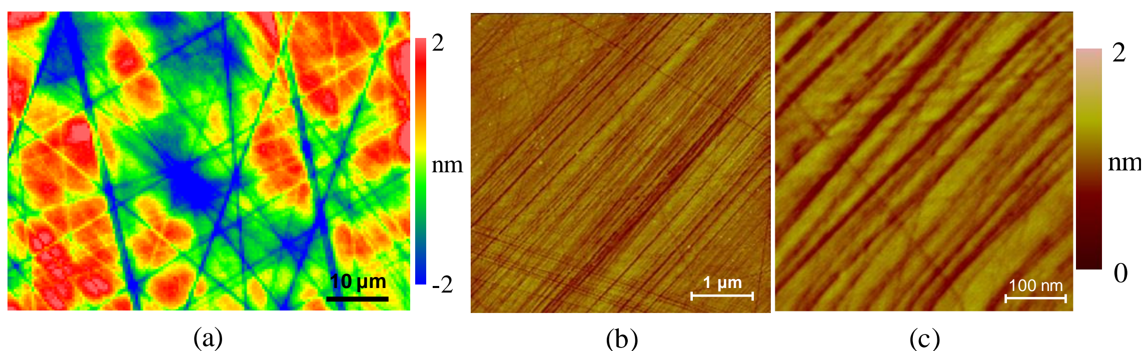

(a) (b) (c)

Figure 4.2 SWLI and AFM images of diamond lapped SiC. (a) SWLI image (p-v: 6.65 nm, rms: 1.02 nm). (b) AFM image (p-v: 3.70 nm, rms: 0.23 nm). (c) AFM image (p-v: 1.26 nm, rms: 0.15 nm).

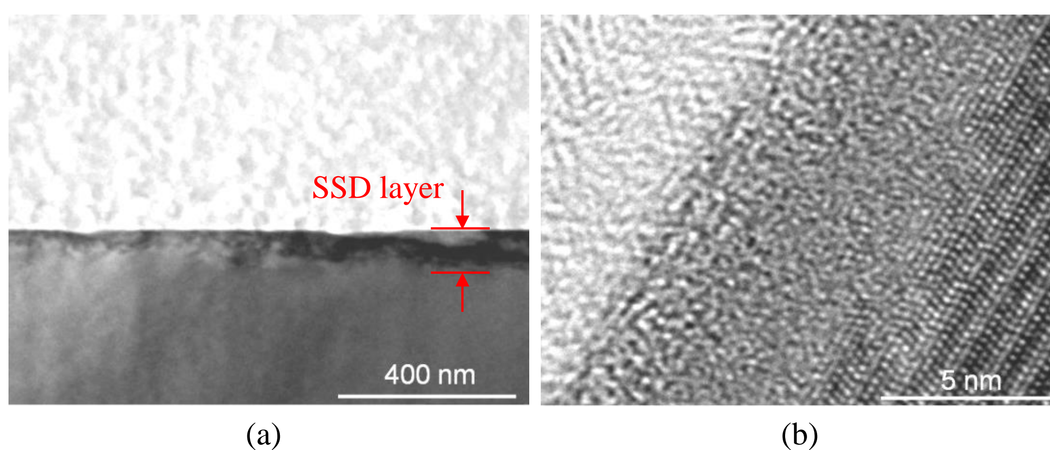

(a) (b)

Figure 4.3 XTEM images of diamond lapped SiC.

though an on-axis substrate was used, the crystal structure (step-terrace structure) of 4H-SiC cannot be observed from the AFM images. Figure 4.3 shows cross-sectional transmission electron microscopy (XTEM) images of the surface of the diamond-lapped SiC substrate. An SSD layer with a thickness of about 100 nm that was formed by diamond lapping can be clearly observed as shown in Figure 4.3(a). As shown in Figure 4.3(b), the existence of an amorphous layer is also confirmed.

The mechanical polishing of SiC using diamond slurry with an abrasive comprising small diamond grains was conducted. With the decrease in the grain size, the scratches became shallow and the formed SSD also became thinner [7]. Figure 4.4

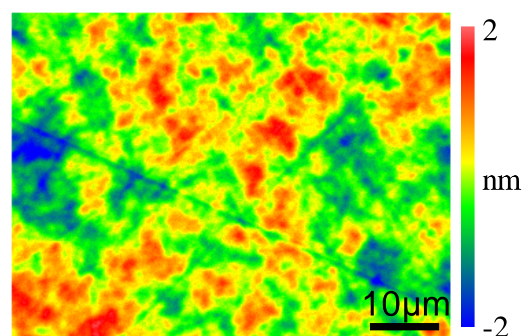

Figure 4.4 SWLI image mechanical polished SiC using diamond slurry. (p-v: 4.41 nm, rms: 0.62 nm)

shows an SWLI image of SiC mechanically polished using a diamond slurry supplied by CREE Co. Ltd. Even though the detailed polishing conditions were not disclosed, it was found that only very shallow scratches were formed. Therefore, the mechanical polishing of SiC using diamond slurry was conducted to reduce the thickness of the SSD and the number of scratches formed by previous grinding or lapping processes.

However, owing to the use of diamond abrasives, many shallow scratches still remained on the polished surface, as shown in Figure 4.4, and there was still a thin SSD layer as previously reported [7]. Thus, a final finishing process of CMP is necessary to remove the residual scratches and the SSD and further improve the surface roughness to the atomic level.

4.2.3 CMP of 4H-SiC

CMP using colloidal SiO_2 slurry is conducted in industry to realize the damage-free and scratch-free finishing of 4H-SiC substrates. As described in Chapter 2, the surface of SiC was modified by the chemicals in a slurry and a modified layer was formed. Compared with the base material, the modified layer was easier to remove. Therefore, soft abrasive polishing using SiO_2 can be conducted to remove the modified layer. SiO_2 is much softer than bulk SiC. Therefore, no scratches or SSD was formed. Finally, a damage-free, scratch-free and atomically flat SiC surface was obtained as widely reported [8].

Figure 4.5 shows SWLI and AFM images of a CMP-processed SiC substrate (on-axis, 0001) supplied by CREE Co. Ltd. As shown in the SWLI image, no scratches were formed by CMP and the surface was very flat with a low surface roughness compared with the diamond-lapped surface and the mechanically polished surface. In the small observation areas shown in Figures 4.5(b) and (c), the step-terrace structure of SiC can be clearly observed even though the step and terraces are not straight and the terrace width is not uniform. This means that an atomically flat surface can be

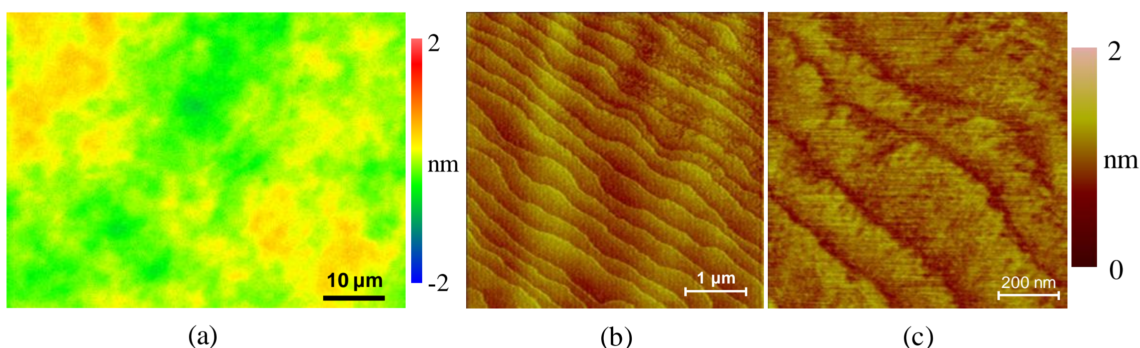

Figure 4.5 SWLI and AFM images of CMP-processed SiC. (a) SWLI image (p-v: 1.57 nm, rms: 0.22 nm). (b) AFM image (p-v: 1.16 nm, rms: 0.14 nm). (c) AFM image (p-v: 1.26 nm, rms: 0.15 nm).

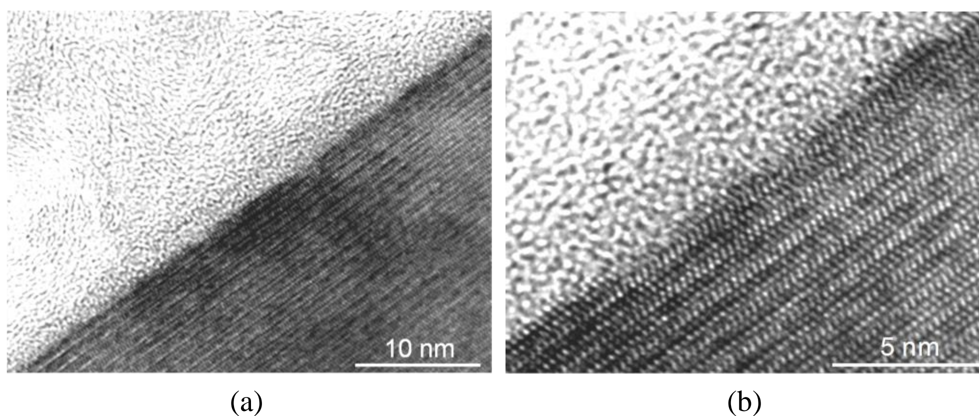

(a) (b)

Figure 4.6 XTEM images of CMP-processed SiC.

Table 4.2 Parameters of slurry polishing of 4H-SiC

Experimental setup	cf. Figure 3.5
Substrate	4H-SiC (on-axis, 0001)
Load	50 g
Pad rotation speed	2000 rpm
Polishing pad	Suede type, NP178 (ϕ10 mm)
Slurry concentration	Diamond: 0.4 wt%, Al_2O_3: 10 wt%, SiO_2: 1 wt%, CeO_2: 1 wt%
Grain size	Diamond: 100 nm, Al_2O_3: 100 nm, SiO_2: 72 nm, CeO_2: 190 nm
Time	3 h

obtained by CMP using SiO_2 slurry. Such a flat surface can be further processed by other semiconductor procedures such as annealing, epitaxial growth, doping, chipping and so forth.

Figure 4.6 shows XTEM images of the SiC surface processed by CMP. The existence of the SSD layer, as shown in Figure 4.3, can no longer be observed. As shown in Figure 4.6(b), an amorphous layer, which is usually formed in mechanical polishing, was not formed after CMP. That is to say, a damage-free 4H-SiC surface was obtained by a conventional CMP process using SiO_2 slurry. Even though an ultrasmooth surface can be obtained by CMP, many extractions of atoms from the surface can be clearly observed.

SiO_2 slurry has been used for finishing SiC substrates in industry. However, it is necessary to evaluate the polishing characteristics of different abrasives to clarify the type of abrasive that can

be used in PAP. Four types of slurry were investigated for polishing SiC: diamond, Al_2O_3, SiO_2 and CeO_2 slurries. Table 4.2 shows the polishing conditions.

Figure 4.7 shows AFM images of the SiC surfaces polished using the different kinds of slurry. In the case of CMP using the diamond slurry, the surface was similar to that shown in Figure 4.2. Many scratches were formed owing to the high hardness of diamond. In the case of CMP using the Al_2O_3 slurry, the polished surface was quite rough. Fewer scratches were formed since the hardness of Al_2O_3 is slightly lower than that of SiC; however, there were many pits, which greatly deteriorated the surface roughness. It was assumed that these pits were formed by the chemicals in Al_2O_3 slurry. In the case of CMP using the SiO_2 and CeO_2 slurries, scratch-free SiC surfaces with a step-terrace structure were obtained. When the SiO_2 slurry was used, a step-terrace structure with four types of terrace that appeared alternately was formed, while the step-terrace structure formed by CeO_2 slurry polishing had a very uniform terrace width. This was considered to be due to the difference in the balance between chemical factors and mechanical factors in the slurry polishing of 4H-SiC, which will be discussed in detail in the next chapter. From the above results, it was concluded that SiO_2

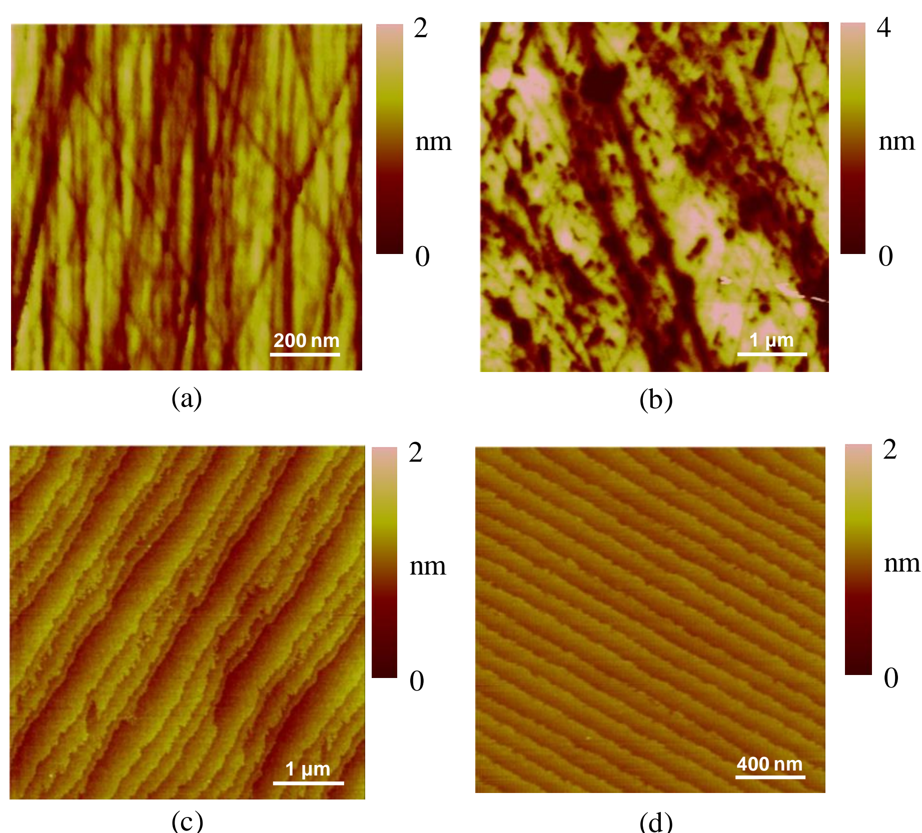

Figure 4.7 AFM images of CMP-processed SiC. (a) Diamond slurry (p-v: 2.46 nm, rms: 0.30 nm). (b) Al_2O_3 slurry (p-v: 30.63 nm, rms: 1.28 nm). (c) SiO_2 (p-v: 2.01 nm, rms: 0.15 nm). (d) CeO_2 (p-v: 0.68 nm, rms: 0.08 nm).

and CeO_2 had the better polishing characteristics for 4H-SiC to obtain scratch-free and atomically flat SiC surfaces. Therefore, in the PAP of 4H-SiC, SiO_2 and CeO_2 grinding stones were used.

4.3 Modification of 4H-SiC by AP-plasma irradiation [9-11)]

To realize the surface modification of 4H-SiC, two types of plasma: oxygen-containing plasma and water-vapor-containing plasma, were investigated. As described in Chapter 3, both plasmas can be used for the surface oxidation of SiC. To compare the surface modification efficiency of the two plasmas, ball-on-disc tests were conducted. Figure 4.8 shows a schematic view of the experimental setup used for the ball-on-disc tests. This setup is very similar to the symmetric-type PAP machine

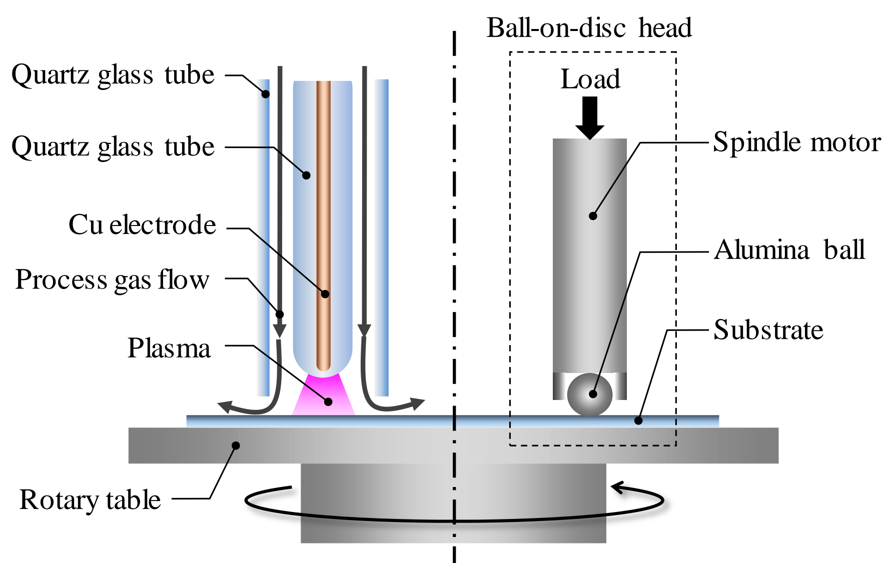

Figure 4.8 Schematic view of the experimental setup used for ball-on-disc tests.

Table 4.3 Parameters of ball-on-disc tests

Ball material	Alumina
Load	100 g
Rotation speed	69.1 mm/s
Process gas	He + H_2O (2.6%), He + O_2 (2.6%)
Flow rate	1.5 slm
RF power	30 W
Processing time	30 min

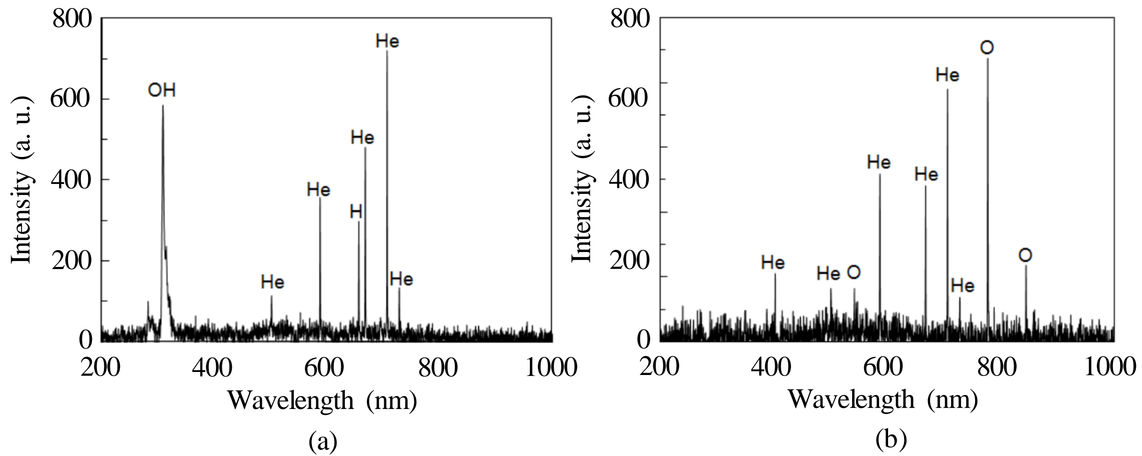

Figure 4.9 OES spectra of water vapor contained plasma (a) and oxygen contained plasma (b).

shown in Figure 3.5, with an alumina ball used instead of the polishing film. The test sample was installed on a rotary table, and surface modification by plasma irradiation and mechanical removal using the alumina ball were alternately conducted.

Figure 4.9 shows the OES spectra of the AP-oxygen-containing plasma and AP-water-vapor-containing plasma. The emission spectra from each plasma were measured using a multichannel spectrometer (Ocean Optics, USB4000). In the case of the water-vapor-containing plasma, strong emissions from OH molecules ($A^2\Sigma^+ \rightarrow X^2\prod$, λ=309 nm) were observed [12)], as shown in Figure 4.9(a), and in the case of the oxygen-containing plasma, emissions from oxygen atoms ($3p^5P \rightarrow 3s^5S$, λ=777 nm and $3p^3P \rightarrow 3s^3S$, λ=845 nm) were observed, as shown in Figure 4.9(b). From these measurement results, the major reactive species inducing surface modification in the water-vapor- and oxygen-containing plasmas were considered to be OH and O radicals, respectively [13)].

Figure 4.10 shows cross sections of the SiC surfaces subjected to the ball-on-disc test under the conditions shown in Table 4.3. These results indicate that the irradiation of the plasma increases the depth of abrasion. In particular, the irradiation of the water-vapor-containing plasma increased the depth of abrasion more than 20-fold in comparison with the case without

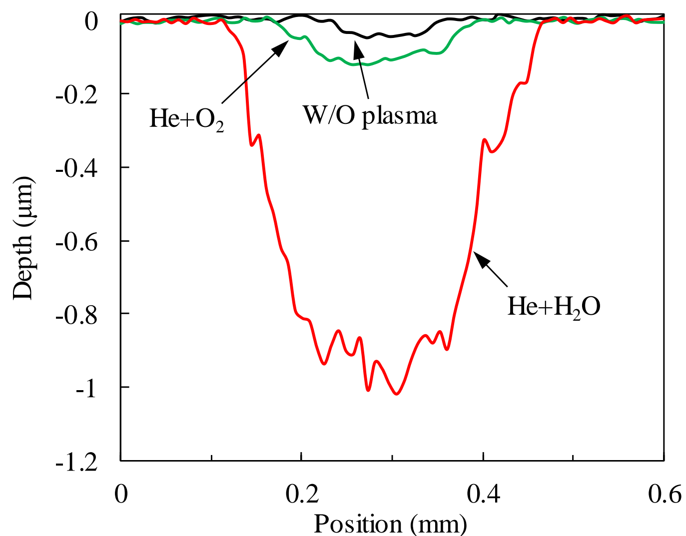

Figure 4.10 Cross-section of SiC surface after ball-on-disc test.

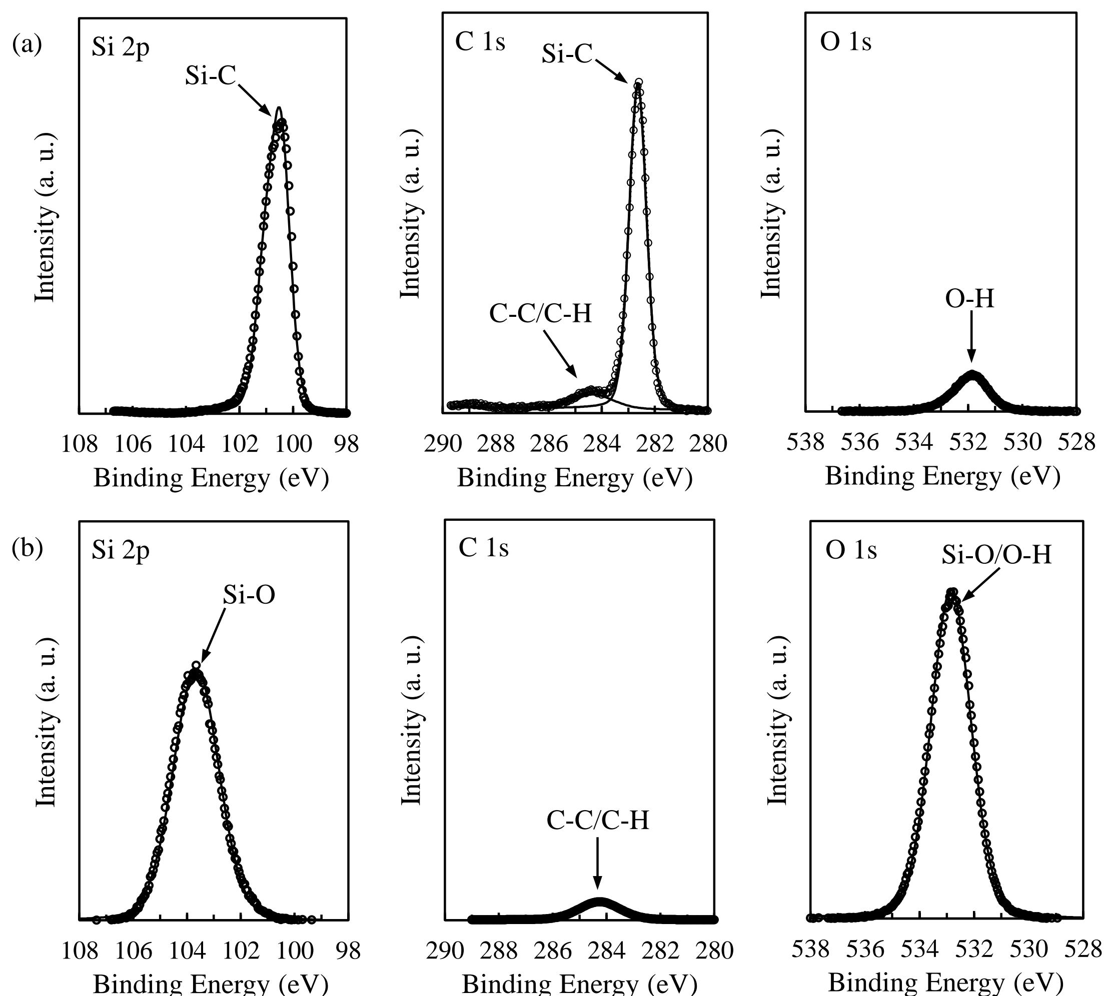

Figure 4.11 XPS spectra of 4H-SiC (0001) surfaces before and after water vapor contained plasma irradiation. (a) Without plasma irradiation. (b) After water vapor contained plasma irradiation for 1 h.

plasma irradiation. The results of the ball-on-disc test imply that the oxidation power of OH radicals was higher than that of O radicals. This is reasonable because the oxidation potential of OH (2.80 V) is greater than that of O (2.42 V).

To determine the composition of the modified layer, X-ray photoelectron spectroscopy (XPS) measurements were conducted. Figures 4.11(a) and (b) respectively show the XPS spectra of the SiC surfaces without and with the irradiation of water-vapor-containing plasma. Before plasma irradiation, as shown in Figure 4.11(a), no peaks corresponding to the oxide layer were observed. A peak from C-C/C-H bonds was observed, which was considered to be due to the contamination from the ambient. O-H bonds existed on the pretreated surface, which originated from the adsorption of water in air or OH termination [14]. After plasma irradiation for 1 h, as shown in Figure 4.11(b),

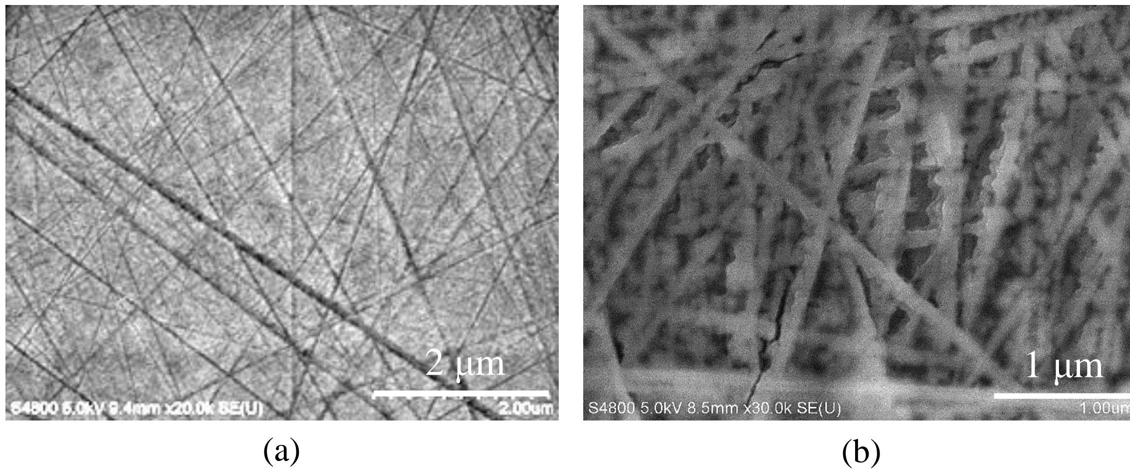

(a) (b)

Figure 4.12 SEM images of 4H-SiC (0001) surface: (a) Unprocessed surface and (b) Processed surface irradiated by water vapor contained plasma.

strong peaks from Si-O bonds were detected, which indicated the generation of an oxide layer. As shown in the Si2p spectra in Figure 4.11(b), Si-C bonds were no longer detected. This means that the thickness of the oxide layer was larger than the detection depth of XPS, which was usually several nm. From the above results, it was concluded that the water-vapor-containing plasma was very effective for the surface modification of 4H-SiC (0001) and that the main oxidation product was SiO_2, which was considered to be softer than SiC.

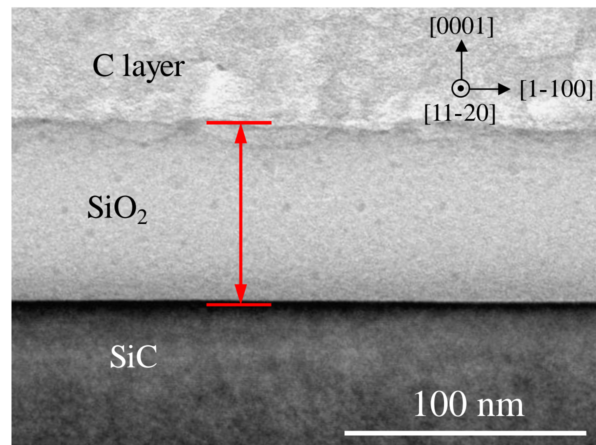

Figure 4.13 XTEM image of surface irradiated by water vapor contained plasma for 1 h.

Table 4.4 Conditions of plasma irradiation

Experimental setup	cf. Figure 3.4
Specimen	4H-SiC (0001)
Process Gas	He + H_2O (2.6%)
Flow Rate	1.5 slm
RF Power	15 W
Processing Time	6 h
Irradiated Area	15 mm × 15 mm

Figure 4.12 shows scanning electron microscopy (SEM) images of a 4H-SiC (0001) surface before and after the irradiation of water-vapor-containing plasma. In this case, surface removal by abrasive polishing was not conducted. After the plasma irradiation, many swelling-like structures were observed along the scratches on the surface. In the case of another specimen having very shallow scratches, there were no swelling-like structures on the surface after

the irradiation of water-vapor-containing plasma. Therefore, it is assumed that the SSD and lattice strain remaining in the vicinity of the deep scratches shown in Figure 4.12(a) enhanced the local oxidation in AP-plasma irradiation. This result implies that the damaged region will be preferentially removed by the subsequent abrasive polishing in PAP.

Figure 4.13 shows an XTEM image of a 4H-SiC (0001) surface irradiated by water-vapor-containing plasma for 1 h using the experimental setup shown in Figure 3.8. He with a flow rate was 3.0 slm was used as the carrier gas. The applied RF electric power was 16 W. As shown in the XTEM image, an oxide layer with a thickness of about 80 nm was formed. Also, although the surface of the oxide layer was very rough, the SiO_2/SiC interface was atomically flat, the reason for which is discussed later.

In PAP, the aim of plasma irradiation is to modify the surface of the substrate and make it softer and easier to remove. Therefore, it is necessary to measure the change in surface hardness. Nanoindentation measurements were conducted using a nanoindenter (Elionix ENT2100) to evaluate the hardness of the surface modified by irradiation of the water-vapor-containing plasma. Table 4.4 shows the conditions of the plasma irradiation and Table 4.5 shows the conditions of the nanoindentation tests. Figure 4.14 shows the hardnesses of the as-received 4H-SiC (0001) wafer and its modified surface, which were measured by the nanoindentation method. A Berkovich-type indenter made of diamond was used,

Table 4.5 Conditions of nanoindentation tests

Approach Speed	1000 nm/min
Delta Slope Contact	50%
Max Load	0.5 mN
Loading Rate	1.0 mN/min
Unloading Rate	1.0 mN/min
Pause	60 s

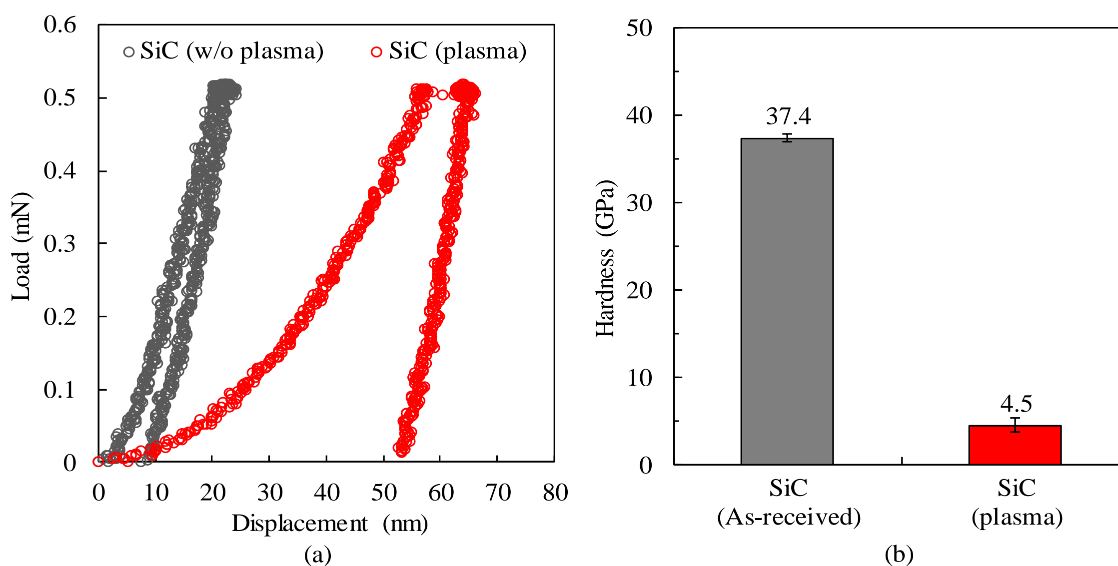

Figure 4.14 Nanoindentation tests of 4H-SiC (0001). (a) Load-displacement curve. (b) Hardnesses caculated from measured data (a).

and the number of measurement points and the maximum load for each sample were 5 and 0.5 mN, respectively. The hardness of the surface was calculated by the Oliver-Pharr method [15]. From this figure, it was found that irradiation of the water-vapor-containing plasma decreased the hardness of the 4H-SiC surface from 37.4 ±0.5 GPa to 4.5 ±0.8 GPa by modifying the surface composition. This result indicates that the irradiation of water-vapor-containing plasma is effective for modifying a hard SiC surface to a soft layer.

To realize the practical use of PAP, a higher MRR than that in commercial CMP processes is crucial. In the PAP process, when the SiC surface is irradiated by water-vapor-containing plasma, it is oxidized and a soft oxide layer is formed. Since the simultaneous conduction of plasma irradiation and abrasive polishing is expected to be carried out, the oxide layer is predicted to be immediately removed by abrasive polishing. Thus, it is necessary to increase the oxidation rate of plasma irradiation to increase the MRR of the PAP process.

Although the oxidation mechanism of SiC by irradiation with water-vapor-containing plasma has not yet been completely clarified, it is considered that this process may be affected by several factors such as the temperature of the substrate, the density of OH radicals, the pressure of the ambient, the flow rate of the process gas and so forth. Since SiC is oxidized by OH radicals, the density of OH radicals appears to be the most important factor in the oxidation. Therefore, in this study, the optical emission intensity from OH radicals in He-based water-vapor-containing plasma was focused on.

As previously reported, the water vapor concentration in the carrier gas (He or Ar) can greatly affect the density of optical emission from OH radicals in the plasma [16]. Therefore, the plasma oxidation process was optimized to find the optimum water vapor concentration

Table 4.6 Conditions of plasma generation

Experimental setup	cf. Figure 3.8
Specimen	4H-SiC (0001), on-axis
Carrier gas	He
Flow rate	2.0 slm
Applied RF power	25 W
Plasma irradiation time	10 min
Acquisition time for OES	60 s

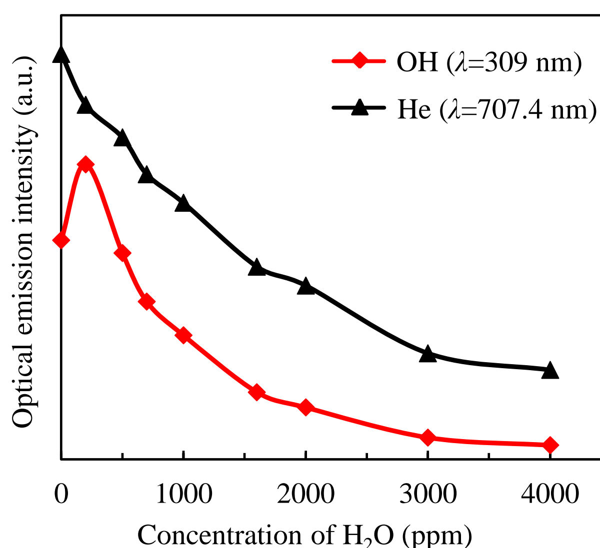

Figure 4.15 Dependence of the OH and He optical emission intensity from water vapor contained plasma on the concentration of water vapor in He.

resulting in the highest oxidation rate. Plasma irradiation was conducted with different concentrations of water vapor in the process gas under the conditions shown in Table 4.6. During plasma irradiation, OES spectra were continuously measured. Figure 4.15 shows the relationship between the intensity of OH and He radicals and the water vapor concentration in He. In this figure, a water vapor concentration of 0 ppm corresponds to the lower limit of detection (LLD: 126 ppm) of the DPM. It was found that the intensity of the head of the OH band (λ=309 nm) was greatest when the water vapor concentration was approximately 200 ppm. OH radicals were generated by the dissociation of water molecules due to electron impact. When the water vapor concentration was lower than 200 ppm, the intensity of OH radicals increased with increasing water vapor concentration because the increase in water vapor concentration promoted the dissociation due to electron impact. On the other hand, when the water vapor concentration exceeded 200 ppm, the excessive supply of water vapor decreased the electron temperature (Te), inhibiting the dissociation of water vapor molecules. Also, the effective quenching of excited states of OH radicals at a high water vapor concentration greatly decreased their density [16]. These factors may explain why there was an optimal water vapor concentration for obtaining the strongest optical emission intensity from the OH radicals in the water-vapor-containing plasma.

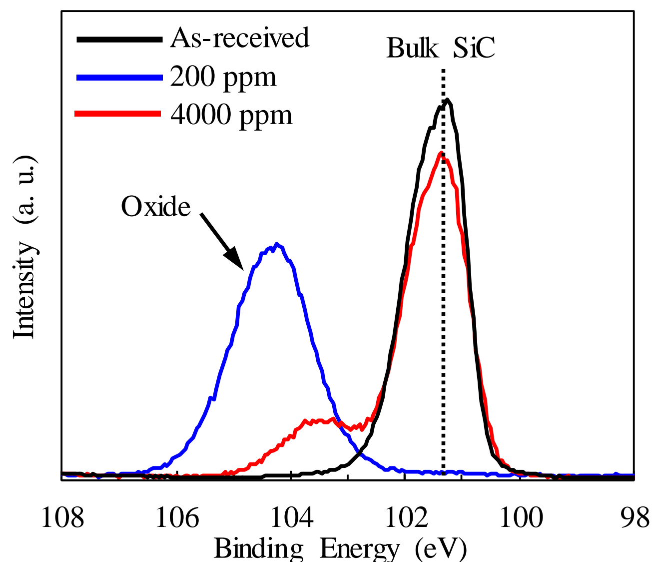

Figure 4.16 Si2p XPS spectra of SiC surfaces with different processes.

Figure 4.16 shows the Si2p XPS spectra of SiC surfaces processed by the irradiation of plasma under the conditions shown in Table 4.6 with water vapor concentrations of 200 ppm and 4000 ppm. In these experiments, the stage with the SiC specimen was heated to 200 ℃ to increase the oxidation rate. As shown in Figure 4.15, when the water vapor concentration was 200 ppm, the intensity of OH radicals was much higher than that for a water vapor concentration of 4000 ppm. Therefore, as revealed in Figure 4.16, the oxide layer on the surface processed by plasma oxidation with a water vapor concentration of 4000 ppm was very thin, while the surface irradiated by plasma with a water vapor concentration of 200 ppm was completely oxidized within the measuring depth of XPS.

4.4 Application of the symmetric PAP machine [17, 18]

The symmetric PAP machine was used to polish a 4H-SiC (0001) on-axis substrate using a polishing film with a ceria abrasive (CE10000-FB GMY-C) supplied by MIPOX Co. Ltd. The substrate was supplied by CREE Co. Ltd. with the surface polished by diamond slurry. The ceria abrasive with an average grain size of 0.5 μm was fixed on the polyethylene terephthalate (PET) polishing film using a polyester-polyurethane adhesive. The hardness of ceria, which is 5-7.5 GPa [19], is lower than that of SiC. Therefore, it was expected that the ceria abrasive would remove only the soft modified layer without the formation of scratches on the SiC surface. The experimental parameters are listed in Table 4.7.

Table 4.7 Conditions of application of symmetric PAP machine

PAP machine	cf. Figure 3.1
Specimen	2 inch, n-type 4H-SiC (0001), 0.29 °-off
Abrasive	CeO_2 polishing film (0.5 μm)
Reactive Gas	He + H_2O (2.0%)
Flow Rate	1.5 slm
RF Power	6 W
Load	30 g
Rotation Speed	Substrate: 120 rpm, Polishing Film: 10,800 rpm
Polishing time duration	3 h

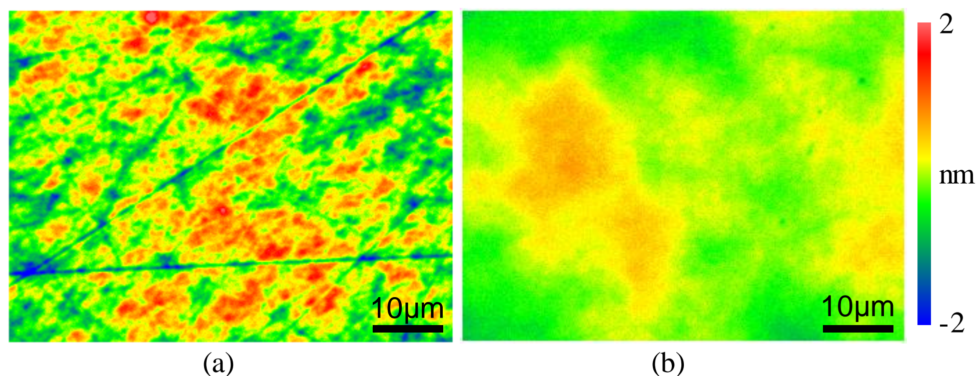

Figure 4.17 SWLI images of processed 4H-SiC wafer. (a) The surface polished by ceria abrasive without plasma irradiation (p-v: 5.49 nm, rms: 0.57 nm). (b) The surface processed by PAP (p-v: 1.89 nm, rms: 0.28 nm).

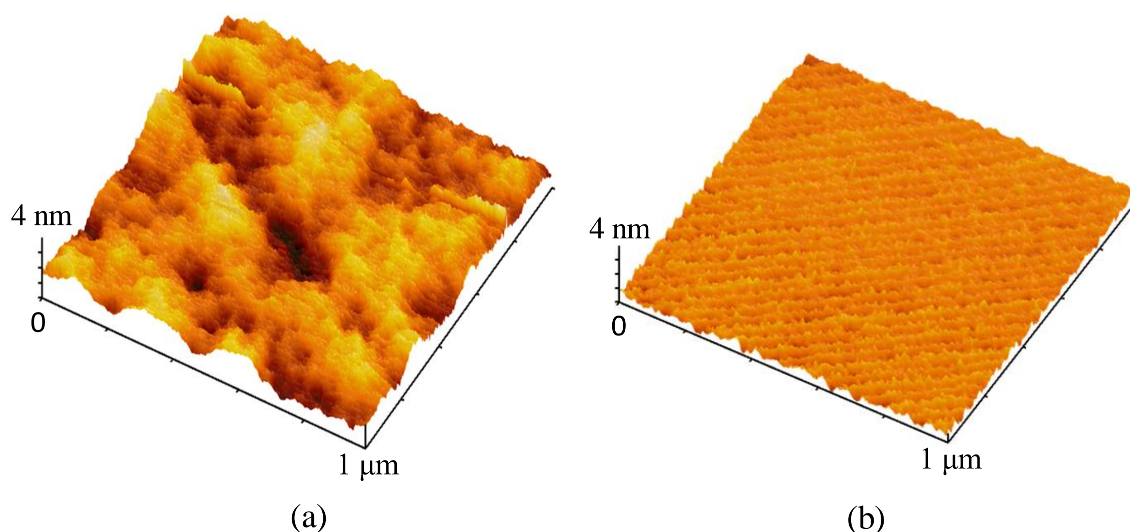

Figure 4.18 AFM images of the 4H-SiC surface. (a) Before PAP. (3.06 nm p-v, 0.42 nm rms) (b) After PAP (1.27 nm p-v, 0.14 nm rms).

Table 4.8 Conditions of application of symmetric PAP machine

PAP machine	cf. Figure 3.1
Specimen	2 inch, n-type 4H-SiC (0001), on-axis
Abrasive	CeO_2 polishing film (0.5 μm)
Reactive Gas	He + H_2O (1.38%)
Flow Rate	1.5 slm
RF Power	18 W
Load	80 g
Rotation Speed	Substrate: 120 rpm, Polishing Film: 10,500 rpm
Polishing time duration	60 min

Figures 4.17(a) and (b) respectively show SWLI images of the surface of the SiC substrate polished by the ceria abrasive without plasma irradiation and the surface processed by PAP. In the case of ceria abrasive polishing, there was no change in the surface morphology compared with that of the as-received wafer. Scratches were still observed and the surface was still very rough. Since the SiC surface was not modified and SiC is much harder than CeO_2, it was considered that the removal of SiC did not occur in this polishing without plasma irradiation. In contrast, the scratches and waviness were completely removed after PAP as shown in Figure 4.17(b).

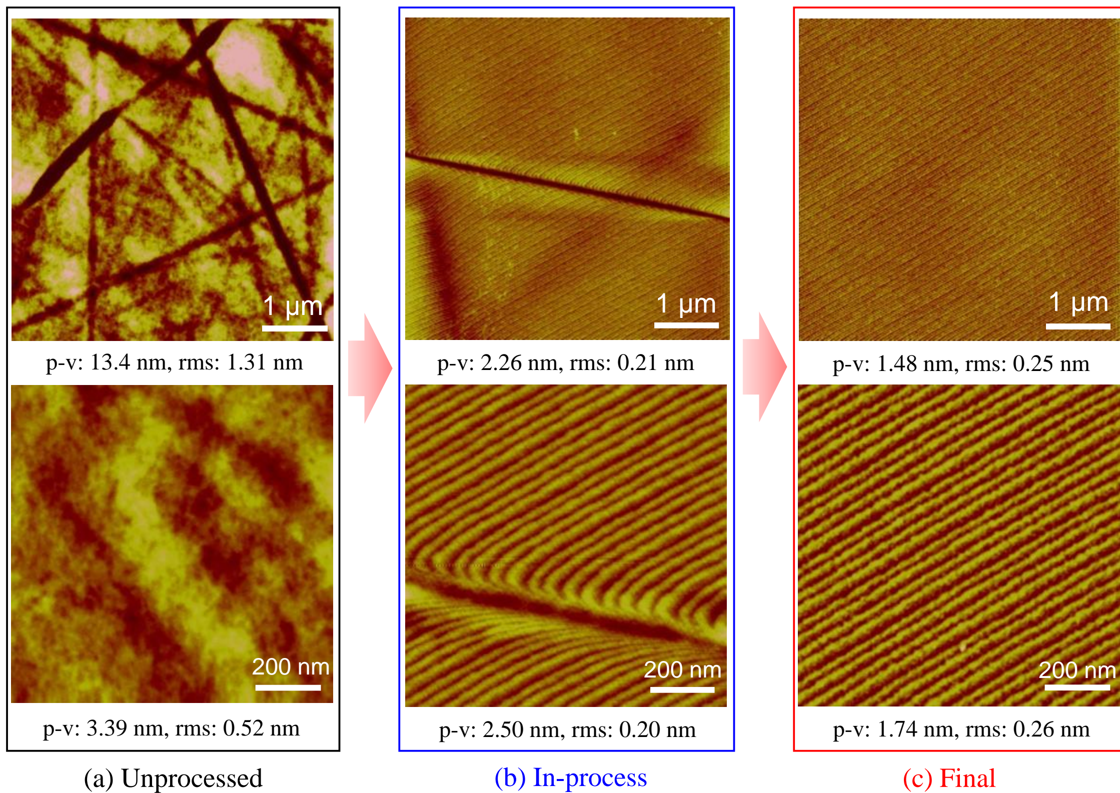

Figure 4.19 AFM images of the surface of SiC substrate during different polishing stage. (a) The unprocessed SiC surface. (b) SiC surface at the in-process stage of PAP. (c) SiC surface at the final stage of PAP.

Figures 4.18(a) and (b) respectively show AFM images of the 4H-SiC substrate before and after processing by PAP. All the scratches formed by diamond slurry polishing were completely removed by PAP, and a well-ordered step-terrace structure, which corresponds to the inclination of the crystal plane (0.29°), was clearly observed. While the step-terrace structure of single-crystal SiC cannot be observed on a surface finished by conventional diamond abrasive polishing, a chemically assisted removal process such as CMP or CARE enables such a structure to be obtained. From these results, it is concluded that PAP enables an atomically flat surface of single-crystal SiC with a micrometer spatial wavelength to be obtained and that a chemical reaction is dominant in the PAP removal process.

Figure 4.19 shows AFM images of the surface of a SiC substrate during different stages of PAP under the polishing conditions shown in Table 4.8. The unprocessed surface was polished using diamond slurry. Thus, many scratches were formed and the step-terrace structure of SiC could not be observed. With the application of PAP, the scratches were gradually removed. Figure 4.19(b) shows the PAP-processed surface of SiC, in which a deep scratch remained. The original shallow

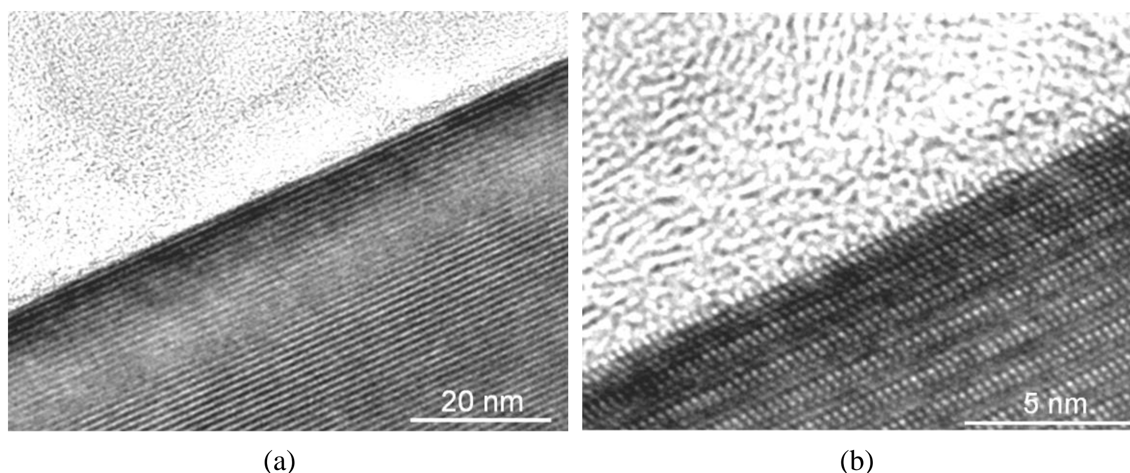

(a) (b)

Figure 4.20 XTEM images of 4H-SiC surface processed by PAP using ceria abrasives. (a) Low resolution image. (b) High resolution image

scratches were completely removed and the area adjacent to the deep scratch was atomically flat with the formation of a well-ordered step-terrace structure. This surface was considered to correspond to the in-process stage of PAP. Figure 4.19(c) shows the surface of the same SiC substrate processed by PAP observed in a scratch-free area. With the continuation of PAP, the deep scratches were also removed. Thus, a scratch-free and atomically flat surface with a well-ordered step-terrace structure, as shown in Figure 4.19(c), was obtained. This surface was considered to correspond to the final stage of PAP.

Figure 4.20 respectively shows low- and high-resolution XTEM images of a 4H-SiC (0001) surface processed by PAP using a ceria abrasive under the polishing conditions shown in Table 4.8. No oxide layer remained on the surface, which indicates that the oxidation rate of the plasma was lower than the removal rate of the oxide layer. Consistent with the SWLI and AFM observations, no scratches exist on the surface. Also, there was no evidence of subsurface damage from the contrast. An enlarged image of the surface is shown in Figure 4.20(b). A periodic well-ordered structure, which corresponds to the crystal structure of 4H-SiC, was continuously observed from the bulk region to the topmost surface. The amorphous layer formed by mechanical polishing was not formed, and the extraction of atoms from the surface, which occurred on surfaces processed by CMP, could not be observed on this surface processed by PAP. This result indicates that almost no crystallographic subsurface damage was formed by PAP using the ceria abrasive. On the top surface, silicon atoms were well ordered and arranged without extractions or cracks, which means that an atomically flat SiC surface was obtained.

In PAP, polishing using a soft abrasive is conducted to remove the modified layer formed by plasma modification. The above results demonstrated that CeO_2 abrasive is very useful for finishing

4H-SiC. For comparison, PAP of 4H-SiC using Al_2O_3 abrasive was also conducted. The experimental parameters are shown in Table 4.9. Figure 4.21(a) shows an SWLI image of the processed surface, which has a p-v roughness of 16.30 nm and an rms roughness of 1.54 nm. Unlike the surface polished by diamond abrasive, many short or shallow scratches can be observed. The above-mentioned XPS results indicate that SiO_2 was formed after 4H-SiC was oxidized by water-vapor-containing plasma. The hardness of Al_2O_3 is much higher than that of SiO_2 [19]; this made it possible for 4H-SiC to be polished by the Al_2O_3 abrasive after it was modified by the water-vapor-containing plasma. Also, a previous study revealed that in the PAP process the oxidation rate of water-vapor-containing plasma was lower than the material removal rate of abrasive polishing. Thus, the SiO_2 layer was immediately removed in the PAP process. Also, it has been widely reported that an intermediate layer consisting of silicon oxycarbide (Si-C-O) was formed after the oxidation of SiC [20]. Since Si-C-O is a product of insufficient oxidation, it is reasonable to assume that its hardness is between that of SiC, which was the base material, and SiO_2, which was the product in the case of sufficient oxidation. After SiO_2 was removed, the polishing of Si-C-O and SiC was conducted. The hardness of the interface oxide layer was comparable to that of Al_2O_3; thus,

Table 4.9 Conditions of PAP using Al_2O_3 abrasives

PAP machine	cf. Figure 3.1
Specimen	2 inch, 4H-SiC (0001), on-axis
Abrasive	Al_2O_3 polishing film (0.5 μm)
Reactive Gas	He + H_2O (1.38%)
Flow Rate	1.5 slm
RF Power	18 W
Load	80 g
Rotation Speed	Substrate: 120 rpm Polishing Film: 10,500 rpm
Polishing time duration	30 min

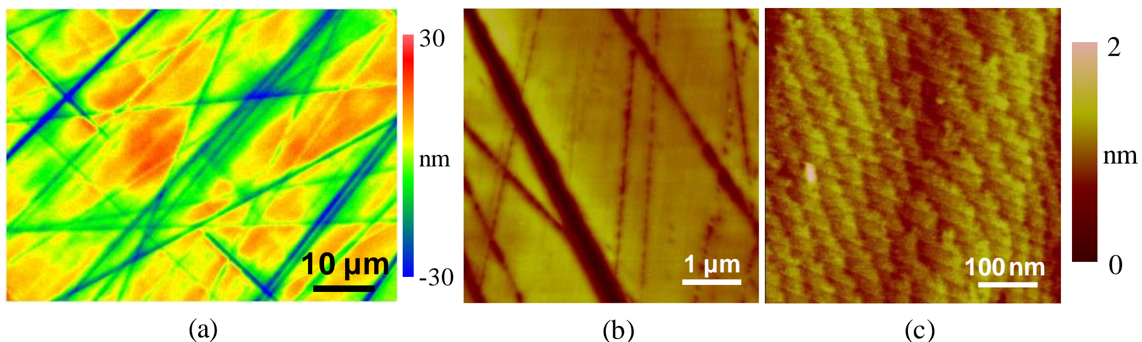

Figure 4.21 SWLI and AFM images of PAP processed SiC using Al_2O_3 abrasives. (a) SWLI image (p-v: 16.30 nm, rms: 1.54 nm). (b) AFM image (p-v: 5.01 nm, rms: 0.57 nm). (c) AFM image (p-v: 1.01 nm, rms: 0.10 nm).

after the top layer was completely removed, the interface oxide layer was destroyed but not completely removed. This is why short and shallow scratches were formed as shown in Figure 4.21(a). The areas without scratches appeared to be very flat as shown in Figure 4.21(b). AFM observation of these scratch-free areas was also conducted as shown in Figure 4.21(c). A disordered step-terrace structure was observed in the scratch-free areas. Even though the step-terrace structure of SiC was formed by PAP using Al_2O_3 abrasive, scratches were formed, which deteriorated the surface integrity as well as the roughness. Therefore, it is concluded that Al_2O_3 is not suitable for the PAP of 4H-SiC.

With the application of the symmetric PAP machine, the finishing ability of PAP for 4H-SiC (0001) has been confirmed. By combining water-vapor-containing plasma modification and CeO_2 abrasive polishing, a scratch-free and atomically flat surface was obtained.

4.5 Application of two-step PAP process

The two-step PAP process was applied to 4H-SiC (0001). In this process, a thick modified layer was first formed by plasma irradiation. After that, the modified layer was removed by polishing using a soft abrasive. In addition to the two-step PAP process, the oxidation process of SiC by water-vapor-containing plasma and the removal process using CeO_2 abrasive were investigated separately.

4.5.1 Oxidation of 4H-SiC (0001) by water-vapor-containing plasma [21)]

To clarify the atomic flattening mechanism of PAP, the oxidation process of 4H-SiC (0001) by irradiation with water-vapor-containing plasma was studied.

As previously mentioned, a thick oxide layer with a thickness of about 80 nm was formed after irradiation with water-vapor-containing plasma for 1 h using the experimental setup shown in Figure 3.8. Also, it was found that the interface between the oxide layer and the bulk SiC was very flat. With the application of the symmetric PAP machine, it has been demonstrated that the removal of the oxide layer is possible by polishing using CeO_2 abrasive. On the basis of the above results, I assumed the flattening mechanism of PAP to be as follows. A rough SiC surface was irradiated by water-vapor-containing plasma, after which an oxide layer was formed with a very flat SiO_2/SiC interface.

Table 4.10 Conditions of plasma irradiation

Experimental setup	cf. Figure 3.8
Specimen	4H-SiC (0001), on-axis
Carrier gas	He
Flow rate	3.0 slm (1.38 %)
Applied RF power	16 W
Plasma irradiation time	1 h

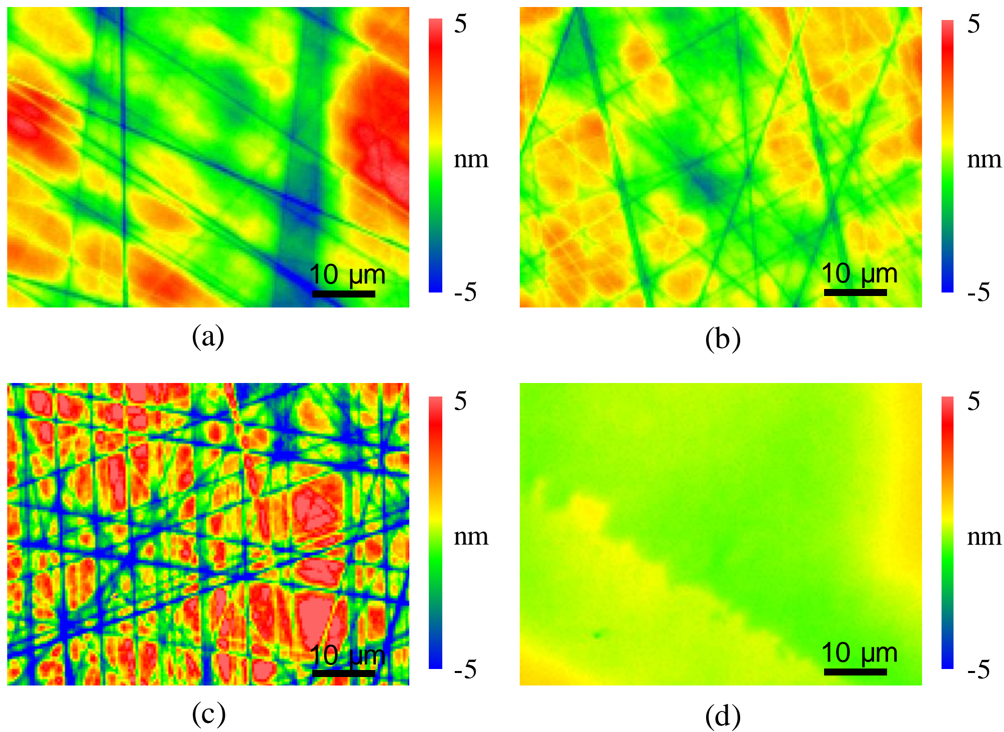

Figure 4.22 SWLI images of processed 4H-SiC surfaces. (a) Diamond lapped surface (11.14 nm p-v, 1.80 nm rms). (b) After first cycle of plasma oxidation and HF dipping (6.65 nm p-v, 1.02 nm rms). (c) After second cycle (8.39 nm p-v, 2.83 nm rms). (d) After third cycle (2.45 nm p-v, 0.45 nm rms).

Then, a soft abrasive, such as CeO_2 was used to remove only the oxide layer to obtain a flat SiC surface. To verify the assumed mechanism, the following experiments were conducted.

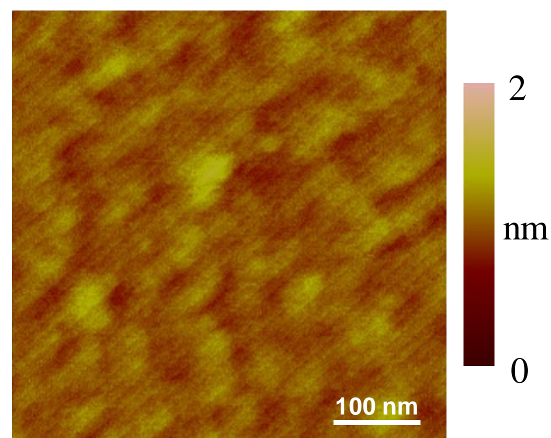

Figure 4.23 AFM image of the surfaces processed by plasma oxidation followed by HF dipping (0.95 nm p-v, 0.11 nm rms).

A new specimen processed by CMP was first lapped by diamond abrasive. Diamond is much harder than SiC; therefore, many scratches were formed as shown in Figure 4.22(a). Then, this surface was irradiated by water-vapor-containing plasma for 1 h to oxidize the surface under the conditions shown in Table 4.10, and the oxide layer was etched off by HF dipping (50 wt%, 10 min). After the removal of the oxide layer, the scratches formed by diamond lapping became much shallower as shown in Figure 4.22(b). Next, a second plasma

irradiation and HF dipping were conducted. As shown in Figure 4.22(c), many deep scratches emerged, which are considered to originate from the subsurface damage layer formed by diamond abrasive lapping. Finally, a third plasma irradiation and HF dipping were conducted. A scratch-free surface was obtained with a much lower surface roughness as shown in Figure 4.22(d). Also, this surface was observed using AFM. Even though it was as flat as the surface processed by PAP shown in Figure 4.19(c), no step-terrace structure of 4H-SiC was observed as shown in Figure 4.23.

The composition of surfaces processed by irradiation with water-vapor-containing plasma and HF dipping was analyzed by angle-resolved XPS (ARXPS). Figure 4.24 shows the Si2p spectra of the surface irradiated by water-vapor-containing plasma for 5 min. Strong peaks corresponding to Si-O bonds and weak peaks corresponding to Si-C-O bonds were observed. The take-off angle of

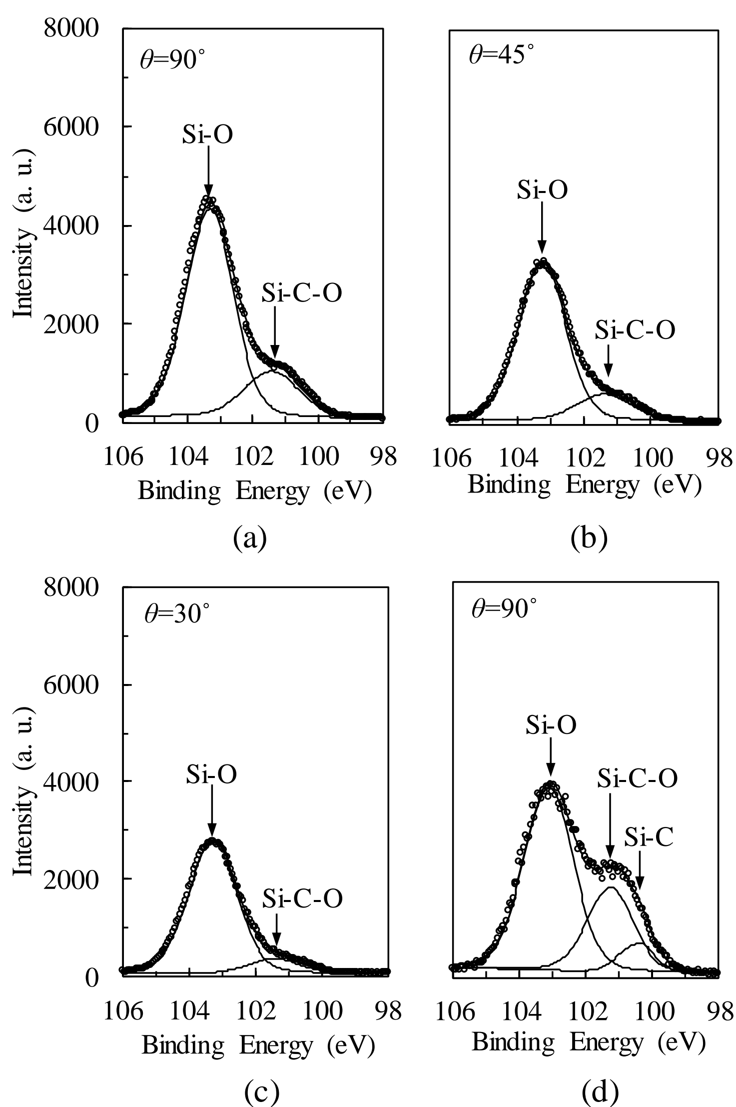

Figure 4.24 ARXPS spectra (Si2p) of water vapor contained plasma irradiated 4H-SiC surface. (θ=take off angle).

the specimen platen was decreased from 90˚ to 45˚ and then to 30˚. The intensity ratio of the Si-O peak and to the Si-C-O peak also increased from 3.75 (a) to 4.98 (b) and 7.67 (c) with the decrease in the take-off angle. These results indicated that there might be a layer structure between silicon oxide and silicon oxycarbide rather than a mixture. A peak corresponding to Si-C bonds was not observed as the thickness of the oxide layer (including silicon oxide and silicon oxycarbide) exceeded the detection depth of XPS, which was only several nm. One min of Ar^+ ion sputtering was conducted on this surface with a low acceleration voltage of about 1.0 kV. Since silicon oxide was partially removed, the peak corresponding to Si-C bonds appeared as shown in Figure 4.24(d). This surface was also observed by XTEM. These observation results are shown in Figure 4.25. Between the oxide layer and the bulk SiC, there was an intermediate layer which had lost the

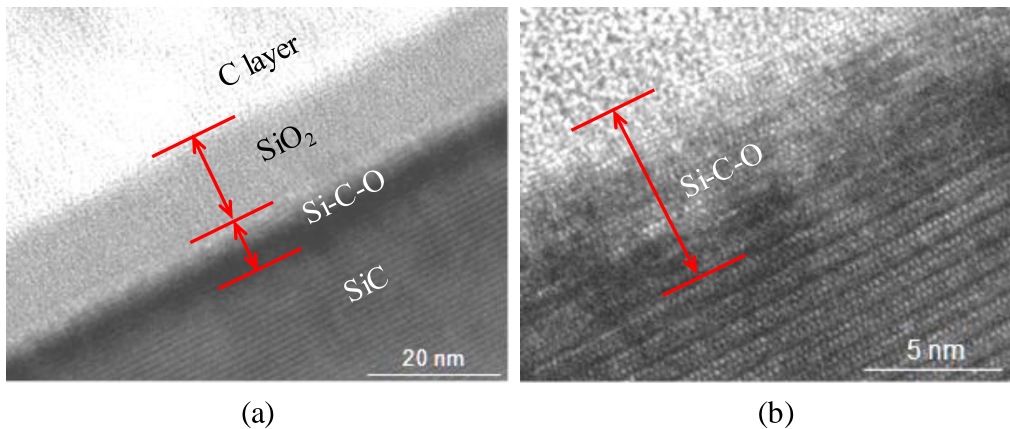

(a) (b)

Figure 4.25 XTEM images of water vapor contained plasma irradiated 4H-SiC surface.

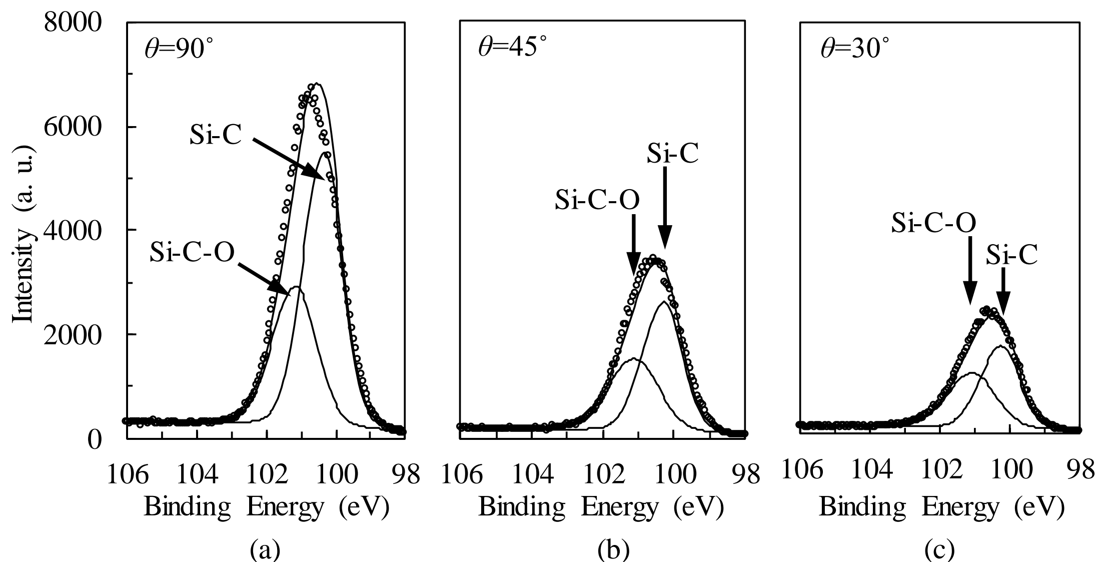

(a) (b) (c)

Figure 4.26 ARXPS spectra (Si2p) of water vapor contained plasma irradiated 4H-SiC surface. (*θ*=take off angle).

periodic structure of 4H-SiC but was also different from the amorphous structure of SiO_2. It was considered that this intermediate layer was silicon oxycarbide, which was detected by ARXPS as previously mentioned. These ARXPS and XTEM results indicate that an intermediate layer of silicon oxycarbide was formed after irradiation with water-vapor-containing plasma. Then, this specimen was etched by HF dipping for 30 min, and Figure 4.26 shows the Si2p spectra of the surface after HF dipping. Peaks corresponding to Si-O bonds disappeared owing to the removal of silicon oxide by HF dipping. However, the peaks of Si-C-O bonds were observed, which indicated that the silicon oxycarbide layer could not be removed by HF dipping. This coincided with the experimental results obtained by R. Palmieri *et al.* [22]. Thus, the surface shown in Figure 4.23 was silicon oxycarbide rather than SiC. This explained why no step-terrace structure of 4H-SiC was observed.

4.5.2 Probable flattening mechanism of PAP [21]

On the basis of the above results, the scratch removal mechanism by plasma oxidation and HF dipping as well as the atomic flattening mechanism of PAP was proposed. Figure 4.27(a) shows the probable mechanism of scratch removal by plasma oxidation and HF dipping. A rough surface with scratches was irradiated by water-vapor-containing plasma, after which an oxide layer that included SiO_2 and silicon oxycarbide was formed. The interface between the oxide layer and SiC was very flat, similar to that shown in Figure 4.13. Therefore, after the specimen was dipped in HF solution, scratches were removed and a flat surface was observed. However, according to the ARXPS measurement results, a silicon oxycarbide layer remained on the surface, which was why a step-terrace structure of SiC was not observed. Figure 4.27(b) shows the probable atomic flattening

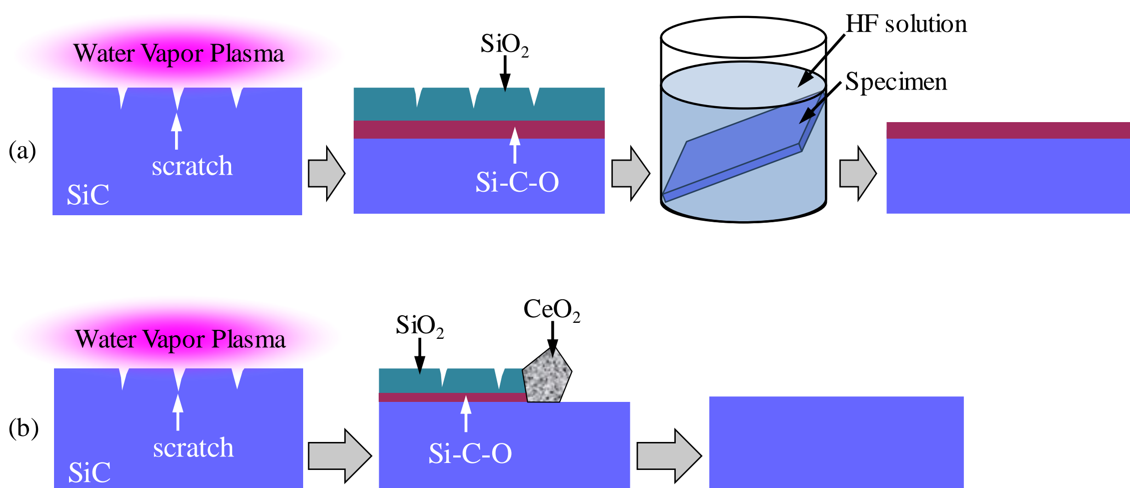

Figure 4.27 Probable mechanism of (a) scratch removal by plasma oxidation and HF dipping, (b) PAP using ceria abrasives.

mechanism of PAP. As previously mentioned, in the PAP process, owing to the rotation of the polishing head and specimen, when an oxide layer was formed, it was removed by the abrasive. Therefore, the duration of oxidation was very short. In this case, both the SiO_2 and silicon oxycarbide layer were very thin and were completely removed by ceria abrasive polishing. Finally, a very flat surface with a well-ordered step-terrace structure and without any residual silicon oxycarbide was obtained. As shown in Figure 4.20, XTEM images of the SiC surface processed by PAP were obtained. The lattice image of 4H-SiC without residual silicon oxycarbide was clearly observed, which supported the proposed mechanism.

4.5.3 Comparison of plasma oxidation and thermal oxidation [23)]

Recently, some other rapid oxidation methods for SiC in addition to oxidation with water-vapor-containing plasma have been widely studied, such as thermal oxidation [24)], anodic oxidation [25)] and ultraviolet-assisted oxidation [26)]. In the case of PAP, atomically flat SiC surfaces with a well-ordered step-terrace structure were obtained. To clarify the flattening mechanism of the oxidation process and further increase the MRR in PAP, clarification of the oxidation process is essential. In this study, two oxidation methods, thermal oxidation, which is a conventional oxidation method, and oxidation with water-vapor-containing plasma, which is applied in PAP, are discussed.

Commercially available single-crystalline 4H-SiC wafers (on axis, n-type) were used in this work. All the experiments were conducted on the Si (0001) face, which is the most commonly used face for epitaxial growth or in power devices. Thermal oxidation was conducted using a miniature lamp annealer (MILA5000, ULVAC Co. Ltd.). Dry oxygen with a flow rate of 22.4 sccm was used as the reactive gas for the thermal oxidation of SiC. The oxidation temperature was 1100 ˚C. In the case of irradiation with water-vapor-containing plasma, the 4H-SiC substrate was set on the ground electrode. Helium-based water vapor was used as the process gas and was introduced into the space between the electrodes. The diameter of the aluminum alloy powered electrode was 4 mm. Atmospheric-pressure helium-based water-vapor-containing plasma was generated by applying a 13.56 MHz RF power between the electrodes. The gap distance between the powered electrode and the SiC wafer was 1 mm. Samples were prepared for XTEM observation using a focused ion beam (FIB) to measure the thickness of the oxide layer.

Table 4.11 Conditions of plasma irradiation

Experimental setup	cf. Figure 3.8
Specimen	4H-SiC (0001), on-axis
Carrier gas	He
Flow rate	1.5 slm
Applied RF power	100 W
Duty ratio	2 %
Pulse frequency	10 Hz
Plasma irradiation time	5, 10, 20, 40, 60 min

To evaluate the oxidation rates of thermal oxidation and plasma oxidation, oxidation experiments with different durations were conducted. The experimental parameters of plasma oxidation are shown in Table 4.11. The Deal-Grove model is widely used for evaluating the oxidation process of Si. Since the oxidation process of SiC is not the same as that of Si, Song *et al*. proposed a modified Deal-Grove model to describe the oxidation process of SiC as follows [27]:

$$X^2 + AX = B(t + \tau), \tag{4.1}$$

where X is the thickness of the oxide and t is the oxidation time. τ is related to the thickness of the initial oxide on the SiC surface. From Equation (4.1), the thickness of the oxide as a function of the oxidation time is:

$$X\,(t) = \frac{-A+\sqrt{A^2+4B(t+\tau)}}{2}. \tag{4.2}$$

In the initial oxidation stage ($t + \tau << A^2/4B$), equation (4.2) can be reduced to

$$X\,(t) = \frac{B\,(t+\tau)}{A}. \tag{4.3}$$

Thus, B/A is called the linear rate constant.

The measured thickness data of the oxide formed by thermal oxidation and plasma oxidation were fitted to the modified Deal-Grove model. Figure 4.28 shows the experimental oxidation growth data as well as the fitting results to the modified Deal-Grove model for plasma oxidation and thermal oxidation of the Si face of 4H-SiC. The two rate constants in the model were calculated from the fitting results shown in Figure 4.28.

In the case of thermal oxidation,

$$X^2 + 0.00655X = 0.00019t. \tag{4.4}$$

In the case of plasma oxidation,

$$X^2 + 0.0033X = 0.00061t. \tag{4.5}$$

The linear rate constant of thermal oxidation was about 0.029 μm/h, whereas that of plasma oxidation was calculated to be 0.185 μm/h. This means that the initial oxidation rate of plasma oxidation was six times higher than that of thermal oxidation. In the case of plasma oxidation, OH radicals, which have a very high oxidation potential [28], reacted with SiC. On the other hand, in the case of thermal oxidation using dry oxygen, the oxidation potential of oxygen molecules was increased owing to the high temperature (about 1100 ℃), and they reacted with SiC. There are two reasons considered to explain why the initial oxidation rate of plasma oxidation was much higher than that of thermal oxidation. First, the oxidation potential of OH radicals is much higher than that of oxygen. Second, OH radicals are much smaller than oxygen molecules; therefore, they can much more easily diffuse through the oxide and react with SiC at the oxide-SiC interface. OH radicals

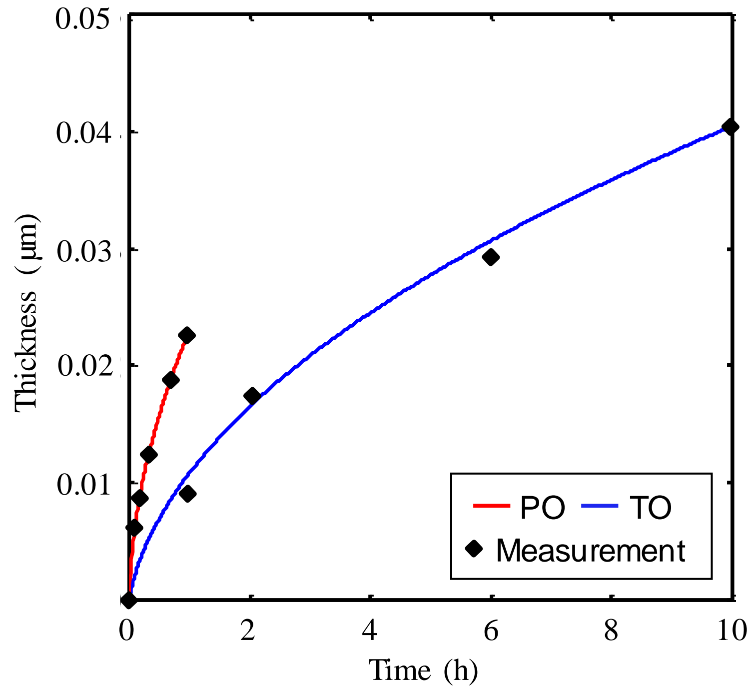

Figure 4.28 Oxide thickness as a function of time for plasma oxidation (PO) and thermal oxidation (TO) of 4H-SiC (0001). Solid lines indicate the fitting results by Eq. (4.1).

diffused into SiC at a high speed, and a high oxidation rate was obtained, particularly in the initial oxidation stage.

When these oxidation methods are used to assist polishing, oxidation and polishing are simultaneously conducted, such as in PAP. When an oxide layer is formed, it is immediately removed by abrasive polishing. That is to say, the oxidation process always maintains the initial oxidation stage and the MRR of the polishing process should be determined by the initial oxidation rate. This is why I have focused on the initial oxidation rates of plasma oxidation and thermal oxidation. To increase the MRR of PAP for practical applications, increasing the initial oxidation rate in plasma oxidation is essential. To obtain a high initial oxidation rate of plasma oxidation, the plasma oxidation process should be optimized by changing the reactive gas, the concentration of water vapor, the structure of the electrode with grinding stones and so forth.

Table 4.12 Conditions of plasma irradiation

Experimental setup	cf. Figure 3.8
Specimen	4H-SiC (0001), on-axis
Carrier gas	He (with bubbling of water)
Flow rate	3.0 slm
Applied RF power	16 W
Plasma irradiation time	1, 5, 60 min

In the oxidation-assisted polishing of SiC, the purpose of oxidation is to form an oxide layer that is much softer than SiC, and this enables

ultraprecision damage-free polishing using a soft abrasive. Since the material used as the abrasive is much softer than SiC, only the oxide layer is removed and the formation of a damaged layer is prevented. Therefore, the base material SiC cannot easily be polished in these oxidation-assisted polishing processes. That is to say, the limitations in oxidation-assisted polishing, *i.e.*, material removal as well as surface roughness, are determined by the oxide-SiC interface.

Next, the oxide-SiC interfaces formed by plasma oxidation and thermal oxidation were investigated by XTEM. Figure 4.29 shows XTEM images of SiC surfaces irradiated by helium-based water-vapor-containing plasma for 1 min, 5 min and 60 min under the conditions shown in Table 4.12. These images were viewed in the [11-20] direction. The thickness of the oxide layer increased from about 6 nm to 80 nm with increasing plasma irradiation time from 1 min to 60 min. It was found that the interface was very rough when the oxide layer was thin and that the interface became flatter when the oxide layer was thicker. When the oxide layer was sufficiently thick, as shown in Figure 4.29(c), an atomically flat interface was formed. A comparison with thermal oxidation was also conducted. As previously mentioned, the oxidation rate of thermal oxidation was very low compared with that of plasma oxidation. Thus, the duration of the thermal oxidation experiments was increased. The oxide-SiC interfaces generated by thermal oxidation for 1 h, 2 h and 10 h were observed. The results are shown in Figure 4.30. It was revealed that in the case of

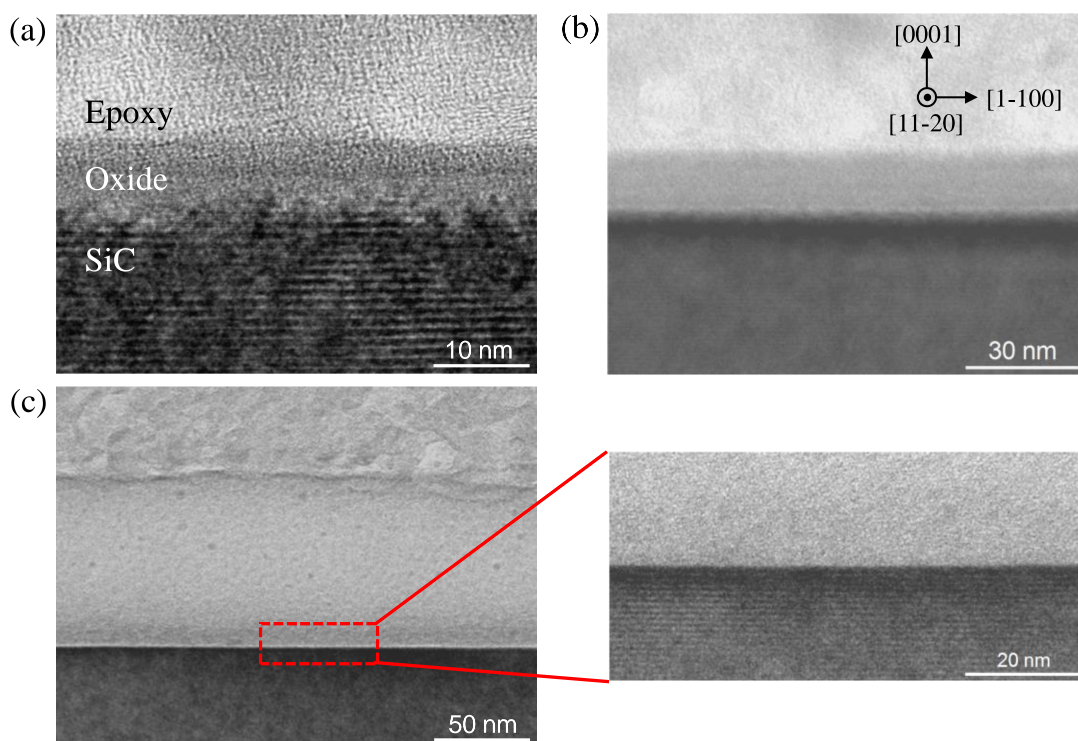

Figure 4.29 XTEM images of the oxide layers formed by plasma oxidation with different durations. (a) 1 min. (b) 5 min. (c) 60 min.

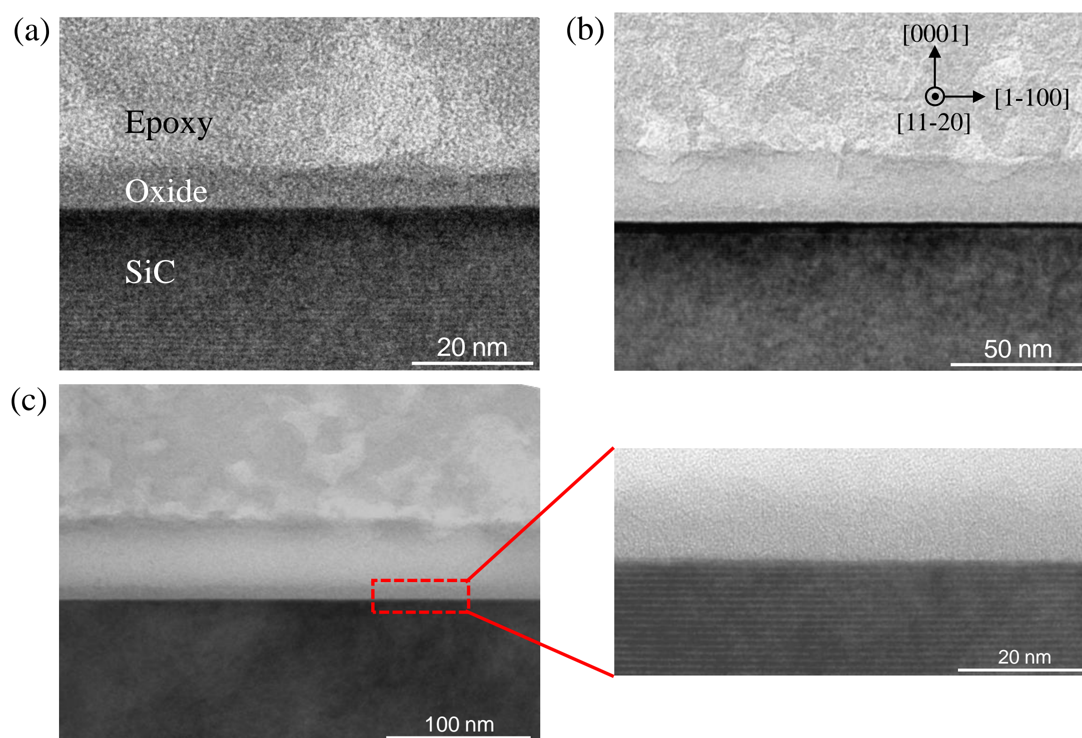

Figure 4.30 XTEM images of the oxide layers generated by thermal oxidation with different durations. (a) 1 h. (b) 2 h. (c) 10 h.

thermal oxidation, the oxide-SiC interface was atomically flat regardless of the thickness of the oxide layer. During the plasma oxidation process, OH radicals diffused through the oxide layer at a high speed and reacted with SiC, particularly when the oxide layer was thin. Thus, it was difficult to realize the uniform diffusion of OH radicals over the whole surface when the oxide layer was thin. This is why the interface was rough in the initial plasma oxidation stage. In the case of a thicker oxide layer, it was more difficult for OH radicals to diffuse through the oxide layer. As shown using the Deal-Grove model, the oxidation rate became extremely low for a thicker oxide layer. In this case, the diffusion of OH radicals was much more uniform in the lateral direction. This may explain why the interface became flatter with increasing thickness of the oxide layer in plasma oxidation. In contrast, for the case of thermal oxidation, the oxidation rate was very low compared with that of plasma oxidation regardless of the thickness of the oxide layer. That is to say, the different oxidation rates of plasma oxidation and thermal oxidation were considered to be the reason for the different flatness of the interfaces, in other words, the roughness of the oxide-SiC interface was determined by the oxidation rate.

To verify the above discussion, it is necessary to examine the oxide-SiC interface generated by plasma oxidation with a low initial oxidation rate. Therefore, plasma oxidation with a low oxidation rate was conducted. Figure 4.31 shows an XTEM image of a SiC (0001) surface irradiated by water-

vapor-containing plasma under the conditions shown in Table 4.13. This experiment was conducted using the same experimental setup as before without the bubbling of water. The thickness of the oxide layer was about 4 nm, which means that the oxidation rate was much lower than that in the plasma oxidation experiments whose results are shown in Figure 4.29. Although the oxide layer was very thin, the oxide-SiC interface was not as rough as the oxide-SiC interface shown in Figure 4.29(a). This result strongly supports my assumption about the relationship between the oxidation rate and interface roughness.

Table 4.13 Conditions of plasma irradiation

Experimental setup	cf. Figure 3.8
Specimen	4H-SiC (0001), on-axis
Carrier gas	He (without bubbling of water)
Flow rate	3.0 slm
Applied RF power	25 W
Plasma irradiation time	30 min

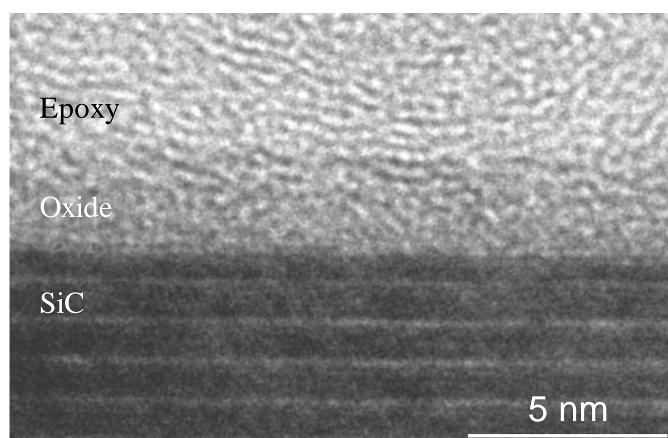

Figure 4.31 XTEM image of the oxide layer generated by PO with an extremely low oxidation rate.

For the flattening of SiC substrates, not only the surface roughness but also the surface integrity is considered very important. As has been widely reported, many types of defect can be found in bulk SiC [29, 30]. During oxidation, pits can be formed, which greatly deteriorate the surface integrity. To confirm the formation of pits during thermal oxidation and plasma oxidation, SiC surfaces oxidized by thermal oxidation for 1 h and by plasma oxidation for 5 min were observed using an SWLI. These samples were chosen because their oxide layers had almost the same thickness. Also, the samples used in thermal oxidation and plasma oxidation were cut from the same bulk wafer; thus, it was considered that they had the same defect density. However, as shown in Figure 4.32, many pits were found on the surface oxidized by thermal oxidation for 1 h, whereas few pits were found on the surface oxidized by plasma oxidation for 5 min. Also, the pits formed on the thermally oxidized surface were much larger than those formed on the surface oxidized by plasma irradiation. The typical morphology of these pits was observed using a scanning electron microscope (SEM) as shown in the inset in Figure 4.32(a). As previously reported, these pits resulted from the preferential oxidation of defects in SiC, such as dislocations and low-angle grain boundaries [31]. In the thermal oxidation process, the temperature of the substrate was very high, which greatly promoted the preferential

oxidation of these defects. In contrast, the temperature of the SiC substrate during plasma oxidation, which increased from room temperature to about 50 ℃ then remained steady when the RF power was 13 W. This means that the temperature of the substrate in plasma oxidation was much lower than that of the substrate in thermal oxidation. Although the high oxidation potential also promoted the preferential oxidation of defects in SiC, it appears that the high temperature was the main reason for the formation of pits according to the above results. This conclusion is supported by the results of anodic oxidation, which was also investigated in my study. The oxidation rate of anodic oxidation was much higher than those of plasma oxidation and thermal oxidation. Also, anodic oxidation was conducted in acid solution without heating, in other words, the temperature during anodic oxidation was also very low compared with that during thermal oxidation. There were no pits on the surfaces processed by anodic oxidation regardless of the oxidation time. The above results proved that the high temperature was the reason why many pits were generated in thermal oxidation.

As previously mentioned in 4.5.1, it was proved that when SiC is oxidized to SiO_2, there is a transition layer of silicon oxycarbide between SiO_2 and SiC [20]. It has been experimentally demonstrated that silicon oxycarbide cannot be removed by dipping in HF solution [22]; however, it can be removed along with SiO_2 by polishing using CeO_2 as an abrasive. Therefore, SiC surfaces processed by thermal oxidation and plasma oxidation were polished using CeO_2 as an abrasive to realize the surface flattening of SiC. According to the above discussion, the pits on the surface oxidized by thermal oxidation should be much deeper than those on the surface oxidized by plasma oxidation. Also, since the pits were generated by the preferential oxidation of defects, these pits should penetrate into the bulk SiC. Figure 4.33 shows AFM images of SiC surfaces processed by thermal oxidation and plasma oxidation followed by polishing using CeO_2, which is widely used as an abrasive material for SiO_2 polishing. In both cases, an atomically flat SiC surface with a well-ordered step-terrace structure was obtained. However, as assumed, some pits remained after the

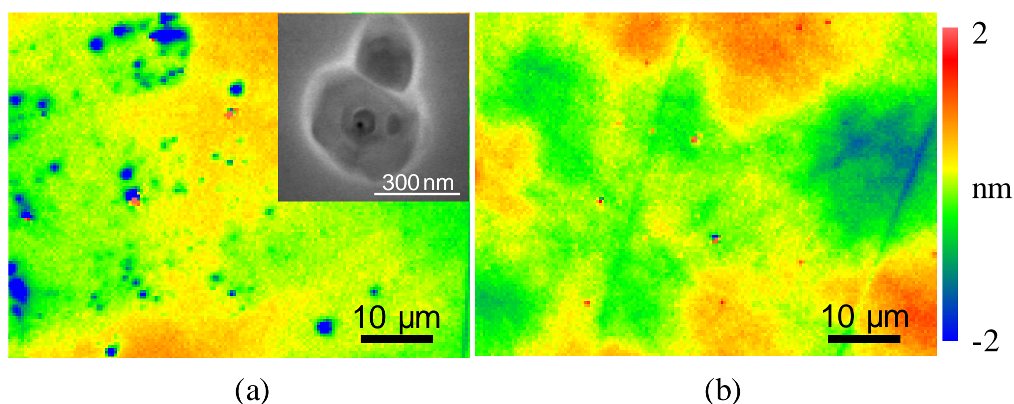

Figure 4.32 SWLI images of SiC surfaces oxidized by thermal oxidation and plasma oxidation. (a) Thermal oxidation for 1 h. The inset figure shows a typical SEM image of the pits observed in (a). (b) Plasma oxidation for 5 min.

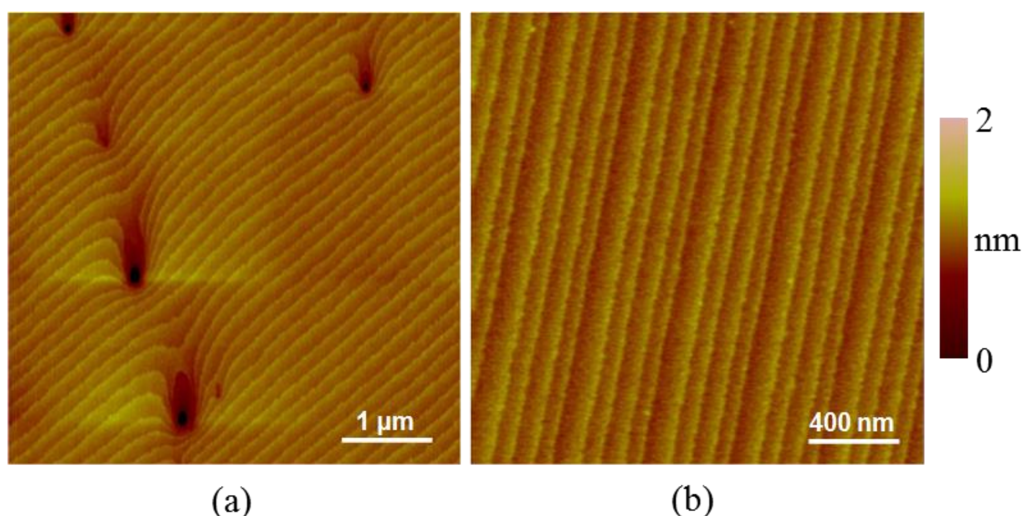

Figure 4.33 AFM images of 4H-SiC (0001) surfaces oxidized by thermal oxidation and plasma oxidation followed by polishing using CeO_2 abrasive. (a) Thermal oxidation. (b) Plasma oxidation.

oxide layer formed by thermal oxidation was removed by polishing. In contrast, the surface oxidized by plasma oxidation was free of pits after polishing.

Since the plasma oxidation process was conducted under atmospheric pressure, layers damaged by the bombardment of ions in water-vapor-containing plasma were not formed because the kinetic energy of the ions in the AP-plasma was very low owing to their small mean free path.

The above results demonstrate that the combination of plasma oxidation and polishing using CeO_2 abrasive was very effective for obtaining atomically flat 4H-SiC substrates. As shown in Figure 4.33(b), a 4H-SiC Si face free of pits and scratches was obtained. Also, the step-terrace structure was very uniform, even compared with that of substrates processed by CMP. Thus, high device performance and high-quality epilayers are strongly expected, which will be experimentally investigated in a future study.

4.6 Flattening of the C-face of 4H-SiC

On the basis of the above results, it has been demonstrated that PAP is very useful for flattening the Si face of 4H-SiC. Scratch-free and damage-free Si faces of 4H-SiC were successfully obtained. In recent years, studies and applications of the C face of 4H-SiC substrates have been widely conducted [32)]. Although the commercially applied polishing technique of CMP and other newly developed polishing techniques have been widely applied to the Si face of 4H-SiC [2, 17, 33)], flattening of the C face to an epi-ready level has been seldom reported. The reason for this is that the chemical and mechanical properties of the Si face and C face are different; therefore the ideal abrasives for

flattening Si faces may not be suitable for flattening C faces. Similarly to the Si faces of 4H-SiC substrates, it is expected that the C faces can also be flattened efficiently by surface oxidation and abrasive polishing because C faces are much easier to oxidize. As the oxidation methods for the C face, anodic oxidation, plasma oxidation, thermal oxidation and so forth can be considered. As a preliminary study, conventional CMP using slurry and the combination of thermal oxidation and abrasive polishing of the C face of 4H-SiC were conducted.

4.6.1 Conventional CMP

To determine the polishing characteristics of the C face of 4H-SiC by conventional CMP, CMP experiments using CeO_2 and SiO_2 slurries were conducted. 4H-SiC substrates from TanKeBlue Co. Ltd. were used. Figure 4.34 shows SWLI and AFM images of an as-received C face processed by polishing using diamond slurry. Many scratches were formed on the surface. For the flattening of such C faces, a special silica slurry for SiC-C faces was developed and reported to be very useful, although its composition has not yet been disclosed [34)]. In this study, commercially available CeO_2 and SiO_2 slurries were used.

Table 4.14 shows the conditions of the CeO_2 slurry polishing of 4H-SiC (000-1). For the same substrate, the total polishing time was increased to 15 h owing to the replacement of the polishing pad and slurry after each step. Figure 4.35 shows AFM images of the polished surfaces after different durations. It was revealed that the shallow scratches on the as-received surface were gradually removed while the deep scratches became deeper and wider. Even after polishing for 9 h, many deep and wide scratches can still be observed. With additional polishing for 6 h, most of the scratches were removed with a few deep scratches still remaining on the polished surface. AFM observation of a small area of 500 nm $\times$ 500 nm was conducted on the scratch-free area, and the step-terrace structure on the C face of 4H-SiC was observed as shown in Figure 4.35(f).

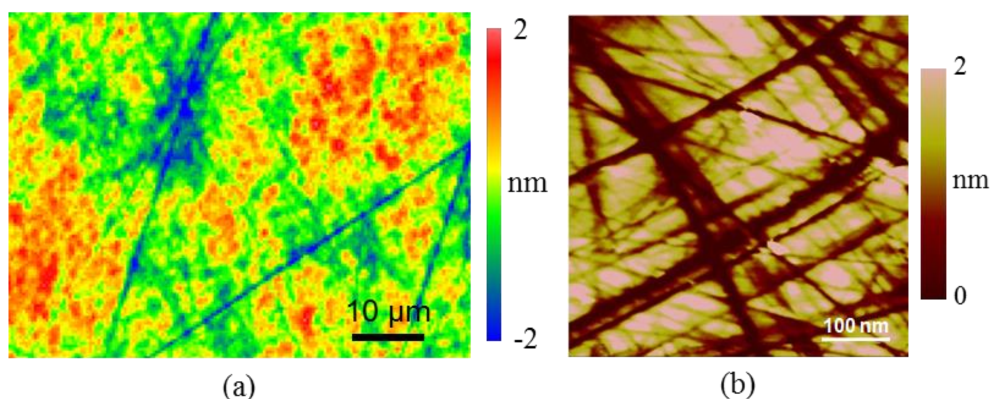

Figure 4.34 SWLI and AFM images of as-received C-face of 4H-SiC. (a) SWLI image (p-v: 4.89 nm, rms: 0.64 nm). (b) AFM image (p-v: 8.34 nm, rms: 0.83 nm).

Table 4.14 Conditions of CeO_2 slurry polishing

PAP machine	cf. Figure 3.5
Polishing pad	Suede type, NP178 (ϕ10 mm)
Abrasive material	CeO_2 (ϕ190 nm, pH: 8.53)
Concentration	1.0 wt%
Load	50 g
Pad rotation Speed	2000 rpm
Polishing time duration	3, 6, 9, 15 h

It has been reported that CeO_2 strongly reacts with 4H-SiC, especially the C-face [35]. In the above experiments, a CeO_2 slurry was used. Thus, two types of surface modification can be considered: the surface modification by chemicals in the slurry and the tribocatalytic reaction between CeO_2 and SiC. Also, there are damaged areas around the scratches, which will increase the efficiency of surface modification. Thus, the scratch areas were preferentially modified and removed. This was why the scratches became wider and deeper as shown in Figure 4.35.

Table 4.15 shows the conditions of the SiO_2 slurry polishing of 4H-SiC (000-1). Similar to the CeO_2 slurry polishing, the polishing pad and slurry were replaced after each step. Figure 4.36 shows

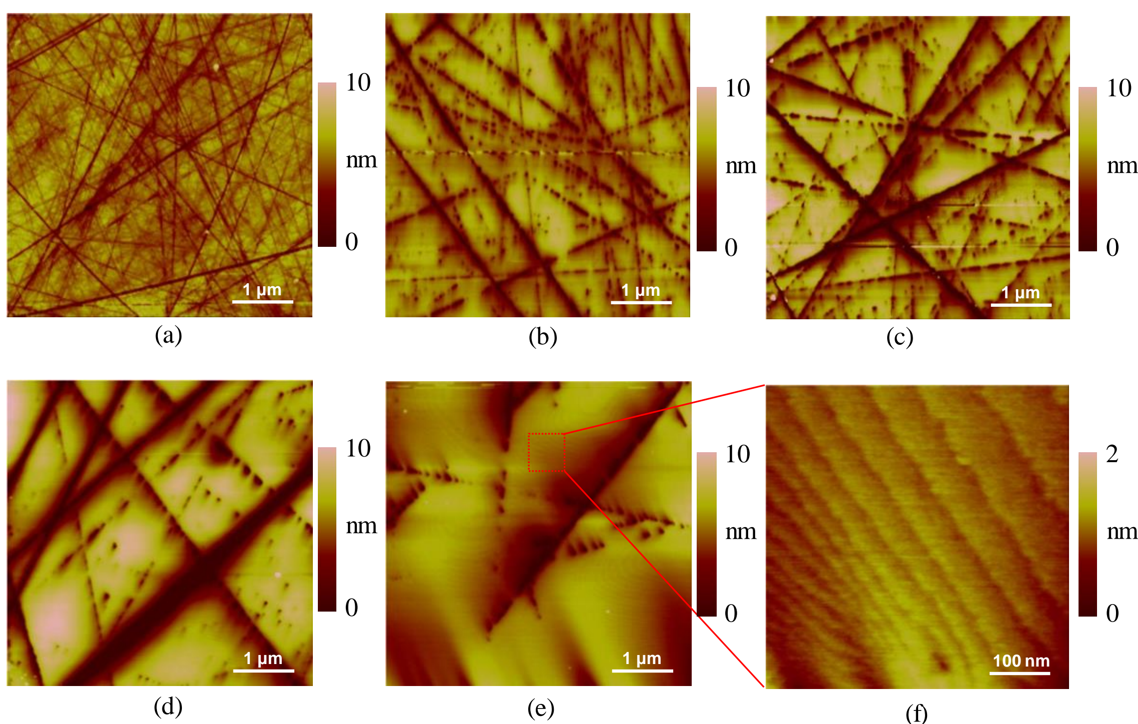

Figure 4.35 AFM images of C-face polished by CeO_2 slurry with different durations. (a) As-received surface (p-v: 21.15 nm, rms: 1.08 nm). (b) 3 h (p-v: 29.25 nm, rms: 1.67 nm). (c) 6 h (p-v: 59.21 nm, rms: 2.77 nm). (d) 9 h (p-v: 35.49 nm, rms: 3.10 nm). (e) 15 h (p-v: 17.03 nm, rms: 1.63 nm).

Table 4.15 Conditions of SiO_2 slurry polishing

PAP machine	cf. Figure 3.5
Polishing pad	Suede type, NP178 (ϕ10 mm)
Abrasive material	CeO_2 (ϕ72 nm, pH: 10.06)
Concentration	10.0 wt%
Load	50 g
Pad rotation Speed	2000 rpm
Polishing time duration	3, 9 h

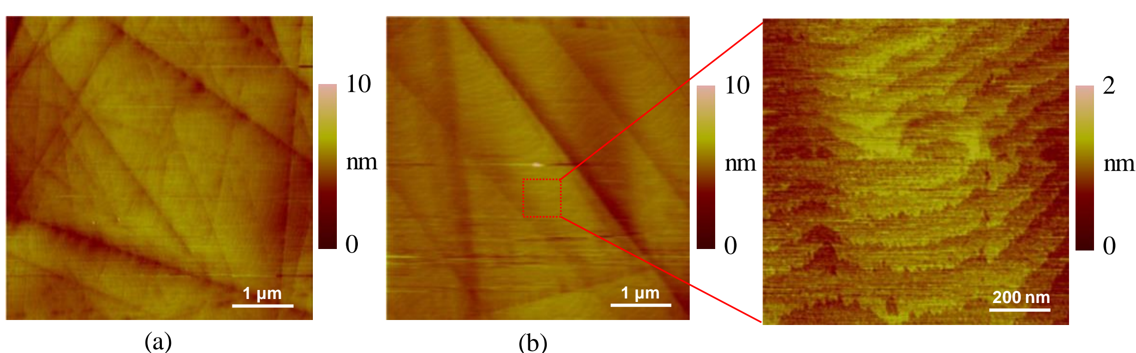

Figure 4.36 AFM images of C-face polished by SiO_2 slurry with different durations. (a) 3 h (p-v: 9.25 nm, rms: 0.63 nm). (b) 9 h (p-v: 5.13 nm, rms: 0.28 nm).

AFM images of the polished surfaces. In contrast to the surfaces polished by the CeO_2 slurry, the widening and deepening of the scratches did not occur in SiO_2 slurry polishing. After polishing for 3 h, the scratches became very shallow. After additional polishing for 6 h, most of the scratches were removed and the step-terrace structure could be observed in the scratch-free areas of the polished surface. Unlike the high surface modification efficiency of CeO_2 slurry polishing, only surface modification by the chemicals in the slurry can be expected in the case of SiO_2 polishing. This was why the C face was removed uniformly.

On the basis of the above results, it was concluded that the polishing efficiency of conventional CMP using a CeO_2 slurry or SiO_2 slurry for the C-face of 4H-SiC was very low. Even after prolonged polishing (15 h for CeO_2 polishing and 9 h for SiO_2 polishing), the scratches were not completely removed.

4.6.2 Combination of thermal oxidation and CeO_2 slurry polishing

The combination of thermal oxidation and abrasive polishing for the finishing of 4H-SiC (000-1) was investigated. In the first step, the substrate was processed by thermal oxidation for 4 h. According to measurement using an ellipsometer, an oxide layer with a thickness of about 33 nm was formed. After thermal oxidation, the surface was polished using CeO_2 slurry to obtain a flat surface. The polishing conditions were the same as those in Table 4.14 and the polishing time was 3 h.

Figure 4.37 shows SWLI and AFM images of the surface after polishing. All the scratches formed by diamond slurry polishing, which can be observed in Figure 4.34, were completely removed and a very low surface roughness was obtained. Furthermore, according to AFM observation of a small area (500 nm $\times$ 500 nm), a well-ordered step-terrace structure was formed on this surface as shown in Figure 4.37(c). Figure 4.37(d) shows a cross-sectional profile of the surface after the slope

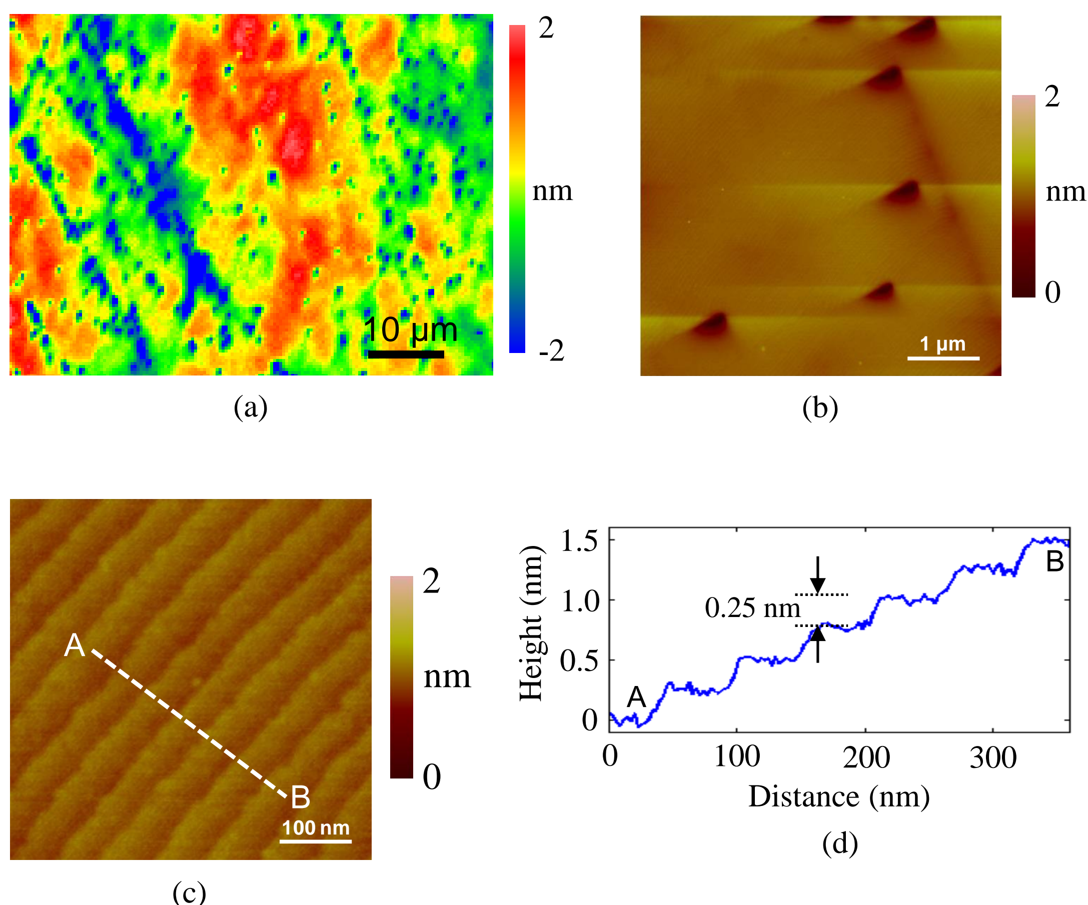

Figure 4.37 SWLI and AFM images of C-face processed by thermal oxidation followed by polishing using CeO_2. (a) SWLI image (p-v: 16.60 nm, rms: 0.94 nm). (b) AFM image (p-v: 25.13 nm, rms: 0.75 nm). (c) AFM image (p-v: 0.41 nm, rms: 0.07 nm). (d) Cross-sectional profile after slope correction.

correction; the step height was measured to be 0.25 nm, corresponding to one bilayer of 4H-SiC, which means that an epi-ready C-face was obtained.

Although an atomically flat SiC-C face was obtained by the combination of thermal oxidation and slurry polishing, many pits were found on the polished surface as shown in Figures 4.37(a) and (b). From a detailed observation of these pits by AFM, it was found that these pits originated from screw dislocations. As previously mentioned in 4.5.3, in the case of thermal oxidation, the preferential oxidation of the defects in SiC occurred owing to the high oxidation temperature, which resulted in the formation of pits after the oxide layer was removed by polishing. Thus, it was concluded that this problem can be resolved by the application of PAP, in which the oxidation process is conducted with a relatively low temperature. Also, the oxidation rate of water-vapor-containing plasma has been proved to be much higher than that of thermal oxidation; thus, the pit-free and highly efficient polishing of the C-face of 4H-SiC can be expected with the application of PAP.

4.7 ECMP of 4H-SiC [36)]

To realize the highly efficient polishing of SiC with minimal subsurface damage, several electrochemical methods have been proposed [26, 37-39)]. Li *et al.* [26)] developed a two-step ECMP process to polish single-crystal SiC. Hydrogen peroxide and potassium nitrate were used as the electrolytes for the anodic oxidation of SiC and the oxide layer was removed by polishing using a colloidal silica slurry. After several cycles of anodic oxidation and slurry polishing, a smooth surface was obtained.

We propose a ceria-slurry-based ECMP process, in which anodic oxidation and soft abrasive polishing are efficiently combined for the highly efficient preparation of a prepolished surface for PAP. A ceria slurry is used as an electrolyte for anodic oxidation as well as a polishing medium to remove the oxide layer. Since oxidation and polishing are simultaneously conducted, a high MRR is expected. Also, since CeO_2 abrasive is very soft compared with SiC, the polishing process will only remove the oxide layer without the formation of any scratches or subsurface damage. Thus, a flat surface without crystallographic defects is expected to be obtained by ceria-slurry-

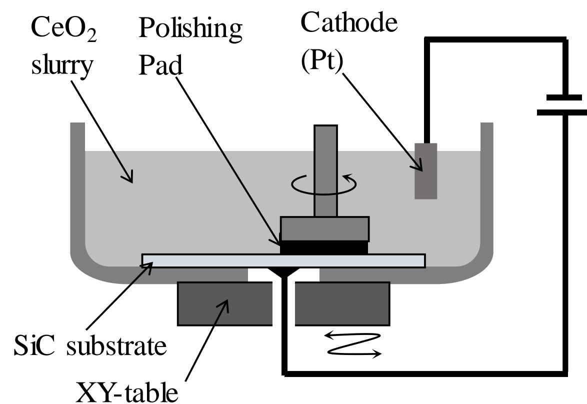

Figure 4.38 Experimental setup of ECMP used for preliminary study.

based ECMP. In this study, the oxidation and polishing characteristics of ECMP applied to SiC were investigated.

Figure 4.38 shows the experimental setup of ECMP used for the preliminary study. A 4H-SiC substrate was immersed in CeO_2 slurry. Direct-current voltage was applied between the SiC substrate and Pt cathode. Anodic oxidation by the following equations occurred on the surface of SiC in contact with the slurry, after which an oxide layer was formed.

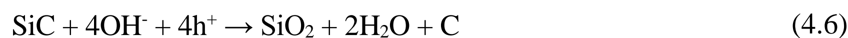

$$SiC + 4OH^- + 4h^+ \rightarrow SiO_2 + 2H_2O + C \tag{4.6}$$

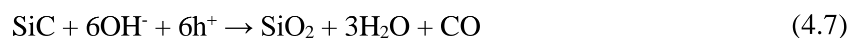

$$SiC + 6OH^- + 6h^+ \rightarrow SiO_2 + 3H_2O + CO \tag{4.7}$$

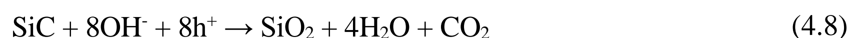

$$SiC + 8OH^- + 8h^+ \rightarrow SiO_2 + 4H_2O + CO_2 \tag{4.8}$$

With the rotation of the polishing pad and the scanning of the stage, the anodic oxidation of SiC and the removal of the oxide layer were simultaneously conducted. Commercially available single-crystal 4H-SiC substrates (on-axis, n-type) with a thickness of 341 μm and a specific resistance of 0.10 Ω·cm supplied by TanKeBlue Co. Ltd. were used in this work. All experiments were conducted on the Si (0001) face, which is the most commonly used face for power device applications. Table 4.16 shows the detailed polishing conditions of ECMP.

Table 4.16 Conditions of ECMP

Electrolyte	CeO_2 slurry (ϕ190 nm, pH: 9.24)
Slurry concentration	2.5 wt%
Electrical conductivity	29.4 mS/m
Polishing pad	Suede type, NP178 (ϕ10 mm)
Pad rotation speed	2000 rpm
Applied voltage	10 V
Load	50 g
Polishing time	30 min

The anodic oxidation layer was observed by XTEM to determine the morphology of

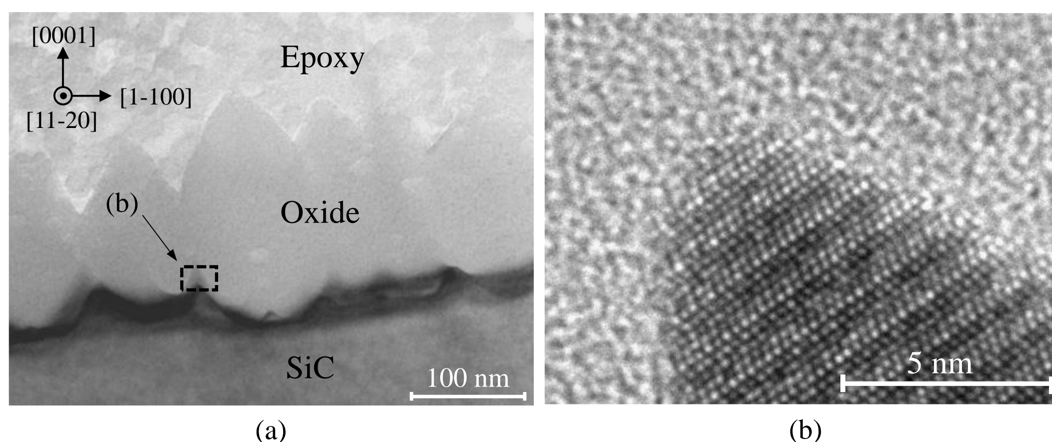

(a) (b)

Figure 4.39 XTEM images of an unpolished surface after anodic oxidation.

the oxide/SiC interface. Figure 4.39 shows an XTEM image of an unpolished surface after anodic oxidation for 10 min with an applied voltage of 5 V. The average thickness of the anodic oxide layer was about 100 nm. It was found that the surface of the oxide layer and the oxide/SiC interface were both very rough and many SiC protrusions existed at the interface. These results indicate that the anodic oxidation of SiC is a less uniform oxidation process than plasma oxidation and thermal oxidation [23]. In the ECMP process, oxidation and polishing are simultaneously conducted. When an oxide layer is formed, it is immediately removed by abrasive polishing. In other words, the oxide layer is removed when it is very thin.

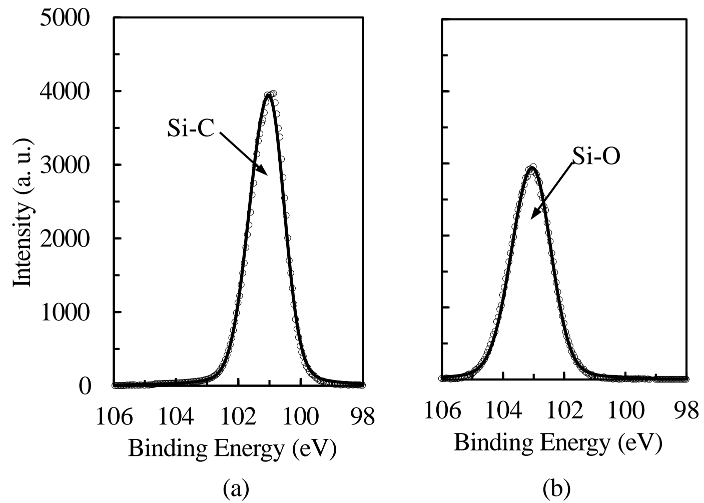

Figure 4.40 Si2p spectra of 4H-SiC (0001) surface before (a) and after anodic oxidation for 5 min (b).

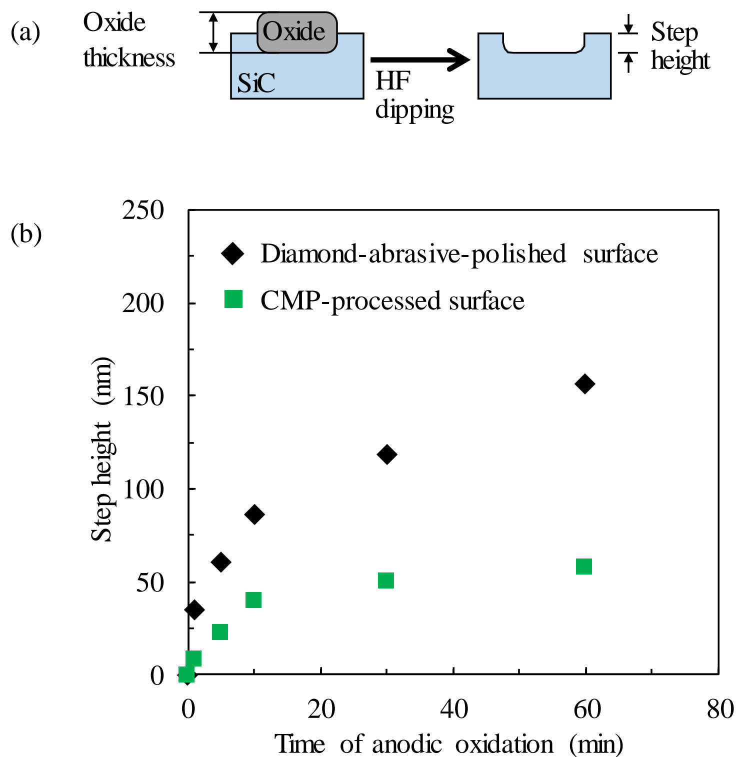

Figure 4.41 Thickness of anodically oxidized SiC with different durations. (a) Schematic image of the measurement flow. (b) Step height.

Therefore, a smooth surface is expected after ECMP even though the oxide/SiC interface formed by prolonged oxidation is rough.

Figure 4.40 shows the Si2p spectra of the as-received and anodically oxidized SiC surface. It was confirmed that SiC was oxidized to SiO_2 after anodic oxidation.

To evaluate the anodic oxidation rate in ECMP, oxidation experiments were conducted on a SiC substrate for different durations. To measure the thickness of SiC which was anodically oxidized, the anodic oxidation area was localized on the substrate and a step was formed after the oxide layer was removed by dipping in HF solution (50 wt%). The thickness of the oxide layer was obtained by conversion from the step height measured by SWLI as shown in Figure 4.41(a).

Owing to the high hardness of SiC, CeO_2 abrasive polishing could only remove the oxide layer formed in the ECMP process. Since the oxidation of SiC and the removal of the oxide layer were simultaneously conducted, the MRR of ECMP was determined by the initial oxidation rate of SiC in anodic oxidation. It was considered that scratches and the existence of a subsurface damaged layer could affect the anodic oxidation rate of SiC. Thus, oxidation experiments on a CMP-processed surface and a diamond-abrasive-polished surface were both conducted. To describe the oxidation process of SiC, the modified Deal-Grove model was proposed and is very widely used [27]. Figure 4.41 shows the measured step heights with different durations of the anodic oxidation of SiC. The thickness data of the oxide converted from the measured step heights with durations from 0 to 10 min were fitted by the modified Deal-Grove model to calculate the initial oxide growth rates. It was found that for the CMP-processed surface, the initial oxide growth rate was 0.92 μm/h, while that for the diamond-abrasive-polished surface was 7.93 μm/h. Owing to the existence of a subsurface damaged layer, the initial oxide growth rate of the diamond-abrasive-polished surface

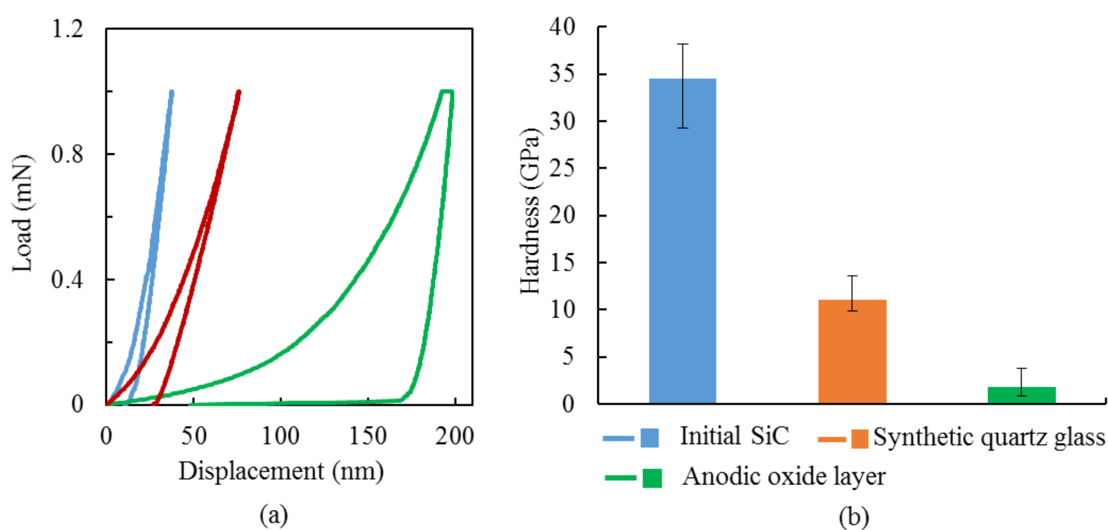

Figure 4.42 (a) Load-displacement curves measured by the nanoindentation method. (b) Hardnesses calculated from measured data (a).

was much higher than that of the CMP-processed surface as anticipated. In consideration of the molecular masses and densities of SiO_2 and SiC, the initial oxide growth rates were converted to the initial oxidation rates of SiC. In ECMP, oxidation and polishing were simultaneously conducted. Therefore, it was assumed that the oxide layer was immediately removed after it was formed because the CeO_2 slurry was very efficient for the polishing of SiO_2. On the basis of this assumption, the MRRs of ECMP were considered equivalent to the initial oxidation rates. The MRRs of ECMP for a CMP-processed SiC surface and diamond-abrasive-polished SiC surface were calculated to be 0.42 μm/h and 3.62 μm/h, respectively. In the conventional CMP process, the MRR of SiC is as low as 0.5 μm/h, although it might increase with the development of new slurry materials [7]. Although the MRR of ECMP for the CMP-processed SiC surface was almost the same as that of the conventional CMP process, that for the diamond-abrasive-polished SiC surface was more than seven times higher. This means that ECMP is very efficient for flattening SiC especially for a damaged substrate surface.

The surface hardness of SiC before and after anodic oxidation was measured using a nanoindenter to determine the change in hardness. In the nanoindentation tests, the maximum load was 1.0 mN and 100 points were measured for each specimen. In the ECMP process, anodic oxidation softens the surface of SiC, which makes it possible for the surface to be polished by a soft abrasive such as CeO_2. Nanoindentation tests were conducted on the surfaces of as-received SiC (CMP-polished), synthetic quartz glass and anodically oxidized SiC to compare their surface hardnesses. Figure 4.42(a) shows the typical load-displacement curves of these three surfaces measured by the nanoindentation method. A Berkovich-type indenter made of diamond was used. The surface hardnesses were calculated by the Oliver-Pharr method [15]. Figure 4.42(b) shows the results of the nanoindentation tests calculated from the load-displacement curves. It was revealed that after anodic oxidation, the surface hardness of SiC greatly decreased from 34.5 GPa to 1.9 GPa. As shown in Figure 4.40(b), it was confirmed that the anodic oxide layer was mainly composed of SiO_2. Although the anodic oxide layer and synthetic quartz glass have the same composition, it was found

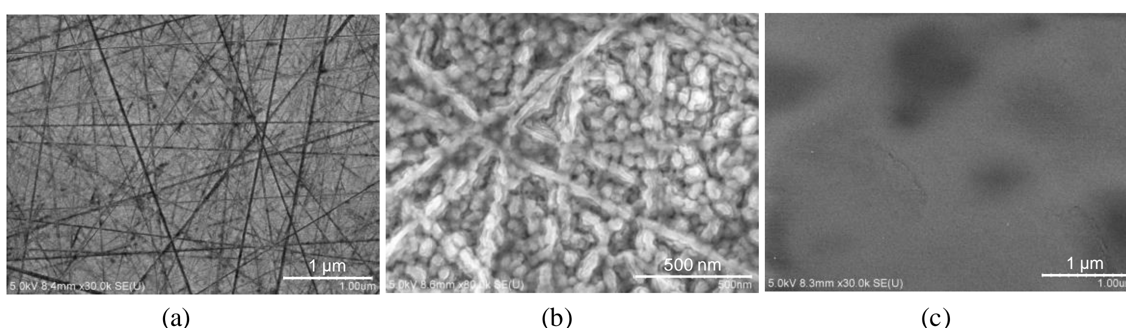

Figure 4.43 SEM images of SiC surfaces. (a) Diamond-abrasive-polished surface. (b) Anodically oxidized surface. (c) ECMP-processed surface.

that the anodically oxidized surface was much softer than the synthetic quartz glass. Therefore, it was concluded that anodic oxidation is very useful for the surface softening of SiC.

Using the experimental setup shown in Figure 4.38, ECMP was conducted on a diamond-abrasive-polished surface for only 30 min. Figure 4.43(a) shows the as-received surface, on which many scratches can be observed. As shown in Figure 4.3, a subsurface damaged layer also exists on such a surface owing to the high hardness of the diamond abrasive. Figure 4.43(b) shows a SEM image of an area outside the ECMP-processed area. Since the entire surface of the specimen was immersed in CeO_2 slurry, anodic oxidation occurred on the surface shown in Figure 4.43(b). The surface morphology of the anodic oxide layer shown in Figure 4.43(b) indicates that scratches were preferentially oxidized. Figure 4.43(c) shows a SEM image of the ECMP-processed area. A very smooth and scratch-free surface was obtained. In Li's work [25)], silica slurry, which is widely used for polishing SiC, was used and they found that scratches could not be removed in simultaneous ECMP. In the ECMP process, the polishing object was the oxide layer (SiO_2) rather than SiC. Thus, CeO_2 slurry was more suitable for the ECMP of SiC than silica slurry. The surface rms roughnesses before and after ECMP were also evaluated using AFM with a measurement area of 1 μm×1 μm. As shown in Figure 4.44, the rms roughness decreased from 0.97 nm to 0.23 nm after 30 min of ECMP. On the ECMP-processed surface, no step-terrace structure of SiC could be observed. It was confirmed that the surface shown in Figure 4.44(b) was covered by a residual oxide layer, which meant that the oxidation rate was higher than the removal rate in ECMP. However, it is expected that with additional abrasive polishing, the residual oxide layer can be completely removed and an atomically flat SiC surface can be obtained. These results indicate that ceria-slurry-based ECMP is very effective for flattening SiC, particularly SiC with a subsurface damaged layer, making it very suitable as a prepolishing process for PAP.

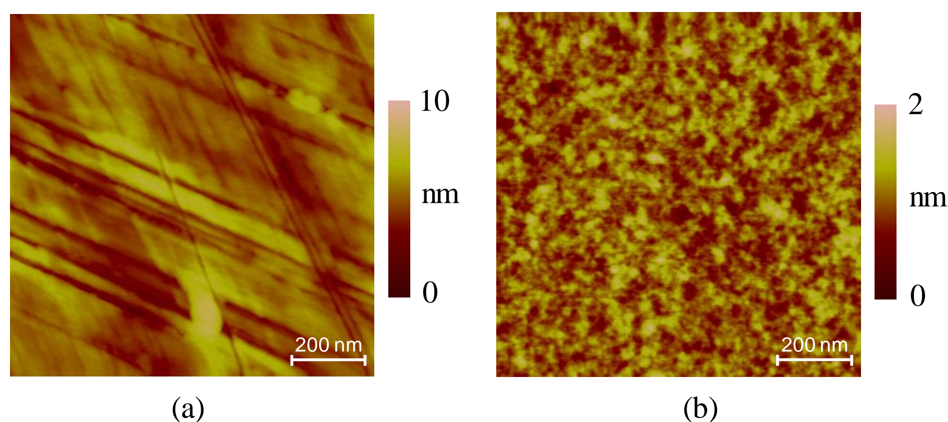

Figure 4.44 AFM images of SiC surfaces. (a) Diamond-abrasive-polished surface (p-v: 7.01 nm, rms: 0.97 nm). (b) ECMP-processed surface (p-v: 1.81 nm, rms: 0.23 nm).

After SiC substrates are sliced from an ingot, several flattening processes, such as grinding, lapping, polishing and finishing, are required before they can be used for the fabrication of electronic devices. The above results demonstrated that SiC surfaces with a subsurface damaged layer are much easier to oxidize, therefore it is considered that the ECMP process can probably be directly applied to sliced or ground substrates with thick subsurface damaged layers. This will be investigated in a future study. For the polishing of SiC, high efficiency and the removal of the damaged layer are usually considered to have a trade-off relationship. On the basis of the above results, this problem can probably be resolved by ceria-slurry-based ECMP.

4.8 Summary

As reported in this chapter, PAP was applied to realize the high-efficiency, low-cost and high-quality polishing of 4H-SiC. The surface modification of SiC by AP-plasma was confirmed, and PAP using the symmetric PAP machine, the two-step PAP process and the prototype PAP machine were conducted. The oxidation mechanism and the material removal mechanism in PAP were also studied. This chapter can be summarized as follows.

(1) It has been confirmed that scratches and SSD were formed in the lapping or polishing of 4H-SiC using diamond abrasive. In the case of conventional CMP, scratch-free surfaces were obtained. However, the step-terrace structure was very disordered and atomic extractions existed on the polished surface.

(2) The surface modification of SiC by the irradiation of AP-plasma was confirmed. It was found that the surface modification efficiency of water-vapor-containing plasma was higher than that of oxygen-containing plasma. It was proved that after the irradiation of the water-vapor-containing plasma, SiC was modified to SiO_2 with a decrease in surface hardness.

(3) In PAP, the density of OH radicals, which were the dominant oxide species, was greatly affected by the concentration of water vapor in the carrier gas. The strongest optical emission intensity from OH radicals was obtained when the water vapor concentration in He was approximately 200 ppm. The increase in surface modification efficiency was confirmed by XPS.

(4) The symmetric PAP machine, which combined irradiation with water-vapor-containing plasma and CeO_2 abrasive polishing, was applied to 4H-SiC (0001). The complete removal of scratches was confirmed and a well-ordered step-terrace structure was formed on the

polished surface without the formation of SSD. PAP using Al_2O_3 was also conducted and many scratches were formed on the surface.

(5) The oxidation process of 4H-SiC (0001) with water-vapor-containing plasma was studied, which indicated that both SiO_2 and a silicon oxycarbide layer were formed as the oxidation products, and the interface between the oxide layer and SiC was found to be very flat. The atomic flattening mechanism of PAP was proposed. Oxidation with water-vapor-containing plasma resulted in the formation of an atomically flat interface; ceria abrasive removed the oxide layer, including the intermediate Si-C-O layer, which could not be removed by dipping in HF solution, to form an atomically flat 4H-SiC (0001) surface with a step-terrace structure.

(6) The thermal oxidation and plasma oxidation processes for 4H-SiC (0001) were compared and discussed to clarify the oxidation process. Plasma oxidation had a higher oxidation rate than thermal oxidation. In particular, the initial oxidation rate of plasma oxidation was six times higher than that of thermal oxidation. Because of the high initial oxidation rate of plasma oxidation, the oxide-SiC interface was very rough when the oxide layer was thin and became flat with increasing thickness of the oxide layer. In contrast, the oxide-SiC interface formed by thermal oxidation was atomically flat regardless of the thickness of the oxide layer owing to its extremely low oxidation rate. Many pits, which penetrated into the bulk SiC, were found on the surface processed by thermal oxidation, whereas few pits were observed on the surface processed by plasma oxidation. These pits were generated by the preferential oxidation of defects in bulk SiC, and the formation of pits was considered to be most affected by the high oxidation temperature in thermal oxidation.

(7) After the oxide layers formed by thermal oxidation and plasma oxidation were removed by polishing using CeO_2 as an abrasive, an atomically flat SiC surface with a well-ordered step-terrace structure was obtained in both cases, although some pits remained on the surface processed by thermal oxidation. It was demonstrated that the combination of plasma oxidation and polishing using CeO_2 is very effective for obtaining atomically flat 4H-SiC substrates without the formation of pits or scratches.

(8) It was found that the polishing efficiency of conventional CMP for the C-face of 4H-SiC was very low regardless of whether SiO_2 slurry or CeO_2 slurry was used. Even after prolonged polishing (15 h for CeO_2 polishing and 9 h for SiO_2 polishing), the scratches were not completely removed. With the combination of thermal oxidation and CeO_2 slurry polishing, an atomically flat C face with a well-ordered step-terrace structure was obtained, although many

pits originating from the dislocations were formed after polishing.

(9) Ceria-slurry-based ECMP, which combined anodic oxidation and abrasive polishing, was proposed as a prepolishing process for the PAP of SiC substrates. In the ECMP process, SiC is anodically oxidized to SiO_2 with a very high initial oxidation rate compared with plasma oxidation and thermal oxidation. Also, it was confirmed that anodic oxidation greatly decreased the surface hardness of SiC, which made it possible to polish the modified surface using CeO_2 slurry. After applying ECMP to a diamond-abrasive-polished SiC surface for 30 min, a scratch-free and smooth surface was obtained. It is expected that with additional abrasive polishing, the residual oxide layer can be completely removed and an atomically flat SiC surface with a step-terrace structure can be obtained.

References

1) G. Ziegler, P. Lanig, D. Theis and C. Weyrich, IEEE Trans. Elect. Devices 30 (1983) 277-281.
2) L. Zhou, V. Audurier, P. Pirouz and J. A. Powell J. Electrochem. Soc. 144 (1997) L161-L163.
3) H. Aida, T. Doi, H. Takeda, H. Katakura, S. W. Kim, K. Koyama, T. Yamazaki and M. Ueda, 12 (2012) S41-S46.
4) https://unit.aist.go.jp/adperc/ci/teams/wpt.html.
5) http://www.shuwaind.com/grinding/sgm8000.html
6) http://www.sicc.cc/en/
7) H. S. Lee, D. I. Kim, J. H. An, H. J. Lee, K. H. Kim and H. Jeong, Ann. CIRP 56 (2010) 333-336.
8) J. R. Grim, M. Benamara, M. Skowronski, W. J. Everson and V. D. Heydemann, Semicond. Sci. Technol. 21 (2006) 1709-1713.
9) K. Yamamura, T. Takiguchi, M. Ueda, A. N. Hattori and N. Zettsu, Adv. Mater. Res. 126-128 (2010) 423-428.
10) H. Deng, T. Takiguchi, M. Ueda, A. N. Hattori, N. Zettsu and K. Yamamura, Jpn. J. Appl. Phys. 50 (2011) 08JG05.
11) H. Deng, K. Monna, T. Tabata, K. Endo and K. Yamamura, Ann CIRP 63 (2014) 529-532.
12) T. Harb, W. Kedzierski and J. W. McConkey, J. Chem. Phys. 115 (2001) 5507-5512.
13) N. Krstulovic, I. Labazan, S. Milosevic, U. Cvelbar, A. Vesel and M. Mozetic, J. Phys. D: Appl. Phys. 39 (2006) 3799-3804.
14) T. L. Barr, J. Phys. Chem. 82 (2001) 1801-1810.
15) W. C. Oliver and G. M. Pharr, J. Mater. Res. 7 (1992) 1564-1583.
16) A. Sarani, A. Yu. Nikiforov and C. Leys, Phys. Plasmas 17 (2010) 063504.
17) K. Yamamura, T. Takiguchi, M. Ueda, H. Deng, A. N. Hattori and N. Zettsu, Ann. CIRP 60 (2011)

571-574.

18) H. Deng, M. Ueda and K. Yamamura, Int. J. Adv. Manuf. Technol. 72 (2014) 1-7.

19) A. B. Shorey, K. M. Kwong, K. M. Johnson and S. D. Jacobs, Appl. Opt. 39 (2000) 5194-5204.

20) B. Hornetz, H. J. Michel and J. Halbritter, J. Mater. Res. 9 (1994) 3088-3094.

21) H. Deng and K. Yamamura, Ann. CIRP 62 (2013) 575-578.

22) R. Palmieri, C. Radtke, H. Boudinov and E. F. Silva, Appl. Phys. Lett. 95 (2009) 113504.

23) H. Deng, K. Endo and K. Yamamura, Appl. Phys. Lett. 104 (2014) 101608.

24) H. Deng, K. Endo and K. Yamamura, Appl. Phys. Lett. 103 (2013) 111603.

25) C. Li, I. B. Bhat, R. Wang and J. Seiler, J. Electron. Mater. 33 (2004) 481-486.

26) Y. Ishikawa, Y. Matsumoto, Y. Nshida, S. Tanigichi and J. Watanabe, J. Am. Chem. Soc. 125 (2003) 6558-6562.

27) Y. Song, S. Dhar, L. C. Feldman, G. Chung and J. R. Williams, J. Appl. Phys. 95 (2004) 4953-4957.

28) H. A. Schwarz and R. W. Dodson, J. Phys. Chem. 88 (1984) 3643-3647.

29) S. Ha, P. Mieszkowski, M. Skowronski and L. B. Rowland, J. Cryst. Growth 244 (2002) 257-266.

30) T. Ohno, H. Yamaguchi, S. Kuroda, K. Kojima, T. Suzuki and K. Arai, J. Cryst. Growth 260 (2004) 209-216.

31) S. E. Saddow, T. E. Schattner, J. Brown, L. Grazulis, K. Mahalingam, G. Landis, R. Bertke and W. C. Mitchel, J. Electron. Mater. 30 (2000) 228-234.

32) K. Fukuda, M. Kato, K. Kojima and J. Senzaki, Appl. Phys. Lett. 84 (2004) 2088-2090.

33) H. Hara, Y. Sano, H. Mimura, K. Arima, A. Kubota, K. Yagi, J. Murata and K. Yamauchi, J. Electron. Mater. 35 (2006) L11-L14.

34) K. Hotta, K. Hirosei, Y. Tanaka, K. Kawata and O. Eryu, Materials Science Forum 600-603 (2009) 823-826.

35) T. Kido, M. Nagaya, K. Kawata and T. Kato, Mater. Sci. Forum 778-780 (2014) 754-758.

36) H. Deng, K. Hosoya, Y. Imanishi, K. Endo and K. Yamamura, Electrochem. Commun. 52 (2015) 5-8.

37) N. Ballarin, C. Carraro, R. Maboudian, L. Magagnin, Electrochem. Commun. 40 (2014) 17-19.

38) K. Yamamura, Japanese patent application No. 2013-060147 (2013).

39) K. Yamamura, K. Hosoya, Y. Imanishi, H. Deng, K. Endo, Adv. Mater. Res., 1017 (2014) 509-514.

Chapter 5

Control of the surface atomic structure of 4H-SiC (0001) [1]

5.1 Introduction

As described in Chapter 1, in recent years, several polishing techniques combining surface modification or etching and mechanical polishing, such as CMP [2-4], CARE [5-8], ultraviolet-assisted polishing [9, 10], PAP [11-14] and so forth [15, 16], have been proposed for the damage-free and atomic-scale flattening of the Si-face of 4H-SiC substrates. In most of these techniques, the surface of the 4H-SiC substrate is modified by chemical reactions, and a modified layer that is easy to remove is formed. The modified layer is removed by abrasive polishing or etching to realize surface flattening. With the application of these polishing techniques, the formation of atomically flat SiC substrate surfaces with a well-ordered step-terrace structure has been reported.

Although the step-terrace structures on the surfaces obtained by these polishing techniques were well-ordered, several types of periodic step-terrace structure were usually formed. In PAP, a step-terrace structure with four types of terrace that appear alternately was generated (a narrow terrace, a wide terrace and two terraces of intermediate width) [12]. This type of step-terrace structure is defined as the a-b-a*-b* type. In the case of catalyst-referred etching, a step-terrace structure with alternating narrow and wide terrace pairs has been reported [6]. This type of step-terrace structure is defined as the a-b type. In the case of SiC surfaces processed by CMP, which is the most widely used method nowadays, an a-b type step-terrace structure or a step-terrace structure with a uniform terrace width, which is defined as the a-a type, can be observed on different substrates [17].

Although the generation of the a-b-a*-b* type, a-b type and a-a type step-terrace structures on 4H-SiC (0001) has been reported and studied in my previous study [14], their generation mechanism has not been thoroughly clarified. Also, these three types of step-terrace structure have occasionally been obtained in different polishing techniques [6, 12, 17], although the process conditions under which they were formed are unclear. Therefore, the control of the step-terrace structure of 4H-SiC has not been realized yet. It is expected that control of the surface atomic structure of 4H-SiC will be highly advantageous for improving its performance in power device applications. In this chapter, the probable formation mechanism of these different types of step-terrace structure is proposed and

experimentally clarified. Furthermore, control of the step-terrace structure of 4H-SiC was realized by adjusting the balance between chemical modification and physical removal in polishing.

5.2 Crystal structure of 4H-SiC

In all the above-mentioned polishing techniques, chemical modification, such as oxidation or etching, and physical removal, such as abrasive polishing, are combined [6, 12, 17]. Chemical modification softens the SiC substrate surface and abrasive polishing removes the modified layer to flatten the surface. Consistent with its name, there are four Si-C bilayers in one unit cell of 4H-SiC single crystal as shown in Figure 5.1. It is considered that there may be a relationship between the generation of these periodic step-terrace structures with different terrace widths and the four Si-C bilayers in a unit cell of 4H-SiC. In fact, it has been reported that there are two types of Si-C terrace, 4H1 and 4H2 terraces, existing in 4H-SiC depending on the physical relationship with the bilayers below [18, 19]. According to a previous calculation result, the extra energy required to deposit a new layer on a 4H1 terrace is much higher than that for a 4H2 terrace [20-22]. In other words, a 4H1 terrace is much more stable than a 4H2 terrace. On the basis of this calculation result, Arima *et al*. proposed that the etching rates of 4H1 and 4H2 terraces are different, resulting in the generation of an a-b type step-terrace structure in a catalyst-referred etching process [23]. However, the difference between 4H1 and 4H2 terraces cannot explain the generation of a-b-a*-b* type and a-a type step-terrace structures.

On the other hand, in the calculation of the extra energy required for deposition, the number of dangling bonds (DBs) at the step edge was not taken into consideration. When 4H-SiC is oxidized

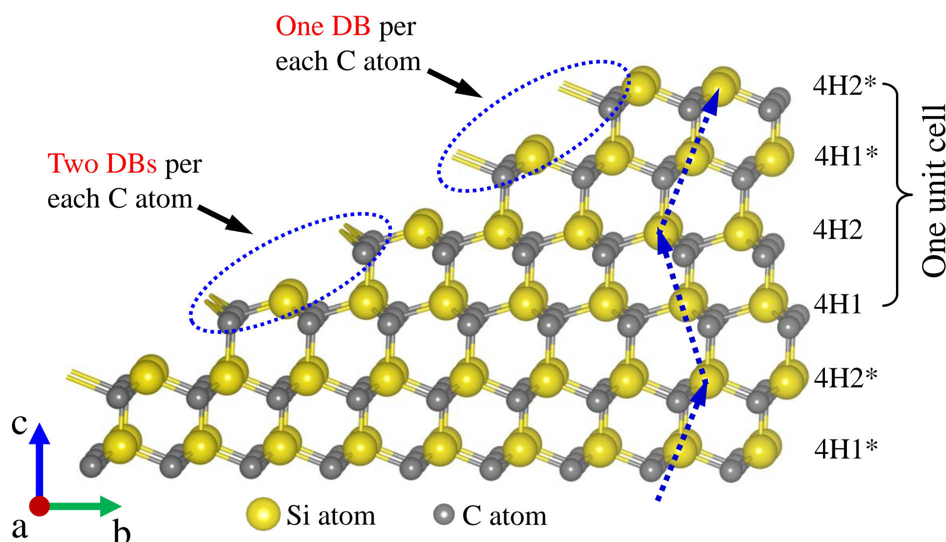

Figure 5.1. Crystal structure of 4H-SiC. Bond configuration of step-terrace structure on a 4H-SiC (0001) surface viewed from the [11-20] direction.

or polished, chemical reactions or physical removal starts from the step edge since the atoms at the step edge are the most unstable. Therefore, the number of DBs at the step edge strongly affects the oxidation rate (r_{oxi}) of the terrace. As shown in Figure 5.1, taking the number of DBs of C atoms at the step edge into consideration, it is found that there are two terrace pairs in a unit cell of 4H-SiC. In one terrace pair, there is only one DB for each C atom at the step edge (4H1* and 4H2*), while in the neighboring terrace pair there are two DBs for each C atom at the step edge (4H1 and 4H2) as shown in Figure 5.1. This means that r_{oxi} for the 4H1-4H2 terrace pair is higher than that for the 4H1*-4H2* terrace pair. Also, in the terrace pairs 4H1-4H2 and 4H1*-4H2*, r_{oxi} for 4H2 or 4H2* is higher than that for 4H1 or 4H1* according to the results of previous first-principles calculations [18, 19].

Correspondingly, it is concluded that these four types of Si-C terrace in a unit cell of 4H-SiC (4H1, 4H2, 4H1* and 4H2*) have different values of r_{oxi}.

5.3 Probable mechanism for controlling the surface atomic structure of 4H-SiC (0001)

When 4H-SiC is oxidized, oxidation starts from the step edges, which are the most unstable areas on the substrate surface. Since there are four values of r_{oxi} in a unit cell of 4H-SiC, the widths of the corresponding oxidized terraces are different. Therefore, it is reasonable to consider that the generation of the a-b-a*-b* type step-terrace structure results from the four types of Si-C terrace with different values of r_{oxi}. However, the a-b type and a-a type step-terrace structures can also be observed in other polishing techniques. Obviously the generation of these two types of step-terrace structure cannot be explained only by the oxidation process.

In the above-mentioned polishing techniques, chemical reactions and abrasive polishing simultaneously occur [6, 12, 17]. Since the values of r_{oxi} for the four types of Si-C terrace in a unit cell are different, the oxidation process preferentially leads to different terrace widths in a unit cell of 4H-SiC, resulting an a-b-a*-b* type step-terrace structure. On the other hand, in the abrasive polishing process, the modified layer is first removed. Then, there is abrasive contact with SiC at the step edge and strain is introduced. With the repetition of this process, Si-C terraces are removed from the step edge. Since abrasive polishing is a physical removal process, the removal rates by polishing (r_{pol}) of the four types of Si-C terrace in 4H-SiC are the same. This means that abrasive polishing preferentially leads to a uniform terrace width, resulting in an a-a type step-terrace structure. In the above polishing techniques, both chemical modification and physical removal occur. It is considered that under different polishing conditions, the balance between chemical modification and physical removal is different, which leads to different types of step-terrace structure.

On the basis of the above analysis, I consider that the generation of the three types of step-terrace structures, a-a type, a-b type and a-b-a*-b* type, can be controlled by changing the balance between chemical modification and physical removal in the polishing of 4H-SiC. The formation mechanism of the three types of step-terrace structure of 4H-SiC is proposed as shown in Figure 5.2. This mechanism is based on the balance between r_{oxi} and r_{pol}. As shown in Figure 5.2(a), in the case that chemical modification plays the main role in slurry polishing, r_{oxi} is higher than r_{pol} and abrasive polishing only removes the modified oxide layer. As previously mentioned, the four types of Si-C terrace in a unit cell of 4H-SiC, 4H1, 4H2, 4H1* and 4H2* have different values of r_{oxi}. The oxidation of SiC starts from the step edge. For these four types of Si-C terrace, the widths of the corresponding oxidized terraces are different. After a modified layer is formed, it is removed by abrasive polishing. Upon the removal of the modified layer, the a-b-a*-b* type step-terrace structure is formed.

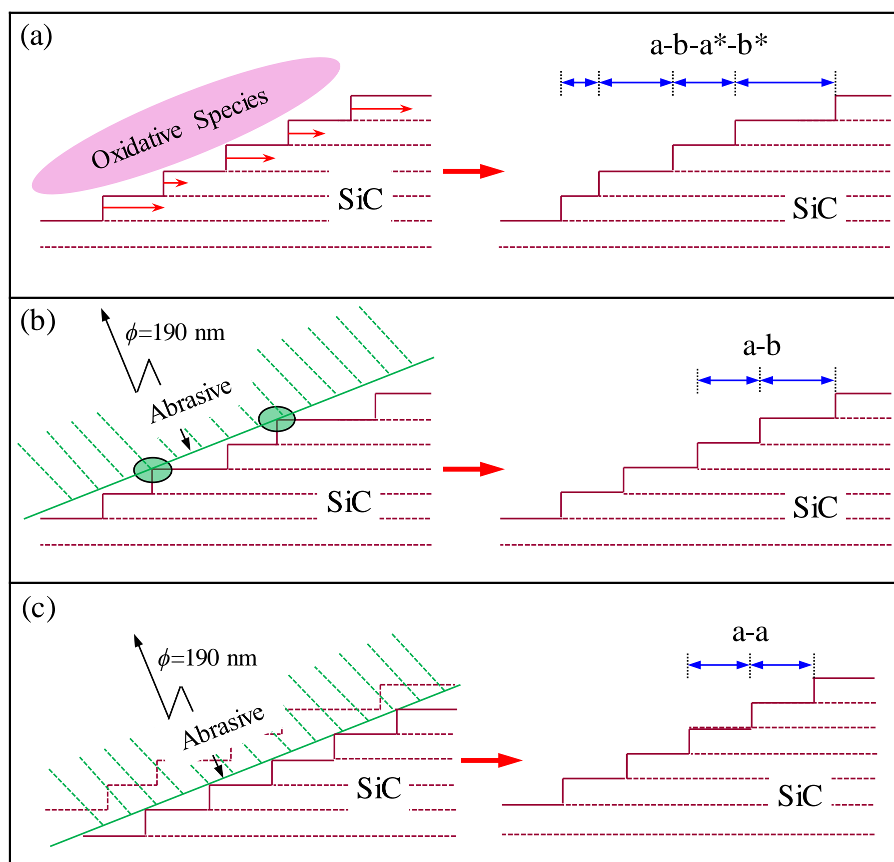

Figure 5.2 Probable formation mechanism of step-terrace structure of 4H-SiC. (a) Surface modification was dominant, resulting in the formation of the a-b-a*-b* type step-terrace structure. (b) Physical removal was comparable with surface modification, resulting in the formation of the a-b type step-terrace structure. (c) Physical removal was dominant, resulting in the formation of the a-a type step-terrace structure.

If the value of r_{pol} for abrasive polishing increases and becomes comparable to r_{oxi} for surface modification, as shown in Figure 5.2(b), contact between the abrasive and the SiC step edges occurs. The diameter of the abrasive particles is very large compared with the height of the SiC steps of 0.25 nm. Thus, after the a-b-a*-b* type step-terrace structure is formed, the step edge of the wide terraces preferentially comes in contact with the abrasive particles. If r_{pol} is low, the amount of physical removal is very limited and the modified layer is mainly removed. However, contact between the abrasive and the wide terraces frequently occurs when the value of r_{pol} for abrasive polishing increases. Owing to the contact between the abrasive and SiC, strain is applied to the contact area. The area subjected to strain is rapidly oxidized and immediately removed by abrasive polishing, *i.e.*, the wide terraces are preferentially removed. Thus, the a-b-a*-b* type step-terrace structure is changed to the a-b type. In this case, the physical removal factor is comparable to the chemical oxidation factor in the polishing of SiC.

Finally, if the value of r_{pol} for abrasive polishing is greatly increased to higher than the value of r_{oxi} for Si-C step edges, physical removal plays the main role as shown in Figure 5.2(c). In the case of a high r_{pol} for abrasive polishing, the modified layer is removed rapidly and physical removal of the Si-C from step edges occurs. Owing to the high r_{pol}, all the terraces in SiC are in uniform contact with the abrasive particles after the oxide layer is removed. Therefore, all the terraces are removed at the same rate and the uniform a-a type step-terrace structure is formed.

5.4 Proof of the proposed removal mechanism

To prove the validity of the proposed removal mechanism, 4H-SiC (0001) substrates were polished using CeO_2 slurry with different rotation speeds of the polishing pad. CeO_2 slurry was used because it has been widely reported that some Si-based materials, such as Si, SiO_2, Si_3N_4 and SiC, can be polished by CeO_2 abrasive owing to its tribocatalytic properties [24-28]. That is to say, both chemical modification and physical removal occur in the polishing of SiC using CeO_2 slurry.

Commercially available single-crystal 4H-SiC substrates (on-axis, n-type, 350 μm in thickness) supplied by TanKeBlue Semiconductor Co. Ltd. were used in this work. All the experiments were conducted on the Si (0001) face, which is the most commonly used face for power devices. The experimental setup shown in Figure 3.5 was used in this study and both the polishing pad and the SiC specimen were immersed in the CeO_2 slurry. The polishing pad was scanned on the specimen with a scanning speed of 200 mm/min for a distance of 10 mm. The pad rotation speed was increased from 500 rpm to 1500 rpm and finally to 2500 rpm. Each specimen was polished for 3 h. In each polishing experiment, a new polishing pad was used and the slurry was replaced. Table 5.1 gives the details of the parameters in the polishing.

A nanoindenter (ENT-2100, ELIONIX Inc.) was used to form some indents on the specimen, which were used as marks in AFM observations. The maximum load applied for indentation was 100 mN. A total of 400 indents (20×20) separated by a distance of 10 μm were formed. The surface morphology of the polished SiC substrates was measured by AFM (D3100, Digital Instruments) in the tapping mode. For each specimen, 100 points that were uniformly distributed over the polished area were observed. The surface composition of the SiC substrates polished with pad rotation speeds of 500 rpm and 2500 rpm was determined by XPS (Quantum 2000, ULVAC-PHI) with AlKα radiation (1486.6 eV). To centralize the XPS observation to the top surface, the stage on which the specimen was located was tilted with a very low takeoff angle of 10˚. Before the XPS measurements, to remove the organic contaminants on the specimen, cleaning in a sulfuric acid (H_2SO_4) and hydrogen peroxide (H_2O_2) mixture (SPM) was conducted for 10 min followed by cleaning in pure water for 10 min. The concentration of the SPM solution was H_2SO_4 (97 wt%): H_2O_2 (30 wt%) =4:1. For each specimen, five points uniformly distributed over the polished area were observed to exclude any area dependence.

In the polishing of 4H-SiC substrates with CeO_2 slurry, modification of the SiC substrate surface and abrasive polishing to remove the modified layer are combined. The surface of SiC is modified to silicon oxycarbide (Si-C-O) and further modified to SiO_2 owing to the tribocatalytic effect of the CeO_2 abrasive [29]. Also, this modification process is promoted by the chemicals in the slurry such as hydroxide (OH) as well as the lattice strain caused by the pressure applied by the polishing pad [30]. After the surface is modified, the modified layer is immediately removed by the CeO_2 abrasive. The composition of the slurry and the load during polishing affect the value of r_{oxi} for SiC in CeO_2 slurry polishing. Therefore, SiC is polished under a constant load with the same slurry, which means that the factors affecting the chemical modification of SiC did not change in the polishing experiments. The pad rotation speed was increased in three stages from 500 rpm to 2500 rpm. According to Preston's law, the value of r_{pol} in abrasive polishing increases linearly with the relative speed between the specimen and the polishing pad. This means that the value of r_{pol} in abrasive polishing increases with the pad rotation speed [31]. In this way, the balance between the chemical modification (r_{oxi}) and physical removal (r_{pol}) of SiC in CeO_2 slurry polishing can be controlled.

Table 5.1. Polishing conditions

Experimental setup	Figure 3.5
Polishing pad	Suede type, NP178 (ϕ10 mm)
Slurry abrasive	CeO_2 (ϕ190 nm)
Slurry concentration & pH	1 wt% (pH: 8.53)
Pressure	3.74 kPa
Time	3 h
Pad rotation speed	500, 1500, 2500 rpm

A SiC specimen was first polished by CeO_2 slurry with a pad rotation speed of 500 rpm. Then, the same specimen was polished by CeO_2 slurry with the pad rotation speed increased to 1500 rpm followed by polishing with a pad rotation speed of 2500 rpm. To confirm the change in the step-terrace structure with the increase in the pad rotation speed, it is very helpful to observe the same area of the same specimen. However, owing to the small observation area in AFM, it was very difficult to find the same place on the same specimen after each polishing experiment. Therefore, a nanoindenter was used to form some fiducial indents on the surface to be polished, which were helpful for finding the same area in AFM observation. Figure 5.3(a) shows an image of the indents obtained by the charge-coupled device (CCD) camera of the microscope. Using these indents as fiducial marks, the AFM observation after each polishing experiment was localized to the area in the lower-left corner, which included four indents as shown in Figure 5.3(b). In this way, the change in the step-terrace structure could be observed at the same area of the same specimen.

The change in the step-terrace structure with the increase in the pad rotation speed is shown in Figure 5.4. When the surface was polished with a pad rotation speed of 500 rpm, the a-b-a*-b* type step-terrace structure was formed as shown in Figure 5.4(a). In such a step-terrace structure, four types of terrace, a narrow terrace, a wide terrace and two terraces with intermediate width, alternately appeared on the polished surface. After this specimen was polished with a pad rotation speed of 1500 rpm, the step-terrace structure changed from the a-b-a*-b* type to the a-b type as shown in Figure 5.4(b). In the a-b type step-terrace structure, terrace pairs with narrow and wide terraces alternately appeared on the polished surface. Finally, after the specimen was polished with a pad rotation speed of 2500 rpm, the step-terrace structure changed from the a-b type to the uniform a-a type, as shown in Figure 5.4(c), in which all the terraces had the same width.

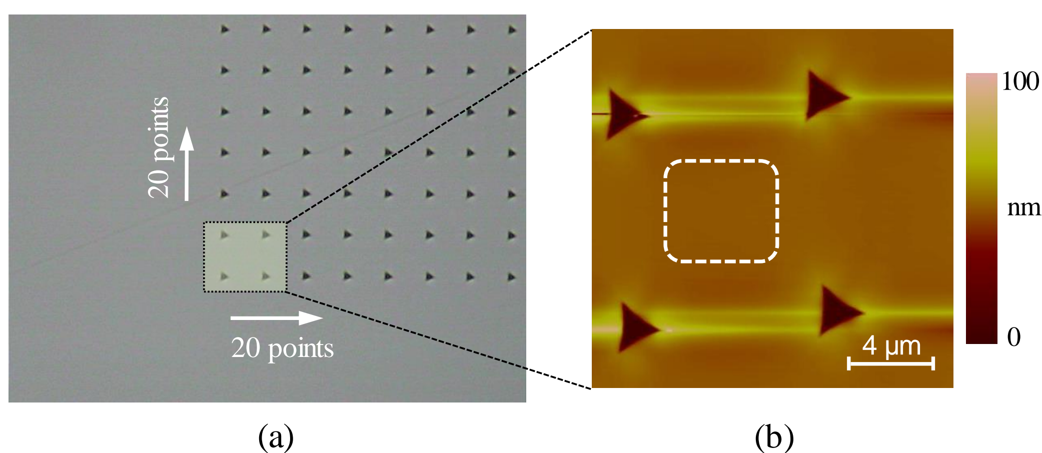

Figure 5.3 Fiducial indents on the SiC surface. (a) CCD image of the fiducial indents formed on the surface of 4H-SiC to be polished. b) AFM image of the lower-left corner of the indented area. The change in the step-terrace structure on the polished surface after each polishing experiment was observed in the same area indicated by the dashed square.

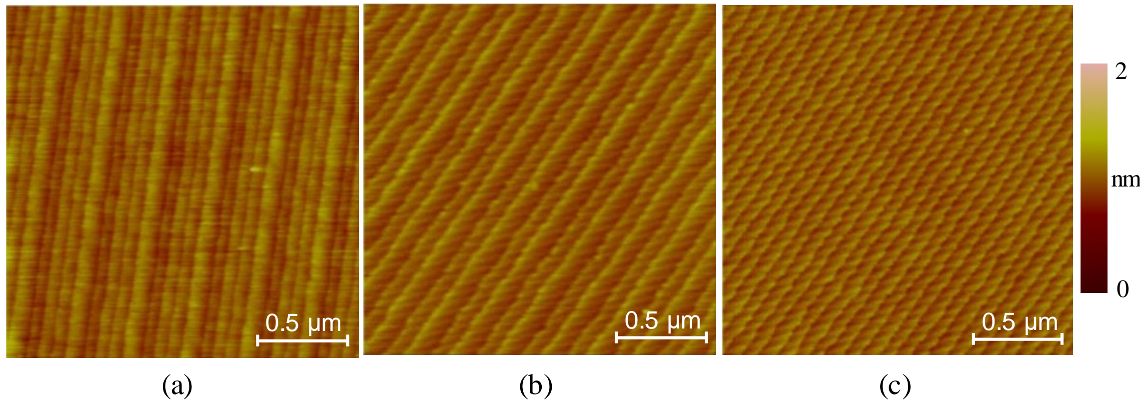

Figure 5.4 AFM observation of polished SiC surfaces. Change in the step-terrace structure with increasing pad rotation speed observed by AFM. (a) 500 rpm. (b) 1500 rpm. (c) 2500 rpm.

It was concluded that the step-terrace structure on the polished 4H-SiC (0001) substrate surface could be changed by changing the pad rotation speed. When the pad rotation speed increased from 500 rpm to 1500 rpm and 2500 rpm, the step-terrace structure changed from the a-b-a*-b* type to the a-b type and the uniform a-a type, respectively. Consistent with the mechanism proposed in Figure 5.2, increasing the pad rotation speed increased the value of r_{pol} for abrasive polishing, resulting in a change in the balance between surface modification and abrasive polishing in the slurry polishing of 4H-SiC.

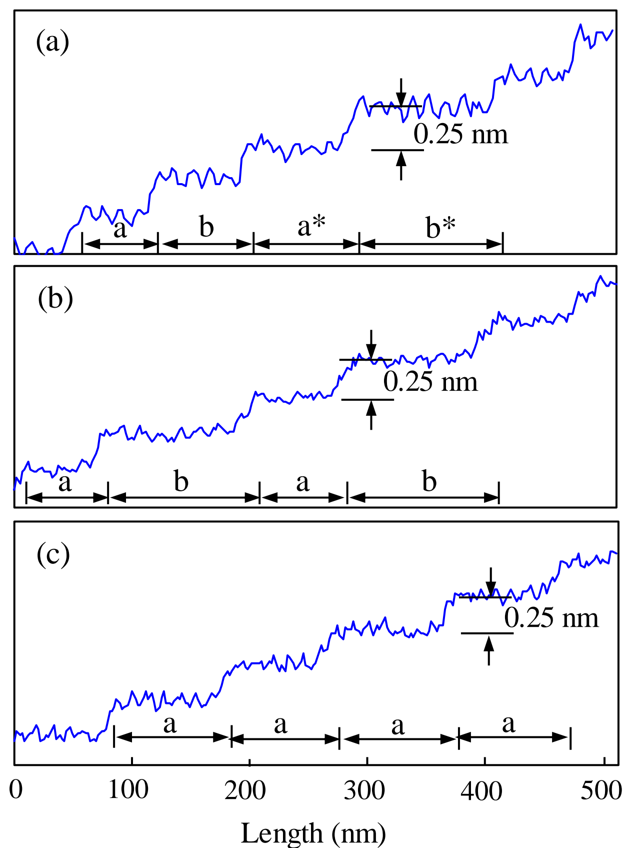

Figure 5.5 Cross-sectional views of the AFM images shown in Figure 5.4 with tilt corrected. (a). Figure 5.4(a). (b). Figure 5.4(b). (c). Figure 5.4(c).

Figure 5.5 shows cross-sectional views of the AFM images shown in Figure 5.4 with the tilt corrected. All the step-terrace structures have a very uniform step height of 0.25 nm, corresponding to a single 4H-SiC bilayer. The terrace widths of these three types of step-terrace structure are shown in Table 5.2. Although the terrace width is different in different types of step-terrace structure, the off-angles of these polished surfaces are almost the same.

Table 5.2 Terrace widths of the a-b-a*-b* type, a-b type and a-a type step-terrace structures and off-angles of the polished surfaces

Type	Width (nm)				Off angle (˚)
	a	b	a*	b*	
a-b-a*-b*	65.8	85.6	92.2	125.1	0.155
a-b	73.5	133.7	-	-	0.138
a-a	95.9	-	-	-	0.149

This means that increasing the pad rotation speed only changed the step-terrace structure and not the off-angle of the polished surface.

According to the results of AFM observation, the change in the step-terrace structure in the same area was confirmed. However, compared with the AFM observation area, the polished area was much larger. Therefore, it was necessary to evaluate the distribution of step-terrace structures on the whole polished area after each polishing experiment. For each specimen, 100 points uniformly distributed over the polished area were observed. Figure 5.6 shows the distribution of different types of step-terrace structure on 4H-SiC substrate surfaces polished with different pad rotation speeds. In the case of a pad rotation speed of 500 rpm, although both the a-b-a*-b* type and a-b type step-terrace structures were observed, the a-b-a*-b* type had a very high frequency of 91% as shown in Figure 5.6(a). Also, in this case, the a-a type step-terrace structure was not found. On the surface polished with a pad rotation speed of 1500 rpm, as shown in Figure 5.6(b), all three types of step-terrace structure were observed and the a-b type step-terrace structure had a high frequency of 81%.

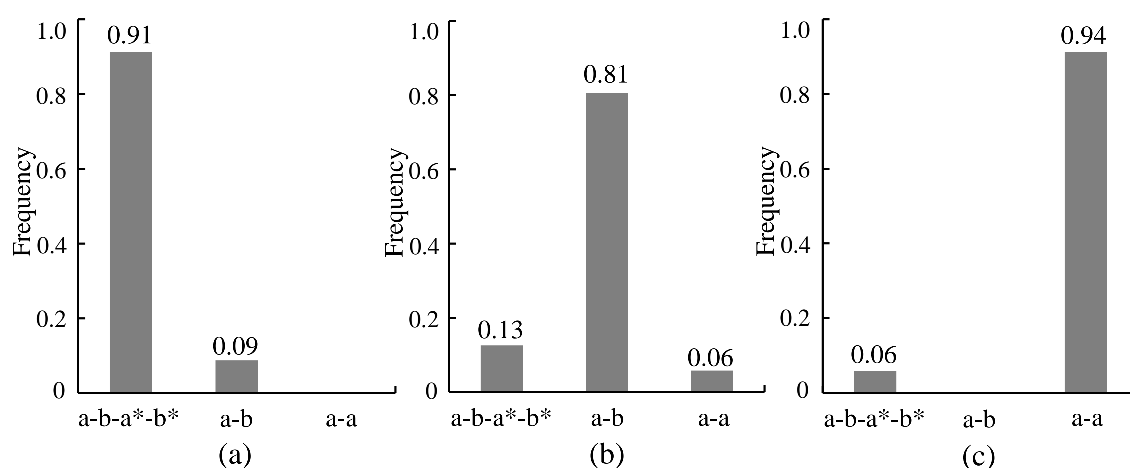

Figure 5.6 Step-terrace structure distribution. Distribution of the a-b-a*-b* type, a-b type and a-a type step-terrace structures on 4H-SiC substrate surfaces polished with different pad rotation speeds. (a) 500 rpm. (b) 1500 rpm. (c) 2500 rpm.

When the pad rotation speed was increased to 2500 rpm, 94% of the observed areas showed the a-a type step-terrace structure.

According to the proposed mechanism, with the change in the balance between chemical modification and physical removal caused by changing the pad rotation speed, there should be more oxidation products on a surface polished with a low pad rotation speed than on a surface polished with a high pad rotation speed. Therefore, the residual oxidation products on the polished surfaces were determined by ARXPS. To increase the difference in the amount of residual oxidation products on the polished surfaces, SiC surfaces polished with the lowest pad rotation speed of 500 rpm and the highest pad rotation speed of 2500 rpm were used for ARXPS measurements. Figure 5.7(a) shows the carbon core-level (C1s) spectra and oxygen core-level (O1s) spectra of the SiC substrate surface polished by CeO_2 slurry with a pad rotation speed of 500 rpm. The strong Si-C peak was assigned to the bulk SiC and a peak of O-H was also observed owing to the adsorption of water

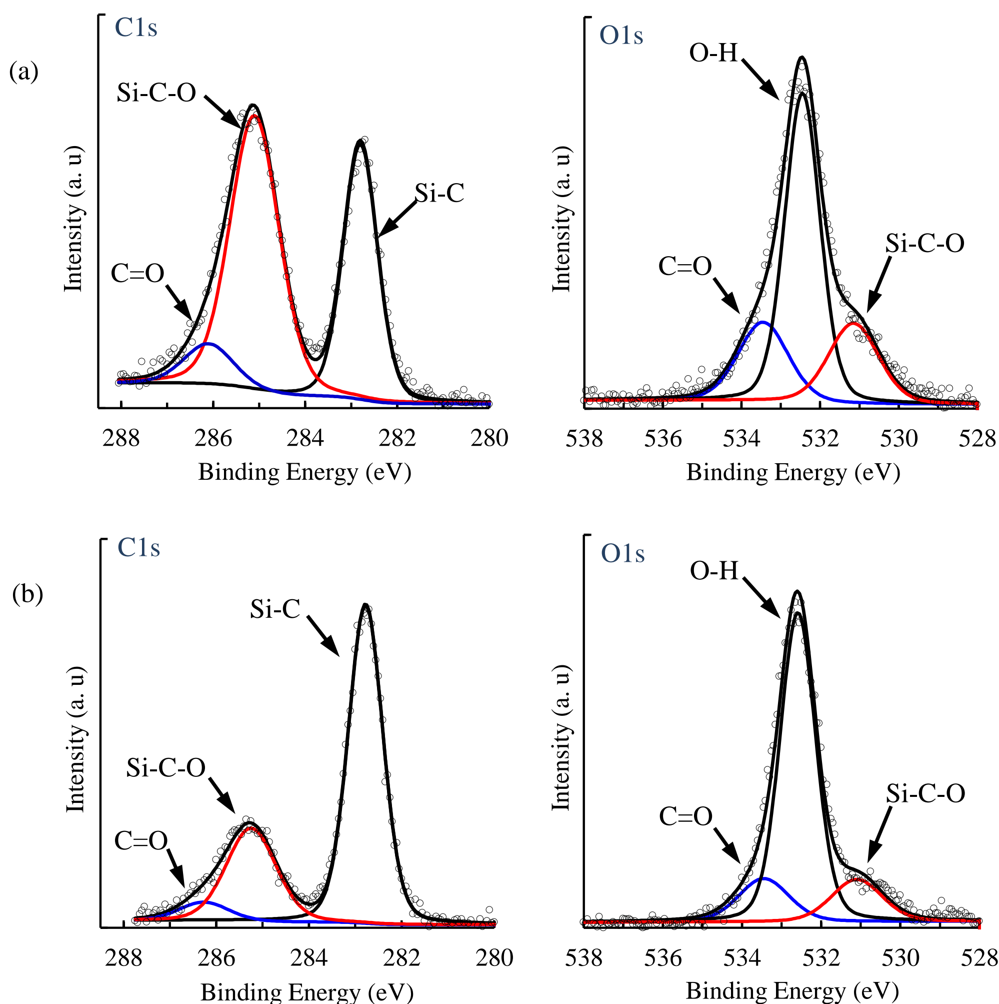

Figure 5.7 C1s and O1s spectra of the polished SiC substrate surface. (a) 500 rpm. (b) 2500 rpm.

vapor or the surface termination of hydroxide. Other peaks, such as Si-C-O and C=O, were considered to originate from residual oxidation products on the polished surfaces [32, 33]. It was found that the Si-C-O peak intensity was even stronger than that of Si-C; thus, the thickness of silicon oxycarbide was greater than that of SiC within the detection depth of XPS. In contrast, Figure 5.7(b) shows the C1s spectra and O1s spectra of a SiC surface polished by CeO_2 slurry with a pad rotation speed of 2500 rpm. The surface composition was the same as the surface shown in Figure 5.7(a). However, the amount of oxidation products on this surface was small since the intensities of the Si-C-O and C=O peaks were relatively weak compared with those of the surface polished with a pad rotation speed of 500 rpm. According to my proposed removal mechanism, for a pad rotation speed of 500 rpm, chemical reactions played the main role in CeO_2 slurry polishing; thus, there should be more oxidation products remaining on the polished surface. On the other hand, for a pad rotation speed of 2500 rpm, r_{pol} was increased and physical removal played the main role, therefore the amount of residual oxidation products should be small. The results of XPS measurement shown in Figure 5.7 support my proposed mechanism.

In my previous study, the a-b-a*-b* type step-terrace structure was obtained by PAP [11-13]. In PAP, the irradiation of atmospheric-pressure water vapor plasma was used for surface modification. Plasma irradiation and abrasive polishing (CeO_2) were simultaneously conducted for surface flattening. For the oxidation of 4H-SiC, water-vapor-containing plasma had a high initial r_{oxi} of 0.185 μm/h [34]. The value of r_{pol} for abrasive polishing was much lower than that of r_{oxi} for oxidation in water-vapor-containing plasma. According to the proposed mechanism, the high r_{oxi} was the reason for the generation of the a-b-a*-b* type step-terrace structure in PAP.

5.5 Summary

By applying different polishing techniques under different polishing conditions, three types of step-terrace structure, the a-b-a*-b* type, a-b type and a-a type, were obtained. By considering the crystal structure of 4H-SiC, a probable mechanism for controlling the surface atomic structure of 4H-SiC (0001) was proposed and experimentally clarified.

(1) By analyzing the crystal structure of 4H-SiC, it was found that there are four types of Si-C terrace in a unit cell of 4H-SiC (4H1, 4H2, 4H1* and 4H2*), which have different values of r_{oxi}.

(2) A probable removal mechanism was proposed for controlling the surface atomic structure of 4H-SiC (0001) by adjusting the balance between chemical modification and physical removal. It was assumed that when r_{pol} for abrasive polishing was lower than the rate of surface modification, the a-b-a*-b* type step-terrace structure was formed. When the pad rotation speed

was increased and r_{pol} for abrasive polishing became comparable to the rate of surface modification, the step-terrace structure changed from the a-b-a*-b* type to the a-b type. When r_{pol} for abrasive polishing was higher than the rate of surface modification, a uniform a-a type step-terrace structure was formed.

(3) CeO_2 slurry polishing of 4H-SiC with different pad rotation speeds was conducted to experimentally clarify the proposed removal mechanism. A change in the surface atomic structure along with the change in the pad rotation speed was confirmed, which supported the proposed removal mechanism.

(4) XPS measurements of the polished surfaces were conducted. The amount of residual oxidation products on the surface polished with a high pad rotation speed was smaller than that on the surface polished with a low pad rotation speed. This result also supported the proposed removal mechanism.

(5) On the basis of this removal mechanism, the results of polishing using existing polishing techniques in which chemical reactions and abrasive polishing are combined can be explained. Furthermore, it is expected that the control of the step-terrace structure on a 4H-SiC substrate will be very advantageous for realizing excellent device performance, which will be experimentally confirmed in a future study.

References

1) H. Deng, K. Endo and K. Yamamura, Sci. Rep. 5 (2015) 8947.
2) L. Zhou, V. Audurier, P. Pirouz and J. A. Powell, J. Electrochem. Soc. 144 (1997) L161-L163.
3) C. L. Neslen, W. C. Mitchel and R. L. Hengehold, J. Electron. Mater. 30 (2001) 1271-1275.
4) H. Aida, T. Doi, H. Takeda, H. Katakura, S. W. Kim, K. Koyama, T. Yamazaki and M. Uneda, Curr. Appl. Phys. 12 (2012) S41-S46.
5) H. Hara, Y. Sano, H. Mimura, K. Arima, A. Kubota, K. Yagi, J. Murata and K. Yamauchi, J. Electron. Mater. 35 (2006) L11-L14.
6) T. Okamoto, Y. Sano, K. Tachibana, K. Arima, A. N. Hattori, K. Yagi, J. Murata, S. Sadakuni and K. Yamauchi, J. Nanosci. Nanotech. 11 (2011) 2928-2930.
7) T. Okamoto, Y. Sano, K. Tachibana, B. V. Pho, K. Arima, K. Inagaki, K. Yagi, J. Murata, S. Sadakuni, H. Asano, A. Isohashi and K. Yamauchi, Jpn. J. Appl. Phys., 51 (2012) 046501.
8) Y. Sano, K. Arima and K. Yamauchi, ECS J. Solid State Sci. Tech. 2 (2013) N3028-N3035.
9) S. H. Hong, J. Watanabe, and M. Touge, Int. J. Manuf. Sci. Technol. 9 (2007) 23-28.

10) J. Watanabe, S. H. Hong, K. Yamaguchi, M. Touge, and N. Kuroda, Proc. Advances in Abrasive Technology (ASAAT 2007) (2007) 91-96.
11) K. Yamamura, T. Takiguchi, M. Ueda, H. Deng, A. N. Hattori and N. Zettsu, CIRP Ann. 60 (2011) 571-574.
12) H. Deng, M. Ueda and K. Yamamura, Int. J. Adv. Manuf. Technol. 72 (2014) 1-7.
13) H. Deng and K. Yamamura, CIRP Ann. 62 (2013) 575-578.
14) H. Deng, K. Monna, T. Tabata, K. Endo and K. Yamamura, CIRP Ann. 63 (2014) 529-532.
15) A. Kubota, M. Yoshimura, S. Fukuyama, C. Iwamoto and M. Touge, Precis. Eng. 36 (2012) 137-140.
16) M. Kikuchi, Y. Takahashi, T. Suga, S. Suzuki and Y. Bando, J. Am. Ceram. Soc. 75 (1992) 189-194.
17) X. L. Shi, G. S. Pan, Y. Zhou, C. L. Zou and H. Gong, Appl. Surf. Sci. 284 (2013) 195-206.
18) J. J. A. Shaw and V. Heine, J. Phys.: Condens. Mater. 2 (1990) 4351-4361.
19) F. R. Chien, S. R. Nutt, W. S. Yoo, T. Kimoto and H. Matsunami, J. Mater. Res. 9 (1994) 940-954.
20) T. Kimoto, A. Itoh, H. Matsunami and T. Okano, J. Appl. Phys. 81 (1997) 3494-3500.
21) V. Heine, C. Cheng and R. J. Needs, J. Am. Ceram. Soc. 74 (1991) 2630-2633.
22) G. R. Yazdi, R. Vasiliauskas, T. Iakimov, A. Zakharov, M. Syvajarvi and R. Yakimova, Carbon 57 (2013) 477-484.
23) K. Arima, H. Hara, J. Murata, T. Ishida, R. Okamoto, K. Yagi, Y. Sano, H. Mimura and K. Yamauchi, Appl. Phys. Lett. 90 (2007) 202106.
24) T. Hoshino, Y. Kurata, Y. Terasaki and K. Susa, J. Non-Cryst Solids 283 (2001) 129-136.
25) M. H. Oh, R. K. Singh, S. Gupta and S. B. Cho, Microelectron. Eng. 87 (2010) 2633-2637.
26) L. Zho, H. Eda, J. Shimizu, S. Kamiya, H. Iwase and S. Kimura, CIRP Ann. 55 (2006) 313-316.
27) Y. B. Tian, L. Zhou, J. Shimizu, Y. Tashiro and R. K. Kang, Appl. Surf. Sci. 255 (2009) 4205-4211.
28) S. Kamiya, H. Iwase, K. Kishita, L. Zhou, H. Eda and Y. Yoshida, J. Vac. Sci. Technol. B 27 (2009) 1496-1502.
29) T. Kido, M. Nagaya, K. Kawata and T. Kato, Mater. Sci. Forum 778-780 (2014) 754-758.
30) A. Rajendran, Y. Takahashi, M. Koyama, M. Kubo and A. Miyamoto, Appl. Surf. Sci. 244 (2005) 34-38.
31) F. W. Preston, J. Soc. Glass Technol. 11 (1927) 214-256.
32) R. Palmieri, C. Radtke, H. Boudinov and E. F. Silva, Appl. Phys. Lett. 95 (2009) 113504.
33) J. M. Knaup, P. Deak, T. Frauenheim, A. Gali, Z. Hajnal and W. J. Choyke, Phys. Rev. B 71 (2005) 235321.
34) H. Deng, K. Endo and K. Yamamura, Appl. Phys. Lett. 104 (2014) 101608.

Chapter 6

Application of PAP to GaN (0001)

6.1 Introduction

As discussed in Chapter 4, PAP has been successfully applied to 4H-SiC (0001) to obtain of scratch-free, damage-free and atomically flat surfaces with well-ordered step-terrace structures. Similar to SiC, GaN is also a difficult-to-machine material with high hardness and chemical inertness. Also, in the case of GaN epilayers, which are widely commercially used, many etch pits are formed on GaN surfaces after conventional CMP using slurry, as has been widely reported [1-3]. Therefore, the damage-free polishing of GaN substrates (epilayer or bulk) to obtain an atomically flat and etch-pit-free surface is a major challenge. Since PAP has been successfully applied to SiC, the damage-free polishing of GaN using PAP is strongly expected. As reported in this chapter, conventional CMP was conducted for comparison, and the surface modification of GaN (0001) using AP-plasma was confirmed. Applications of the two-step PAP process and the prototype PAP machine are discussed. The probable removal mechanisms of conventional CMP and the proposed PAP are also discussed.

6.2 CMP of GaN [4]

In this study, commercially available undoped GaN epilayers with a thickness of 8 μm grown on 2 inch or 3 inch sapphire substrates (thickness: 430 μm) supplied by POWDEC Co. Ltd. were used. The surface modification and polishing experiments were all conducted on the Ga-faces. Figure 6.1 shows an AFM image and surface cross-sectional profile of the epitaxially grown GaN surface used in this work. This surface was not subjected to a flattening process after epitaxial growth; thus, the step-terrace structure on this surface was very disordered. Many small pits can be observed at the dislocation sites. As has been widely reported, these dislocations are defined as screw dislocations or a mixture of screw dislocations and edge dislocations [3]. As shown in the cross-sectional profile, the step height was about 0.5 nm, corresponding to a two-bilayer step-terrace structure of GaN. This means that step bunching occurred in the epitaxial growth process of GaN.

The epitaxially grown GaN substrate was polished by conventional CMP using SiO_2 slurry and CeO_2 slurry under the polishing conditions shown in Table 6.1. SiO_2 slurry has been widely used

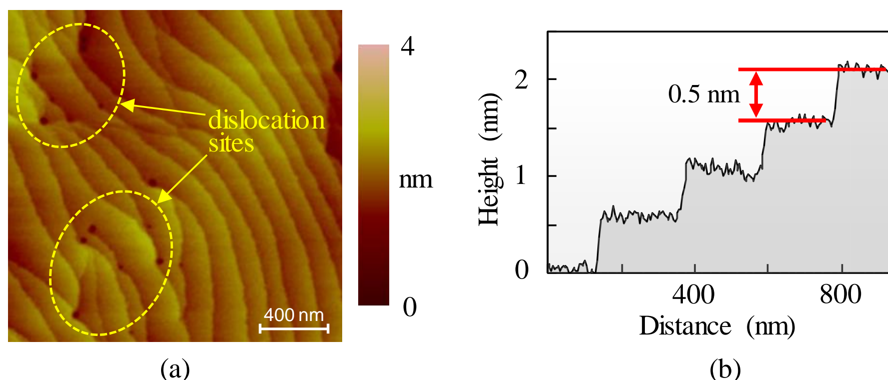

Figure 6.1 AFM image (a) and the surface cross-sectional profile after slope correction (b) of the as-grown GaN surface (p-v: 3.65 nm, rms: 0.28 nm).

Table 6.1 Conditions of CMP

Experimental setup	cf. Figure 3.5
Polishing pad	Suede type, NP178 (ϕ10 mm)
Abrasive material	SiO_2 (ϕ72 nm), CeO_2 (ϕ190 nm)
Slurry pH	SiO_2: 9.4, CeO_2: 8.5
Concentration	1.0 wt%
Load	50 g
Pad rotation speed	2000 rpm
Polishing time duration	3 h

for the CMP of semiconductor materials such as Si and SiC [5, 6)]. Recently, the CMP of GaN using SiO_2 slurry has also been frequently performed [1-3)]. For comparison, GaN was also polished with CeO_2 slurry because it has been reported that CeO_2 slurry has better polishing characteristics for GaN than SiO_2 slurry [7)]. Figure 6.2 shows AFM images of the slurry-polished surfaces. Many enlarged pits, which deteriorated the surface roughness, can be observed after slurry polishing, particularly when SiO_2 slurry was used.

As shown in the surface cross-sectional profiles in Figures 6.2(c) and (d), it was confirmed that the depth of these etch pits was usually less than 10 nm [8)]. These pits greatly affected the surface integrity as well as the surface roughness. As clearly demonstrated in Figure 6.2(b), these etch pits originated from the dislocations in GaN since they were only generated at the dislocation sites. They were also much larger than the pits on the as-grown surface shown in Figure 6.1(a),

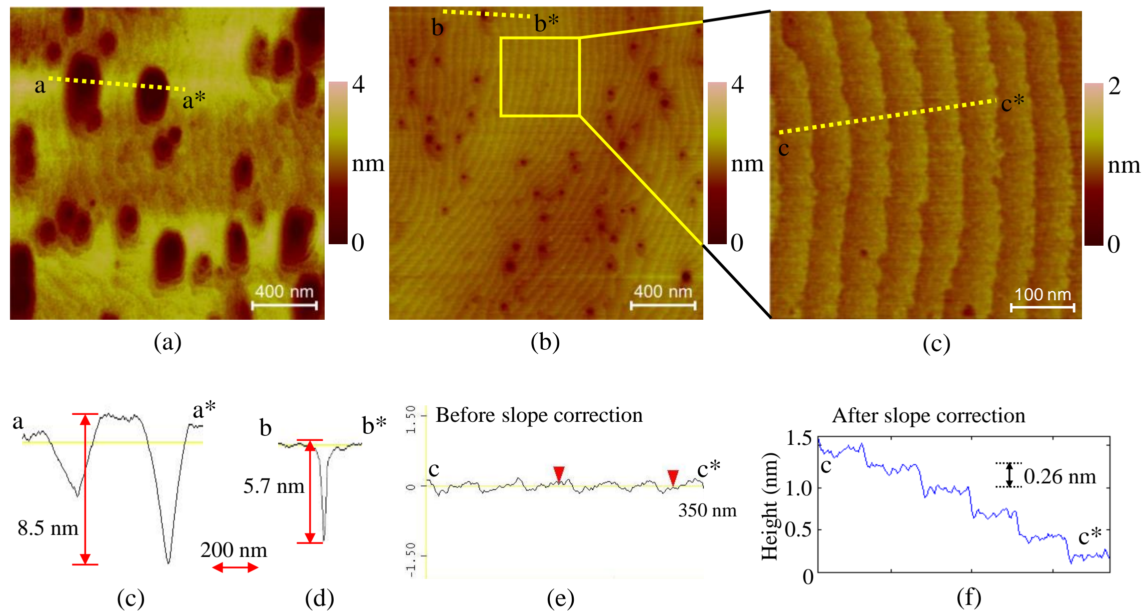

Figure 6.2 (a) AFM image of SiO_2 slurry polished surface (p-v: 4.04 nm, rms: 0.43 nm). (b) AFM image of CeO_2 slurry polished surface (p-v: 7.28 nm, rms: 0.21 nm). (c) AFM image of the pit-free area in Figure (b). (c-f) Surface cross sectional profiles.

which proved that the preferential removal of dislocation sites occurred in the slurry polishing of GaN. Figures 6.2(e) and (f) show cross-sectional profiles of a pit-free area on the CeO_2-slurry-polished surface. It was found that the step height was about 0.26 nm, corresponding to the height of one bilayer of GaN. This means that the problem of step bunching on the as-received surface can be resolved by CeO_2 slurry polishing even though many etch pits are generated.

In the above polishing experiments, the GaN substrates were locally polished by the scanning of a small polishing pad. Figure 6.3 shows a SEM image of the boundary between the unpolished area and the CMP-processed area using SiO_2 slurry. The difference can be clearly observed between these two areas. In the unprocessed area, only very few small pits existed, while the amount and size of the pits both greatly increased in the slurry-polished area. At the edge of the polished area, the density of pits was very high, which was considered to be due to the high rotation speed of the periphery of the polishing pad. Thus, it was concluded that not only the chemical reaction but also the mechanical action promoted the generation of the etch pits.

CMP using SiO_2 slurry is a very common finishing technique for GaN. Therefore, many similar results in which etch pits were generated have been reported [1-3]. The reason why these etch pits were generated is also discussed. Figure 6.4 shows the probable mechanism by which large pits are generated in the slurry polishing of GaN. The SiO_2 and CeO_2 slurries used in this work are both alkaline. There are many chemicals including species such as hydroxide radicals existing in both slurries. Generally, these OH radicals oxidize the surface of GaN by the following reaction

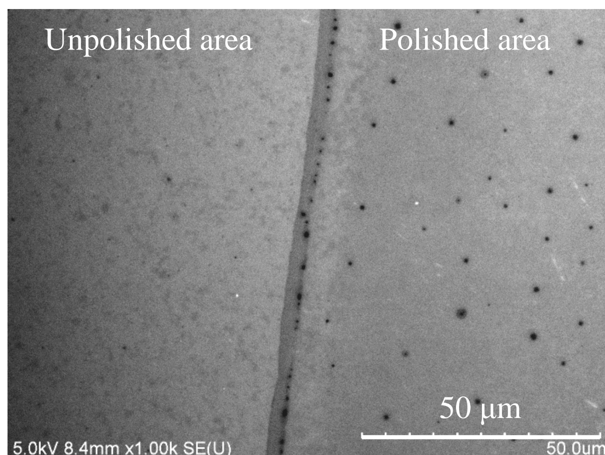

Figure 6.3 SEM image of the boundary between the unpolished area and the CMP process area using SiO_2 slurry.

and realize the removal using a soft abrasive in CMP [3].

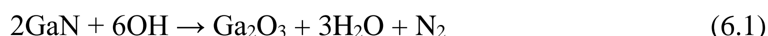

$$2GaN + 6OH \rightarrow Ga_2O_3 + 3H_2O + N_2 \tag{6.1}$$

The dislocation sites in GaN are chemically unstable owing to the existence of strain and DBs. Therefore, reactions such as etching and oxidation by chemicals in the slurry preferentially occur at these dislocation sites [3, 7]. Moreover, the mechanical abrasion of the abrasive promotes the preferential removal at these sites. Thus, the dislocation sites are preferentially polished, resulting in many large pits as shown in Figures 6.2 and 6.3.

6.3 Surface modification of GaN by AP-plasma irradiation [4]

To realize the application of PAP to GaN, the surface modification of GaN by AP-plasma irradiation needs to be confirmed. Both O_2-containing plasma and CF_4-containing plasma were examined in this work. Table 6.2 shows the conditions used for plasma modification. Figure 6.5

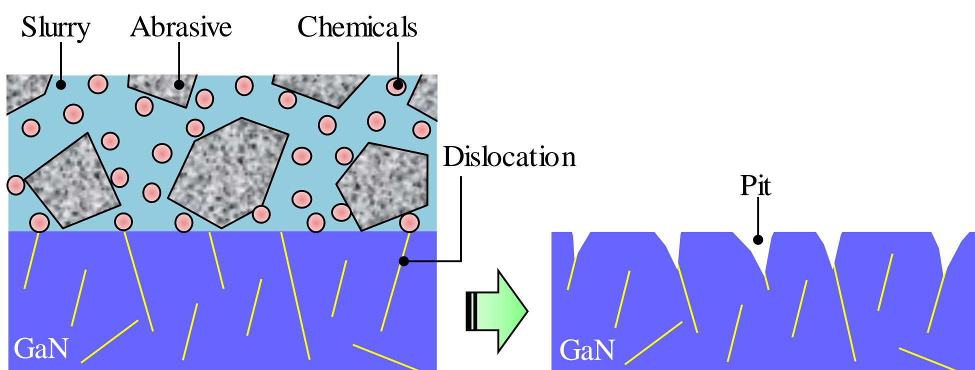

Figure 6.4 Probable pit generation mechanism in the slurry polishing of GaN.

shows the surface morphologies of GaN irradiated by O_2-containing plasma and CF_4-containing plasma under the same conditions. In the case of irradiation with O_2-containing plasma, the step-terrace structure of GaN can still be observed, while that on the CF_4-plasma-irradiated surface almost disappeared. This means that the CF_4-containing plasma had higher efficiency than the O_2-containing plasma for the modification of GaN. This result also coincides with the calculated Gibbs free energies of GaF_3 (-591.96 kJ/mol) and Ga_2O_3 (-396.26 kJ/mol) [9]. Thus, CF_4-plasma-modified specimens were used in the subsequent experiments.

The surface composition of GaN was analyzed by XPS before and after irradiation with CF_4-containing plasma. As shown in Figure 6.6, no signal from F1s was detected from the as-grown GaN surface, while a strong peak corresponding to GaF_3 was observed after irradiation with CF_4-containing plasma [10]. This means that GaN was modified to GaF_3 after irradiation by the CF_4-containing plasma. Figure 6.6(c) shows the F1s spectrum of the GaN surface modified by the CF_4-containing plasma with the substrate heated to 100 ˚C. It was found that heating of the substrate was very effective for promoting the surface fluoridation of GaN. Therefore, in the following experiments, the substrate was heated to 100 ˚C to increase the surface fluoridation rate.

The thickness of the fluoridated layer generated by the irradiation of CF_4-containing plasma (applied RF power: 18 W) was measured by XTEM. The irradiation conditions were the same as

Table 6.2 Conditions of plasma irradiation

Experimental setup	cf. Figure 3.4
Carrier gas	He (1.0 slm)
Reactive gas	O_2 (10 sccm) or CF_4 (25 sccm)
Applied RF power	7 W
Gap distance	1.6 mm
Polishing time duration	30 min

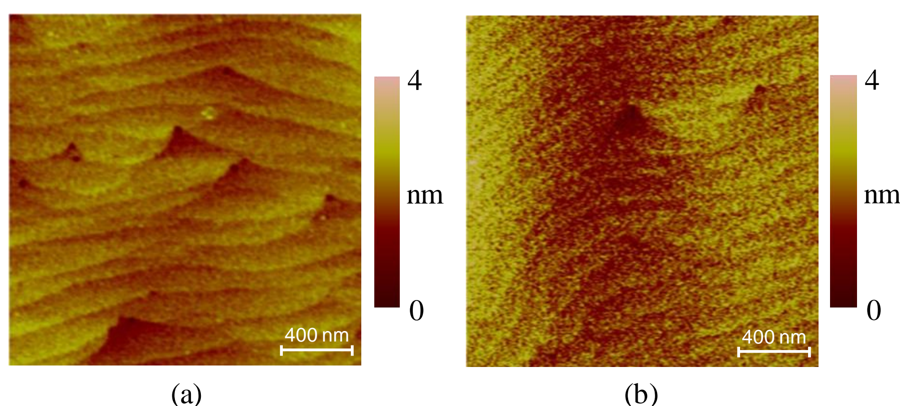

Figure 6.5 AFM images of plasma irradiated GaN surfaces: (a) O_2 contained plasma, (b) CF_4 contained plasma.

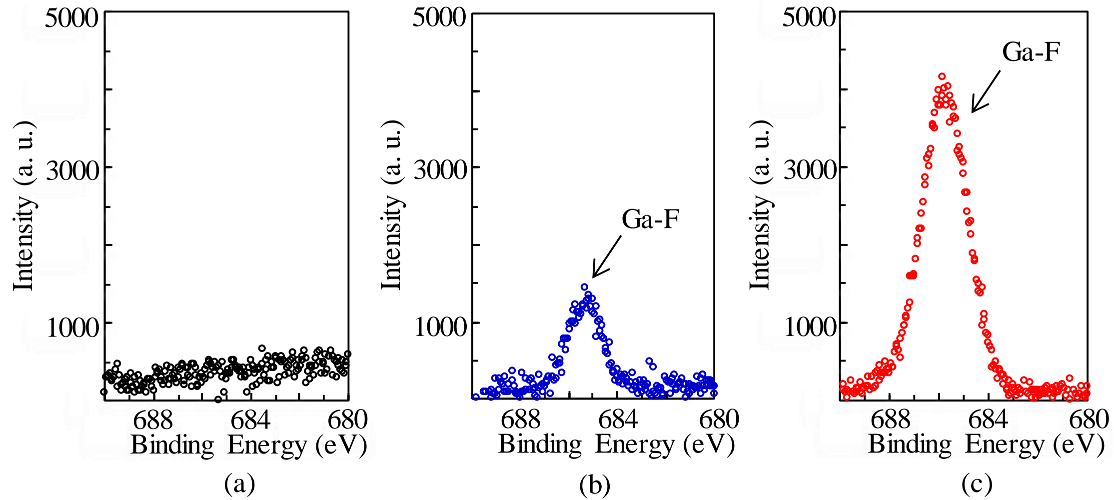

Figure 6.6 F1s spectra of GaN surfaces. (a) The as-received surface. (b) CF_4 contained plasma irradiated surface without heating. (c) CF_4 contained plasma irradiated surface with heating (100˚C).

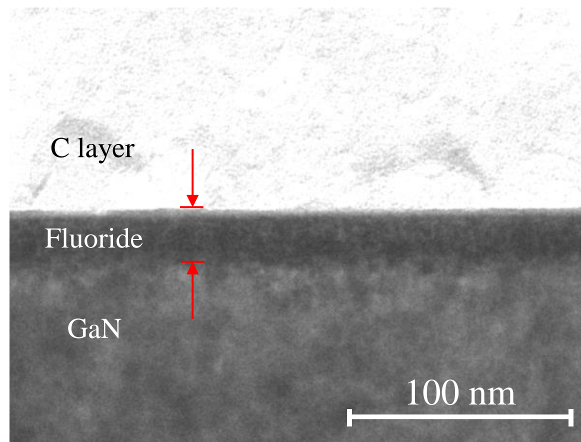

Figure 6.7 XTEM image of the CF_4 contained plasma-modified surface.

shown in Table 6.2, and heating of the substrate to 100 ˚C was also conducted. Figure 6.7 shows an XTEM image of the fluoridated layer. After irradiation with the CF_4-containing plasma for 30 min, the formation of a modified layer with a thickness of about 30 nm was confirmed. Taking the densities and mass numbers of GaN (ρ=6.15 g/cm^3, M=84) and GaF_3 (ρ=4.47 g/cm^3, M=127) into consideration, the average modification rate of this process was about 14.4 nm/h. Similar to SiC [11)], the growth of the modified layer decreased the modification rate. Therefore, it was considered that the initial fluoridation rate of GaN for irradiation with CF_4-containing plasma should be much higher.

Nanoindentation tests were conducted to examine the surface hardness before and after irradiation with CF_4-containiing plasma. The maximum load in the nanoindentation tests was 0.1 mN and 100 points uniformly located on the surface were measured to calculate the average

hardness. The maximum load was very small and thus only the top surface was examined. A Berkovich-type indenter made of diamond was used. Figure 6.8(a) shows typical load-displacement curves measured by the nanoindentation method. It was revealed that the displacements for the as-received surface and plasma-modified surface were about 10 nm and 15 nm, respectively. The surface hardnesses were calculated by the Oliver-Pharr method [12]. Figure 6.8(b) shows the hardnesses calculated from the load-displacement curves shown in Figure 6.8(a). The error bars of measured hardnesses were considered to originate from the surface nonuniformity such as step edges and dislocation sites. It was revealed that after irradiation with CF_4-containing plasma for 30 min, the surface hardness of GaN greatly decreased from 22.7 GPa to 13.9 GPa. This means that GaF_3 is much softer than GaN. In other words, the plasma irradiation of GaN made it easier for the surface to be polished using a soft abrasive.

6.4 Applications of two-step PAP

6.4.1 Plasma pretreatment and slurry polishing [8]

Owing to the large lattice mismatch and the difference between the thermal expansion of the GaN epilayer and the sapphire substrate, many crystal defects exist in the GaN epilayer including screw dislocations, edge dislocations and mixed dislocations [3, 7]. When a GaN epilayer is processed by CMP using a silica slurry, many etch pits originating from the defects are formed, as previously mentioned and widely reported [1-3].

To resolve the problem of etch pit formation in conventional CMP, a two-step PAP process in which AP-plasma pretreatment and slurry polishing are combined is considered. Since the preferential removal of dislocation sites was the reason for pit formation in CMP, it is considered

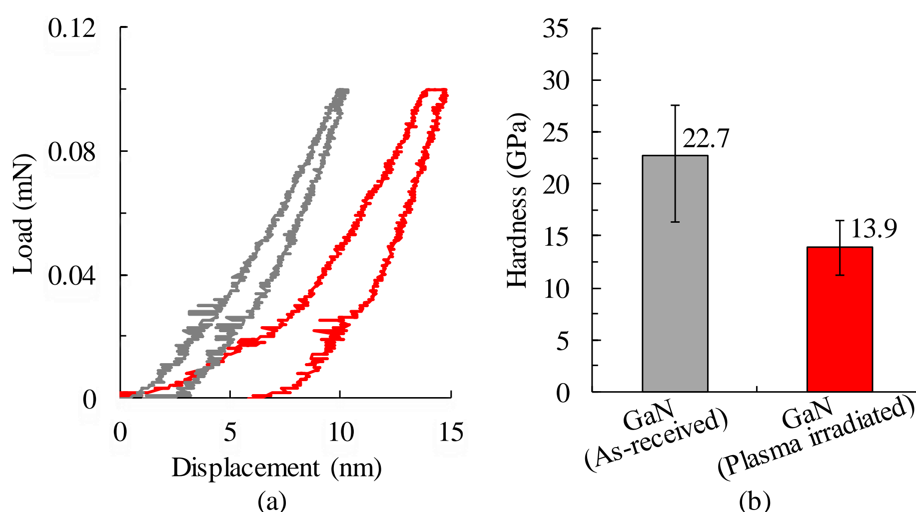

Figure 6.8 Nanoindentation tests of GaN: (a) Load-displacement curves measured by the nanoindentation method, (b) Hardnesses calculated from measured data (a).

that a protective layer that can prevent the preferential removal of dislocation sites will be very useful for avoiding the formation of pits. In this study, AP-plasma irradiation was used for the surface modification of GaN. The surface of the GaN epilayer was first modified by the irradiation of AP-plasma to form a soft and protective layer, and then the modified surface was polished by time-controlled CMP using slurry. As previously mentioned, the modified layer was much softer than GaN. Therefore, it is considered that the modified layer can be removed by slurry polishing. Also, if the polishing time of CMP is controlled to ensure that only the modified layer is removed, a pit-free surface can be expected to be obtained since the bulk GaN is protected by the modified layer from preferential etching and removal by an alkaline agent.

In the first step, for the surface modification of GaN to form a protective layer, the irradiation of CF_4-containing plasma was conducted under the conditions shown in Table 6.2 with the applied RF power increased to 18 W. According to the previous XTEM observation, the thickness of the modified layer on the GaN surface should be about 30 nm.

After irradiation with the CF_4-containing plasma for 30 min, time-controlled CMP using CeO_2 slurry was conducted on the modified surface. The polishing time of CMP was increased from 5 min to 8 min and then to 15 min to observe the change in the surface morphology with increasing polishing time. Table 6.3 shows the polishing conditions. The CeO_2 slurry was used because it had better polishing characteristics for GaN than the SiO_2 slurry as shown in Figure 6.2. Figure 6.9(a) shows an AFM image of the modified surface before CMP. Since this surface was covered with an amorphous GaF_3 layer, no step-terrace structure can be observed. After it was polished by CMP for 5 min, no step-terrace structure was observed as shown in Figure 6.9(b). The surface composition was determined by ARXPS with a take-off angle of 10° so that only the top surface

Table 6.3 Conditions of CMP

Experimental setup	cf. Figure 3.5
Specimen	CF_4-plasma modified GaN (30 min)
Polishing pad	Suede type, NP178 (ϕ10 mm)
Abrasive material	CeO_2 (ϕ190 nm)
Slurry pH	8.5
Concentration	1.0 wt%
Load	50 g
Pad rotation speed	2000 rpm
Polishing time duration	5 min, 8 min, 15 min

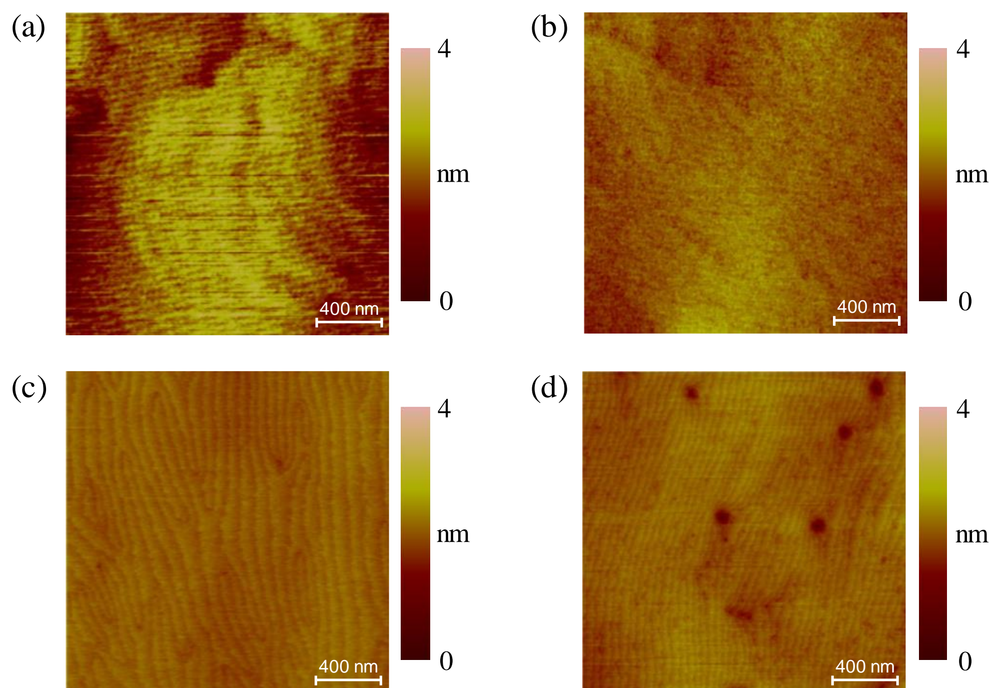

Figure 6.9 AFM images of plasma-modified and CeO_2 slurry-polished GaN surfaces. (a) Surface irradiated by CF_4 contained plasma. (b) Surface after CeO_2 slurry polishing for 5 min. (c) Surface after CeO_2 slurry polishing for 8 min. (d) Surface after CeO_2 slurry polishing for 15 min.

was evaluated. As shown in Figure 6.10(a), GaF_3 remained on this surface, which means that the modified layer was not completely removed. This state is defined as under-polishing. Since GaN was protected by the modified layer, pits formed by conventional CMP were not observed on the surface. After that, the surface was polished for another 3 min (total 8 min). As shown in Figure 6.9(c), an atomically flat GaN surface with a step-terrace structure was obtained. Although many dislocation sites could still be observed on the polished surface, no pits were formed at the dislocation sites. The composition of this surface was also determined by ARXPS. As shown in Figure 6.10(b), the peak corresponding to GaF_3 was not detected. This surface is defined as the just-polished surface. In the cases of under-polishing and just-polishing, GaN was protected by the modified GaF_3 layer. Therefore, no pits originating from the preferential removal of the dislocation sites were formed. The just-polished surface was then polished for another 7 min (total 15 min). Some pits appeared at the dislocation sites as shown in Figure 6.9(d). This state is defined as the over-polished surface. Since the modified layer had already been removed in the just-polishing stage, no protective layer existed in the over-polishing stage. Therefore, preferential removal of the dislocation sites occurred similarly to in the conventional CMP process and many etch pits were formed.

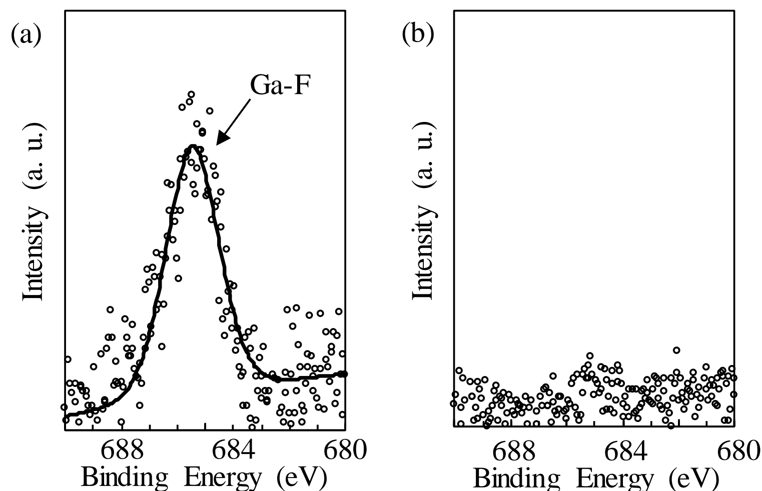

Figure 6.10 F1s spectra of polished GaN surfaces after (a) 30 min of CF_4 contained plasma irradiation followed by 5 min of polishing and (b) 30 min of CF_4 contained plasma irradiation followed by 8 min of polishing.

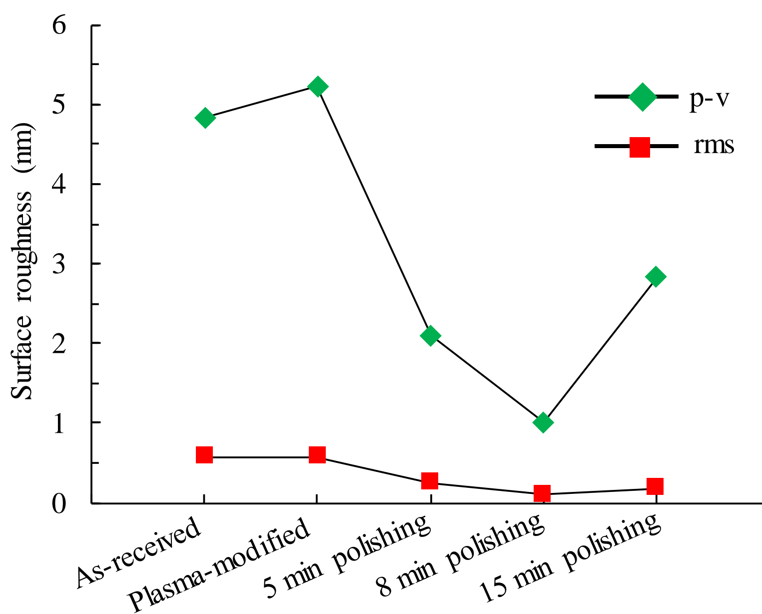

Figure 6.11 Change in surface roughnesses of GaN processed by plasma irradiation and CMP.

Figure 6.11 shows the change in the surface peak-to-valley (P-V) and rms roughnesses of GaN measured by AFM with an area of 2 μm × 2 μm after CMP with different polishing times with pretreatment by irradiation with He-based CF_4-containing plasma. The as-received surface was rough owing to the disordered and bunched step-terrace structure. After plasma irradiation, the surface roughness was not decreased. After the modified surface was polished by CMP for 5 min, although the modified layer remained on the polished surface, the surface roughness was greatly

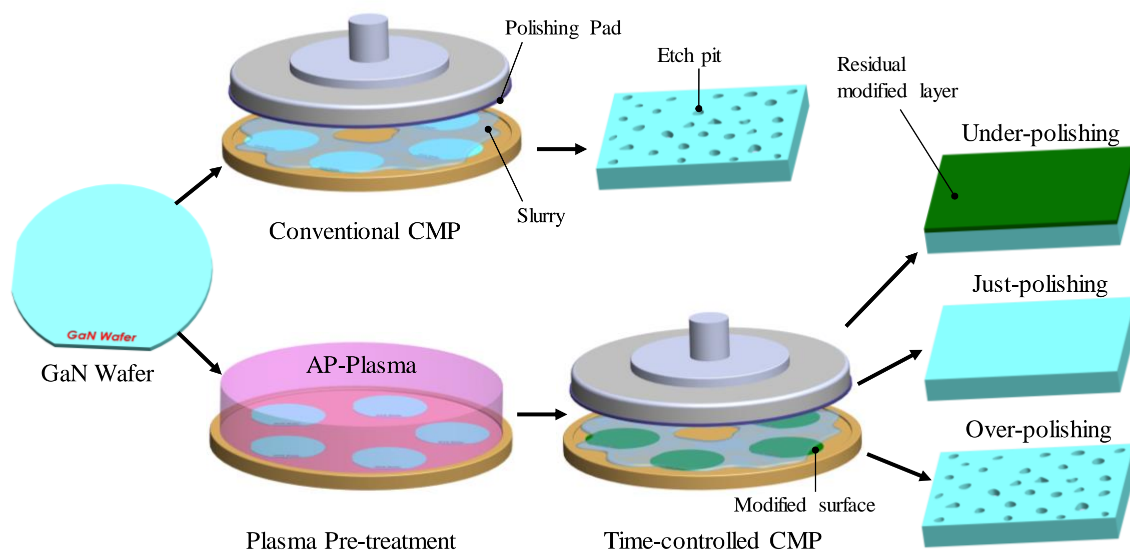

Figure 6.12 Comparison of conventional CMP and time-controlled CMP with plasma pretreatment.

decreased. In the case of CMP for 8 min, an atomically flat surface with 1.00 nm P-V roughness and 0.11 nm rms roughness was obtained. When this surface was over-polished by performing CMP for 15 min, the surface roughness increased owing to the formation of pits as shown in Figure 6.9(d).

Figure 6.12 shows a schematic summary of this study. In the case of conventional CMP, many etch pits were formed on the polished surface. In contrast, for CMP with plasma pretreatment, a pit-free surface was obtained with the time-controlled polishing. Under-polishing resulted in a GaN surface with the modified layer remaining, whereas a rough surface with many etch pits was formed in the case of over-polishing. Only in the case of just-polishing was a pit-free and atomically flat surface obtained. On the basis of the above results, it is concluded that the combination of plasma pretreatment and time-controlled CMP is very effective for obtaining a pit-free and atomically flat GaN surface. With this combination, the surface integrity, flatness, and uniformity of the surface atomic structure are all improved compared with those of a surface polished by conventional CMP without plasma pretreatment. Thus, high device performance is strongly expected as a result of using GaN with a surface polished by the proposed methods, which will be experimentally investigated in future study.

6.4.2 Plasma pretreatment and dry polishing using grinding stone [4)]

Even though the pit-free polishing of GaN can be realized by AP-plasma pretreatment and time-controlled CeO_2 slurry polishing, the use of slurry is still undesirable owing to its high cost.

PAP was developed to realize the dry polishing of difficult-to-machine materials. Therefore, the dry polishing of GaN using grinding stones rather than slurry is a promising method. Meanwhile, many etch pits are formed in wet slurry polishing (CMP) as previously mentioned. Even if a plasma pretreatment is conducted, the polishing time of CMP must be controlled to realize damage-free polishing, which also makes the process complicated. Obviously, these problems will not exist if a dry polishing process is developed. Therefore, the dry polishing of GaN combined with AP-plasma modification and grinding stone polishing was conducted. First, plasma pretreatment and grinding stone polishing were combined in a preliminary study.

In the first step, the surface modification of GaN by irradiation with CF_4-containing plasma was conducted. The conditions for surface modification were the same as those in Table 6.2 but with the applied RF power increased to 18 W. The formation of a modified layer was confirmed by XPS. To remove the modified layer, grinding stone polishing was conducted. Therefore, evaluation of the polishing characteristics of different types of grinding stone was required to optimize the process.

In this two-step PAP process, polishing using grinding stones is conducted to remove the modified layer. After removal of the modified layer, friction between the grinding stone and the bulk GaN occurs. This dry friction will greatly affect the surface quality of the two-step PAP-processed GaN substrate. Therefore, the polishing of GaN using grinding stones without plasma pretreatment was conducted. Three types of grinding stone were evaluated: loose-held-type SiO_2 grinding stone, fixed type SiO_2 grinding stone and fixed-type CeO_2 grinding stone. Table 6.4 shows the conditions of grinding stone polishing without plasma pretreatment.

Figure 6.13 shows SEM images of the fixed-type SiO_2 grinding stone. Even though the abrasive

Table 6.4 Conditions of grinding stone polishing

Experimental setup	cf. Figure 3.5
Specimen	GaN (0001) without plasma modification
Grinding stone	SiO_2: loose held type and fixed type. CeO_2: fixed type
Grain size	SiO_2: 0.3 μm. CeO_2: 1.2 μm
Grinding stone size	$\phi 5.1 mm \times 1.6 mm^t$
Bonding material	resin
Load	50 g
Rotation speed	2000 rpm
Polishing time duration	1 h

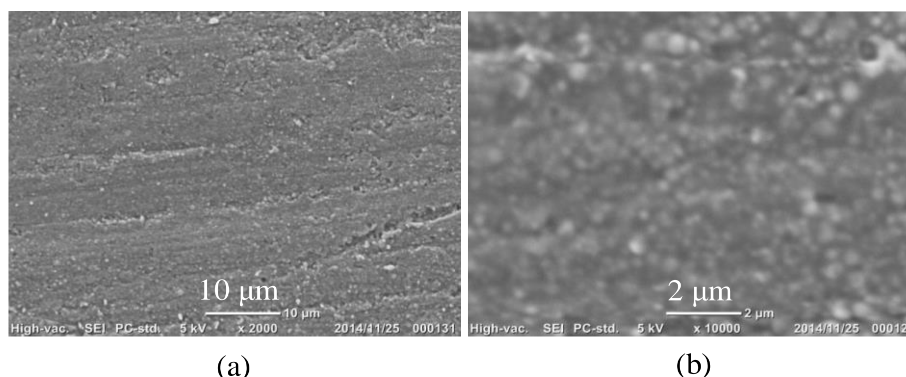

Figure 6.13 SEM images of the fixed type SiO_2 grinding stone. (a) Magnification: 2000. (b) Magnification: 10000.

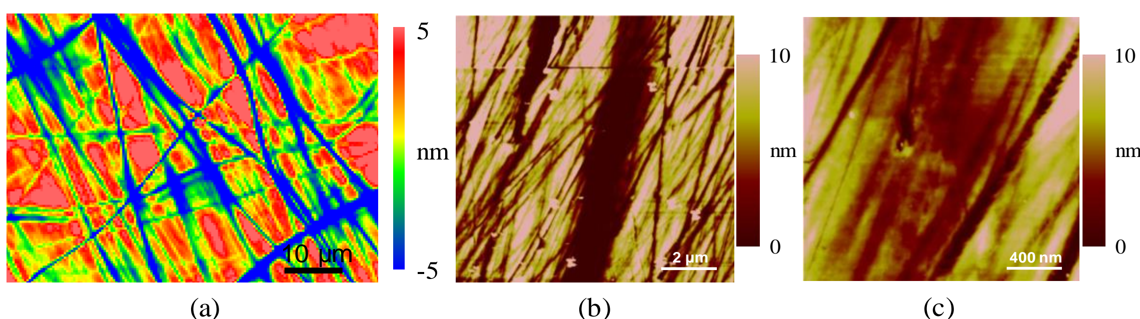

Figure 6.14 Surface morphology of GaN polished by the fixed type SiO_2 grinding stone. (a) SWLI image (p-v: 15.15 nm, rms: 2.71 nm). (b) AFM image (p-v: 97.73 nm, rms: 5.58 nm). (c) AFM image (p-v: 29.99 nm, rms: 2.57 nm).

SiO_2 and the bonding resin are both very soft compared with GaN, a large number of scratches were formed as shown in the SWLI and AFM images in Figure 6.14. For a fixed-type grinding stone, the elasticity must be very low. Therefore, it was considered that very strong friction occurred in the areas of contact between the grinding stone and the substrate. It was assumed that these scratches were formed by the pressure concentration and increase in temperature (friction heat) in the local friction areas. The MRR in the polishing of GaN using this grinding stone without plasma pretreatment was also measured using the indents (depth: 175 nm) formed by nanoindentation tests as references. These indents completely disappeared after polishing. Thus, the MRR should be higher than 175 nm/h, which was much higher than that in the conventional CMP process, which is usually less than 80 nm/h. However, owing to the introduction of scratches and SSD, it was concluded that the fixed-type SiO_2 grinding stone was not suitable for the PAP of GaN.

Since it was found that the fixed-type SiO_2 grinding stone was not suitable for the PAP of GaN, the loose-held-type was also investigated. Figure 6.15 shows SEM images of the loose-held-type

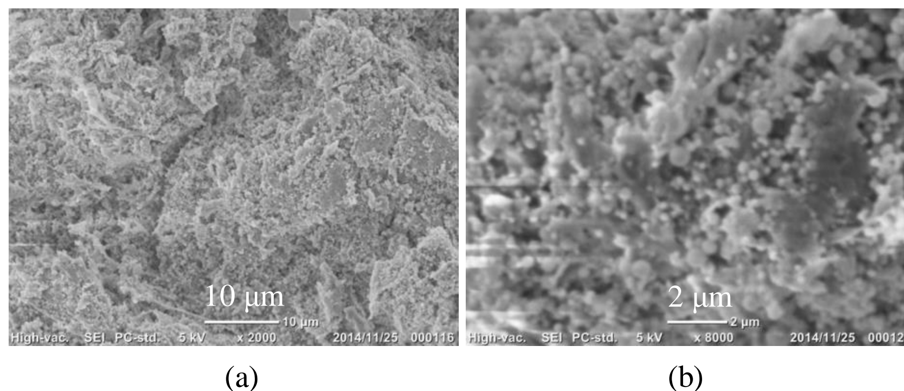

(a) (b)

Figure 6.15 SEM images of the loose held type SiO_2 grinding stone. (a) Magnification: 2000. (b) Magnification: 10000.

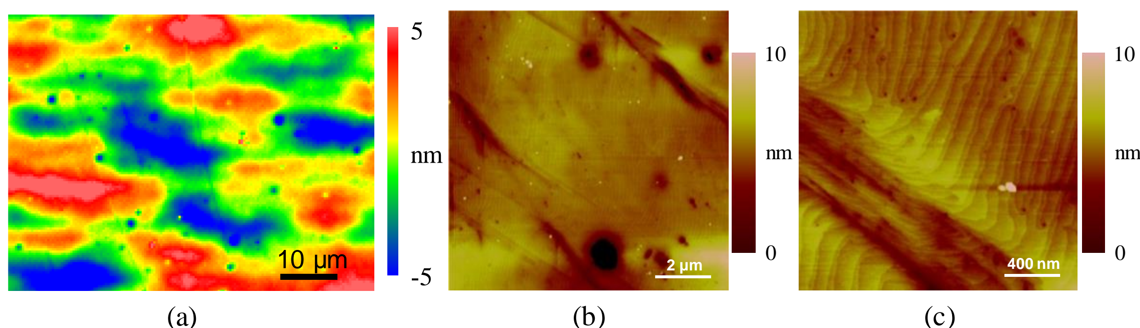

(a) (b) (c)

Figure 6.16 Surface morphology of GaN polished by the loose held type SiO_2 grinding stone. (a) SWLI image (p-v: 19.63 nm, rms: 2.48 nm). (b) AFM image (p-v: 23.52 nm, rms: 1.34 nm). (c) AFM image (p-v: 9.54 nm, rms: 0.41 nm).

SiO_2 grinding stone. While the grinding stone shown in Figure 6.13 was very dense, the loose-held-type grinding stone shown in Figure 6.15 was rather loose. Therefore, strong elasticity of the grinding stone was expected.

Figure 6.16 shows SWLI and AFM images of the surface polished by the loose-held-type SiO_2 grinding stone. Compared with the surface shown in Figure 6.14, only a very limited number of small and shallow scratches were observed, which was considered to result from the loose-held structure of the grinding stone. In the SWLI image shown in Figure 6.16(a), many etch pits were observed. Even though pits can also be observed on the as-received surface shown in Figure 6.1, they were formed in the epitaxial growth process and they are very small and can only be observed by AFM. Thus, it was considered that pits shown in Figure 6.16(a) were formed in the polishing process. It was assumed that the SiO_2 abrasive reacted with GaN and that the preferential removal of the dislocation sites also occurred, just as in slurry polishing, resulting in the formation of etch pits. From the above results and discussion, it was concluded that the loose-held-type SiO_2

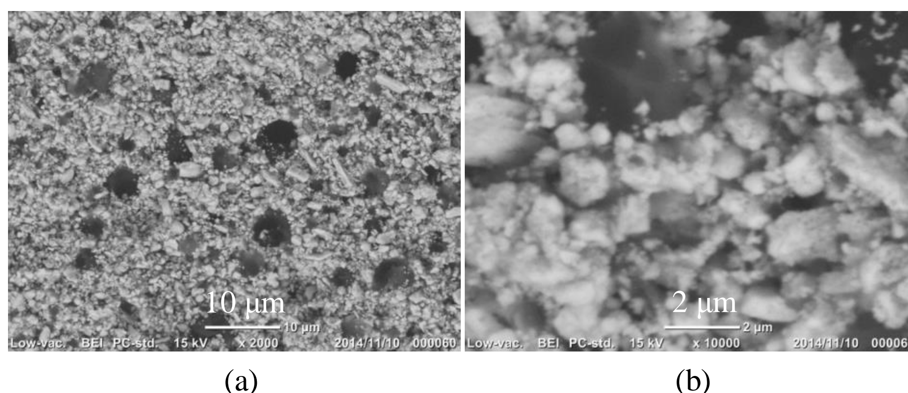

Figure 6.17 SEM images of the fixed type CeO_2 grinding stone. (a) Magnification: 2000. (b) Magnification: 10000.

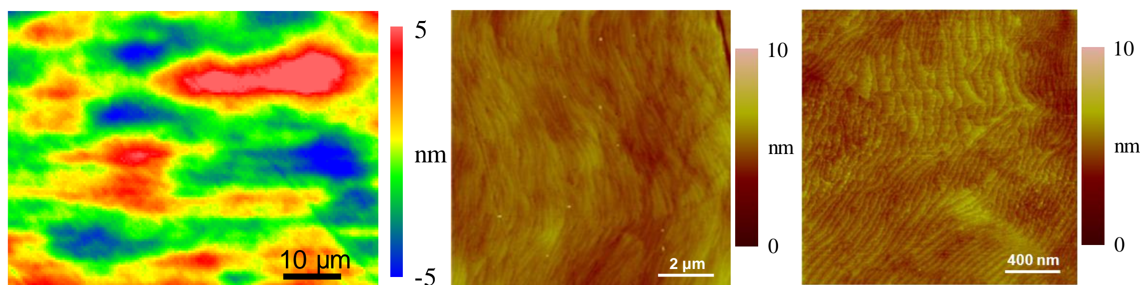

Figure 6.18 Surface morphology of GaN polished by the fixed type SiO_2 grinding stone. (a) SWLI image (p-v: 13.90 nm, rms: 2.17 nm). (b) AFM image (p-v: 13.16 nm, rms: 0.51 nm). (c) AFM image (p-v: 1.86 nm, rms: 0.22 nm).

grinding stone was also not suitable for the PAP of GaN.

Next, polishing using the fixed-type CeO_2 grinding stone was conducted. Figure 6.17 shows SEM images of the grinding stone. The grain size of CeO_2 was much larger than that of the SiO_2 abrasive in the SiO_2 grinding stones. Even though it was a fixed-type grinding stone, pocket structures can be observed. Figure 6.18 shows SWLI and AFM images of the polished

Table 6.5 Conditions of grinding stone polishing

Experimental setup	cf. Figure 3.5
Specimen	CF_4-plasma modified GaN (30 min)
Grinding stone	fixed type CeO_2 grinding stone (resin bonded, ϕ1.2 μm)
Grinding stone size	ϕ5.1mm×1.6mm^t
Load	50 g
Rotation speed	2000 rpm
Polishing time duration	3 h

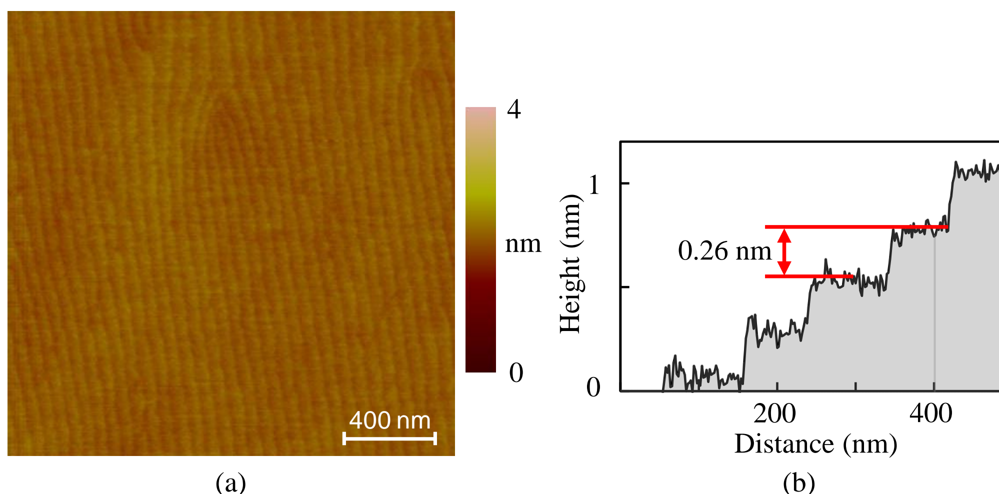

(a) (b)

Figure 6.19 AFM image (a) and the surface profile (b) of the PAP processed GaN surface (p-v: 0.67 nm, rms: 0.08 nm).

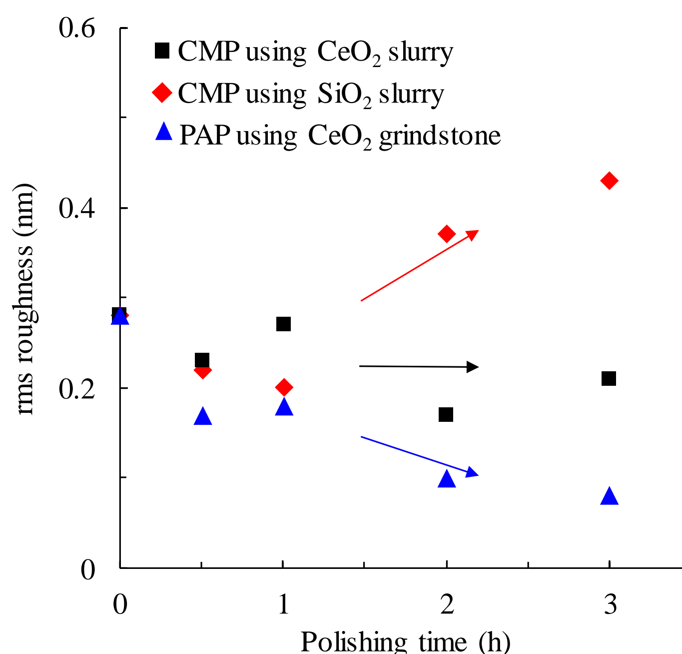

Figure 6.20 Changes in rms roughness of polished GaN surfaces with different polishing duration in different methods.

surface. Almost no scratches were formed. As shown in the AFM images, the step-terrace structure was still very disordered, which means that the removal volume was very limited since no surface modification was conducted. In contrast to the surface polished by the SiO_2 grinding stone, the formation of etch pits was not observed after polishing by the CeO_2 grinding stone. From the above results, it was concluded that the CeO_2 grinding stone was very suitable for the PAP of GaN to realize damage-free and etch-pit-free polishing.

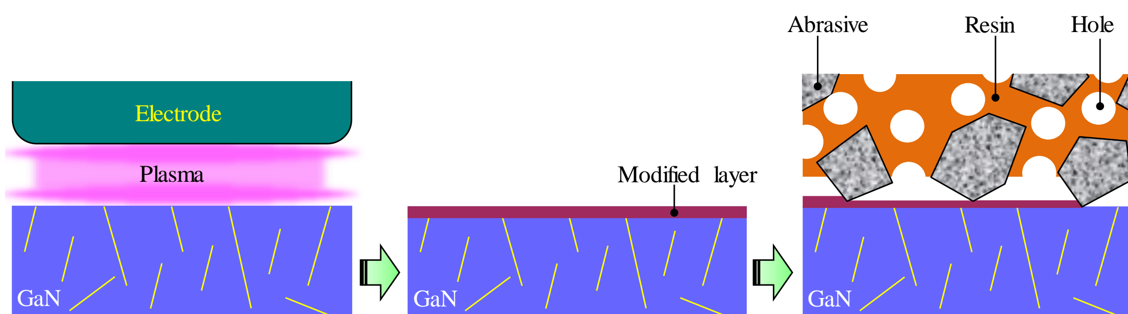

Figure 6.21 Probable mechanism of PAP applied to GaN.

Two-step PAP, which combined surface modification with CF_4-containing plasma and polishing with a CeO_2 grinding stone, was conducted on GaN. The plasma irradiation conditions and polishing conditions are respectively shown in Table 6.2 and 6.5. Figure 6.19 shows an AFM image of the GaN surface processed by plasma irradiation followed by polishing using a CeO_2 grinding stone. No scratches were formed and the step-terrace structure is very uniform. As shown in the cross-sectional profile, the step height was about 0.26 nm, corresponding to a one-bilayer step-terrace structure of GaN. This means that the step-bunched surface was atomically polished by the grinding stone. Dislocations can still be observed on this polished surface, as shown in the AFM image. However, no pits were formed at these dislocation sites. This means that a scratch-free, pit-free and atomically flat surface was obtained by PAP.

Figure 6.20 shows the changes in the rms surface roughness of GaN processed by different polishing methods with different polishing durations under the conditions shown in Table 6.1 and 6.5. All these polishing experiments were conducted on as-received GaN (0001) substrates. The rms roughness of the polished surfaces was evaluated by AFM with an observation area of 2 μm×2 μm. The as-received surface was rough owing to its disordered and bunched step-terrace structure. When it was polished by SiO_2 slurry, many large pits were formed, which greatly increased the surface roughness. In the case of CMP using CeO_2 slurry, although many pits were still formed on the polished surface, as shown in Figure 6.2(b), these pits were much smaller than those formed by SiO_2 slurry polishing, as shown in Figure 6.2(a). Therefore, the surface roughness was not greatly affected. In the case of two-step PAP using a CeO_2 grinding stone, the surface roughness gradually decreased with the removal of the modified layer. After polishing for 3 h, an atomically flat surface with an rms roughness of less than 0.1 nm was obtained as shown in Figure 6.19(a).

Figure 6.21 shows the probable removal mechanism for the PAP of GaN. GaN is irradiated by CF_4-containing plasma, which results in the formation of a soft modified layer. When the modified surface is polished by a CeO_2 grinding stone under a dry condition, only the modified layer is

removed and no scratches are formed since CeO_2 is very soft compared with GaN. Because it is a dry polishing process, preferential etching or oxidation of the dislocation sites, both of which occur in slurry polishing, does not occur in this process. Thus, no pits are formed. Finally, an atomically flat GaN surface free from scratches and pits is obtained.

6.5 Application of prototype PAP machine

As previously mentioned, AP-plasma has been demonstrated to be very useful for the surface modification (softening) of GaN. Also, the two-step PAP processes (time-controlled wet polishing using slurry and dry polishing using a grinding stone) were successfully conducted and scratch-free, etch-pit-free and atomically flat GaN surfaces were obtained. However, there are still some challenges in realizing the whole-surface polishing of large GaN substrates with high polishing efficiency and a low polishing cost. As described in Chapter 3, the prototype PAP machine was developed to realize the dry polishing of large substrates. Therefore, the prototype PAP machine was applied to GaN.

For the application of the prototype PAP machine, the plasma generation conditions were first optimized to increase the surface modification rate of GaN, which should also increase the MRR of PAP. After that, the MRR of PAP for GaN using the prototype PAP machine was investigated as well as the roughness and morphology of the polished surface. Finally, the deterioration of the grinding stones during polishing was confirmed and the effect of dressing was evaluated.

6.5.1 Optimization of plasma generation conditions

To increase the polishing efficiency of PAP, the conditions under which GaN will be most efficiently modified should be found, in other words, the plasma generation conditions need to be optimized. There are many factors that will affect the surface modification efficiency of GaN, such as the substrate temperature, the applied RF power, the gap distance and so forth. In this study, the effects of the composition of the reactive gas, the flow rate of the carrier gas and the type of carrier gas on the surface modification efficiency of GaN were investigated.

In the prototype PAP machine, water-vapor-containing plasma was used for the surface modification of GaN because it has no toxic gas component. Figure 6.22 shows a photograph and the OES spectrum of the AP-plasma. With the scanning of the stage, the whole surface of the substrate was modified. As shown in the OES spectrum, a large amount of optical emission from N_2 can be observed. This is owing to the open-air ambient, which includes N_2 molecules and He atoms with a low mass, making the substitution of N_2 by He difficult [13]. The existence of OH radicals was also confirmed.

As described in Chapter 4, the water vapor concentration in He will affect the intensity of OH

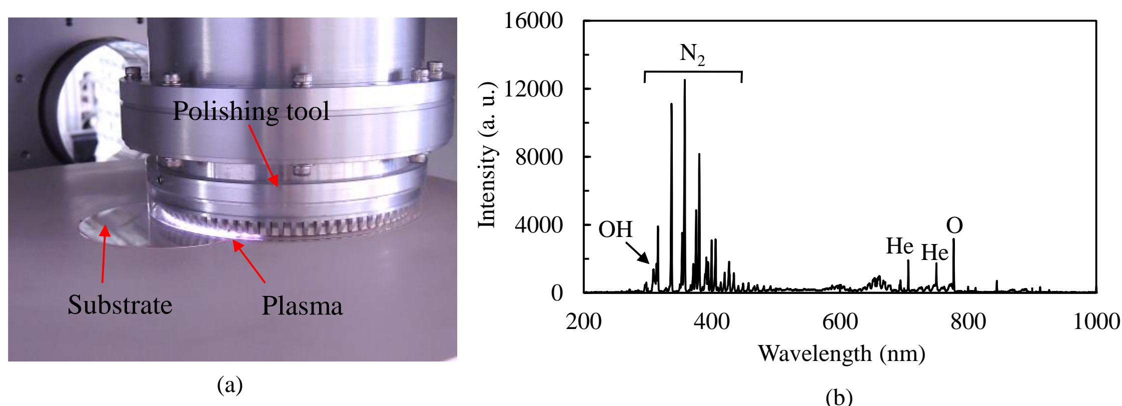

Figure 6.22 Photo of experimental setup (a) and OES spectra of He-based water vapor contained plasma used in the prototype PAP machine (Gap: 1 mm, He flow rate: 3 slm, Applied RF power: 30 W) (b).

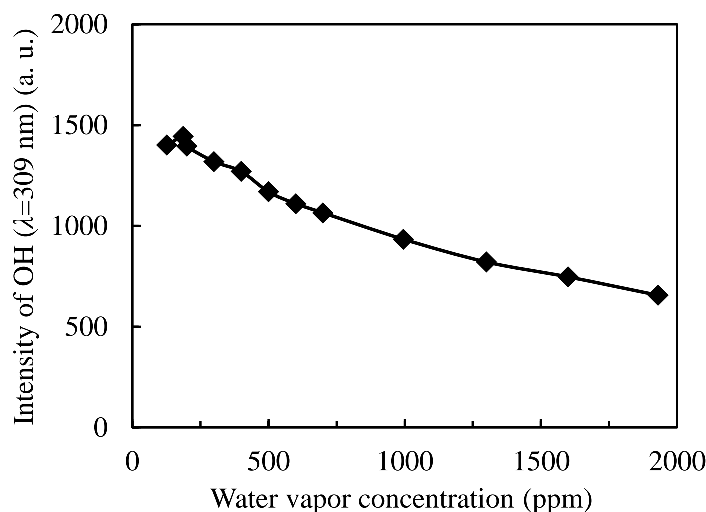

Figure 6.23 Dependence of the OH optical emission intensity from water vapor contained plasma on the content of water vapor in He.

radicals in the plasma. Therefore, the dependence of the OH optical emission intensity from the water-vapor-containing plasma on the concentration of water vapor in the He carrier gas was investigated. The water vapor concentration was measured using a dew point meter (DPM) and it could be adjusted by using a mass flow controller (MFC) to control the flow rate of the He flowing through the water vessel. Figure 6.23 shows the OES measurement results. The intensity of OH radicals gradually decreased with increasing water vapor concentration. It was considered that with increasing water vapor concentration, the excessive supply of water vapor decreased the electron temperature, inhibiting the dissociation of water molecules. Also, the effective quenching of excited states of OH radicals at a high water vapor concentration greatly decreased their density

[14]. Therefore, in the following experiments, a noble gas (He or Ar) with a relatively low water vapor concentration (lower than the LLD of the DPM) was used for surface modification.

The surface modification of GaN by water-vapor-containing plasma irradiation was conducted under the conditions shown in Table 6.6. Before and after plasma irradiation, the surface composition of the GaN substrate was determined by XPS (take-off angle: 45 °). Figure 6.24 shows the measured O1s spectra. On the as-received surface, a thin native oxide layer was confirmed. However, after the irradiation of water-vapor-containing plasma for 1 h, the intensity of the peak corresponding to Ga-O greatly increased, which proved the formation of a modified oxide layer. Even though the thickness of the oxide layer formed by irradiation with the water-vapor-containing plasma could not be calculated from the O1s spectrum, the feasibility of the surface modification of GaN by water-vapor-containing plasma has been demonstrated.

Table 6.6 Conditions of plasma irradiation

Experimental setup	cf. Figure 3.10
Specimen	As-received GaN
Carrier gas	He (3.0 slm, WVC<LLD)
Scanning length	30 mm
Scanning speed	5 mm/s
Applied RF power	30 W
Irradiation time duration	1 h

The inclusion of N_2 from the ambient affected the surface modification efficiency of GaN. This

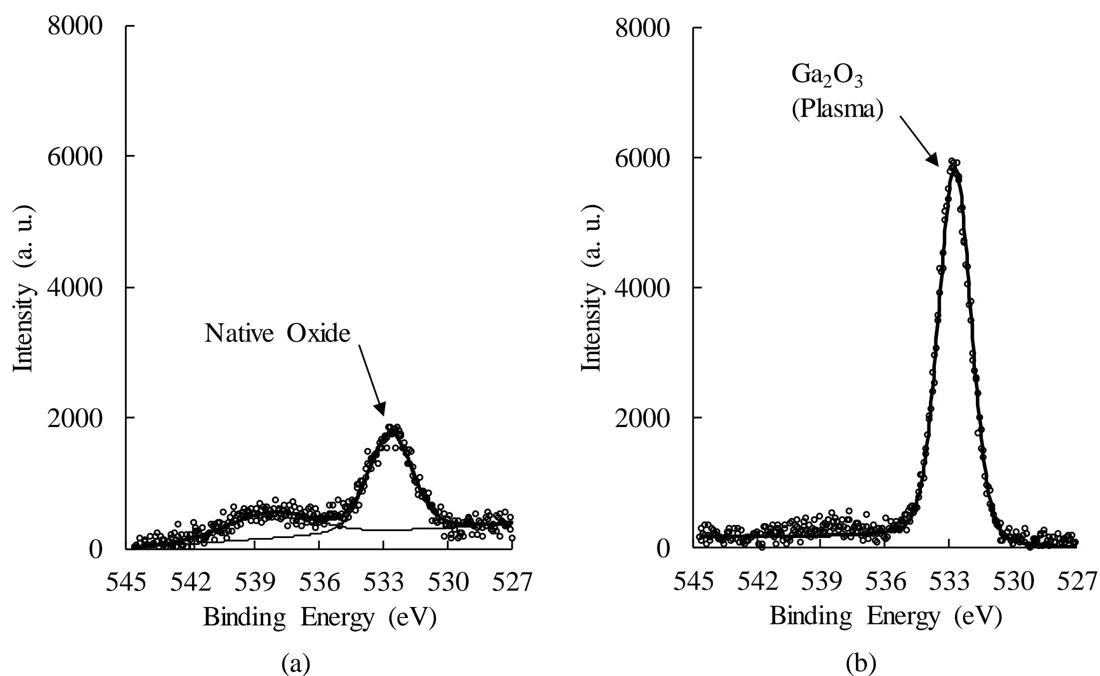

Figure 6.24 O1s spectra of GaN surfaces before (a) and after water vapor contained plasma irradiation for 1 h (b).

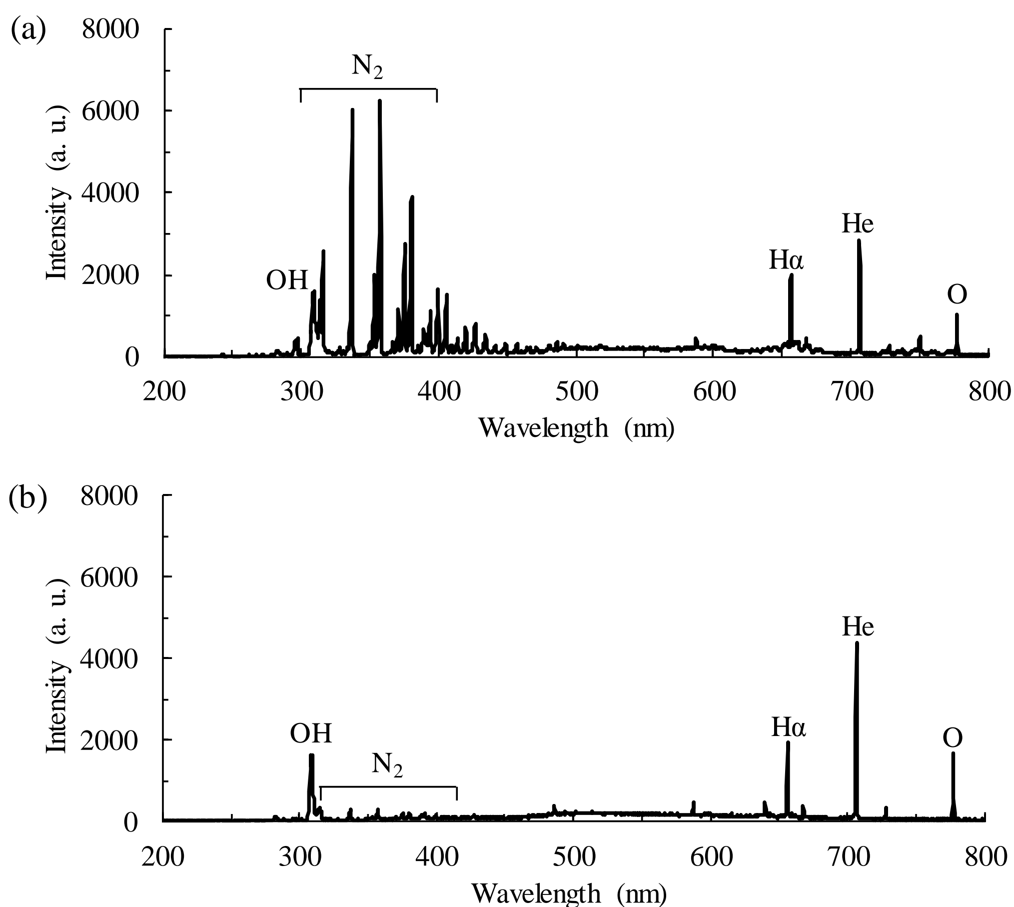

Figure 6.25 OES spectra of He-based water vapor contained plasma. (a) 3 slm. (b) 10 slm.

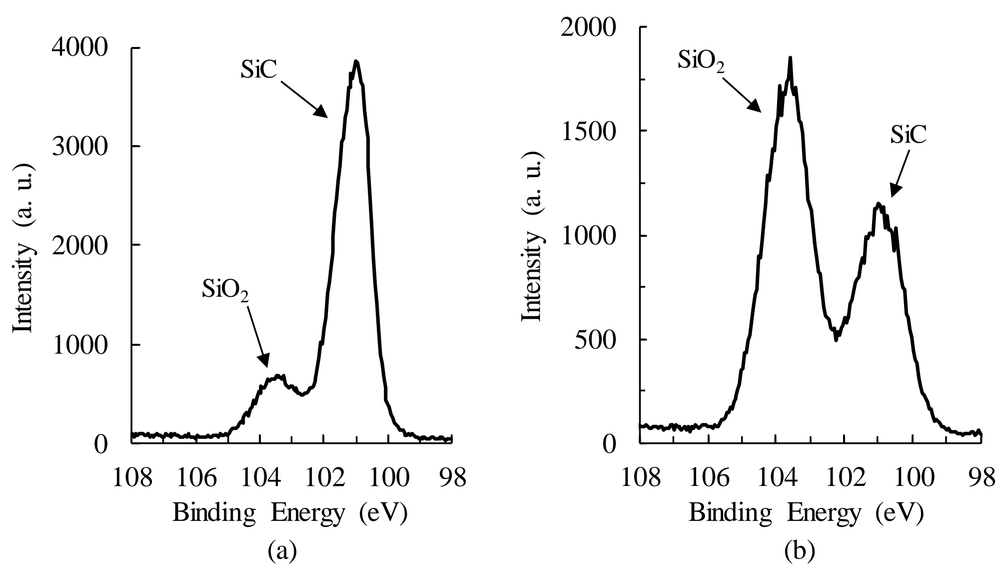

Figure 6.26 Si2p spectra of SiC surfaces irradiated by water vapor contained plasma with different flow rate of He. (a) 3 slm. (b) 10 slm.

is because the excitation energy of N_2 is very low (5.23 eV), making it easy to excite in the plasma region, which will decrease the dissociation efficiency of water molecules. Even though the substitution of N_2 by He was difficult owing to their large difference in molecule mass, it is assumed that a large flow rate will probably resolve this problem. Therefore, the surface modification efficiency of irradiation with He-based water-vapor-containing plasma with different He flow rates was compared.

Figure 6.25 shows OES spectra of the He-based water-vapor-containing plasmas with He flow rates of 3 slm and 10 slm. The applied RF power was 18 W in both experiments. It was found that for the lower He flow rate of 3 slm, a large amount of optical emission from N_2 was observed owing to the inclusion of N_2 from the ambient. When the He flow rate was increased to 10 slm, the optical emission from N_2 became very weak, which means that the substitution of N_2 was efficiently performed with a large flow rate of He.

To determine the surface modification efficiency of the above water-vapor-containing plasmas with different He flow rates, XPS measurements of the modified GaN surfaces were conducted. As previously mentioned, when a GaN substrate was used, the thickness of the modified layer could not be calculated. Thus, a 3 inch 4H-SiC (0001) substrate was used instead. The plasma irradiation time was 30 min and the take-off angle of the XPS measurements was 45 °. Figure 6.26 shows the Si2p spectra of the plasma-modified surfaces. From a qualitative evaluation, the oxide layer formed by irradiation with water-vapor-containing plasma with a He flow rate of 10 slm was much thicker than the modified layer formed with a He flow rate of 3 slm, which supported my assumption.

Equation (6.2) has been widely used to determine the surface layer thickness from XPS measurements. To carry out the calculation, an XPS spectrum with peaks from the surface layer and the bulk material is necessary.

$$d = \lambda_{\mathrm{ox}} \cdot \sin\theta \cdot \ln\left[\left(\frac{N_{\mathrm{m}} \cdot \lambda_{\mathrm{m}}}{N_{\mathrm{ox}} \cdot \lambda_{\mathrm{ox}}}\right) \cdot \frac{I_{\mathrm{ox}}}{I_{\mathrm{m}}} + 1\right] \tag{6.2}$$

In the above equation, d represents the thickness of the surface layer; λ_{m} and λ_{ox} respectively represent the escape depths of a photon from the bulk material and the surface oxide layer; θ represents the take-off angle, which was 45 ° in my measurements; N (N_{m} and N_{ox}) represents atomic densities and I (I_{m} and I_{ox}) represents the intensities of peaks in the XPS spectra.

From equation (6.2) and some previous studies [15, 16], the thickness of the oxide layer shown in Figure 6.26(a) was about 0.83 nm, while that of the oxide layer shown in Figure 6.26(b) was about 3.45 nm, which was about four times thicker. It was concluded that the increase in the He flow rate greatly increased the surface oxidation efficiency.

Although the effect from the included N_2 could be avoided by increasing the flow rate of He,

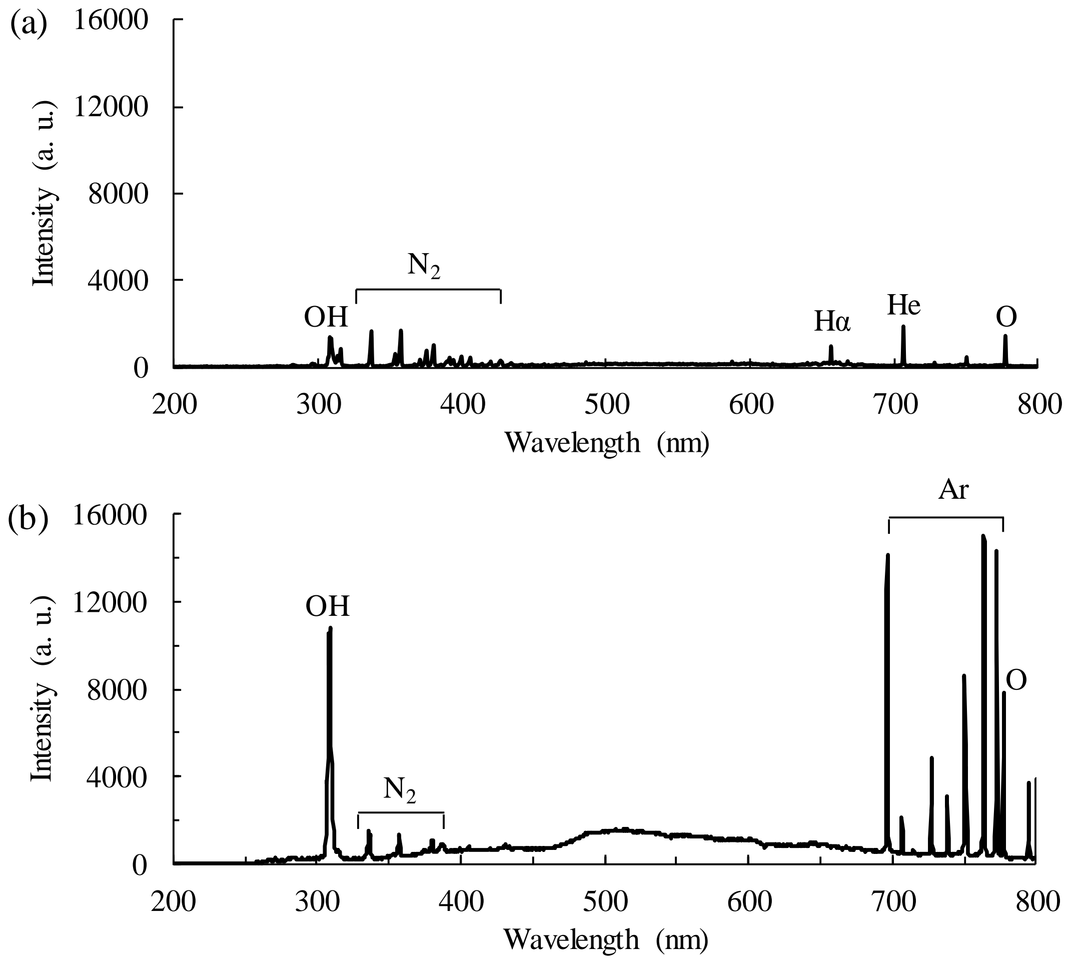

Figure 6.27 OES spectra of water vapor contained plasma with different kinds of carrier gas. (a) He. (b) Ar.

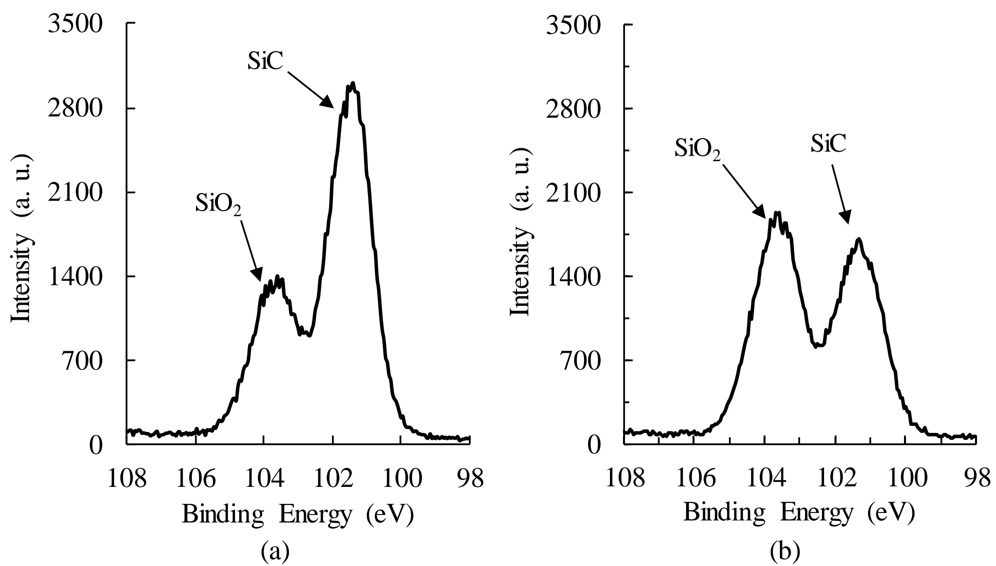

Figure 6.28 Si2p spectra of SiC surfaces irradiated by water vapor contained plasma with different kinds of carrier gas. (a) He. (b) Ar.

this is not a cost-effective method owing to the increase in the price of He in recent years. Compared with He, Ar is relatively inexpensive. We assume that the surface modification efficiency of Ar plasma is higher than that of He plasma for the following two reasons. First, Ar has a larger atomic mass than He. Therefore, a good substitution effect can be expected with the use of Ar. Second, the ionization energy of Ar (15.75 eV) is much lower than that of He (24.58 eV); thus, the electron density in Ar plasma is higher than that in He plasma under the same discharge conditions, which is expected to result in a high radical density. On the basis of the above assumption, a comparison between He and Ar in terms of surface modification efficiency was conducted.

Figure 6.27 shows OES spectra of the He-based and Ar-based water-vapor-containing plasmas. The OES spectra were measured under the same plasma generation conditions (gas flow rate of 5 slm and applied RF power of 18 W). It was found that in the case of He-based plasma, a large amount of emission from N_2 was observed owing to the inclusion of N_2 from the ambient. Also, the intensity of the peak corresponding to OH radicals was very weak. In contrast, with the change in the carrier gas from He to Ar, the emission intensity from N_2 became very weak while the intensity of OH radicals greatly increased. Since OH radicals played the main role in surface modification, it was assumed that the Ar-based water-vapor-containing plasma had higher surface modification efficiency than the He-based plasma.

The surface modification of 4H-SiC (0001) substrates using He-based and Ar-based water-vapor-containing plasmas was conducted. The plasma generation conditions were the same as those in the OES experiments and the irradiation time was 30 min. The modified surfaces were measured by XPS to evaluate the thickness of the oxide layer. Figure 6.28 shows the Si2p spectra of the modified SiC surfaces. From equation (6.2), the thickness of the oxide layer generated by the He-based water-vapor-containing plasma was about 1.75 nm while that of the oxide layer generated by the Ar-based water-vapor-containing plasma was about 3.12 nm. It was concluded that the Ar-based water-vapor-containing plasma had a higher surface modification efficiency than the He-based water-vapor-containing plasma.

On the basis of the above results and discussion, conditions for improving the surface modification efficiency of water-vapor-containing plasma have been determined. It was revealed that a lower water vapor concentration, a higher carrier gas flow rate and the replacement of He with Ar are very effective for improving the surface modification efficiency.

6.5.2 Deterioration of grinding stone during polishing

In the prototype PAP machine, the surface modification efficiency as well as the status of the grinding stone surface will affect the polishing efficiency of PAP. Since dry polishing was conducted, it was considered that deterioration of the grinding stone occurred. There are two

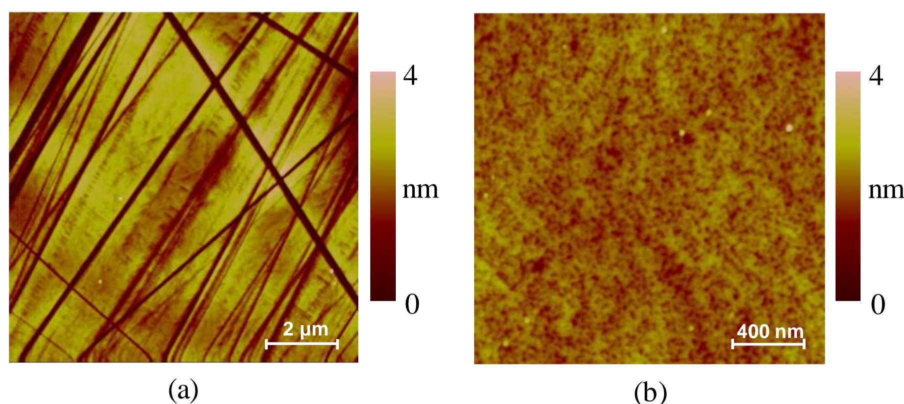

Figure 6.29 AFM images of a polished GaN surface. (a) 10 μm×10 μm (p-v: 32.16 nm, rms: 2.26 nm). (a) 2 μm×2 μm (p-v: 4.62 nm, rms: 0.26 nm).

consequences of using a deteriorated grinding stone: deterioration of the surface quality and a decrease in the MRR.

As previously mentioned, a scratch-free and etch-pit-free surface could be obtained by the combination of irradiation with CF_4 containing plasma for 30 min and dry polishing using a resin-bonded CeO_2 grinding stone for 3 h. However, when the polishing time was increased, deterioration of the grinding stone surface morphology occurred.

Figure 6.29 shows AFM images of a GaN surface polished with the resin-bonded CeO_2 grinding stone for 8 h. The plasma irradiation conditions and polishing conditions were those in Tables 6.2 and 6.5, respectively. Many scratches were formed and the surface roughness was greatly increased. Even in a small area (2 μm ×2 μm), as shown in Figure 6.29(b), the step-terrace structure of GaN could no longer be observed.

It was assumed that the deterioration of the grinding stone was the reason why the surface shown in Figure 6.29 was generated. Therefore, the change in the grinding stone resulting from polishing was evaluated. Figure 6.30 shows surface profiles of the resin-bonded CeO_2 grinding stone before and after polishing for 8 h. While many protrusions existed on the as-received grinding stone surface, as shown in Figure 6.30(a), these protrusions disappeared after polishing for 8 h, as shown in Figure 6.30(b). Detailed observation of the surface morphology of the grinding stone was conducted by SEM. Figure 6.31 shows SEM images of the grinding stone surface before and after polishing. Compared with the as-received surface, the surface of the grinding stone after polishing was very flat. Abrasion clearly occurred on the grinding stone surface after polishing. It was considered that the deterioration of the grinding stone surface was the reason why many scratches were generated.

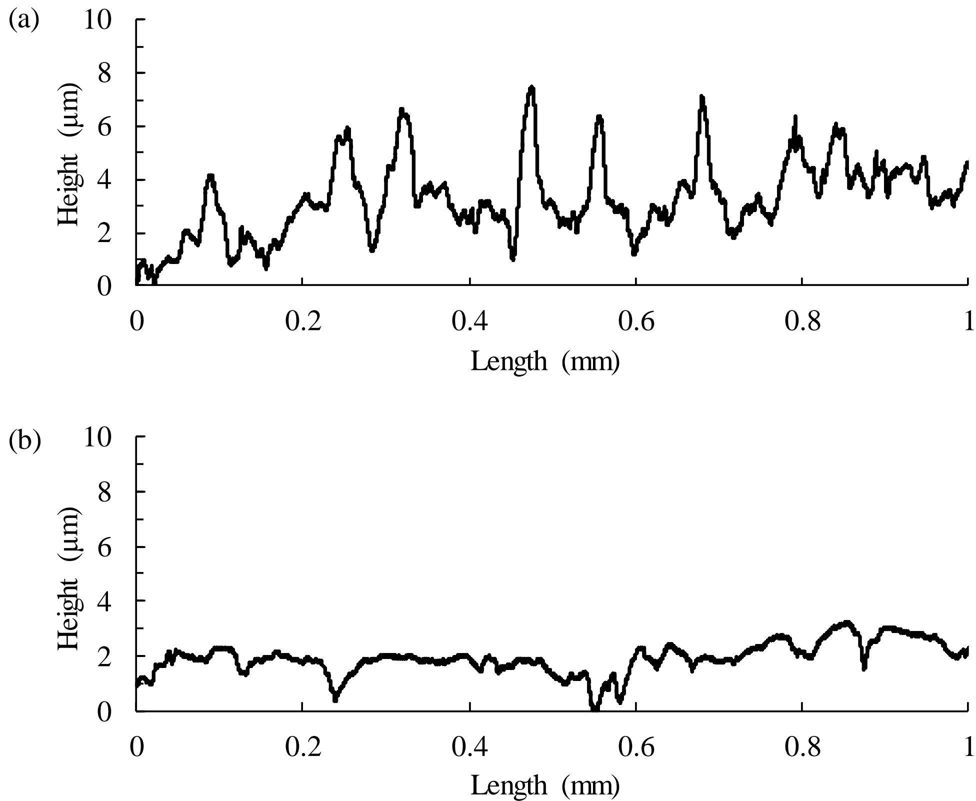

Figure 6.30 Surface profiles of the resin-bonded CeO_2 grinding stone. (a) Before polishing. (b) After polishing for 8 h.

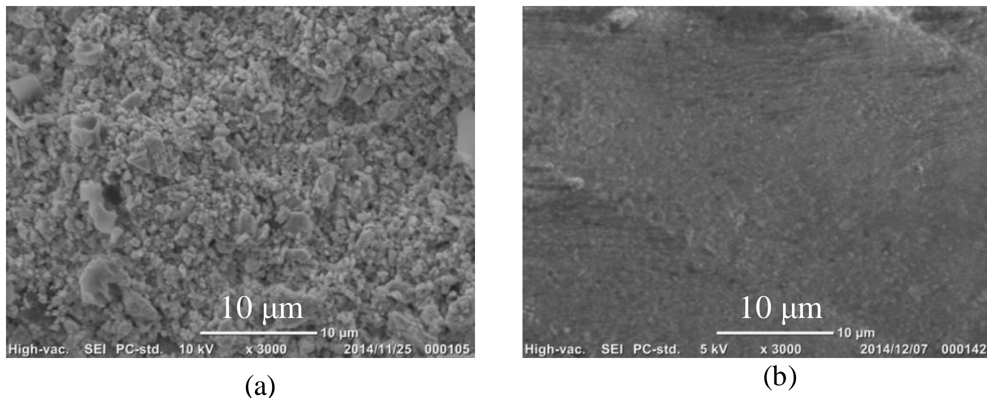

Figure 6.31 SEM images of the resin-bonded CeO_2 grinding stone surface. (a) Before polishing. (b) After polishing for 8 h.

On the grinding stone surface, the protrusions shown in Figure 6.30(a) and the grains shown in Figure 6.31(a) can be considered to behave as small cutting edges, resulting in material removal during polishing. Therefore, it was assumed that the MRR greatly decreased in PAP owing to the surface deterioration of the grinding stone. To confirm this assumption, the MRR of PAP for GaN

using the prototype PAP machine was evaluated after different durations of PAP without changing the polishing tool (grinding stones) or dressing.

Table 6.7 shows the conditions of PAP. Before and after polishing, the weight of the substrate was measured using a high-precision balance (resolution: 0.1 mg) and the difference in weight was used to calculate the average MRR for different polishing durations. To sustain a stable glow discharge in PAP, the rotation speed of the stage was quite low (about 200 rpm) and the polishing

Table 6.7 Conditions of PAP

Experimental setup	cf. Figure 3.10
Specimen	3 inch GaN (0001)
Grinding stone	Resin-bonded SiO_2 grinding stone (LHA type)
Average grain size	0.7 μm
Carrier gas	Ar (10 slm)
Rotation speeds	Stage: 200 rpm. Polishing tool: 0
Scanning of the stage	Length: 30 mm. Speed: 5 mm/s
Applied RF power	18 W
Pressure	50 kPa
Polishing time duration	1 min, 4.5 min, 8.5 min, 30 min

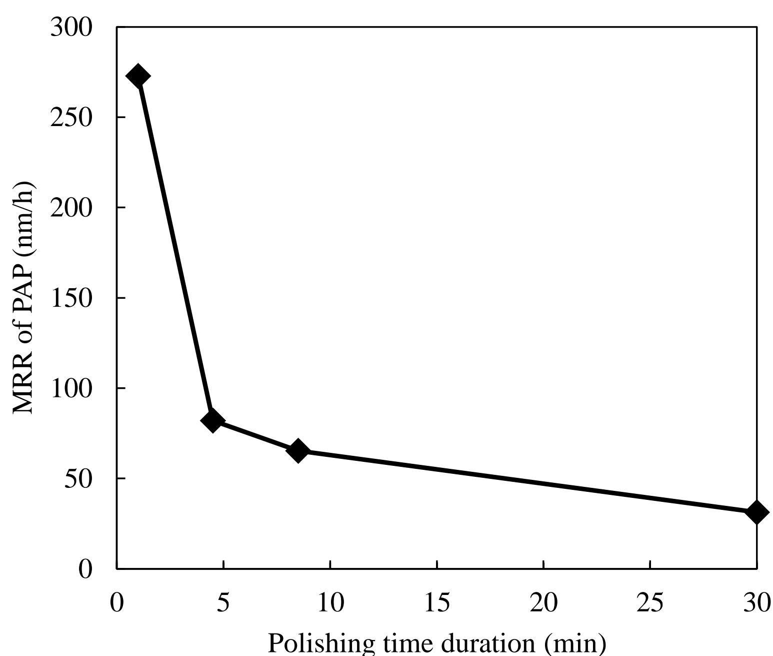

Figure 6.32 Change of MRR of PAP with different polishing time duration.

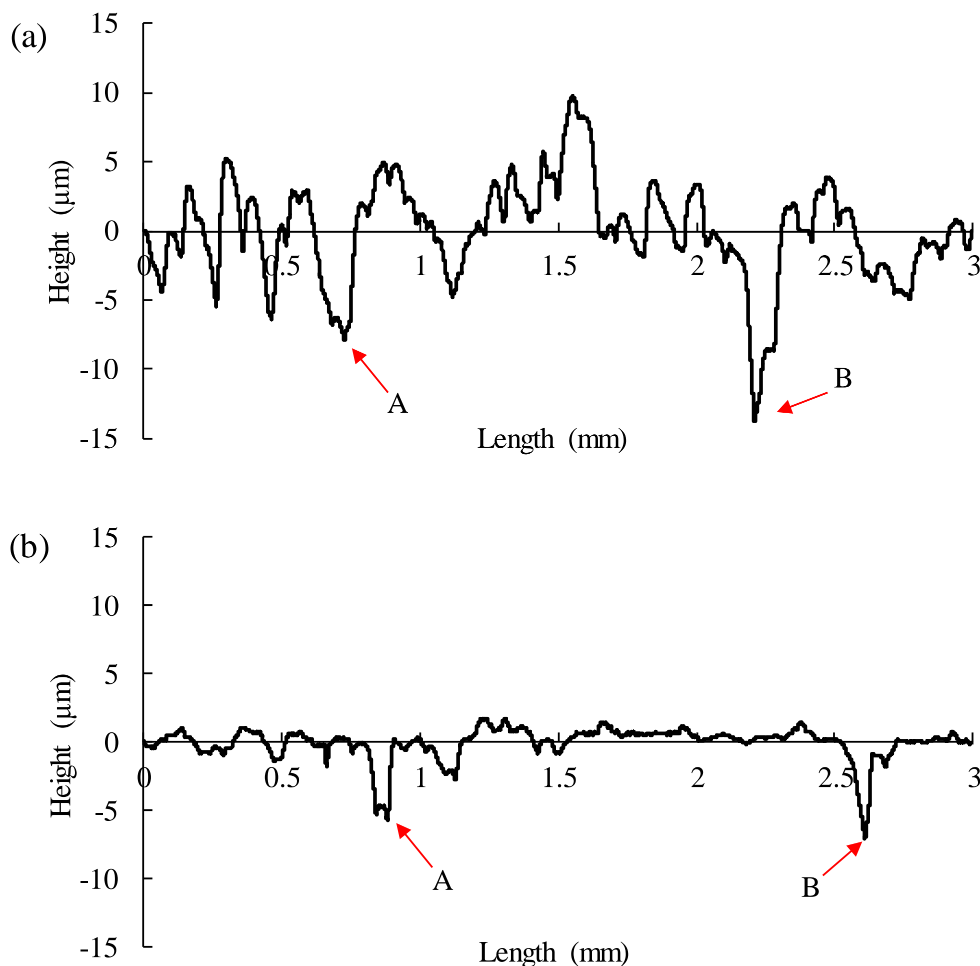

Figure 6.33 Surface profiles of the resin-bonded SiO_2 grinding stone used in the prototype PAP machine. (a) Before polishing. (b) After PAP for 4.5 min.

tool (hybrid electrode) did not rotate. To increase the surface modification rate in PAP, Ar was used as the carrier gas with a high gas flow rate of 10 slm.

Figure 6.32 shows the change in the MRR of PAP for different durations. In the case of 1 min of PAP, a very high MRR of about 272.8 nm/h was obtained. This MRR was much higher than that of the conventional CMP process, which is usually less than 80 nm/h [3)]. However, with increasing polishing time, the MRR greatly decreased. After PAP for 4.5 min, the MRR was greatly decreased to 82 nm/h. In the case of PAP for 30 min, the average MRR was further decreased to 31.4 nm/h, which was even lower than that of the conventional CMP process. It was assumed that the deterioration of the grinding stone was the reason why the MRR decreased with increasing polishing duration.

To confirm this assumption, the change in the surface morphology of the grinding stone

resulting from polishing was evaluated. Figure 6.33 shows surface profiles of the grinding stone before and after PAP for 4.5 min. The grinding stone was measured at the same location using the two valleys marked as A and B as references. Even though the polishing time was only 4.5 min, the surface of the grinding stone after polishing was reasonably flat and the protrusions that existed on the initial grinding stone surface almost disappeared. That is to say, deterioration of the grinding stone surface was confirmed, which was the reason why the MRR of PAP markedly decreased.

On the basis of the above discussion, it was concluded that dressing is necessary to refresh the surface of the polished grinding stone to obtain a scratch-free surface and sustain the high MRR of PAP.

6.5.3 Effect of dressing in PAP

To determine the effect of dressing, the PAP of GaN was conducted with and without dressing. Currently, *in situ* dressing of the grinding stone cannot be conducted using the prototype PAP machine. Therefore, the PAP and dressing were separately conducted. After PAP for 10 s under the conditions shown in Table 6.8, the grinding stone was dressed using a diamond plate for 5 s under the dressing conditions shown in Table 6.9. An image of the dressing setup was shown in Figure 3.17. PAP and dressing were repeated several times and the total polishing time of PAP was 5 min. For comparison, PAP was also conducted for 5 min under the conditions shown in Table 6.8 without dressing.

Figure 6.34(a) shows the surface profile of the grinding stone after dressing. Many protrusions can be observed, which means that the diamond plate was very useful for dressing the grinding stone to provide it with a rough surface. Figure 6.34(b) shows the surface profile of the grinding

Table 6.8 Conditions of PAP

Experimental setup	cf. Figure 3.10
Specimen	3 inch GaN (0001)
Grinding stone	Resin-bonded SiO_2 grinding stone (LHA type)
Average grain size	0.7 μm
Carrier gas	Ar (10 slm)
Rotation speeds	Stage: 100 rpm. Polishing tool: 0
Scanning of the stage	Length: 30 mm. Speed: 5 mm/s
Applied RF power	18 W
Pressure	30 kPa

stone after PAP for 5 min without dressing. Protrusions almost disappeared on the polished grinding stone surface. Abrasion of the grinding stone clearly occurred. The abraded grinding stone surface was not flat, which was considered to be due to the nonuniform abrasion of the grinding stone or the accumulation of scraps from the abrasion.

The weight of the substrate was measured before and after PAP to calculate the MRR of PAP. Figure 6.35 shows the MRR of PAP with and without dressing. In the case of PAP with intermittent dressing, the MRR was calculated to be 193 nm/h, which was about 2.5 times higher than that of the conventional CMP process. In contrast, the MRR of PAP without dressing was 90 nm/h, which was much lower than that of PAP with intermittent dressing. This means that dressing is very effective for obtaining a high MRR of GaN in PAP.

In the future, the prototype PAP machine will be optimized to realize *in situ* dressing in PAP. On the basis of the above results, it is strongly expected that a higher MRR can be obtained with the application of *in situ* dressing, which will be experimentally confirmed in a future study. The PAP of GaN using other types of grinding stone will also be investigated.

Table 6.9 Conditions of dressing

Experimental setup	cf. Figure 3.10
Diamond plate	#100
Rotation speeds	Stage: 50 rpm. Polishing tool: 100 rpm
Pressure	10 kPa
Time	5 s

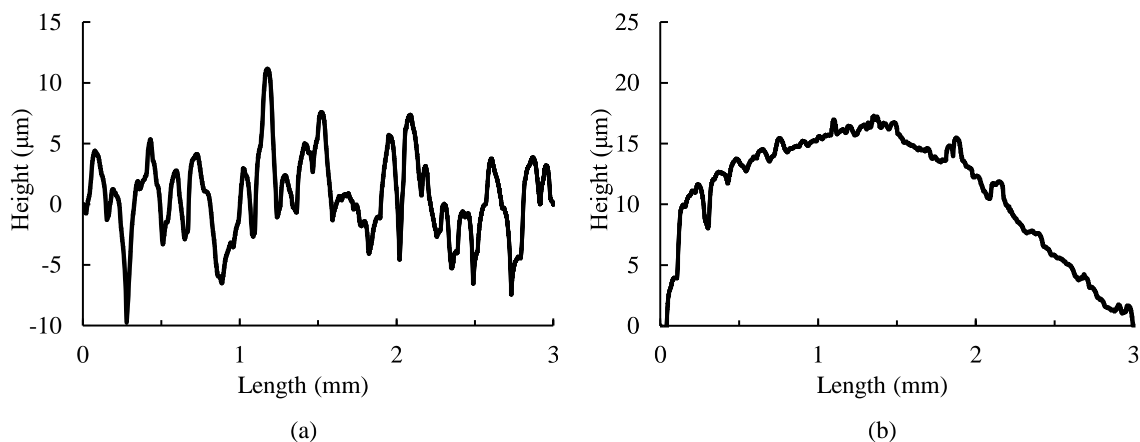

Figure 6.34 Surface profiles of the resin-bonded SiO_2 grinding stone used in the prototype PAP machine. (a) After dressing. (b) After PAP for 5 min.

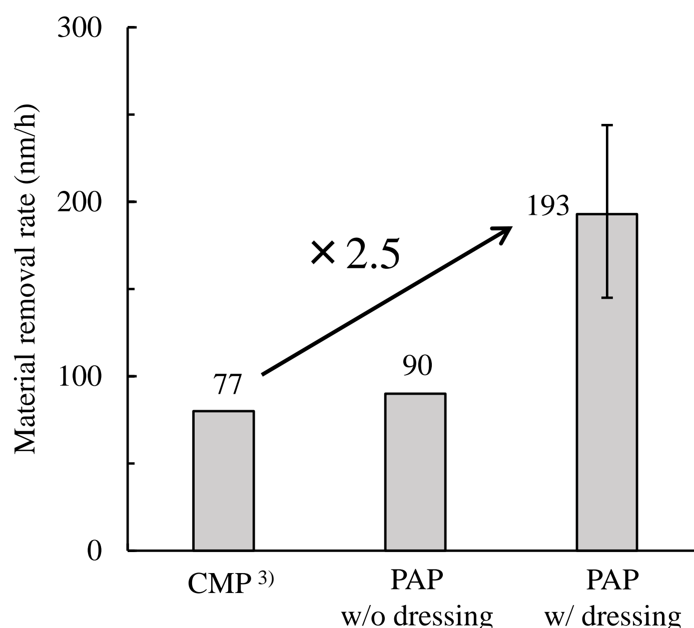

Figure 6.35 MRRs of PAP with and without dressing.

6.6 Summary

PAP was applied to GaN (0001) to resolve the problems of the conventional CMP process such as the low MRR and the formation of etch pits. The surface modification of GaN by AP-plasma was confirmed. The application of the two-step PAP process and the prototype PAP machine were separately investigated.

(1) It was confirmed that in the conventional CMP process, regardless of whether SiO_2 or CeO_2 slurry was used, many etch pits, which deteriorated the surface integrity and roughness, were generated, which originated from the dislocations in the GaN epilayer. It was considered that these pits were formed by the preferential etching or removal of the dislocations by the chemicals in the slurry.

(2) The surface modification of GaN by AP-plasma irradiation was confirmed. It was found that the surface modification efficiency of CF_4-containing plasma was higher than that of O_2-containing plasma and that the heating of the substrate greatly promoted the surface modification reaction. After plasma irradiation, the surface hardness of GaN decreased, which was confirmed by nanoindentation tests.

(3) The CMP of GaN with plasma pretreatment was conducted and a pit-free surface was

obtained with time-controlled polishing. Under-polishing resulted in a GaN surface with the modified layer remaining, whereas a rough surface with many etch pits was generated in the case of over-polishing. Only in the case of just-polishing was a pit-free and atomically flat surface obtained.

(4) Several types of grinding stone were used to polish GaN without plasma pretreatment. It was revealed that the fixed-type CeO_2 grinding stone had better polishing characteristics without the generation of scratches and etch pits. Plasma irradiation was combined with dry polishing using a CeO_2 grinding stone, and a scratch-free and pit-free surface with a well-ordered step-terrace structure was obtained.

(5) The plasma generation conditions in the prototype PAP machine were optimized. It was found that a lower water vapor concentration, a higher carrier gas flow rate and the replacement of He with Ar were very effective for improving the surface modification efficiency in PAP.

(6) The prototype PAP machine was used to polish the whole-surface of 3 inch GaN substrates. A high MRR of 272.8 nm/h was obtained in the case of short-time polishing. The deterioration of the grinding stone surface in PAP was confirmed, which increased the surface roughness, resulted in the formation of scratches and decreased the MRR of PAP.

(7) The effect of dressing in PAP was confirmed. With intermittent dressing using a diamond plate, a high MRR of PAP of 193 nm/h was obtained, while it was only 90 nm/h without dressing. In a future study, the prototype PAP machine will be optimized to realize *in situ* dressing in PAP to obtain higher MRRs.

References

1) H. Aida, S. Kim, T. Suzuki, K. Koyama, N. Aota, T. Doi and T. Yamazaki, ECS J. Solid Stae Sci. Technol. 3 (2014) P163-P168.

2) P. R. Tavernier, T. Margalith, L. A. Coldren, S. P. DenBaars, and D. R. Clarke, Electrochem. Solid-State Lett. 5 (2002) G61-G64.

3) H. Gong, G. Pan, Y. Zhou, X. Shi, C. Zou and S. Zhang, Appl. Surf. Sci. 338 2015) 85-91.

4) H. Deng, K. Endo and K. Yamamura, Ann. CIRP 64 (2015) 531-534.

5) W. J. Patrick, W. L. Guthrie, C. L. Standley and P. M. Schiable, J. Electrochem. Soc. 138 (1991) 1778-1784.

6) L. Zhou, V. Audurier, P. Pirouz and J. A. Powell, J. Electrochem. Soc. 144 (1997) L161-L163.

7) P. Kumar, S. Rao, J. Lee, D. Singh and R. K. Singh, ECS J. Solid Stae Sci. Technol. 2 (2013) P1-P4.
8) H. Deng, K. Endo and K. Yamamura, Appl. Phys. Lett. 107 (2015) 051602.
9) D. D. Wagman, W. H. Evans, V. B. Parker, R. H. Schumm, I. Halow, S. M. Bailey, K. L. Churney and R. L. Nuttall, J. Phys. Chem. Ref. Data 11 (1982) 1-392.
10) Y. Kawamoto, K. Ogura, M. Shojiya, M. Takahashi and K. Kadono, J. Flourine Chem. 96 (1999) 135-139.
11) H. Deng, K. Endo and K. Yamamura, Appl. Phys. Lett. 104 (2014) 101608.
12) W. C. Oliver and G. M. Pharr, J. Mater. Res. 7 (1992) 1564-1583.
13) V. Anand and M. R. Gowravaram, IEEE Trans. Plasma Sci. 37 (2009) 1811-1816.
14) A. Sarani, A. Yu. Nikiforov and C. Leys, Phys. Plasmas 17 (2010) 063504.
15) B. R. Strohmeier, Surf. Interface Anal. 15 (1990) 51-56.
16) S. Tanuma, C. J. Powell and D. R. Penn, Surf. Interface Anal. 43 (2011) 689-713.

Chapter 7
AP-plasma-based figuring and finishing of CVD-SiC

7.1 Introduction

The excellent properties of CVD-SiC, such as high hardness, light weight and high thermal conductivity, make it a very good candidate material for space telescope mirrors and molds for optical components [1-3]. As reported in this chapter, the characteristics of the CVD-SiC substrates used in my study were investigated. To resolve the problems and challenges in the machining of CVD-SiC using conventional methods, a highly efficient and damage-free figuring and finishing process for CVD-SiC based on AP-plasma is proposed.

7.2 CVD-SiC used in the study

CVD-SiC is usually grown on other substrates such as reaction-sintered SiC (RS-SiC), graphite and so forth. For different CVD-SiC manufacturers, even though their growth processes have the same mechanism, the growth parameters, such as the temperature, pressure, and gas flow rates, are considerably different. Therefore, CVD-SiC substrates from different manufacturers may have different properties such as purity, crystallinity, surface morphology and so forth. The CVD-SiC substrates used in this study were supplied by Tokai Fine Carbon Co. Limited [4].

Figure 7.1(a) shows a photograph of the CVD-SiC substrate used in this study. SiC was grown on a graphite substrate (40 mm × 40 mm × 10 mm ^{t}) on both sides and the thickness of the SiC

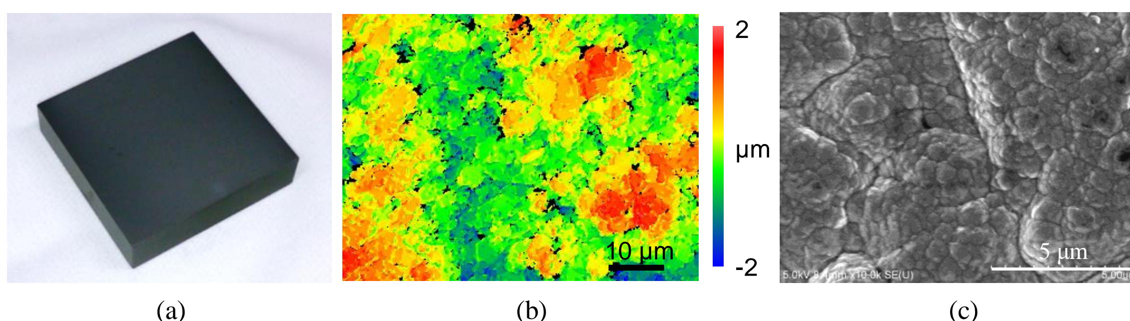

(a) (b) (c)

Figure 7.1 CVD-SiC substrate used in my research. (a) Photograph. (b) SWLI image (p-v: 4643.5 nm, rms: 621.0 nm). (c) SEM image.

layer is about 100 μm. Figure 7.1(b) shows an SWLI image of the substrate. No flattening process was conducted after CVD growth. Therefore, the surface is very rough. As shown in Figure 7.1(c), the SiC grains in the substrate are very small (less than 1 μm in diameter). It is considered that the smaller the SiC grains, the better the properties obtained, such as good surface roughness after polishing, high hardness and high strength. Therefore, it was assumed that excellent properties could be obtained with the application of this substrate.

Figure 7.2 shows XPS spectra of the substrate. All the elements existing in the substrate surface are shown in the wide-scan spectrum, which indicates that only Si, C and O exist in the CVD-SiC layer. As indicated by the O1s and Si2p spectra, a thin oxide layer was observed, which is considered to be owing to the native oxide. Also, as shown in the C1s spectrum, a small amount of organic contamination (C-C/C-H) exists on the substrate surface.

The crystalline orientation of the SiC layer was investigated by XRD. The XRD pattern is shown in Figure 7.3, which indicates very high crystallinity. Two obvious characteristic peaks at 35.7° and 73.8°, corresponding to the diffraction from the (111) and (222) crystal planes of β-SiC [5, 6], were observed. This means that the SiC grains in the CVD-SiC substrate have a phase structure of β-SiC and that all the grains are highly oriented.

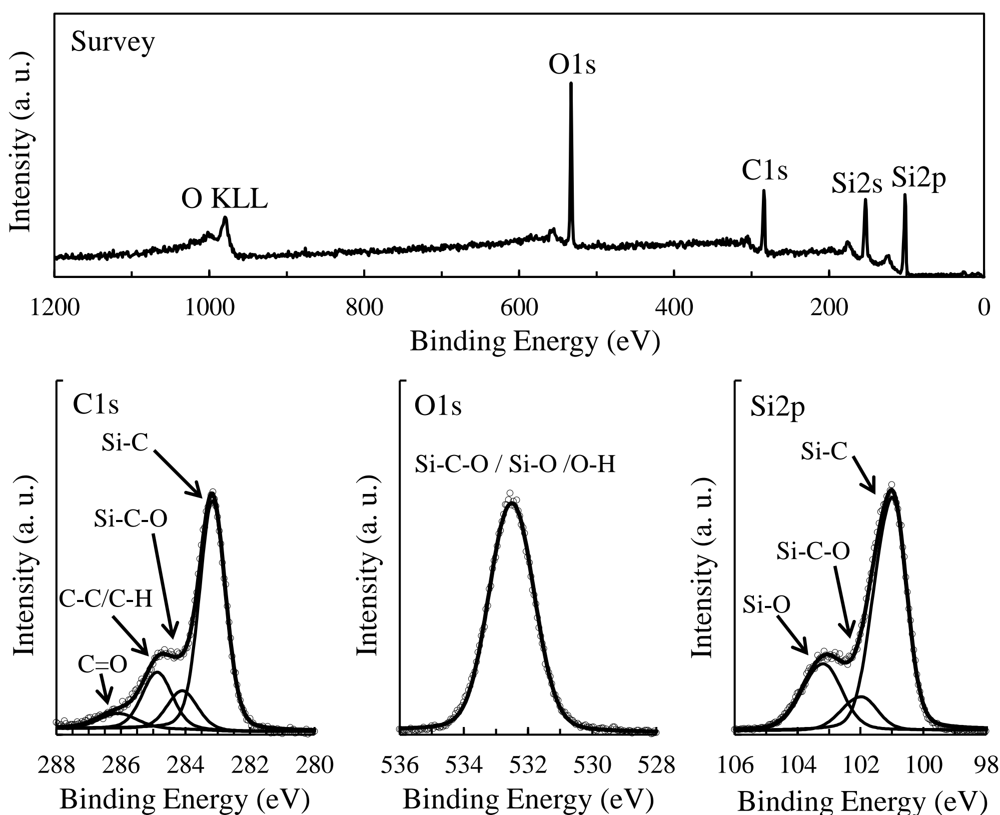

Figure 7.2 XPS spectra of the CVD-SiC substrate.

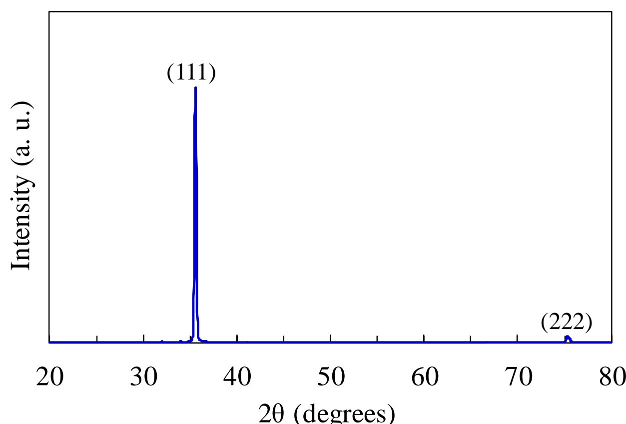

Figure 7.3 XRD patterns of the CVD-SiC substrate.

7.3 Lapping and CMP of CVD-SiC

CVD-SiC has a very high hardness, which makes it difficult to mechanically machine. Therefore, for the figuring of CVD-SiC, diamond tools for turning or diamond grinding stones for grinding are widely used [7, 8]. Figure 7.4 shows a schematic view of the conventional figuring and finishing of CVD-SiC. After figuring using mechanical methods, finishing using CMP is usually conducted to remove the SSD formed by the previous mechanical processes and decrease the surface roughness.

Diamond lapping was conducted on a CVD-SiC substrate under the conditions shown in Table 7.1. Since there were components with a large spatial wavelength on the as-grown surface, the

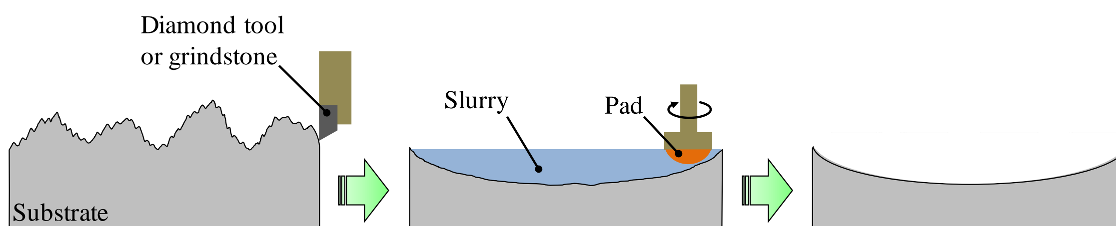

Figure 7.4 Schematic view of conventional figuring and finishing of CVD-SiC.

Table 7.1 Parameters of diamond lapping

Load	4000 g
Diamond grain size	5-15 μm
Rotation speed (substrate)	350 rpm
Rotation speed (Platen)	150 rpm
Time duration	48 h

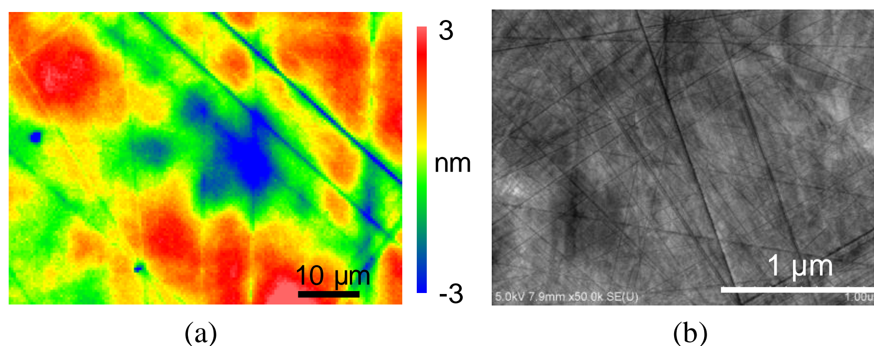

(a) (b)

Figure 7.5 CVD-SiC after diamond lapping. (a) SWLI image (p-v: 24.86 nm, rms: 1.16 nm). (b) SEM image.

polishing time was set to a quite long duration to smooth the whole substrate surface. Figure 7.5 shows SWLI and SEM images of the lapped surface. Even though the surface roughness was greatly decreased to a mirror level, deep scratches can be observed in the SWLI image and a large number of shallow scratches were formed as shown in the SEM image. In my previous study on the finishing of single-crystal SiC, the diamond lapping of 4H-SiC under the same conditions was also conducted, as described in Chapter 4 and an SSD layer with a thickness of about 100 nm was formed [9]. Therefore, it was considered that there was also a thick SSD layer on the CVD-SiC surface after lapping.

The formed scratches will deteriorate the surface roughness and figure accuracy of the substrate surface, which will affect the performance of mirrors and molds. Also, the SSD will affect the durability of these components. Therefore, it was concluded that diamond lapping is not a suitable finishing method for CVD-SiC and that a damage-free finishing technique with a high efficiency and low cost is required.

CMP is widely used as a damage-free finishing technique for semiconductor and optical components [10, 11]. Using the experimental setup shown in Figure 3.5, CMP using CeO_2 slurry was conducted on an as-grown CVD-SiC substrate. Table 7.2 shows the conditions of CMP. A high slurry concentration, a high pressure and a high pad rotation speed were applied to realize a high polishing efficiency in accordance with Preston's law [12]. Figure 7.6 shows the CMP-processed surfaces after different durations of CMP. After CMP for 2 h, the surface roughness was decreased but the surface was still very rough as shown in

Table 7.2 Parameters of CMP

Experimental setup	cf. Figure 3.5
Concentration	40 wt% (CeO_2)
Pad type	Suede type (ϕ10 mm)
Pad rotation speed	2000 rpm
Load	25.5 kPa
Time	2+5 h

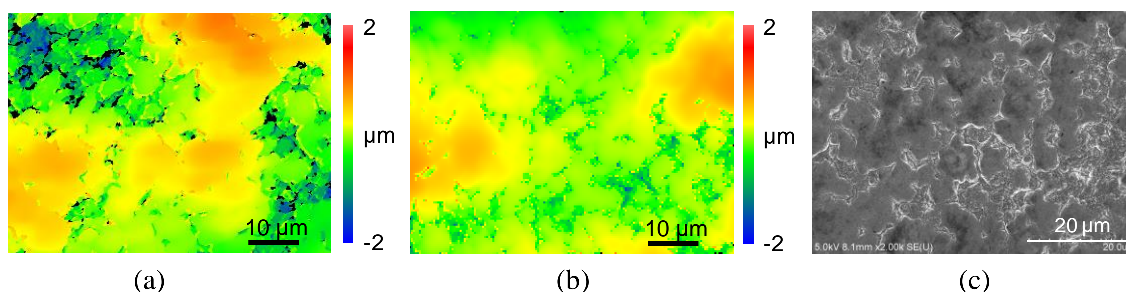

Figure 7.6 CMP-processed CVD-SiC surface (p-v: 3517.0 nm, rms: 457.1 nm). (a) SWLI image after CMP for 2 h. (b) SWLI image after CMP for 7 h (p-v: 2571.1 nm, rms: 312.8 nm). (c) SEM image after CMP for 7 h.

Figure 7.6(a). With additional CMP for 5 h, a flatter surface was obtained but the surface roughness was still unsatisfactory for applications such as mirrors and mold components. As shown in Figure 7.6(c), even after CMP for 7 h, there were still many unpolished areas on the surface. The CMP of CVD-SiC using a commercially available SiO_2 slurry was also conducted and very similar results were obtained. This means that the efficiency of CMP for CVD-SiC is very low.

7.4 AP-plasma-based figuring and finishing of CVD-SiC

7.4.1 Concept

An AP-plasma-based process is proposed to realize the highly efficient, low-cost and damage-free figuring and finishing of CVD-SiC. Figure 7.7 shows a schematic view of the proposed concept. In the figuring stage, conventional methods such as turning and grinding using diamond are used to realize figuring with a low cost and high efficiency. However, scratches and SSD are inevitably formed. After that, PCVM, which is a chemical etching process, is used for figure correction and the removal of the SSD. Etching in PCVM is isotropically performed, therefore an ultrasmooth surface cannot be obtained using PCVM only. Thus, a finishing process is necessary and PAP is conducted for damage-free finishing to decrease the surface roughness.

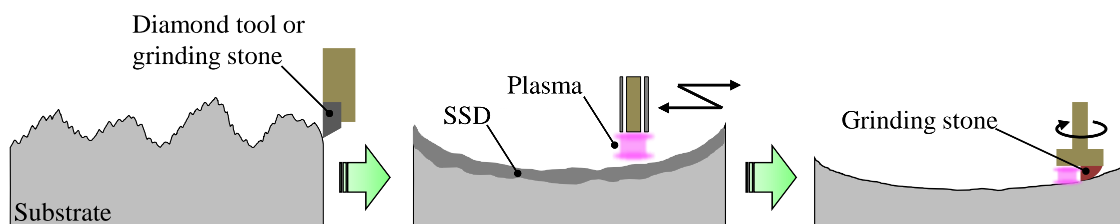

Figure 7.7 Schematic view of plasma-based figuring and finishing of CVD-SiC.

PCVM is a non-contact figuring process with a very high efficiency [13, 14]. Therefore, it is considered that the SSD and scratches formed by previous mechanical processes can be completely removed by PCVM in a very short time without the formation of further damage. On the other hand, PAP is a dry polishing process without the use of slurry. SiC grains in CVD-SiC are oxidized by the irradiation of AP-plasma and the oxide layer is removed by a soft grinding stone. Therefore, highly efficient figuring and damage-free finishing can be realized by the proposed plasma-based process.

7.4.2 PCVM of CVD-SiC

As previously mentioned, a CVD-SiC substrate consists of SiC, SiO_2 (native oxide) and contamination (C-C/C-H). In PCVM, CF_4 plasma is used to etch the CVD-SiC substrate on the basis of the following reactions.

$$SiC + CF_4 + O_2 \rightarrow 2CO\uparrow + SiF_4\uparrow \quad (7.1)$$

$$SiO_2 + CF_4 \rightarrow CO_2\uparrow + SiF_4\uparrow \quad (7.2)$$

$$C_xH_y + O/OH/F \rightarrow CO/CO_2/H_2O/CF_4\uparrow \quad (7.3)$$

Table 7.3 Parameters of PCVM

Experimental setup	Figure 3.4
RF power	20, 30 W
Gas flow rate	He: 1.0 slm, CF_4: 20 sccm
Gap	1.6 mm
Scanning speed	5 mm/s
Feed pitch	0.5 mm
Processing time	30 min

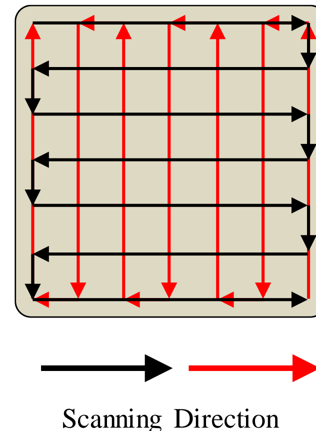

Figure 7.8 Scanning path of PCVM.

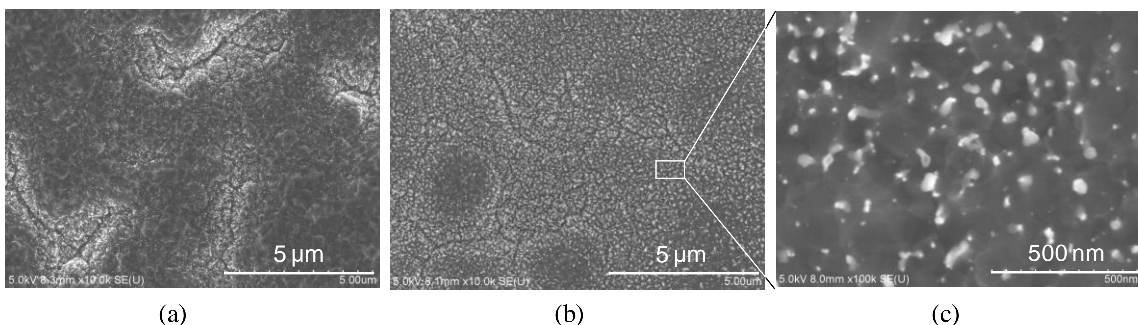

(a) (b) (c)

Figure 7.9 SEM images of PCVM-processed CVD-SiC surface. (a) 20 W. (b) 30 W. (c) An enlarged image.

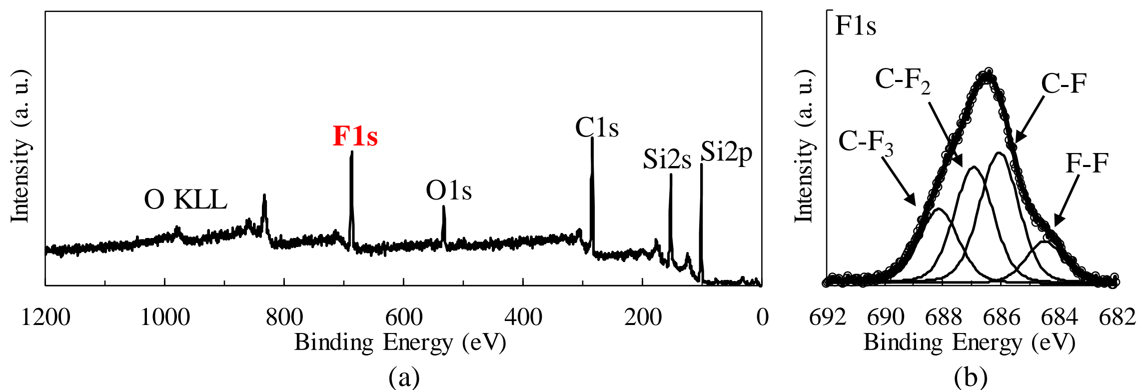

Figure 7.10 XPS measurements of PCVM-processed CVD-SiC surface. (a) Wide scan spectrum. (b) F1s spectrum.

It was found that when CVD-SiC is irradiated by CF_4 plasma, chemical reactions occur and all the reaction products are volatile. Therefore, the machining (etching) of CVD-SiC using CF_4 plasma is possible.

Table 7.3 shows the conditions of PCVM. The experimental setup shown in Figure 3.4 was used. PCVM was conducted using a localized plasma with the scanning path shown in Figure 7.8. The surface after PCVM was observed by SEM. Figure 7.9 shows the observation results. Compared with the as-received surface shown in Figure 7.1(c), the surface became smoother with the increase in the removal volume. However, many small particles with a size of 10 nm order were observed as shown in Figure 7.9(c).

It is considered that these small particles originated from the nonvolatile reaction products generated in the PCVM process. To clarify the composition of these small particles, XPS measurements of PCVM-processed surfaces were conducted. Figure 7.10 shows the measurement results. As can be observed from the wide-scan spectrum, fluorine exists on the processed surface. Figure 7.10(b) shows the result of peak separation of the F1s spectrum. It was confirmed that these particles are carbon fluorides (C_xF_y), which were generated in the PCVM process. These residual particles increased the surface roughness. Therefore, they need to be efficiently removed.

Taking the composition of these particles into consideration, it is assumed that the addition of O_2 to the reactive gas should be very useful for removing these particles. This is because O_2 will be dissociated in the plasma area to generate O radicals, which will react with the carbon fluorides and remove them by the reaction:

$$C_xF_y + O \rightarrow CO/CO_2/F\uparrow. \quad (7.4)$$

The above assumption was experimentally confirmed. PCVM with the additive of O_2 (2 sccm) was conducted with the other parameters given in Table 7.3. Figure 7.11 shows a SEM image of

the processed surface. The surface is very smooth and no C_xF_y particles can be observed. This means that O_2 is a very useful additive to prevent the generation of C_xF_y particles as assumed. On the basis of the above results, He-based CF_4 and O_2 were used as the plasma gas for the PCVM of CVD-SiC in the following experiments.

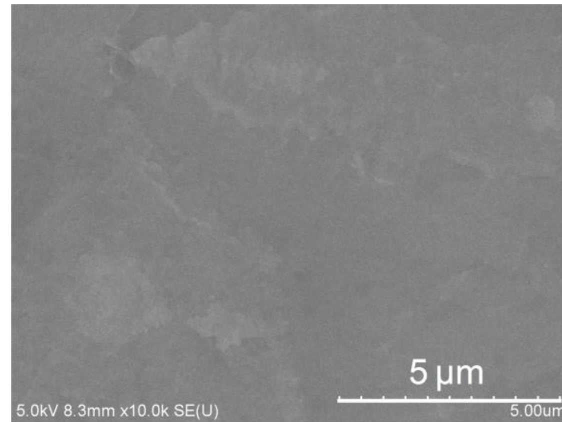

Figure 7.11 SEM image of PCVM-processed CVD-SiC surface.

PCVM is mainly conducted to remove the SSD formed by previous mechanical processes. The thickness of the SSD varies with the machining conditions. In a typical figuring process using turning or grinding, SSD with micrometer thickness is formed [15, 16]. Therefore, a high MRR is required for PCVM to remove the SSD with high efficiency. The static etching of CVD-SiC was conducted under the conditions shown in Table 7.4 to evaluate the MRR of PCVM. Figure 7.12 shows an SWLI image of the removal spot as well as its cross section, which can be considered as the removal footprint of PCVM. It was confirmed that under the conditions shown in Table 7.4, PCVM has a very high MRR of about 14 μm/h, which is much higher than that of the conventional CMP process for SiC.

Table 7.4 Parameters of static plasma etching

Experimental setup	cf. Figure 3.4
RF power	20 W
Gas flow rate	He: 1.0 slm CF_4: 20 sccm, O_2: 2 sccm
Gap	1.6 mm
Processing time	30 min

Even though PCVM has a very high MRR, it is considered that the surface of a CVD-SiC

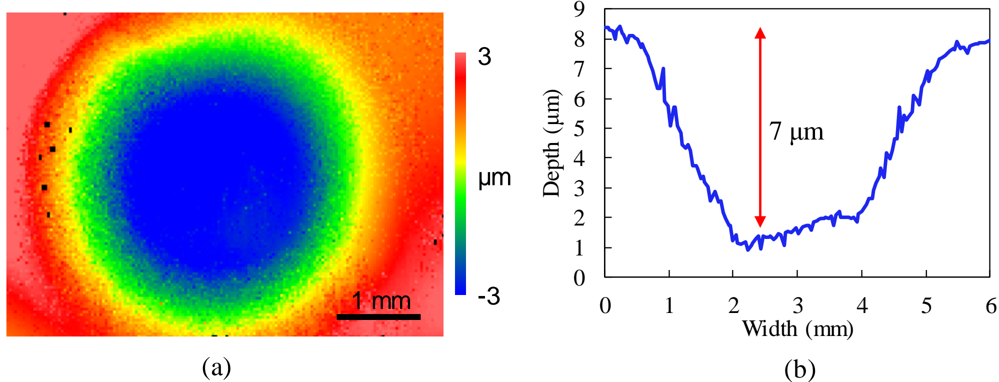

Figure 7.12 Removal footprint of PCVM. (a) SWLI image. (b) Cross-sectional image.

substrate subjected to PCVM will become rough since PCVM is an isotropic etching process. The PCVM of a diamond-lapped CVD-SiC substrate was conducted for different durations under the conditions shown in Table 7.5. According to my previous study, scratches and SSD with a thickness of about 100 nm were formed on the substrate. Figure 7.13 shows SWLI images of PCVM-processed CVD-SiC surfaces and a graph indicating the change in the rms roughness with the duration of PCVM. After PCVM for a short time (5 min), the scratches formed by diamond lapping completely disappeared even though the surface roughness also increased as assumed. It is clear that the surface roughness increased with the duration of PCVM. Taking the MRR of PCVM and the probable thickness of the SSD layer into consideration, PCVM for 5 min was sufficient to completely remove the SSD formed by diamond lapping. Therefore, the surface shown in Figure 7.13(a) is considered to be damage-free. To decrease the roughness of this damage-free surface, additional finishing is required.

Table 7.5 Parameters of PCVM

Experimental setup	Figure 3.4
RF power	20 W
Gas flow rate	He: 1.0 slm, CF_4: 20 sccm, O_2: 2 sccm
Gap	1.6 mm
Scanning speed	5 mm/s
Feed pitch	0.5 mm
Processing time	30 min

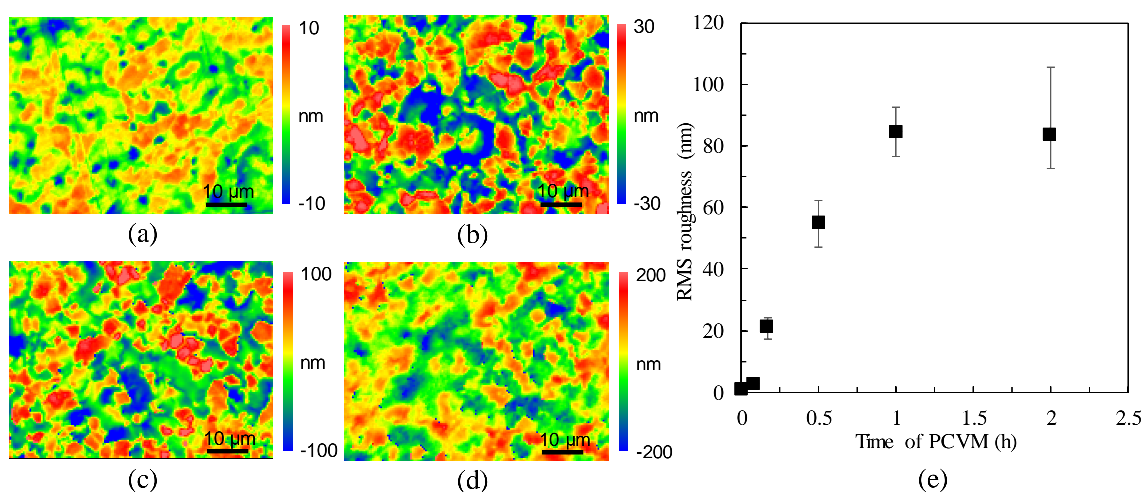

Figure 7.13 (a-d) SWLI image of PCVM-processed surfaces. (a) 5 min. (b) 10 min. (c) 30 min. (d) 1 h. (e) Change of rms with the increase of duration of PCVM.

7.4.3 PAP of CVD-SiC

The surface processed by PCVM for 5 min shown in Figure 7.13(a) was finished by PAP, in which plasma modification and abrasive polishing were combined. Similar to the case of 4H-SiC, water-vapor-containing plasma was used for the surface modification of CVD-SiC. For removal of the modified layer, resin-bonded grinding stones were used.

Figure 7.14 shows schematic views of the PAP setup and an enlarged image of the polishing tool. A resin-bonded grinding stone (ϕ 8 mm) was fixed on the bottom of the electrode (ϕ 20 mm), which was made of Al alloy with an offset of 4 mm from the rotation center. A mixture of He and water vapor, which was used as the process gas for plasma generation, was supplied into the glass cover and flowed through the space between the electrode and the substrate. The gap distance between the electrode and the substrate was 1 mm. Water-vapor-containing plasma was generated around the grinding stone by applying an RF power between the electrode and the stage. With the rotation of the electrode with a constant load, which could be adjusted via the weight, plasma modification and abrasive polishing were simultaneously conducted.

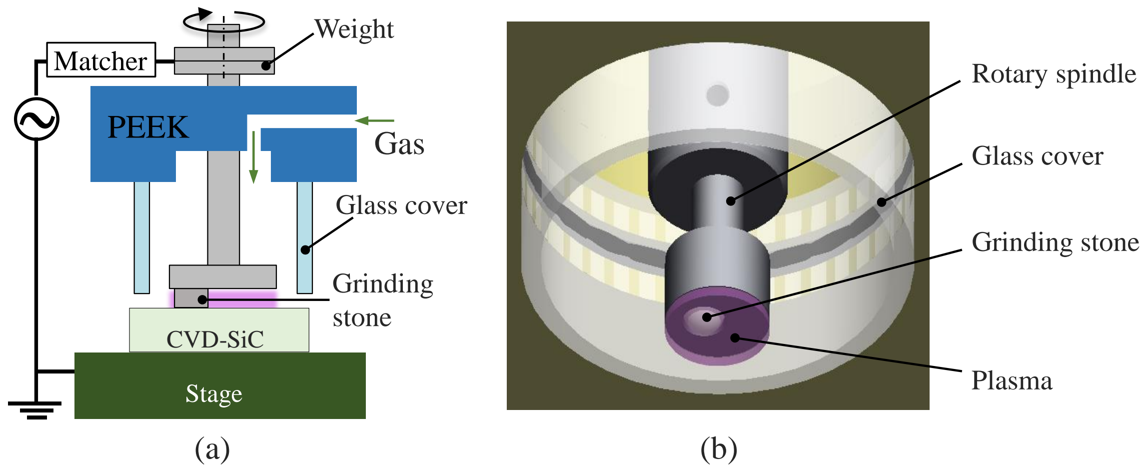

Figure 7.14 (a) Schematic view of the PAP setup. (b) CAD image of the polishing tool.

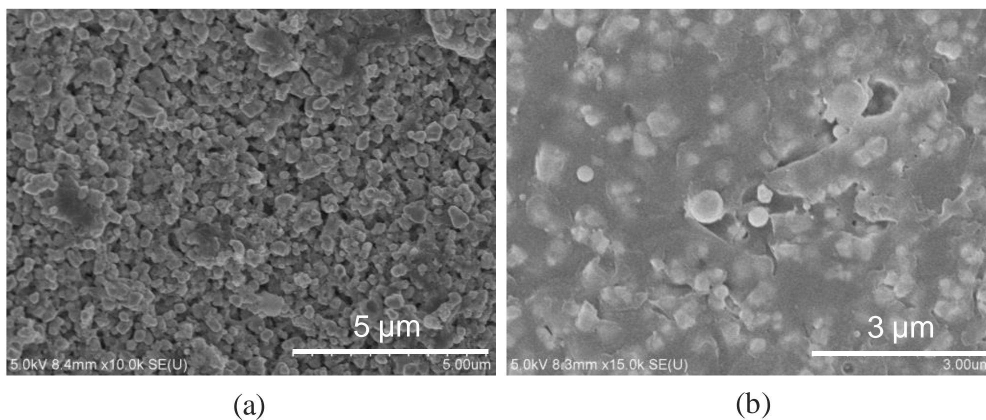

Figure 7.15 SEM images of the grinding stones. (a) Regular fixed type. (b) Loose held type.

To realize damage-free finishing, resin-bonded CeO_2 grinding stones were used. Two types of grinding stone: the regular fixed-type and loose-held-type were investigated. Figure 7.15 shows SEM images of these two types of grinding stone. The average diameter of the CeO_2 grains was 0.7 μm. Both the resin and the CeO_2 are soft materials compared with SiC, therefore it was considered that a layer of damage would not be formed in PAP.

Table 7.6 shows the conditions of PAP. When the regular fixed-type grinding stone was used in PAP, hardly any polishing occurred owing to its very rapid abrasion in PAP. It was considered that the parameters of the fixed-type grinding stones needed to be optimized such as the concentration of CeO_2 grains, the grain size, the structure of the resin and so forth. In the case of the loose-held-type grinding stone, PAP was effectively conducted. Figure 7.16 shows an SWLI image of the polished CVD-SiC surface after PAP for 3 h using a loose-held-type grinding stone. The protrusions existing on the PCVM-processed surface shown in Figure 7.13(a) were completely removed and a smooth surface was obtained. The surface rms roughness in a 64 μm×48 μm area was also improved from 2.93 nm to 0.69 nm.

Table 7.6 Parameters of PAP

Experimental setup	cf. Figure 7.14
RF power	15 W
Gas flow rate	He: 1.5 slm, H_2O: 20 sccm
Load	180 g
Rotation speed	500 rpm
Processing time	3 h

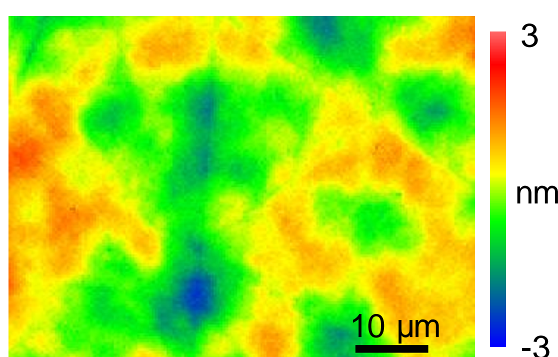

Figure 7.16 SWLI image of the PAP-processed surface (p-v: 4.41 nm, rms: 0.69 nm).

Even though PAP has been proved to be very useful for the finishing of CVD-SiC, there are still several problems. Figure 7.17 shows an optical microscope image of the grinding stone after PAP. Areas with a different color can be clearly observed. It is assumed that the resin in the grinding stone was oxidized owing to the high

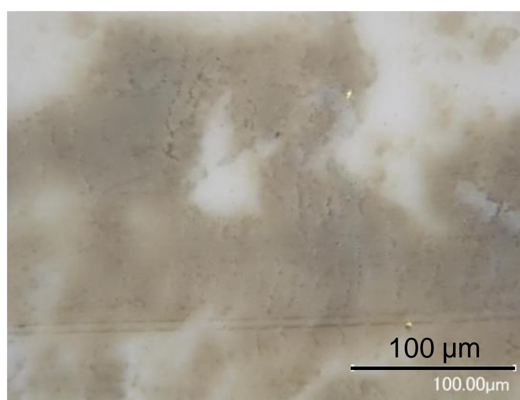

Figure 7.17 Optical microscope image of the grinding stone after PAP.

friction heat in the area of contact between the grinding stone and the substrate during abrasion. That is to say, resin with stronger heat resistance should be used in PAP. Also, similar to the PAP of GaN, deterioration of the grinding stone surface also occurred even after a short polishing time. Therefore, a dresser that can be applied in the PAP of CVD-SiC substrates should be developed. The experimental setup shown in Figure 7.14 was used for a fundamental study of PAP, for which only a localized plane area can be polished. Therefore, a PAP machine that can be practically used for finishing the curved surfaces of substrates with different sizes will be developed in my future study. Finally, the conditions of PAP should also be optimized to obtain a high polishing efficiency and decrease the finishing time. Also, better surface roughness with a subnanometer-order rms (in a 64 μm × 48 μm area) is expected.

7.5 Summary

To realize the damage-free figuring and finishing of CVD-SiC substrates, which are used as materials for space telescope mirrors and glass molds, PCVM and PAP were combined. As reported in this chapter, the properties of the CVD-SiC substrates used in this study were investigated. Diamond lapping and CMP were conducted for comparison with the proposed plasma-based figuring and finishing process. PCVM was performed for the removal of the SSD layer while PAP was performed for damage-free surface finishing.

(1) The as-grown surface of the CVD-SiC substrate was very rough and its surface composition was determined by XPS, which indicated that a thin oxide layer and a contamination layer existed. The high crystallinity of the substrate was proved by XRD measurements and all the SiC grains had the same (111) surface orientation.

(2) Many scratches and an SSD layer were formed by the diamond lapping of CVD-SiC, which means that it is not a suitable finishing process for CVD-SiC. Conventional CMP using CeO_2 slurry was conducted for the damage-free finishing of CVD-SiC. However, the polishing efficiency was very low.

(3) PCVM was conducted on a diamond lapped CVD-SiC surface. After PCVM for a short duration of 5 min, scratches and the SSD layer formed by lapping were completely removed, although the surface roughness was slightly increased.

(4) PAP using a resin-bonded CeO_2 grinding stone was conducted to decrease the surface roughness of CVD-SiC processed by diamond lapping and PCVM for 5 min. The loose-held-

type grinding stone was demonstrated to be very useful. A flat and scratch-free surface with an rms roughness of 0.6 nm was obtained.

References

1) C. Hall, M. Tricard, H. Murakoski, Y. Yamamoto, K. Kuriyama and H. Yoko, Proc. SPIE 5868 (2005) 58680V-1-10.
2) N. Ebizuka, Y. Dai, H. Eto, W. Lin, T. Ebisuzaki, H. Omori, T. Handa, H. Takami and Y. Takahashi, Proc. SPIE 4842 (2003) 329-334.
3) J. Casstevens, A. Rashed, R. Plummer, D. Bray, R. Gates, E. Curzio, M. Ferber and T. Kirkland, Proc. SPIE 4451 (2001) 458-467.
4) http://www.tokaicarbon.co.jp/index.html
5) T. Bun, J. Plasma Fusion Res. 90 (2014) 47-51.
6) D. Huang, M. Zhang, Q. Huang, L. Xue, P. Zhong and L. Li, Corros. Sci. 87 (2014) 134-140.
7) N. Ebizuka, Y. Dai, H. Eto, W. Lin, T. Ebisuzaki, H. Omori, T. Handa, H. Takami and Y. Takahashi, Proc. SPIE 4842 (2003) 329-334.
8) C. Hall, M. Tricard, H. Murakoski, Y. Yamamoto, K. Kuriyama and H. Yoko, Proc. SPIE 5868 (2005) 58680V-1-10.
9) H. Deng, M. Ueda and K. Yamamura, Int. J. Adv. Manuf. Technol. 72 (2014) 1-7.
10) H. Aida, T. Doi, H. Takeda, H. Katakura, S. Kim, K. Koyama, T. Yamazaki and M. Uneda, Curr. Appl. Phys. 12 (2012) 541-546.
11) E. Becker, A. Prange and R. Conradt, Mater. Res. Soc. Symp. Proc. 1157 (2009) 1157-E03-02.
12) F. Preston, J. Soc. Glass Tech. 11 (1927) 214-256.
13) K. Yamamura, S. Shimada and Y. Mori, Ann. CIRP 57 (2008) 567-570.
14) Y. Mori, K. Yamamura and Y. Sano, Rev. Sci. Instrum. 75 (2004) 942-946.
15) X. Tonnellier, P. Shore, P. Morantz, A. Baldwin, D. Walker, G. Yu and R. Evans, Proc. Of SPIE 7018 (2008) 70180F.
16) S. Goel, J. Phys. D: Appl. Phys. 47 (2014) 243001.

Chapter 8
Summary

A novel finishing technique named plasma-assisted polishing (PAP) was proposed for the damage-free, slurryless and low-cost finishing of difficult-to-machine materials such as 4H-SiC, GaN and CVD-SiC. A symmetric PAP machine, a two-step PAP process and a prototype PAP machine were developed. The usefulness of PAP was confirmed using the symmetric PAP machine. The surface modification and material removal mechanisms in PAP were clarified by the two-step PAP process. The slurryless and whole-surface polishing of large substrates with high efficiency was realized using the prototype PAP machine.

In Chapter 1, the background to this study, the properties and applications of the difficult-to-machine materials that were polished in this study and the aims of this study were introduced.

In Chapter 2, PAP was proposed and its concepts were introduced. To realize the highly efficient, cost-effective and damage-free polishing of the difficult-to-machine materials, which cannot be realized by conventional polishing techniques, PAP was proposed. In this chapter, the conventional polishing techniques, the basics of the generation of AP-plasma, and the concepts and strategies of PAP were introduced.

(1) The damage-free and ultraprecision polishing of difficult-to-machine materials is difficult owing to their high hardness and chemical inertness. Currently, several polishing techniques are being developed for these materials. However, there are still several challenges associated with these polishing techniques such as the low polishing efficiency and high cost.

(2) AP-plasma has been successfully used in PCVM for the ultraprecision machining of Si-based materials. The major advantages of AP-plasma in machining, such as the high efficiency, good form accuracy, low cost and the ability of damage-free machining, have been proved.

(3) PAP, which combines AP-plasma surface modification and soft abrasive polishing, was proposed, in which the surfaces of difficult-to-machine materials are modified by the irradiation of AP-plasma and a soft modified layer is formed. Then the modified layer is removed by polishing using a soft abrasive. Thus, a damage-free and atomic-scale flat surface

can be expected. Plasmas containing water vapor, oxygen and CF_4 are used in PAP for the polishing of different materials.

In Chapter 3, the development of the PAP machine was discussed. PAP was developed from a symmetric machine used for fundamental study to a prototype for practical application. In this chapter, the background to the development to the PAP machine and the details of the prototype PAP machine were introduced.

(1) To demonstrate the usefulness of PAP, a symmetric PAP machine that combines localized AP-plasma modification and polishing using polishing films was developed. An annular polishing area can be obtained after polishing.

(2) To clarify the oxidation and removal mechanism in PAP, a two-step PAP process was developed. The surface modification process by AP-plasma and the removal process by abrasive polishing will be investigated using this machine.

(3) To realize the polishing of large substrates, the generation of large-area AP-plasma was experimentally confirmed. Homogeneous glow discharges in large areas with diameters of 85 mm and 150 mm were realized.

(4) A prototype PAP machine was developed for the practical application of PAP to 3 inch substrates of SiC, GaN and sapphire. Slurry is not used in this machine, which is an open-air-type polishing machine without the use of a vacuum chamber, therefore it is expected to be a very cost-effective polishing technique for difficult-to-polish materials compared with conventional processes.

In Chapter 4, PAP was applied to realize the high-efficiency, low-cost and high-quality polishing of 4H-SiC. The surface modification of SiC by the irradiation of AP-plasma was confirmed, and PAP was conducted using the symmetric PAP machine, the two-step PAP process and the prototype PAP machine. The oxidation mechanism and material removal mechanism in PAP were also studied.

(1) It has been confirmed that scratches and SSD were formed in the lapping or polishing of 4H-SiC using diamond abrasive. In the case of conventional CMP, scratch-free surfaces were obtained. However, the step-terrace structure was very disordered and atomic extractions existed on the polished surface.

(2) The surface modification of SiC by the irradiation of AP-plasma was confirmed. It was found that the surface modification efficiency of water-vapor-containing plasma was higher than that of oxygen-containing plasma. It was proved that after the irradiation of the water-vapor-containing plasma, SiC was modified to SiO_2 with a decrease in surface hardness.

(3) In PAP, the density of OH radicals, which were the dominant oxide species, was greatly affected by the concentration of water vapor in the carrier gas. The strongest optical emission intensity from OH radicals was obtained when the water vapor concentration in He was approximately 200 ppm. The increase in surface modification efficiency was confirmed by XPS.

(4) The symmetric PAP machine, which combined irradiation with water-vapor-containing plasma and CeO_2 abrasive polishing, was applied to 4H-SiC (0001). The complete removal of scratches was confirmed and a well-ordered step-terrace structure was formed on the polished surface without the formation of SSD. PAP using Al_2O_3 was also conducted and many scratches were formed on the surface.

(5) The oxidation process of 4H-SiC (0001) with water-vapor-containing plasma was studied, which indicated that both SiO_2 and a silicon oxycarbide layer were formed as the oxidation products, and the interface between the oxide layer and SiC was found to be very flat. The atomic flattening mechanism of PAP was proposed. Oxidation with water-vapor-containing plasma resulted in the formation of an atomically flat interface; ceria abrasive removed the oxide layer, including the intermediate Si-C-O layer, which could not be removed by dipping in HF solution, to form an atomically flat 4H-SiC (0001) surface with a step-terrace structure.

(6) The thermal oxidation and plasma oxidation processes for 4H-SiC (0001) were compared and discussed to clarify the oxidation process. Plasma oxidation had a higher oxidation rate than thermal oxidation. In particular, the initial oxidation rate of plasma oxidation was six times higher than that of thermal oxidation. Because of the high initial oxidation rate of plasma oxidation, the oxide-SiC interface was very rough when the oxide layer was thin and became flat with increasing thickness of the oxide layer. In contrast, the oxide-SiC interface formed by thermal oxidation was atomically flat regardless of the thickness of the oxide layer owing to its extremely low oxidation rate. Many pits, which penetrated into the bulk SiC, were found on the surface processed by thermal oxidation, whereas few pits were observed on the surface processed by plasma oxidation. These pits were generated by the preferential oxidation of

defects in bulk SiC, and the formation of pits was considered to be most affected by the high oxidation temperature in thermal oxidation.

(7) After the oxide layers formed by thermal oxidation and plasma oxidation were removed by polishing using CeO_2 as an abrasive, an atomically flat SiC surface with a well-ordered step-terrace structure was obtained in both cases, although some pits remained on the surface processed by thermal oxidation. It was demonstrated that the combination of plasma oxidation and polishing using CeO_2 is very effective for obtaining atomically flat 4H-SiC substrates without the formation of pits or scratches.

(8) It was found that the polishing efficiency of conventional CMP for the C-face of 4H-SiC was very low regardless of whether SiO_2 slurry or CeO_2 slurry was used. Even after prolonged polishing (15 h for CeO_2 polishing and 9 h for SiO_2 polishing), the scratches were not completely removed. With the combination of thermal oxidation and CeO_2 slurry polishing, an atomically flat C face with a well-ordered step-terrace structure was obtained, although many pits originating from the dislocations were formed after polishing.

(9) Ceria-slurry-based ECMP, which combined anodic oxidation and abrasive polishing, was proposed as a prepolishing process for the PAP of SiC substrates. In the ECMP process, SiC is anodically oxidized to SiO_2 with a very high initial oxidation rate compared with plasma oxidation and thermal oxidation. Also, it was confirmed that anodic oxidation greatly decreased the surface hardness of SiC, which made it possible to polish the modified surface using CeO_2 slurry. After applying ECMP to a diamond-abrasive-polished SiC surface for 30 min, a scratch-free and smooth surface was obtained. It is expected that with additional abrasive polishing, the residual oxide layer can be completely removed and an atomically flat SiC surface with a step-terrace structure can be obtained.

In Chapter 5, by applying different polishing techniques under different polishing conditions, three types of step-terrace structure, the a-b-a*-b* type, a-b type and a-a type, were obtained. By considering the crystal structure of 4H-SiC, a probable mechanism for controlling the surface atomic structure of 4H-SiC (0001) was proposed and experimentally clarified.

(1) By analyzing the crystal structure of 4H-SiC, it was found that there are four types of Si-C terrace in a unit cell of 4H-SiC (4H1, 4H2, 4H1* and 4H2*), which have different values of r_{oxi}.

(2) A probable removal mechanism was proposed for controlling the surface atomic structure of 4H-SiC (0001) by adjusting the balance between chemical modification and physical removal. It was assumed that when r_{pol} for abrasive polishing was lower than the rate of surface modification, the a-b-a*-b* type step-terrace structure was formed. When the pad rotation speed was increased and r_{pol} for abrasive polishing became comparable to the rate of surface modification, the step-terrace structure changed from the a-b-a*-b* type to the a-b type. When r_{pol} for abrasive polishing was higher than the rate of surface modification, a uniform a-a type step-terrace structure was formed.

(3) CeO_2 slurry polishing of 4H-SiC with different pad rotation speeds was conducted to experimentally clarify the proposed removal mechanism. A change in the surface atomic structure along with the change in the pad rotation speed was confirmed, which supported the proposed removal mechanism.

(4) XPS measurements of the polished surfaces were conducted. The amount of residual oxidation products on the surface polished with a high pad rotation speed was smaller than that on the surface polished with a low pad rotation speed. This result also supported the proposed removal mechanism.

(5) On the basis of this removal mechanism, the results of polishing using existing polishing techniques in which chemical reactions and abrasive polishing are combined can be explained. Furthermore, it is expected that the control of the step-terrace structure on a 4H-SiC substrate will be very advantageous for realizing excellent device performance, which will be experimentally confirmed in a future study.

In Chapter 6, PAP was applied to GaN (0001) to resolve the problems of the conventional CMP process such as the low MRR and the formation of etch pits. The surface modification of GaN by the irradiation of AP-plasma was confirmed. The application of the two-step PAP process and the prototype PAP machine were separately investigated.

(1) It was confirmed that in the conventional CMP process, regardless of whether SiO_2 or CeO_2 slurry was used, many etch pits, which deteriorated the surface integrity and roughness, were generated, which originated from the dislocations in the GaN epilayer. It was considered that these pits were formed by the preferential etching or removal of the dislocations by the chemicals in the slurry.

(2) The surface modification of GaN by AP-plasma irradiation was confirmed. It was found that the surface modification efficiency of CF_4-containing plasma was higher than that of O_2-containing plasma and that the heating of the substrate greatly promoted the surface modification reaction. After plasma irradiation, the surface hardness of GaN decreased, which was confirmed by nanoindentation tests.

(3) The CMP of GaN with plasma pretreatment was conducted and a pit-free surface was obtained with time-controlled polishing. Under-polishing resulted in a GaN surface with the modified layer remaining, whereas a rough surface with many etch pits was generated in the case of over-polishing. Only in the case of just-polishing was a pit-free and atomically flat surface obtained.

(4) Several types of grinding stone were used to polish GaN without plasma pretreatment. It was revealed that the fixed-type CeO_2 grinding stone had better polishing characteristics without the generation of scratches and etch pits. Plasma irradiation was combined with dry polishing using a CeO_2 grinding stone, and a scratch-free and pit-free surface with a well-ordered step-terrace structure was obtained.

(5) The plasma generation conditions in the prototype PAP machine were optimized. It was found that a lower water vapor concentration, a higher carrier gas flow rate and the replacement of He with Ar were very effective for improving the surface modification efficiency in PAP.

(6) The prototype PAP machine was used to polish the whole-surface of 3 inch GaN substrates. A high MRR of 272.8 nm/h was obtained in the case of short-time polishing. The deterioration of the grinding stone surface in PAP was confirmed, which increased the surface roughness, resulted in the formation of scratches and decreased the MRR of PAP.

(7) The effect of dressing in PAP was confirmed. With intermittent dressing using a diamond plate, a high MRR of PAP of 193 nm/h was obtained, while it was only 90 nm/h without dressing. In a future study, the prototype PAP machine will be optimized to realize *in situ* dressing in PAP to obtain higher MRRs.

In Chapter 7, the combination of PCVM and PAP was applied to realize the damage-free figuring and finishing of CVD-SiC substrates, which are used as materials for space telescope mirrors and glass molds. As reported in this chapter, the properties of the CVD-SiC substrates used in this study were investigated. Diamond lapping and CMP were conducted for comparison

with the proposed plasma-based figuring and finishing process. PCVM was performed for the removal of the SSD layer while PAP was performed for damage-free surface finishing.

(1) The as-grown surface of the CVD-SiC substrate was very rough and its surface composition was determined by XPS, which indicated that a thin oxide layer and a contamination layer existed. The high crystallinity of the substrate was proved by XRD measurements and all the SiC grains had the same (111) surface orientation.

(2) Many scratches and an SSD layer were formed by the diamond lapping of CVD-SiC, which means that it is not a suitable finishing process for CVD-SiC. Conventional CMP using CeO_2 slurry was conducted for the damage-free finishing of CVD-SiC. However, the polishing efficiency was very low.

(3) PCVM was conducted on a diamond lapped CVD-SiC surface. After PCVM for a short duration of 5 min, scratches and the SSD layer formed by lapping were completely removed, although the surface roughness was slightly increased.

(4) PAP using a resin-bonded CeO_2 grinding stone was conducted to decrease the surface roughness of CVD-SiC processed by diamond lapping and PCVM for 5 min. The loose-held-type grinding stone was demonstrated to be very useful. A flat and scratch-free surface with an rms roughness of 0.6 nm was obtained.

In this study, PAP was applied to 4H-SiC, GaN and CVD-SiC. When PAP was applied to 4H-SiC (0001), a scratch-free and damage-free surface with a well-ordered step-terrace structure was obtained. Also, the mechanism for controlling the surface atomic structure of 4H-SiC (0001) was proposed and experimentally confirmed. When PAP was applied to GaN (0001), the problem of etch pit formation in the conventional CMP process was successfully resolved. The polishing conditions of PAP were optimized and a high MRR of 277 nm/h for a 3 inch GaN substrate was obtained. By the combination of PCVM and PAP, the slurryless and damage-free figuring and finishing of CVD-SiC was realized.

PAP is a slurryless and dry polishing technique in which damage-free and atomic-scale flat surfaces can be obtained. This is the greatest advantage of PAP compared with conventional polishing techniques such as CMP, in which a large amount of expensive slurry is required. On the basis of the results of PAP described in this study, the industrial application of PAP to wide-gap semiconductor substrates, glass lens molds and telescope mirrors is strongly expected and will be attempted in future studies.

Acknowledgements

After graduating from Huazhong University of Science & Technology (Wuhan, China), I was very lucky to have the opportunity to study at Osaka University with my supervisor Associate Professor Kazuya Yamamura. I have spent more than 5 years in this lab, the place where I lived the longest time in my life except for my hometown. I believe that this experience will become a very precious part of my life which I will never forget.

I would like to sincerely thank many people who have contributed to the completion of this work. First, I wish to express my gratitude to my supervisor Associate Professor Kazuya Yamamura for his supervision throughout this research, for his encouragement regarding my professional development and for his advice on organizing and writing this thesis. I want to thank Professor Katsuyoshi Endo for his valuable advice on this research and I appreciate the enormous amount of time he spent with me discussing my research and correcting this dissertation. I am also grateful to Assistant Professor Yuji Ohkubo for discussing my research at lab meetings and for his advice on writing this dissertation. I would like to thank all the professors in the Department of Precision Science and Technology of Osaka University including Professor Kazuto Yamauchi, Professor Kiyoshi Yasutake, Professor Mizuho Morita, Professor Yuji Kuwahara, Professor Yoshitada Morikawa, Professor Heiji Watanabe and so forth for their valuable comments and advice on my research.

I would like to thank the current members of the PAP Group including Ms. Chika Kageyama and Mr. Hisaya Dojo and the graduate members including Mr. Kohki Monna, Mr. Takaaki Tabata, Mr. Masaki Ueda and Mr. Tatsuya Takiguchi for their support and help. I sincerely appreciate the support from other members of our lab. Also, I would like to sincerely thank Ms. Yuko Miyazaki, the secretary of our lab, for her patient and kind support and for giving me courage in my daily life.

This research was partially supported by a Grant-in-Aid for Scientific Research (A) (25249006) from MEXT, Japan; a research grant from the Adaptable and Seamless Technology Transfer Program through Target-driven R&D. JST; and a Grant-in-Aid for JSPS Research Fellows (25-581 2013). Furthermore, I would like to express my gratitude to NORITAKE Co., Ltd., for providing the SiO_2 and CeO_2 grinding stones and to TOKAI Fine Carbon Co., Ltd., for providing the CVD-SiC substrates.

Finally, I thank my parents and my wife, who have always believed in me, encouraged me, and given me all their support whenever I have needed it.